# WATER USE ESTIMATION FOR POMEGRANATE ORCHARDS USING DRONE TECHNOLOGY

Report to the
Water Research Commission

by

T Volschenk[1], C Munghemezulu[2], E Economon[2], M van der Rijst[3], M Ravuluma[1], D Havenga[4], PE Ratshiedana[2], M Makghato[1], G Chirima[2] and R Mulidzi[1]

[1]Soil and Water Science Programme, Agricultural Research Council Infruitec-Nietvoorbij
[2]Agricultural Research Council Natural Resources and Engineering
[3] Biometry, Agricultural Research Council Central Office

WRC Report No. 3217/1/25
ISBN 978-0-6392-0727-8

July 2025

Obtainable from

Water Research Commission

Private Bag X03

Gezina, 0031

hendrickm@wrc.org.za or download from www.wrc.org.za

This is the final report of WRC project no. C2020/2021-00943.

# EXECUTIVE SUMMARY


BACKGROUND

Global warming-induced climatic changes, limited water resources and water restrictions for agriculture during drought force producers to invest in crops that are more suited to the potential future climate, such as drought-tolerant pomegranate (*Punica granatum*) trees. In South Africa, the pomegranate industry is small but expanding and in 2023, 79% of the plantings under this crop were in the Western Cape. The Western Cape has a semi-arid climate and the predictions of climate change are that the province can expect more water stress with increasing temperatures, increasing evaporation and increasing occurrence of droughts. The province is considered particularly vulnerable to climate change as the region is highly dependent on water storage capacity due to the dominant winter rainfall patterns and the success of the agricultural sector depends to a large extent on irrigation water availability. In Western Cape agriculture, water demands are likely to increase in the future with the expected increased temperatures and evaporation, which will result in an increased irrigation demand for orchards. According to the most recent complete dataset for the Water Management Areas (WMAs), water use in the Breede-Olifants WMA (Berg-Olifants and Breede-Gouritz WMAs amalgamated) exceeds water supply and irrigation is by far the dominant water use sector in the WMA, representing about 85% of the local water requirements. There has been a major drive in the Western Cape in recent years to increase irrigation efficiency, to promote water conservation and to manage water demand in the agricultural sector. Although irrigated agriculture in the Western Cape is one of the largest water users, there is a lack of reliable agricultural water use data.

A baseline survey on irrigation and pomegranate tree performance was undertaken during 2017/18 and 2018/19 by the Agricultural Research Council (ARC) (co-funded by the Alternative Crop Fund of the Western Cape Department of Agriculture through the Pomegranate Producers Association of South Africa (POMASA) and the Water Research Commission (WRC)). Results of the study (WRC Project K5/2958) confirmed that although pomegranate trees are considered drought-tolerant, irrigation is required during the dry summer to optimise growth, yield and fruit quality for commercial production. Furthermore, there is potential for some production areas to increase yield and fruit quality through improved irrigation scheduling. Lack of local research information on water use and crop coefficients to improve irrigation scheduling of pomegranate trees prompted the WRC (C2020/2021-00404, KSA4, Agricultural water use) and National Research Foundation (NRF) to fund research to determine water use and water productivity of pomegranate orchards from 2021/22 until 2024/25. This research measured water use for pomegranate orchards varying in canopy size and aimed to develop a method for practical estimation of crop coefficients for application in a water use model to enable calculation of individual orchard water requirements. The ground-based methods used to quantify the water use included a soil water balance, sap flow (transpiration) and micrometeorological methods (eddy covariance, surface renewal), whereas the canopy cover and tree dimensions of selected trees were monitored throughout the season.

The abovementioned research paved the way to investigate the potential use of drones or unmanned aerial vehicles (UAVs) to improve pomegranate orchard irrigation management. Drones are used as tools to efficiently monitor orchards for precision orchard management as they supply data at practical spatial, spectral and temporal resolutions. Drone technology is therefore useful to quantify the between-tree variability for the orchards where water use is measured (size could be up to c. 7 hectares). Previous research showed a good correlation between aerial-based NDVI measured for trees and canopy cover, and between canopy cover and basal crop coefficients. The latter can be used with ground-based measurements of reference evapotranspiration (ETo) to schedule irrigation. Tree height and canopy cover can, in addition to crop aerodynamic and internal resistance information, be used to estimate crop coefficients for purposes of irrigation scheduling. Dimensional estimates of canopy cover based on crop diameter or width and row spacing can be reasonably accurate, but should be calibrated with other objective techniques to improve accuracy.

The purpose of the current research was to relate drone image-derived tree geometric dimensions, spectral band reflectance, vegetation indices and thermal infrared temperature with seasonal canopy development and water use for pomegranate orchards in the Western Cape to determine if it could aid in on-farm irrigation and catchment-scale water resource management. It also aimed to provide supplementary information on the orchard properties, such as canopy cover and tree homogeneity, underlying water use values obtained via micrometeorological methods that will be made available for decision support and policy making in the water sector. Supplying information on water use and crop coefficients to improve irrigation scheduling of pomegranate trees will in principle address the goals of the Western Cape Sustainable Water Management Plan for 2017-2022 regarding water availability (Enable the sustainability of water resources for growth and development) and water quality (Enable integrity and sustainability of socio-ecological systems). It falls within the focus area of Water Smart Agriculture with regard to improved water use efficiency and management and

could reduce the ecological impact of excessive leaching on river catchments and groundwater resources. As such it can support the formation of a water-wise agriculture sector that promotes sustainable and optimal agricultural production and thereby improve water security.

## AIMS

The current research project intended to refine pomegranate orchard irrigation management by using the water use data generated by WRC Project C2020/2021-00404 and drone technology by pursuing the following aims:

Aim 1: To assess if drone-technology derived attributes for individual pomegranate trees can be related accurately to in-field measured tree dimensions and light interception.

Aim 2. To relate drone-determined tree geometric traits and NDVI to actual water use and crop coefficients on tree and orchard scale.

Aim 3. To determine orchard homogeneity for two orchards varying in canopy cover using drone technology-derived tree attributes.

## METHODOLOGY

Drone surveys were conducted at five pomegranate development stages during the 2023/2024 growing season for two pomegranate orchards varying in canopy cover. The ARC Natural Resources and Engineering Institute collected thermal and multispectral data around solar noon using the specific cameras and sensors required and conducted the data processing to supply the data outputs per tree. Geometric traits (tree height and volume), spectral band reflectance (blue, green, red, near-infrared and RedEdge), six vegetative indices (NDVI - Normalized Difference Vegetation Index, NDRE - Normalized Difference Red Edge Index, GNDVI - Green Normalized Difference Vegetation Index, RVI - Ratio Vegetation Index, CVI - Chlorophyll vegetation index, CIRE - Chlorophyll index – Red edge) and thermal infrared temperature (TIR) were derived from the drone images using the appropriate data processing steps.

On the same day or at least within three days after the drone surveys, ground-based tree canopy measurements (dimensions, fractional interception and leaf area index) were conducted. Canopy dimensions were determined using a measuring stick. Two Accupar LP-80 ceptometers were used to measure fractional light interception (FI) of eight trees around solar noon. Leaf area index (LAI) was obtained as an output from the LP-80 ceptometer and an *in situ* calibration was performed to obtain canopy area-based and orchard leaf area index (Tr-LAI and OLAI, respectively). Leaf chlorophyll content data were collected during survey 1 and for surveys 3-5 for 11 and 17 trees, respectively, using a SPAD-502 chlorophyll meter. Stem water potential measurements were determined for six selected trees using a pressure chamber (PMS Model 1505D-EXP). Tree physiological measurements were conducted on the same six trees during surveys 2-5 using a LI6400 XT infrared gas analyser. Orchard water use data were collected for the day the drone surveys were conducted through soil water balance (two trees) and sap flow (transpiration, four trees) techniques at individual trees. On an orchard scale, individual tree transpiration was upscaled and evapotranspiration (ETc) was determined by using a surface renewal system at a young orchard and an eddy covariance system at a full bearing orchard. A weather station at each site collected the data required to calculate ETo to determine the ratios of transpiration and ETc to ETo (crop coefficients).

Simple linear regressions were conducted between all data and indices derived from drone images for selected individual trees to individual tree data measured in orchards for orchards combined (young and full bearing), per orchard (five surveys combined) and per survey per orchard (individual trees combined). Linear regressions were also conducted at orchard scale – i.e. orchard averaged values of all individual tree data derived from drone images compared to averaged ground measured tree dimensions or orchard upscaled transpiration or orchard level evapotranspiration, also for orchards combined and per orchard (five surveys combined). Regression models were considered significant at 95% level of confidence ($p = 0.05$). Spectral profiles were provided for the two orchards and the homogeneity of the orchard canopy characteristics was reported as the average of the individual tree metrics ± standard error and in the form of histograms depicting the size distribution or various tree canopy-related variables per orchard.

## RESULTS AND DISCUSSION

Simple linear regressions were used to assess the potential of using multispectral drone image-derived variables and thermal infrared temperature to estimate various ground-measured pomegranate tree canopy properties for orchards varying in canopy size and differing in location. From regressions which included data for individual trees from both the young and the full bearing orchard and all five surveys combined, drone image estimated tree height and volume appeared to be the variables that related most frequently to the ground-measured tree variables, especially at the young orchard. There were no good, significant regression relationships between the drone image-derived variables and in-field measured tree properties for the full bearing orchard, probably due to a lack of variation

in the properties of the trees required for strong linear regression relationships. At the individual tree level, for data of orchards combined, drone estimated tree height had significant regression relationships with all tree canopy properties except for OLAI ($R^2$ values between 0.09 and 0.53). The coefficients of determination for all measured canopy properties with drone image-derived tree height were higher than those with all the other drone image-derived variables, except for FI, which had a better regression relationship with CVI.

At the orchard level, for data from orchards combined, orchard-averaged tree height, across row width, tree volume, FI and CP-LAI related relatively well to orchard-averaged drone-estimated tree height, with $R^2$-values ranging between 0.73 and 0.87. Reliability of these regression models could be improved by the collection of more data to address a paucity of data points existing in the mid-range between that available for the young and the full bearing orchard of the current research. Unexpectedly, there were no significant linear regression relationships at a 95% confidence level of the orchard averaged canopy dimensions, FI or LAI variables with NDVI, except for tree height of the young orchard, which increased with decreasing NDVI. The variability in NDVI was partially ascribed to a decrease in NIR from summer to fall, simultaneous with a general increase in red spectral band reflectance over the season.

Using orchard-averaged ground-measured and drone image-derived data improved the regression relationships considerably, especially for the young orchard considered on its own. For the young orchard, the orchard averaged blue spectral band reflectance was the best suited to estimate the orchard's average tree height. Although CVI had the best regression relationship with FI and the LAI variables ($R^2$ values > 0.94), it appeared to be more sensitive to chlorophyll changes in the canopy than to changes in FI and LAI, with the latter variables increasing with decreasing CVI. Although the regression relationships of FI and LAI with the RedEdge spectral band had $R^2$ values of only 0.77 and 0.7, respectively, it was due to the positive regression relationships preferred to provide FI and OLAI estimates. Tree height, FI and OLAI are important input parameters to estimate crop coefficients as an alternative if crop coefficients cannot be acquired directly from regression relationships with drone image-derived variables. The full bearing orchard only had one significant regression relationship at a 5% significance level, i.e., between orchard averaged across tree row canopy width and TIR ($R^2$ =0.78). Poor relationships of orchard averaged FI and LAI variables with NDVI were perplexing. Some of the variability in NDVI may be related to seasonal effects induced by phenological changes, while the saturation of vegetation indices could have been affected by changes in soil background reflectance, leaf properties and canopy structures over the season.

Water use includes tree transpiration, which is, among other factors, controlled by or related to plant physiological variables such as leaf stomatal conductance and leaf-level transpiration rate. Since such data can be usefully applied to support decision making in orchard irrigation management, the relationships between drone image-derived variables and individual tree plant physiological parameters were also investigated. There were several linear regression relationships significant at a 95% confidence level, with coefficients of determination ranging between 0.104 and 0.584 for data of orchards combined, and the $R^2$ value increased in some cases up to 0.866, where orchards were considered on their own. However, in most cases, there was a clear paucity of mid-range data to strengthen the regression relationships. This was more frequently the case for individual tree data for orchards combined and for the young orchard considered on its own. In most cases, there was a clear distinction between data collected after harvest and that derived from the surveys done in summer. Regressions using orchard-averaged data for orchards combined rendered $R^2$ values of between 0.5 and 0.87. When regressions were conducted for the orchard averaged data of individual orchards, the coefficients of determination were, in general, higher, i.e., between 0.74 – 0.997. In some cases, data from orchards combined may render significant regression relationships at a 95% confidence level, whereas it will not necessarily be significant for both orchards at the individual orchard level (e.g., stem water potential and chlorophyll content).

Individual tree midday stem water potential data of orchards combined were not significantly related to any drone image-derived variables, whereas it related poorly, but significantly, with a negative correlation to RVI at the young ($R^2$ = 0.27) and NIR at the full bearing orchard ($R^2$ = 0.2). Predawn stem water potential at the full bearing orchard related better to NIR, with a coefficient of determination of 0.46. Orchard averaged midday stem water potential was not related significantly to any drone image-derived variables at a 95% confidence level for the data of orchards combined, nor for the young or full bearing orchards considered individually. Data for the young orchard lacked a clear trend in stem water potential over the season. However, at the full bearing orchard midday stem water potential tended to decrease with decreasing NDVI as the season progressed, albeit at a lower significance level ($R^2$ = 0.74, p = 0.062). Leaf chlorophyll content data for orchards combined related significantly to CVI, with $R^2$ values of 0.42 and 0.61 for regressions based on individual tree and orchard averaged data, respectively. However, regression relationships based on individual tree data were, in general, poor for the individual orchards ($R^2$ values of 0.28 or less), with no consistent drone image-derived variable that resulted in the best regression relationship (CIRE for the young / TIR for the full bearing). Based on orchard averaged data, there was no significant regression relationship for the young orchard, but a highly significant one for the full bearing orchard ($R^2$ = 0.92) in which leaf chlorophyll content increased with NIR spectral reflection.

Concerning leaf physiological parameters, for data of orchards combined, the carbon dioxide assimilation rate ($A_n$) at 10h00 related significantly to NIR based on individual tree data ($R^2$ = 0.56) as well as orchard averaged data ($R^2$ = 0.71). For the individual orchards,

there was once again variation in the drone image-derived variables, which resulted in the best regression relationships. Based on individual tree data, $A_n$ at 10h00 related the best to NDRE for the young orchard ($R^2$ = 0.7), whereas at the full bearing orchard, NIR was the best related variable ($R^2$ = 0.24). For orchard averaged data, $A_n$ at 10h00 related best to RedEdge spectral reflectance for the young orchard (R2 = 0.96), while at the full bearing orchard, only $A_n$ at 14h00 related significantly to RVI ($R^2$ = 0.997). Stomatal conductance ($g_s$) at 12h00 for data of orchards combined related significantly to GNDVI based on individual tree data ($R^2$ = 0.37) as well as orchard averaged data ($R^2$ = 0.54). At the individual tree level at the young orchard, the $g_s$ at 12h00 related significantly the best to NDVI ($R^2$ = 0.74), but at the full bearing orchard $g_s$ at 10h00 related the best to RVI ($R^2$ = 0.27). Based on orchard averaged data, $g_s$ at 12h00 related at the young orchard the best to RedEdge spectral reflectance ($R^2$ = 0.88) or RVI ($R^2$ = 0.82) and, at the full bearing orchard and to RVI ($R^2$ = 0.993). Based on individual tree data for orchards combined, Leaf level transpiration rate ($Tr_L$) at 10h00 related significantly to RVI ($R^2$ = 0.58), whereas amongst regressions based on orchard averaged data for orchards combined, $Tr_L$ at 12h00 related the best to RVI ($R^2$ = 0.87), In contrast with that found for individual tree data of orchards combined, the time and drone image derived variables that $Tr_L$ related to the best changed for the individual orchards. For the young orchard, $Tr_L$ related at 12h00 the best to NDRE ($R^2$ = 0.87) and for the full bearing orchard at 14h00 to RVI ($R^2$ =0.45). The time and drone variable resulting in the best regression relationship of $Tr_L$ with orchard averaged data for orchards combined remained similar for the individual orchards, with $Tr_L$ at 12h00 giving the best relationship with either RVI or RedEdge spectral reflectance for the young orchard ($R^2$ = 0.98) and with RVI at the full bearing orchard ($R^2$ = 0.993).

For producers that have frequent access to drone services or own drones themselves, the possibility exists to apply precision irrigation management if tree transpiration, orchard water use or crop coefficients can be predicted accurately from variables derived from the drone multispectral and thermal imagery. Linear regressions of the drone image-derived variables with water use determined for individual trees resulted in general in poor regression relationships. At the individual tree level, for orchards combined, transpiration related best to drone-estimated tree height or RVI ($R^2$ values around 0.46). The ratio of transpiration to ETo related significantly at a 95% confidence level the best to drone estimated tree height ($R^2$ = 0.367). The linear regression relationships of transpiration and transpiration:ETo ratio with NDVI was poor ($R^2$ = 0.37) and not significant, respectively. Soil water balance determined ETc related well at tree row and orchard level, especially to RedEdge spectral reflectance and CVI ($R^2$ values of between 0.79 and 0.9), with no significant linear regression relationships for either water use indicator with NDVI. The ETc:ETo ratio in the tree row related significantly to the green, blue and RedEdge spectral band reflectance ($R^2$ values between 0.58 - 0.615), with no significant regression relationships between the ETc:ETo ratio at orchard level and any of the drone image-derived variables. Individual tree transpiration data of surveys combined for the young orchard related best to drone estimated tree height and RedEdge spectral band reflectance ($R^2$ values ≤ 0.355), whereas the regression relationship to NDVI was poorer ($R^2$ = 0.208). Individual tree transpiration at the full bearing orchard and the transpiration: ETo ratio at both sites were not significantly related to any of the drone-derived variables at a 5% significance level. Soil water balance-based ETc datasets were limited and did not render significant regression relationships that could aid in irrigation scheduling of the orchards. At the survey level at the full bearing site, regressions significant at a 95% confidence level were limited to that between transpiration and the ratio thereof to ETo with NIR and RedEdge spectral band reflectance, respectively, during the fourth survey. Soil water balance-derived ETc data were too limited to use for survey-level regression purposes.

Fortunately, the regression relationships between pomegranate tree water use and drone image-derived variables improved as data processing moved from individual trees towards orchard orchard-averaged scale. At the orchard averaged level, for sites combined, orchard upscaled tree transpiration related at a 5% significance level linearly the best to orchard averaged RVI ($R^2$ = 0.92, $SE_{est}$ = 0.061 mm $d^{-1}$). Orchard transpiration ranged in a narrow band between 0.8 and 1.4 mm per day and increased with increasing RVI. Regressions of orchard transpiration with NDVI and drone-estimated tree height resulted in coefficients of determination of 0.71 and 0.7, respectively, at a similar significance level, with standard error of the estimates around 0.11 mm $d^{-1}$. Micrometeorological system determined orchard level ETc for sites combined ranged between 1 and 4.6 mm and related significantly only to RVI at a 10% significance level ($R^2$ value of 0.42) with a large standard error of the estimate, i.e. 0.956. The poor regression relationships with the drone-derived variables were mostly due to an outlying value originating from January 2024 for the full bearing orchard, but in some cases, one from October 2023 for the young orchard as well. For data of orchards combined, the ratio of orchard transpiration to ETo related significantly only to drone estimated tree height and volume at a 10% significance level ($R^2$ values 0.41 and 0.45, respectively), with a standard error of the estimate of about 0.2 for both variables. The ratio of orchard level ETc to ETo related significantly at the 10% significance level, reasonably only to drone estimated tree height, with an $R^2$ value of 0.44, but the standard error of the estimate was 0.12, which is too large to allow accurate estimates of the ratio.

Orchard upscaled transpiration data for the young orchard considered on its own, related linearly the best to the orchard averaged RedEdge spectral band reflectance ($R^2$ = 0.96, standard error of the estimate 0.03), whereas NDVI comparatively correlated poorer ($R^2$ = 0.811) while the standard error of the estimated transpiration increased to 0.068. There were no significant relationships at a 95% confidence level between orchard upscaled transpiration of the full bearing orchard and any drone image-derived variables at the site level, most likely due to the variability of the limited data set available. There were no significant relationships between orchard-level ETc of the young orchard and the drone image-derived variables, even at a 90% confidence level. For the full bearing orchard, orchard level ETc can be estimated from a linear regression relationship with TIR based on a limited number of datapoints ($R^2$ = 0.999), with no other significant regression relationships between orchard level ETc and other drone-derived variables, probably due to the

variation of a limited dataset. Furthermore, there were no significant regression relationships for the young or full bearing orchards between the orchard upscaled transpiration:ETo ratio and any drone image-derived variables at a 5% significance level. However, the orchard level ETc:ETo ratio for the young orchard can be estimated from NIR at a %5 significance level with a standard error for the ETc:ETo estimate of 0.03. There were no significant regression relationships for the full bearing orchard level ETc:ETo ratio with any of the drone image-derived variables, probably due to limited data points available for regression analysis.

Estimation of transpiration and especially the ETc:ETo ratio for the five-year-old orchard from the regression relationships with RedEdge and NIR spectral band reflectance, respectively, indicated the presence of large variability in the orchard, which will benefit from the application of precision irrigation. The estimated orchard mean transpiration (±standard error) for summer amounted to 1.01(±0.02) mm $d^{-1}$, but individual tree position transpiration could reach a maximum of 1.24 mm $d^{-1}$. The estimated orchard mean Kc during summer was 0.29, which could increase by almost 70% for individual trees. If you irrigate according to the mean, underirrigation will be inevitable for some trees in the orchard, which might affect the orchard canopy development goals or productivity negatively. On the other hand, overirrigation could result in loss of precious water resources and expensive fertilizers beyond the root zone.

Existing research proposes estimation of crop coefficients from mathematical relationships containing tree height, fractional interception and LAI. Since our research endeavoured to estimate these variables, amongst others, from drone image-derived variables on orchard scale, it was considered fit to compare the measured water use and ratios thereof to ETo to the in-field measured tree canopy properties. The regression relationships between measured tree water use and tree geometric properties of the young and full-bearing pomegranate orchards were poorer than expected. For individual tree data of both orchards combined, transpiration and its ratio to ETo related best to tree height, across row canopy width, FI and ceptometer-derived LAI, with the highest coefficient of determination reaching only 0.588. At the individual orchard level, only the young orchard acquired significant linear regression relationships, with a limited dataset hampering proper evaluation for the full bearing orchard. Transpiration in the young orchard related significantly to all the tree canopy-related variables measured, but the best to calculated tree volume ($R^2$ = 0.538) and unexpectedly the poorest to tree height ($R^2$ = 0.23) and FI ($R^2$ = 0.238). Transpiration of the individual trees in the young orchard was not related to any tree geometric properties early in the season and after harvest, but it related well to and increased with FI and LAI after most of the fruit set in December 2023, at full canopy development stage in January 2024 and shortly before harvest in February 2024 ($R^2$ values> 0.9). For the full bearing orchard, transpiration and the ratio thereof to ETo were only significantly related to FI early in the season during October 2023 and to across row canopy width during October 2023 and January 2024. Lack of significant regression relationships for the full bearing orchard can be explained by the absence of variation in canopy dimensions and a limited water use dataset.

For data of orchards combined, the ratio of orchard upscaled transpiration to ETo as well as ETc:ETo were significantly linearly related at a 5% significance level to tree height, FI and ceptometer-based LAI. The respective ratios increased with increasing tree height, FI and ceptometer-based LAI, but additional data are required mid-range to improve the regressions and to validate it. The orchard level ETc:ETo ratio was also significantly related to across row width and tree volume at a 5% significance level with $R^2$ values of 0.72 and 0.78, respectively. However, the standard error of the estimate was quite high for both variables, being more than 0.075. More research is required in this regard. There were no significant regression relationships of orchard upscaled transpiration at the full bearing orchard with other tree canopy measured variables. Nor were orchard ETc or the ratio of transpiration or ETc to ETo, respectively, significantly related to any of the field-measured canopy properties for the orchards considered separately. Several anomalous significant regression relationships were obtained between orchard upscaled transpiration and selected tree canopy variables for the orchards combined and for the young orchard on its own. A collection of additional datasets are recommended to improve regression relationships and to resolve atypical linear regression trends found for transpiration with tree height, fractional interception and LAI at orchard scale.

Orchard homogeneity for the two orchards varying in canopy cover was quantified and compared. Spectral profiles provided valuable insight on the changes in spectral band reflectance at selected crop development stages and highlighted the main differences between the young and the full-bearing pomegranate orchards in two production areas. The dynamics of especially the NIR, red and blue bands are especially useful to determine differences in reflection that might be related to differences in canopy development or stress-induced chlorophyll degradation. According to the seasonal means, there were no differences in spectral band reflectance between the orchards. Amongst the vegetation indices, CVI was significantly higher for the young compared to the full bearing orchard, indicating higher chlorophyll content of the canopies. Drone-estimated tree height and volume was also significantly different between the two orchards. Drone estimated tree height ranged between 0.675 m and 0.982 m for the young orchard and 1.59 m and 2.04 m for the full bearing orchard, whereas drone estimated tree volume reached a maximum of 4.55 $m^3$ for the young and 10.85 $m^3$ for the full bearing orchard.

GENERAL

All three project aims were achieved successfully. More value was added by assessing the relationship between water use and crop coefficients, respectively, to drone image-derived spectral band reflectance and five spectral vegetation indices in addition to NDVI and the tree geometric traits (Refer Aim 2).

NEW KNOWLEDGE CREATED

New knowledge to be created by this project included correlation of drone technology-based information on seasonal canopy development to ground-measured tree characteristics and water use dynamics for pomegranate trees under South African conditions and assessing the viability of using drone technology to assist in estimation of crop coefficients to estimate water use for irrigation scheduling. The research gap on usefulness of drones to assist in estimation of crop coefficients for orchards differing in canopy size and location was addressed by conducting drone surveys earlier and later during the canopy development stage, at full canopy, during ripening before harvest and after harvest and by strategically using selected tree and water use data from project C2020/2021-00404. Linear regression relationships between drone image derived spectral band reflectance, tree geometrical canopy characteristics, six vegetative indices (including NDVI) and thermal infrared temperature, respectively, to in field measured tree canopy properties (dimensions, FI, LAI); selected tree physiological parameters and tree water use (transpiration, evapotranspiration and crop coefficients), respectively, were obtained. The statistical significance of these relationships has been summarized and this information can be used to select appropriate regression relationships to estimate selected tree canopy or water use-related variables from drone image-derived variables. Regressions were conducted on individual tree scale (combining data of orchards/ surveys per site/ trees per survey per site) and orchard averaged scale (combining data of orchards/ surveys per site).

Products produced by this research included:

- For the young orchard considered on its own, orchard averaged tree height can be estimated from orchard averaged blue spectral band reflectance ($R^2$ = 0.993) with a low standard error of the estimate, whereas FI and OLAI can be estimated from regression relationships with RedEdge spectral band reflectance with lower accuracy ($R^2$ values of 0.77 and 0.7, respectively).

- Significant regression relationships to estimate transpiration or crop coefficients for irrigation scheduling of a young orchard from orchard averaged drone image derived RedEdge and NIR reflectance, respectively, was obtained. Collection of additional data is recommended improve and to validate the abovementioned regression relationships.

- Orchard transpiration and Kc (ETc: ETo ratio) values was estimated for individual trees for different growth stages for the young pomegranate orchard using the regression relationships obtained and the variation over the season tabulated.

To our knowledge similar research using drones to determine canopy characteristics to estimate crop coefficients or for estimation of evapotranspiration or crop coefficients directly has not been done for pomegranate orchards varying in canopy cover and location in South Africa. Crop coefficients for pomegranates have previously been related to drone image derived NDVI by the USDA. Our research related it best to NIR reflectance.

CAPACITY BUILDING

Uncertainties with regard to suppliers to conduct the drone surveys and lack of funding for a bursary hampered recruitment of a student for this project. The stem water potential and physiological data collected in 2023/2024 was related to the drone image derived spectral bands and indices and will be included in the thesis of Daniel Havenga supervised by Dr Dzikiti (Stellenbosch University) on the water use and water productivity project (C2020/2021-00404). He assisted in the writing of Chapter 6 of the final report for project C2020/2021-00943. In terms of institutional capacity building, Dr T. Volschenk attended an online short course: “Introduction to field data collection and UAV data pre-processing” held by the ARC Natural Resources and Engineering institute, on 17 October 2023.

CONCLUSIONS

Drone-technology derived attributes for individual pomegranate trees can, based on the existing dataset, not be related accurately to in-field measured tree dimensions and light interception, but it is possible for selected tree properties on an orchard scale.

- Linear regressions using individual tree data for orchards combined, orchards on their own or phenological growth stages (surveys) separately did not render regression models for a single specific drone image-derived variable that could be used to estimate the canopy tree dimensions, fractional interception or LAI over the whole season. Factors contributing to the poor

regression relationships could include variation in spectral reflectance between soils and/ or trees of orchards, within orchards as well as between phenological growth stages, and specifically for the full bearing orchard, lack of variation in the canopy properties of the trees required for strong linear regression relationships. Amongst the multispectral and thermal drone image-derived variables, drone image estimated tree height and volume related most significantly via linear regression to in-field measured tree canopy properties of individual selected trees, especially at the young orchard. At the individual tree level, for data of orchards combined, drone estimated tree height rendered the best significant regression relationships with all tree canopy properties except for OLAI (which was not significantly related) and FI (which related better to CVI), with $R^2$ values ranging between 0.09 and 0.53.

- Regression relationships improved where orchard averaged data from the various drone surveys were used, compared to those based on individual tree data. For data of the young and full bearing orchard combined, orchard averaged drone estimated tree height related significantly at a 95% confidence level to orchard averaged tree height, across row width, tree volume, FI and ceptometer based LAI ($R^2$-values ranging between 0.73 and 0.87), but with a relatively high standard error of the estimate for tree height and FI. Reliability and accuracy of these regression models could possibly be improved by collection of more data to address a paucity of mid-range data points.

- For the young orchard, orchard averaged blue spectral band reflectance was the best suited to estimate orchard averaged tree height with a low standard error of the estimate. It was recommended to rather estimate FI and OLAI from regression relationships with RedEdge spectral band reflectance instead of using the regression relationship with CVI, which correlated better, but appeared to be sensitive to seasonal chlorophyll content changes.

- Tree height, FI and OLAI are important input parameters to estimate crop coefficients as an alternative if crop coefficients cannot be acquired directly from regression relationships with drone image derived variables., Poor, atypical or lack of significant relationships of orchard averaged tree height, FI and LAI variables with NDVI was partially ascribed to NDVI variability, which may be related to phenological changes or changes over the season in soil background reflectance, leaf properties and canopy structures.

With regard to relating drone image derived variables to individual tree plant physiological parameters (stem water potential, leaf chlorophyll content, $A_n$, $g_s$ and $Tr_L$) there were several linear regression relationships significant at a 95% confidence level, with maximum coefficients of determination for data of orchards combined being 0.58 and 0.87 where orchards were considered on their own. In most cases, additional data points are required mid-range to strengthen and validate the regression relationships. Using orchard-averaged data rendered $R^2$ values of up to 0.87 and 0.997 for orchards combined and for individual orchards, respectively.

- For stem water potential data of orchards combined, neither individual tree nor orchard-averaged midday stem water potential was significantly related to any drone image-derived variables. For orchards separately, individual tree midday stem water potential related poorly ($R^2 < 0.27$), but significantly with a negative correlation to RVI at the young and NIR at the full bearing orchard, whereas orchard averaged midday stem water potential was not related significantly to any drone image derived variables at a 95% confidence level for either orchard. Data for the young orchard lacked a clear trend in stem water potential over the season. However, the full bearing orchard averaged midday stem water potential tended to decrease with decreasing NDVI as the season progressed, albeit at a lower significance level ($R^2 = 0.74$, $p = 0.062$).

- Although leaf chlorophyll content data for orchards combined related significantly to and increased with CVI based on individual tree and orchard averaged data ($R^2$ values of 0.42 and 0.61, respectively), data distribution patterns were not convincing. Regression relationships based on individual tree data were, in general, poor for the individual orchards with no common drone image-derived variable resulting in the best regression relationships. Based on orchard-averaged data, leaf chlorophyll content for the full bearing orchard increased with NIR spectral reflection ($R^2 = 0.92$), with no significant regression relationship identified for the young orchard.
- For data of orchards combined, $A_n$ at 10h00 related significantly to and increased with NIR based on individual tree data ($R^2 = 0.56$) as well as orchard averaged data ($R^2 = 0.71$). Stomatal conductance at 12h00, for data of orchards combined, related significantly to and increased with GNDVI based on individual tree data ($R^2 = 0.37$) as well as orchard averaged data ($R^2 = 0.54$). For the individual orchards, there was for both $A_n$ and $g_s$ variation in the drone image-derived variables, which resulted in the best regression relationships.

- Based on individual tree data for orchards combined, $Tr_L$ at 10h00 related significantly to RVI ($R^2 = 0.58$), whereas amongst regressions based on orchard averaged data for orchards combined, $Tr_L$ at 12h00 related the best to RVI ($R^2 = 0.87$), Individual tree data of orchards considered separately displayed variability in terms of the $Tr_L$ time and drone image derived

variables that related the best. However, the orchard averaged data of the young orchard displayed the best regression relationship between $Tr_L$ at 12h00 with either RVI or RedEdge spectral reflectance and at the full bearing orchard, with RVI.

Drone image-derived spectral band reflectance, tree geometric traits and spectral indices were related to actual water use and crop coefficients on tree and orchard scale, with mixed success rates at individual tree and orchard scale. Some of the regression relationships could be used to derive useful information for irrigation scheduling, but they still need to be validated before they can be endorsed and recommended for use on farms. The regression relationships between pomegranate tree water use and drone image-derived variables improved from individual tree towards orchard-averaged scale.

- Transpiration:

***At the individual tree level, f****or* ***orchards combined***, *transpiration* related best to drone estimated tree height or RVI ($R^2$ values around 0.46), whereas t*ranspiration* data of ***surveys combined*** for the *young orchard* related best to drone estimated tree height and RedEdge spectral band reflectance ($R^2$ values ≤ 0.355). Individual tree transpiration at the full bearing orchard did not relate significantly to any of the drone-derived variables at a 95% confidence level. Regression relationships of individual tree transpiration with NDVI for data of orchards combined or for the young orchard considered on its own were poor ($R^2$ = 0.37 and 0.208, respectively) and for the full bearing orchard, not significant. Regressions ***per survey*** were only significant at a 95% confidence level at the *full bearing site* between *transpiration* with NIR and RedEdge spectral band reflectance, respectively, during the fourth survey.

***At the orchard averaged level***, for ***sites combined***, *orchard upscaled tree transpiration* related at a 5% significance level linearly the best to and increased with orchard averaged RVI ($R^2$ = 0.92, $SE_{est}$ = 0.061 mm $d^{-1}$). Regressions of orchard transpiration with NDVI and drone-estimated tree height resulted in poorer coefficients of determination (c. 0.7), with standard errors of the estimates increasing to around 0.11 mm $d^{-1}$. ***Orchard upscaled transpiration*** *data for the* ***young orchard*** considered on its own, related linearly the best to the orchard averaged RedEdge spectral band reflectance ($R^2$ = 0.96, standard error of the estimate 0.03), whereas NDVI comparatively correlated poorer ($R^2$ = 0.811) with the standard error of the estimated transpiration increasing to 0.068. There were no significant relationships at a 95% confidence level between *orchard upscaled transpiration of the* ***full bearing orchard*** and any drone image-derived variables at the site level, most likely due to the variability of the limited data set available.

- Transpiration: ETo ratio

***At*** the ***individual tree level***, the *ratio of transpiration to ETo* for ***orchards combined*** related significantly at a 95% confidence level, the best to drone estimated tree height ($R^2$ = 0.367), but the linear regression relationship of the transpiration: ETo ratio with NDVI was not significant. For the data of ***surveys combined,*** the *transpiration: ETo ratio* at neither site was significantly related to any of the drone-derived variables at a 5% significance level. ***At the survey level,*** regressions significant at a 95% confidence level were limited to that between *transpiration* and the *ratio thereof to ETo* with NIR and RedEdge spectral band reflectance, respectively, during the fourth survey at the *full bearing orchard.*

***At the orchard averaged level,*** for data of ***orchards combined***, the ratio of orchard transpiration to ETo related significantly only to drone estimated tree height and volume at a 10% significance level ($R^2$ values 0.41 and 0.45, respectively), with a standard error of the estimate of about 0.2 for both variables. Furthermore, there were no significant regression relationships for the young or full-bearing orchards considered on their own between the orchard upscaled transpiration: ETo ratio and any drone image-derived variables at a 5% significance level.

- ETc

***At*** the ***individual tree level***, for ETc data of ***orchards combined***, soil water balance determined *ETc* related well at tree row and orchard full surface area level especially to RedEdge spectral reflectance and CVI ($R^2$ values of between 0.79 and 0.9), with no significant linear regression relationships for either water use indicator with NDVI. For ***surveys combined and at the survey level,*** soil water balance-based *ETc* datasets were limited and did not render significant regression relationships that could aid in irrigation scheduling of the orchards.

***At the orchard level***, for ***sites combined, the*** micrometeorological system determined *orchard level ETc* for sites combined related significantly only to RVI at a 10% significance level ($R^2$ value of 0.42) with a large standard error of the estimate, i.e. 0.956. Outlying values originating from January 2024 for the full bearing orchard and, in some cases, October 2023 for the young orchard caused the poor regression relationships. There were no significant relationships between ***orchard-level ETc*** *of the* ***young orchard*** and the drone image-derived variables even at a 90% confidence level. For the ***full bearing orchard,*** *orchard level ETc* can be estimated from a linear regression relationship with TIR based on a limited number of datapoints ($R^2$ = 0.999, n = 3), but might not be reliable.

- ETc:ETo ratio

*At individual tree level*, for *orchards combined,* the soil water balance based *ETc:ETo ratio* in the tree row related significantly to the green, blue and RedEdge spectral band reflectance ($R^2$ values between 0.58 - 0.615), with no significant regression relationships between the ETc:ETo ratio at orchard full surface level and any of the drone image derived variables. For ***surveys combined and at the survey level*** soil water balance-derived *ETc* data were too limited to use for survey-level regression purposes.

*At orchard averaged level*, for ***sites combined,*** the *ratio of orchard level ETc to ETo* related significantly at the 10% significance level reasonably only to drone estimated tree height with an $R^2$ value of 0.44, but the standard error of the estimate was 0.12, which is too large to allow accurate estimates of the ratio. However, the orchard level ETc:ETo ratio for the ***young orchard*** can be estimated from NIR at a %5 significance level with a standard error for the estimate of 0.03. There were no significant regression relationships for the ***full bearing orchard*** level ETc:ETo ratio with any of the drone image-derived variables, probably due to limited data points available for regression analysis.

Estimation of transpiration and especially the ETc:ETo ratio for the five-year-old orchard from the regression relationships with RedEdge and NIR spectral band reflectance, respectively, indicated the presence of large variability in the orchard, which will benefit from the application of precision irrigation. The estimated orchard mean transpiration (±standard error) for summer amounted to 1.01(±0.02) mm $d^{-1}$, but individual tree position transpiration could reach a maximum of 1.24 mm $d^{-1}$. The estimated orchard mean Kc during summer was 0.29, which could increase by almost 70% for individual trees. If you irrigate according to the mean, underirrigation will be inevitable for some trees in the orchard, which might affect the orchard canopy development goals or productivity negatively. On the other hand, overirrigation could result in loss of precious water resources and expensive fertilizers beyond the root zone.

Collection of additional data sets in different orchards and/ or over more seasons are required to increase the database and to validate statistically significant regression relationships to enable reliable estimation of orchard-level transpiration, ETc and crop coefficients from drone image-derived variables for pomegranate orchards varying in canopy size. The poor relationships between the water use indicators and NDVI might be explained by site-specific differences in the spectral profiles of the orchards researched here compared to those reported on by other researchers.

The regression relationships between measured tree water use and tree geometric properties of the young and full-bearing pomegranate orchards were poorer than expected.

- This can partially be explained by transpiration not being significantly related to any tree geometric properties early in the season and after harvest, whereas data representative of the whole season were used for the linear regressions.
- Transpiration related well to and increased with FI and LAI during the middle of December after most fruit set, at full canopy development stage in January and shortly before harvest near the end of February ($R^2$ values> 0.9).
- For the full bearing orchard, the lack of significant regression relationships between transpiration and the ratio thereof to Eto, with the majority of tree canopy properties can partially be explained by the absence of variation in canopy dimensions and a limited dataset, which was due to temporary malfunctioning of the sap flow and eddy covariance systems.
- The ratio of orchard upscaled transpiration to ETo as well as ETc:ETo were significantly linearly related at a 5% significance level to tree height, FI and ceptometer-based LAI for data of orchards combined. Additional data are required for mid-range to improve the regressions and to validate it.
- The orchard level ETc:ETo ratio was also significantly related to across row width and tree volume at a 5% significance level with $R^2$ values of about 0.73, but the standard error of the estimate was quite high for both variables and exceeded 0.075, which is considered too high to estimate the ratio accurately.

Drone technology-derived tree attributes were used to determine orchard homogeneity for two orchards varying in canopy cover.

- Spectral profiles provided valuable insight into the changes in spectral band reflectance at selected crop development stages and highlighted the main differences between the young and the full-bearing orchard in two production areas.
- According to the seasonal means, there were no differences in spectral band reflectance between orchards.
- Amongst the vegetation indices, CVI was significantly higher for the young compared to the full bearing orchard, indicating higher chlorophyll content of the canopies.
- Drone-estimated tree height and volume were also significantly different between the two orchards.

RECOMMENDATIONS

Selected drone-technology derived attributes for individual pomegranate trees were related accurately to in-field measured tree water use, tree physiology, tree dimensions, light interception and LAI. However, collection of additional data sets representative of more

growing seasons and/or more pomegranate orchards varying in canopy cover are required. This is necessary to validate or improve regression relationships between the drone image-derived spectral bands, indices, tree geometric dimensions and thermal infrared temperature with tree water use variables, tree height, fractional interception, leaf area index, stem water potential, leaf level transpiration and $g_s$. It is recommended to collect in future more detailed information over the growing season on soil background reflectance, leaf and tree canopy structure properties, to assist in the identification of the most appropriate vegetation indices to estimate tree height, FI and LAI or to clarify why certain vegetation indices (e.g. NDVI) does not relate well. The fusion of morphological (canopy height, canopy cover and canopy volume) and vegetation indices for more accurate estimation of LAI over the season can also be investigated. The use of machine learning to identify appropriate algorithms to estimate physiological variables accurately from drone image-derived variables is strongly recommended for further research.

It is important to further explore the feasibility of extrapolating and reliably estimating orchard level transpiration, ETc and the ETc:ETo ratio for other full-bearing and/ or young pomegranate orchards varying in canopy size. The accurate in-field measurement of fractional interception and leaf area index of orchards to aid in estimation of crop coefficients is not easily achieved, and it would really aid farm and irrigation management (through estimation of crop coefficients) if these variables could be estimated accurately from drone imagery. A collection of additional datasets are also recommended to improve and/or validate significant regression relationships and to investigate and resolve atypical linear regression trends found.

Future research could expand to other pomegranate orchard sites, even outside the Western Cape. In addition, the prospects of obtaining existing drone imagery and water use data from the USDA on pomegranate orchards to relate to the current South African dataset should be investigated. It may require reprocessing of the images to be comparable to our datasets, but could potentially supplement or be used to validate our dataset, or provide explanations why NDVI did not relate well to ETc;ETo for the Western Cape orchards. Furthermore, the simplistic linear regression approach should be expanded to include non-linear regression statistical techniques, including training at centres of excellence on more advanced data analysis techniques such as machine learning.

# ACKNOWLEDGEMENTS

The project team wishes to thank the following institutions and people for their contributions to the project.

| Reference Group | Affiliation |
|---|---|
| Prof NS Mpandeli | Water Research Commission |
| Dr L Nhamo | Water Research Commission (Chairperson) |
| Dr SN Hlophe-Ginindza | Water Research Commission |
| Prof A Clulow | University of KwaZulu-Natal |
| Prof N Jovanovic | University of the Western Cape |
| Prof T Mabhaudhi | University of KwaZulu-Natal |
| Dr S Dzikiti | Stellenbosch University |
| Dr N Taylor | University of Pretoria |
| Ms M Kapari | Water Research Commission |
| Mr M Masevhe | University of Limpopo |
| Mr C Nortjé | Pomegranate Producers Association of South Africa |

The financing of the project and allowing use of WRC project C2020/2021-00404 data for this research by the Water Research Commission is acknowledged gratefully. Additional funding of pomegranate orchard water use research by the National Research Foundation is also acknowledged gratefully.

This project was only possible with the co-operation of many individuals and institutions. The authors therefore wish to record their sincere thanks to the following:

The Pomegranate Producers Association of South Africa for their support of the research proposal.

*Participating producers:*
Avontuur (Mr A Pretorius) for the use of their orchard, orchard information and assistance with field work from October 2024.
Avontuur (Mr H Smith) for the use of the orchard, orchard information and assistance with field work until July 2024 (Mr E Baard and Mr A Esterhuysen).
Welgemoed (Mr P Nell) for the use of the orchard, orchard information and assistance with field work (Mr R Botha and Mr M Prins).

# CONTENTS

LIST OF FIGURES

# LIST OF TABLES

# ACRONYMS & ABBREVIATIONS

| | |
|---|---|
| $A_n$ | Net carbon dioxide assimilation rate |
| ANN | Artificial neural networks |
| ATNS | Air Traffic and Navigation Services |
| AOI | Area of interest |
| ARC | Agricultural Research Council |
| CIRE | Chlorophyll Index-Red-Edge |
| CP-LAI | Accupar LP-80 ceptometer modelled leaf area index |
| CV | Coefficient of variation |
| CVI | Chlorophyll Vegetation Index |
| CWSI | Crop water stress index |
| DTD | Dual temperature difference |
| DSM | Digital Surface Model |
| DTM | Digital Terrain Model |
| EC | Eddy covariance |
| ENDVI | Enhanced normalized difference vegetation index |
| ET | Evapotranspiration |
| ETc | Crop evapotranspiration |
| ETo | Reference evapotranspiration |
| FAO | Food and Agriculture Organisation |
| FI | Fractional light interception |
| GNDVI | Green Normalized Difference Vegetation Index |
| GNSS | Global Navigation Satellite Systems |
| GPR | Gound penetrating radar |
| GPS | Global Positioning System |
| $g_s$ | Stomatal conductance |
| HRMET | High resolution mapping of evapotranspiration |
| INS | Inertial Navigation Systems |
| Kc | Crop coefficient |
| Kcb | Basal crop coefficient |
| LAI | Leaf area index |
| LIDAR | Light detecting and ranging |
| LM | Landsat METRIC |
| METRIC | Mapping evapotranspiration at high resolution with internalized calibration |
| ML | Machine learning |
| NDGNI | Normalized difference green near-infrared index |
| NDRE | Normalized Difference Red-Edge |
| NDVI | Normalized Difference Vegetation index |
| NIR | Near-infrared |
| NOTAM | Notice to Airmen |
| NRF | National Research Foundation |

| | |
|---|---|
| OLAI | Orchard leaf area index |
| OSEB | One source energy balance |
| RGB | Red, Green, Blue |
| RMSD | Root mean square deviation |
| RSEB | Remote sensing energy balance |
| RVI | Ratio Vegetation Index |
| S | Saturation |
| SEBAL | Surface energy balance algorithm for Land |
| $SE_{est}$ | Standard error of the estimate |
| SR | Surface renewal |
| T | Transpiration |
| TIR | Thermal infrared |
| $Tr_L$ | Leaf transpiration rate |
| Tr-LAI | Canopy area-based leaf area index |
| TSEB | Two source energy balance |
| UAS(s) | Unmanned Aerial System(s) |
| UASM | Mapping evapotranspiration at high resolution with internalized calibration with unmanned aerial system imagery inputs |
| UAST | Mapping transpiration at high resolution with internalized calibration with unmanned aerial system imagery inputs |
| UAV(s) | Unmanned Aerial Vehicle(s) |
| VHR | Very-high-resolution |
| WRC | Water Research Commission |

# CHAPTER 1: BACKGROUND

## 1.1 INTRODUCTION

Global warming-induced climatic changes, limited water resources and water restrictions for agriculture during drought force producers to invest in crops that are more suited to the potential future climate, such as drought-tolerant pomegranate (*Punica granatum*) trees (DEA, 2016; WCDoA, WCDEA and DP, 2016; Botai et al., 2017; Galindo et al., 2018; Otto et al., 2018; Burls et al., 2019,). In South Africa, the pomegranate industry is small but expanding. Of the 1167 ha in 2023 under this crop, 79%, 9% and 11% of the plantings are in the Western Cape, Limpopo and Northern Cape provinces, respectively (POMASA, 2024). The Western Cape has a semi-arid climate and the predictions of climate change are that the province can expect more water stresses with increasing temperatures, increasing evaporation and increasing occurrence of droughts. The Western Cape is considered particularly vulnerable to climate change as the region is highly dependent on water storage capacity due to the dominant winter rainfall patterns and the success of the agricultural sector depends to large extent on irrigation water availability (WCDEA and DP, 2018a). With increased urbanisation and the perceived impact of climate change, the Western Cape needs to manage rising water demand and increasing climate uncertainty which enhances the risk of water scarcity (WCDEA and DP, 2018b). Although irrigated agriculture in the Western Cape is one of the largest water users - utilising approximately 40% of available water resources - there is a lack of reliable agricultural water use data (WCDEA and DP, 2018a). In Western Cape agriculture, water demands are likely to increase in future with the expected increased temperatures and evaporation (DEA, 2016; WCDoA, WCDEA and DP, 2016; WCDEA and DP, 2018b; Otto et al., 2018) which will result in an increased irrigation demand According to the most recent complete dataset for the Water Management Areas (WMAs), water use in the Breede-Olifants WMA (Berg-Olifants and Breede-Gouritz WMAs amalgamated) exceeds water supply and irrigation is by far the dominant water use sector in the WMA, representing about 85% of the local water requirements (DWS, 2022). There has been a major drive in the Western Cape in recent years to increase the efficiency of irrigation, to promote water conservation and to manage water demand in the agricultural sector (WCDEA and DP, 2018a).

A baseline survey on irrigation and pomegranate tree performance was undertaken during 2017/18 and 2018/19 by the Agricultural Research Council (ARC) (co-funded by the Alternative Crop Fund of the Western Cape Department of Agriculture through the Pomegranate Producers Association of South Africa (POMASA) and the Water Research Commission (WRC)). Results of the scoping study (WRC Project K5/2958) confirmed that although pomegranate trees are considered drought-tolerant, irrigation is required during the dry summer to optimise growth, yield and fruit quality for commercial production. Furthermore, there is potential for some production areas to increase yield and fruit quality through improved irrigation scheduling. Supplying information on water use and crop coefficients to improve irrigation scheduling of pomegranate trees will in principle address the goals of the Western Cape Sustainable Water Management Plan for 2017-2022 (WCDEA and DP, 2018b) regarding water availability (Enable the sustainability of water resources for growth and development) and water quality (Enable integrity and sustainability of socio-ecological systems). It falls within the focus area of Water Smart Agriculture with regard to improved water use efficiency and management and could reduce the ecological impact of excessive leaching on river catchments and groundwater resources. As such, it can support the formation of a water-wise agriculture sector that promotes sustainable and optimal agricultural production and thereby improves water security.

The WRC recently funded a project to determine water use and water productivity of pomegranate orchards from 2021/22 until 2024/25 (C2020/2021-00404, KSA4, Agricultural water use). The aims of this project, relevant to the current proposal, were 1) to measure pomegranate orchard water use for orchards varying in canopy size and 2) to develop a method for practical estimation of crop coefficients for application in a water use model to enable calculation of individual orchard water requirements. The methods used to quantify the water use included a soil water balance, sap flow (transpiration) and micrometeorological methods (eddy covariance, surface renewal). Of these methods, the eddy covariance/ surface renewal methods monitored the evapotranspiration for the orchard overall, while the soil water balance was measured at only two trees per orchard and sap flow in four trees per orchard. The canopy cover of selected trees was monitored manually at selected intervals throughout the season to relate it to the water use measured by the soil water balance and sap flow. However, to biweekly to monthly manually measure the canopy cover and tree dimensions of all the trees in each orchard (one of the selected orchards spans c. 7 hectares planted to c. 5600 trees) to relate to the water use monitored using meteorological techniques, is inefficient and costly, if not impossible.

Drone surveys and subsequent data processing can provide fruit tree geometric traits for orchards at the individual tree level, such as canopy area and vegetative volume (Zhang et al., 2021 and references therein). Drones installed with RGB (red, green and blue) and multispectral sensors, combined with the necessary image processing, could provide reliable alternatives for manual fruit tree

geometric measurements. The drone estimated tree geometric properties such as tree height and canopy cover, in turn, have the potential to be used in the estimation of crop coefficients (Pereira et al, 2020). Dimensional estimates of canopy cover based on crop diameter or width and row spacing can be reasonably accurate, but should be calibrated with other objective techniques to improve accuracy. Based on the scale of measurement, remote sensing and specifically the use of drone or unmanned aerial vehicle (UAV) technology was considered to be the appropriate monitoring method to determine the canopy cover for all the trees per orchard. Drones are used as tools to efficiently monitor orchards for precision orchard management as they supply data at practical spatial, spectral and temporal resolutions (Zhang et al., 2021 and references therein). Conventional remote sensing technology, aerial sensing and spectral satellite sensing are all limited by weather conditions and monitoring costs, whereas a lack of imagery with optimum spatial and spectral resolutions and re-visit time issues renders spectral satellite sensing less useful. Advantages of drones are that they are – compared to satellite-based remote sensing – less dependent on weather conditions (capture data above orchards, but below cloud cover), data acquisition is fast and images are georeferenced. Limitations of drones, though, are the battery life (suitable for small- to medium-sized orchards) and operational speed, which plays an important role in the quality of data collected.

The focus of this project was to use drone technology to refine pomegranate orchard irrigation management. In addition to estimating orchard tree geometric properties on a large scale, drone image-derived spectral band reflectance and vegetation indices can also be related to tree physiology and orchard water use. The normalized difference red-edge (NDRE) index derived from drone imagery can be used for monitoring irrigation variability and identification of uneven growth (Jorge et al., 2019). Research furthermore showed a good correlation between aerial-based NDVI measured for trees and canopy cover (almond, olive, pear, lemon, pistachio), and between canopy cover and basal crop coefficients. Researchers from the USA recently published a highly significant validated linear regression relationship between single crop coefficients and NDVI for pomegranate trees using data from several drone surveys and individual tree water use data derived from weighing lysimeters (Niu et al, 2022). This information can be used to estimate the water use of crops from ground-based measurements of reference evapotranspiration (ETo).

The purpose of the current research was to relate drone image derived tree geometric dimensions, spectral band reflectance, vegetation indices (including NDVI and NDRE) and thermal infrared temperature with seasonal canopy development and water use for pomegranate orchards in the Western Cape to determine if it could aid in on-farm irrigation and catchment scale water resource management. It also aimed to provide supplementary information on the orchard properties, such as canopy cover and tree homogeneity, underlying water use values obtained via micrometeorological methods that will be made available for decision support and policy making in the water sector.

## 1.2 PROJECT AIMS

The following were the aims of the project:

1. To assess if drone-technology derived attributes for individual pomegranate trees can be related accurately to in-field measured tree dimensions and light interception.
2. To relate drone-determined tree geometric traits and NDVI to actual water use and crop coefficients on tree and orchard scale.
3. To determine orchard homogeneity for two orchards varying in canopy cover using drone technology-derived tree attributes.

## 1.3 SCOPE AND LIMITATIONS

The original research proposed entailed frequent drone surveys over two growing seasons. However, problems acquiring a suitable drone survey service supplier and sufficient supplementary funding delayed and decreased the scope of the project such that only five drone surveys could be conducted over one growing season. At project inception a literature review regarding the use of drones to assist in water resource management in the horticultural industry was completed (Chapter 2). The possibility to use drones to refine irrigation management for pomegranate orchards was investigated by comparison of the drone image derived variables to ground measured canopy properties (Chapter 5), selected plant physiological variables (Chapter 6) and water use (Chapter 7) on individual tree and orchard scale, and by quantifying and comparing orchard homogeneity (Chapter 9). In addition, tree water use was related to in-field measured tree properties, whereas fractional interception and LAI measured using a ceptometer, tree canopy area-based LAI and OLAI was compared to a manual method capturing the shaded orchard area (Chapter 8).

Drone surveys were conducted at five pomegranate development stages during one growing season (2023/2024) for two pomegranate orchards varying in canopy cover and location. The ARC Natural Resources and Engineering Institute collected thermal and multispectral data using the specific cameras and sensors required and conducted the data processing. Geometric traits (tree height and volume), spectral band reflectance (blue, green, red, near infrared and RedEdge), several vegetative indices (NDVI, NDRE, GNDVI, RVI, CVI, CIRE) and thermal infrared temperature were derived from the drone images using the appropriate data processing steps. The homogeneity of the orchard canopy characteristics was reported as the average of the drone image derived individual tree metrics ± standard error and in the form of histograms depicting the size distribution or various tree canopy related variables for the orchard.

Ground-based tree canopy measurements (dimensions for 11 or 17 trees, fractional interception for eight trees, shadowed area photos for three trees) were conducted on the same day of, or at least within a week of the drone surveys. On the day of the drone survey, leaf chlorophyll content (Survey1, 3-5; 11 or 17 trees) and physiological measurements (Survey 2-5, six trees) were also done. Water use was determined at individual tree scale through soil water balance (two trees) and sap flow (transpiration, four trees) techniques. Orchard evapotranspiration was determined using a surface renewal system at a young orchard and an eddy covariance system at a full bearing orchard. Weather data collected at each site were used to calculate ETo which was used to obtain the ratio of transpiration and evapotranspiration to ETo (transpiration and single crop coefficients).

Simple linear regressions were conducted between all data and indices derived from drone images for selected individual trees to individual tree data measured in orchards for orchards combined (young and full bearing), per orchard (five surveys combined) and per survey per orchard (individual trees combined). Linear regressions were also conducted at orchard scale – i.e. orchard averaged values of all individual tree data derived from drone images compared to averaged ground measured tree dimensions or orchard upscaled transpiration or orchard level evapotranspiration, also for orchards combined and per orchard (five surveys combined). Regression models were considered significant at 95% level of confidence ($p=0.05$).

Datasets available for regression purposes were limited at times by the malfunctioning of equipment used for monitoring physiology and water use. In addition, regression relationships were in some cases poor or insignificant due to a lack of variability in ground-measured datasets, as different treatments were not applied that could add variability. Since data was collected for only over one growing season, there was not data available to validate highly significant regression relationships. A collection of additional data is recommended to improve and validate regression relationships. The simplistic linear regression approach to data processing could in future be improved by using more advanced statistical techniques with non-linear modelling approaches and machine learning techniques and artificial neural networks.

The research supply knowledge to different user groups in support of more accurate irrigation scheduling. Producers that do not have frequent access to drones or drone services can estimate crop coefficients for critical growth stages in the growing season. Those that own drones or access drone services frequently can use estimations of transpiration, evapotranspiration or crop coefficients to improve their irrigation applications through precision management.

# CHAPTER 2: LITERATURE REVIEW ON THE USE OF DRONES TO ASSIST IN WATER RESOURCE MANAGEMENT IN THE HORTICULTURAL INDUSTRY

The objective of this chapter was to review literature on the use of drones (unmanned aerial vehicles/ UAVs) to assist in water resource management for the horticultural industry. In the context of this review, water resources at farm level were considered.

## 2.1 INTRODUCTION

The scenario of increased population growth in addition to the destabilizing effects of climate change on available water resources and agriculture worldwide, makes for an increase in focus on sustainable farming to supply increasing demands for food production while using less water (Alvino and Marino, 2017; Acharya et al., 2021; Mohamed et al., 2021; Zhang et al., 2021). To pursue sustainable farming and food security, especially under climate change conditions, it is critical to optimize physical and economic water productivity (Fernandez et al., 2020). To achieve this, knowledge and application of water-efficient production practices are required. Water-efficient production practices such as irrigation scheduling, the use of appropriate irrigation systems, mulches and water-saving irrigation strategies can result in several water resource-related benefits (WCDEADP, 2018). Water savings in the agricultural sector can be made available to other sectors during conditions of drought, and the environment could benefit through the efficient use of limited water resources and reduced leaching of fertilizers to groundwater. In the horticultural industry, production-related benefits of water-efficient production practices could include increased production, high-quality products, increased product volumes for local and export markets, increased income, and sustainable work and income opportunities.

Estimation of evapotranspiration (ET), the main component of the water cycle and agricultural water balance, is important for agricultural water resources planning, management and regulation (Wanniarachchi and Sarukkalige, 2022). The process of evapotranspiration consumes irrigation water and rainfall and accurate estimation of ET is a prerequisite to improve water use efficiency and sustainable water management in agriculture. Application of precision and digital agricultural technologies, integration of advanced techniques, including remote sensing (satellite and drone), and use of machine learning algorithms could aid in increased accuracy of ET estimation for agricultural water management (Alexandris et al., 2021; Gautam et al., 2021; Mohamed et al., 2021; Niu et al., 2020; Wanniarachchi and Sarukkalige, 2022). Considering the increased dire effects of climate change worldwide, the adoption of precision irrigation and advanced technologies is inevitable to sustain the horticulture industry and agriculture, also in developing countries where the agricultural sector is one of the most important contributors to national income (Mohamed et al, 2021).

## 2.2 UAV PLATFORMS

A drone can be defined as a remotely controlled aircraft flying in a set direction at a set speed (Zhang et al., 2021).The weight of the drone will determine the set of regulations and restrictions it has to comply with to fly as drones that weigh 25 kg or more on take-off, will be required to fly under a different set of regulations (Delavarpour and references therein, 2021). Drones are classified based on the take-off weight and categories include super heavy (> 2 tons, fly at high altitudes serving military reconnaissance), heavy weight (200 to 2000 kg), medium-weight (50–200 kg), light-weight (5–50 kg, useful in agricultural fields) and micro (<5 kg, quick to lift off and fly at relatively lower altitudes, more common in agricultural fields, portable). Mini and Nano UAVs are two kinds of micro drones with reduced size and weight so that it can be carried by one person and they have reduced associated costs of technology. Small drones (<25 kg) can be operated remotely by human pilots or operate independently (Delavarpour et al., 2021). The drone can be automatically piloted by an autopilot based on two main navigation technologies, Global Navigation Satellite Systems (GNSS) (such as, for example, GPS) and Inertial Navigation Systems (INS), in a GNSS-only mode or INS/GNSS coupling (Colomina and Molina (2014). The UAS generally has three main components namely the unmanned aerial vehicle, the ground control station and a communication data link (Colomina and Molina, 2014). Other UAS components considered critical are autopilots, navigation sensors, imaging sensors, mechanical control systems and wireless systems.

Based on literature regarding the use of lightweight drones/ UAVs in orchards for 17 fruit species in 24 countries; basically three types of UAV crafts are currently used for orchard management i.e.: fixed-wing, rotary-wing and multi-rotor (Zhang et al., 2021). The specific UAV type selected depends on the requirements and limitations of the application. Multirotor crafts are the most widely used since

these helicopters with four to eight rotors can fly at different altitudes and manoeuvring abilities include hovering over a specific location, using global positioning system-based navigation, flying horizontally and vertically, and it only need a small take-off and landing space. The main limitations of the rotor – compared to fixed-wing craft – are the lower speed and reduced flight time (c. 30 minutes) (Niu et al., 2020, Zhang et al., 2021). Advantages of the fixed wing vs multi-rotor UAVs is the capability of high payload, longer flight times (c. 2 hours) and faster travel speeds. The cost of the fixed-wing UAV is higher than that for the multi-rotor and the high speed can cause image blurring, which can be solved by using specialized imaging sensors. Specialized orchard precision management requirements can be addressed through the development of customized UAVs, hybrid UAVs, and UAVs having vertical take-off and landing (Delavarpour, 2021; Zhang et al., 2021).

## 2.3 REMOTE SENSING SYSTEMS ON UAVS

For orchard management purposes, the UAVs described above are mainly used as imaging and remote sensing platforms, although the UAVs can also be applied for activities such as pesticide spraying (Zhang et al., 2021). Of the sensors mounted on UAVs, mainly RGB and multispectral sensors are used for orchard management, while hyperspectral and thermal sensors are used in fewer applications. Niu et al. (2020) indicated that UAV multispectral and thermal images are useful for ET estimation, whereas a light detecting and ranging (LIDAR) system was found to be excellent for determining apple tree geometric traits (Hadas et al., 2019).
Zhang et al. (2021) classed sensors used for UAV orchard management according to their application, i.e., for resource efficiency, tree geometric and biophysical trait classification, productivity estimation, disease detection and other applications. Of these, the first three classes appear to be most relevant for water resource management, although disease detection may also have implications for the water use of crops. The percentage use of UAV-mounted spectral sensors in 59 research studies is listed per orchard management objective in Table 1.

Table 1. Use of UAV (unmanned aerial vehicle) mounted spectral sensors per orchard management objective (% of studies evaluated, n=59). Adapted from Zhang et al. (2021).

| **Objective** | **Degree of sensor application (% of 59 research studies)** | | | |
|---|---|---|---|---|
| | **RGB** | **Multispectral** | **Thermal** | **Hyperspectral** |
| Resource efficiency | 2 | 14 | 15 | 5 |
| Tree geometric and bio-physical trait quantification | 22 | 14 | 0 | 0 |
| Productivity estimation | 8 | 17 | 0 | 3 |

Of the 59 studies reviewed 36% were focused on resource efficiency (improving irrigation efficiency), 36% on tree geometrical and biophysical trait quantification and 29% on productivity (yield estimation models). Of the sensors, multispectral and thermal were used the most for resource efficiency studies, whereas RGB and thermal were used more for tree geometric and biophysical quantification and productivity estimations.

## 2.4 WATER RESOURCE MANAGEMENT

The main aim of irrigation scheduling in horticulture is knowledgeable management of water resources to maintain or increase crop yield and quality (Guantam and Pagay, 2021). To apply irrigation scheduling strategies accurately, knowledge is required on the water use and water status of the crops (Alvino and Marino, 2017). Conventional decision-making for irrigation of horticultural crops are based on historical regimes, soil water content measurements, visual assessments of the soil and/or crop, weather data including evapotranspiration (ET) estimates and measurements of crop water status using direct-, proximal- or remote-sensing techniques (Guatam and Pagay and references therein, 2020). These ground-based measurements have several drawbacks in terms of logistics, cost and representativeness of the irrigation blocks monitored.

For proper irrigation scheduling, information is required on when, where and how much to irrigate. Three main methods are being used for scientific irrigation scheduling, namely crop evapotranspiration calculations based on weather data/ models, monitoring of soil water status and monitoring of plant water status (O'Shaughnessy and Rush, 2012). The decision when to irrigate is generally based on monitoring of a threshold that has been established based on soil water depletion levels in the root zone or as thermal-based stress indices. These thresholds are usually correlated to plant physiological measurements such as stem water potential and leaf stomatal conductance, which indicate actual tree water status and plant stress levels.

Researchers typically obtain ET data using a water balance (soil water content sensors, weighing lysimeters) or an energy balance approach (Bowen ratio, eddy covariance), which is also point specific or area-weighted and cannot be extended to large scale (Niu et al., 2020). Although satellite-based remote sensing images can provide spatially distributed measurements, the spatial resolution is often not fine enough for crops with clumped canopy structures such as trees and vines, and revisit time is not suitable for many agricultural applications. Despite the introduction of new satellite platforms with significant improvement in revisit time and multispectral capability (Pôças et al., 2020), the synchronization of satellite overpass and research requirements can be challenging. According to Niu et al. (2020) availability of higher temporal and spatial resolution images, relatively low operational costs and nearly real-time image acquisition make the UAVs ideal for mapping and monitoring ET.

The technology of UAVs includes high spatial resolution and rapid collection of data over large areas, which could enable producers to increase the precision of irrigation both spatially and temporally (Ezenne et al. 2019) for them to achieve high biophysical and economic water productivity (Fernandéz et al., 2020; Knox et al, 2012). UAVs have been used in smart water management platforms (SWAMP) for precision irrigation (Kamienski et al., 2019). In the horticultural industry, water resource management drone technology can potentially be applied to improve irrigation scheduling and increase water use productivity through 1) representative estimation of crop water demand and 2) monitoring of crop water status.

### 2.4.1 Estimation of crop water demand

Methods are being progressively developed to apply very high-resolution UAV imagery for precision ET monitoring (Nieto et al. and references therein, 2019). With regard to the estimation of soil moisture content. Acharya et al. (2021) listed several studies between 2015 and 2020 that used UAV-obtained hyper-spatial imagery, including thermal techniques, optical data and their synergy and ground penetrating radar (GPR) systems/microwave. UAV-obtained GPR data are used progressively more to create high-resolution soil moisture maps for up to a depth of 20 cm. According to Acharya et al. (2021) soil and moisture mapping using UAVs improves agricultural water use and management from field- to regional scale.

#### *2.4.1.1 Satellite remote sensing-based UAV ET estimation methods*

Satellite remote sensing-based methods are mainly used to estimate ET from UAV imagery (Niu et al., 2020). These include the One source energy balance (OSEB), high resolution mapping of evapotranspiration (HRMET), two source energy balance (TSEB), dual temperature difference (DTD), surface energy balance algorithm for Land (SEBAL) and mapping evapotranspiration at high resolution with internalized calibration (METRIC). In addition, machine learning (ML) and artificial neural networks (ANN) are also employed to estimate ET. The details of these methods are presented by Niu et al. and references therein (2020). Factors to consider when choosing the appropriate algorithms for ET estimation include, among others, the capabilities of the UAV and sensors, field size, flight time and weather conditions.

Park et al. (2021) estimated instantaneous ET using very-high-resolution (VHR) multispectral and thermal imagery (ground sampling distance < 8 cm) collected using a single flight of a UAV over a high-density peach orchard with a discontinuous canopy. The energy balance component estimation was based on the HRMET model. The canopy surface temperature and the leaf area index, resampled at the corresponding scale via a systematic feature segmentation method based on pure canopy extraction, was used to produce a tree-by-tree ET map. Data indicated a strong linear relationship between the estimated ET and the leaf transpiration measured using a gas exchange sensor ($n = 42$, $R^2 = 0.89$). Daily ET (5.5 mm $d^{-1}$) derived from the instantaneous ET map was comparable with daily crop ET (6.4 mm $d^{-1}$) estimated using the meteorological approach for the study site. The proposed approach can potentially provide a practical method of assessing the intra-field variability of tree-by-tree ET at the sub-field scale for the irrigation scheduling, but further

research is proposed to include various remote sensing energy balance models and different field sites to develop robust water management information and strategies.

In Chile, a UAV had been employed in an olive orchard to obtain multispectral and thermal imagery to compute ET at high spatial resolution (Ortega-Farías et al., 2019). The field experiment was carried out to develop a remote sensing energy balance (RSEB) algorithm for estimating evapotranspiration (ET) for a drip-irrigated olive orchard using multispectral and thermal sensors placed aboard an unmanned aerial vehicle (UAV) during February and March 2014. Measurements of micrometeorological variables, surface energy balance components and remote sensing data were obtained from the orchard. Compared to measurements of ET obtained from an eddy correlation system the RSEB algorithm overestimated ET by about 13% with a root mean squared error and mean absolute error of 0.43- and 0.29-mm $d^{-1}$, respectively. Major errors were associated with the estimation of sensible heat flux from the canopy and soil, especially when the wind speed was greater than 2.5 m $s^{-1}$. According to Niu et al. (2020), this research confirmed that the use of a UAV platform to evaluate the spatial variability of ET in the olive orchard could work exceptionally well. Experiment results indicated that the RSEB algorithm can estimate latent heat flux and sensible heat flux with errors of 7% and 5%, respectively.

Research by Chandel et al. (2021) confirmed that small UAS (unmanned-aerial-system)-based multispectral and thermal imaging can be used to reliably estimate ET and T at high geospatial resolution for heterogeneous crops such as vineyards and fruit trees. Grapevine ET was estimated using a satellite remote sensing energy balance model, METRIC, with UAS imagery inputs implemented (UASM approach) (Chandel et al., 2020; Chandel et al., 2021). In addition, soil background was segmented in the UASM ET maps to obtain canopy transpiration (T) maps (UAST) (Chandel et al., 2021). The high-resolution ET was compared to ET estimates from the conventional satellite Landsat-METRIC (LM) model and a soil water balance, whereas UAST was compared to transpiration estimated from the conventional basal crop coefficient approach according to FAO56 (Allen et al., 1998). The mean daily UASM ET was 0.31 mm $day^{-1}$ less than that obtained from the conventional satellite approach, and the mean root mean square deviation (RMSD) for two years did not exceed 0.76 mm $day^{-1}$ (<22%). The UASM and LM-ET estimates were strongly positively correlated ($r=0.7$-$0.81$, $p<0.01$). The enhanced ability of the UAS compared to the Landsat 7/8 satellite to capture spatial variation in ET for a vineyard is indicated by the mean CV (±std. dev.) of 68±6.67% for UASM compared to 11.85±1.77% for LM (Chandel et al., 2021). This highlights the importance of the UAS smaller ground sampling distance (GSD) (spectral data resolution 7 cm/ pixel, thermal data resolution 13 cm/ pixel) compared to that of Landsat 8 (visible and near-infrared band resolution 30 m /pixel; thermal band resolution 100m/ pixel) (Niu et al., 2022). The UASM daily ET estimates were significantly higher compared to those obtained using the soil water balance approach (Chandel et al., 2021). This was attributed to some roots of the vines being outside of the area sampled by the soil water content monitoring equipment. The UASM and soil water balance ET estimates were still positively correlated with each other in both seasons ($r=0.64$-$0.81$; $p<0.01$). The cumulative water use estimated from the UASM approach was higher than, but within 5-11% of the soil water balance-based water use calculations. The UASM approach slightly overestimated T compared to the FAO-Kcb approach, but transpiration trends were strongly correlated ($r=0.95$, $p<0.001$). The mean estimated transpiration did not differ significantly for the two approaches. The UASM-T maps indicated a significant effect of different irrigation rates on transpiration for both seasons, which highlights the applicability of the UAS for management of deficit irrigation strategies.

Chandel et al. (2022) also used METRIC modified for drone-based multispectral and thermal imagery inputs to estimate ET for an apple orchard. The images were taken 100 m above the ground and the spatial resolution for the multispectral images was 7.1 cm/ pixel and for thermal infrared 13 cm / pixel. The mean daily ET estimated from drone imagery (6.4 mm $d^{-1}$, relative deviation 12.3%) was similar to that of the satellite-based approach (7.1 mm $d^{-1}$) and the estimates derived from the two methods had a strong correlation ($r=0.82$). The satellite-based approach slightly overestimated the ET, likely due to the spatial resolution that could have affected the identification of the hot and cold anchor pixels near the research site. According to the drone imagery, the spatial water use variability was 31% for the experimental block, which indicates that irrigation management intervention is required. Drone imagery-based daily canopy transpiration estimates for the season correlated well with those estimated according to the FAO56 crop coefficient approach ($r=0.95$, Allen et al., 1998) and had a relative deviation of less than 10%. Transpiration estimates were in the range of 4.3 to 7.9 mm $d^{-1}$ compared to basal crop coefficient estimates of 4.6 to 8.6 mm $d^{-1}$ (Chandel et al., 2022). The relatively higher basal crop coefficient approach estimates were attributed to the use of non-stressed and generalized crop coefficients with minimal adjustments for local conditions.

For irrigation management in orchards and vineyards, water use of both the vineyard/ tree row and the inter-row (cover crop or bare soil) is important to consider. Thermal and visible/ near-infrared imagery of fine enough resolution to discriminate between the interrow and crop row could provide the means to properly partition the energy fluxes and ET between the two sources (Nieto et al., 2019). In

California, Nieto et al. (2019) used a UAV to obtain very high spatial resolution remote sensing data over two vineyards to estimate the component soil and canopy temperatures and ET partitioning between soil and canopy using a thermal-based Two-Source-Energy-Balance model. The results indicated that a simple contextual algorithm based on the inverse relationship of a vegetation index and bulk composite surface radiometric temperature to derive soil and canopy temperatures yielded the closest agreement with eddy covariance measurements of ET. This study assumed that cover crop contribution to water fluxes was negligible and it was included in a bulk layer with the underlying soil. Future research plan for a simplified three-source model for flux partitioning between the grapevine, cover crop and soil. In addition, Aboutalebi et al. (2018) indicated that grapevine ET estimation improved significantly where high-resolution images were used to fill shadowed pixels.

The UAVs can be used for modelling ET estimation with high confidence since the UAV platform and lightweight cameras can estimate the surface energy fluxes with similar accuracy to that of traditional satellite remote sensing approaches (Niu et al., 2020). The METRIC and SEBAL methods - which are more accepted by remote sensing researchers - are based on satellite (Landsat) platforms and according to Niu et al. (2020) significant modification would be required to make them work with UAV images. The TSEB model is less widely known but offers more potential for UAV applications for many crop settings, especially for tree crops such as almonds, pomegranates or peaches. The TSEB and DTD models are considered to have great potential for ET estimation, since they can separate the soil and canopy with high-resolution UAV imagery. This will make research relating to individual tree-level ET estimation possible and will be useful for analysing the temporal and spatial variability of the crops in the field. Deep learning algorithms can be used for processing high-resolution UAV imagery such as individual tree-level canopy or soil segmentation.

#### *2.4.1.2 Crop coefficient approach*

The ET for horticultural crops can also be estimated using the widely adopted single or dual crop coefficient approach, combined with Penman-Monteith reference evapotranspiration (Allen et al., 1998). The Penman-Monteith reference evapotranspiration (ETo) is calculated from micrometeorological data obtained from ground-based automatic weather stations. The product of ETo and crop coefficients is used to estimate ET. The crop coefficients are closely related to the light interception of the canopy (Williams and Ayars, 2005). In orchard management, the UAVs are used to derive crop geometric traits for purposes of pruning and crop selection (Zhang et al., 2021). This information could therefore potentially be used to predict crop coefficients from the fraction of ground cover and height (Allen and Pereira, 2009; Pereira et al., 2020, Pereira et al. 2021).

Satellite-based remote sensing at a coarser resolution is used to estimate single and basal crop coefficients from vegetation indices to estimate ET (Pôças et al., 2020), but it is limited by both its temporal (revisit time) and spatial resolutions for irrigation scheduling applications when compared to a UAV. Satellite image pixels furthermore contain multiple objects with different spectral signatures (e.g. plants and soil), whereas the high spatial resolution images of UAVs provide mixed-free pixels, making detection and differentiation of vegetation easier and allowing precise estimation of the vegetation cover fraction (Chen et al., 2018).

According to Pôças et al. (2020), single and basal crop coefficients estimated from UAV-based vegetative indices determined at higher resolution still need further assessment over a longer period. Using UAV remote sensing, Gautam et al. (2021) used a UAV to remotely determine Kc for sprawling Cabernet Sauvignon wine grapes with similar accuracy to that of ground-based measurements ($R^2$=0.675, root mean square error:0.062, mean absolute error: 0.047). Spectral and structural information obtained using a multispectral sensor at various phenological stages of the vine over two seasons was used to model Kc using univariate, multivariate and machine learning (convolution neural network and random forest) model frameworks. The structural information (e.g. canopy top view area) had the strongest correlation with Kc throughout the season, while the spectral indices became less sensitive at the onset of ripening of grapes. Combining structural and spectral information improved model performance.

In 2020, Niu et al. stated that there is a strong correlation between the NDVI and the crop coefficient at individual tree-level ET and that further study can be conducted to create new vegetation indexes using machine learning and deep learning algorithms (Niu et al., 2020). In 2021, they published research conducted in California, which related NDVI derived from high spatial resolution multispectral UAV imagery of a 12-year-old pomegranate orchard to Kc values determined from ET using weighing lysimeters and ETo derived from weather data (Niu et al., 2021). The spatial and temporal variability of Kc and NDVI was analysed by using a stochastic configuration networks model, which made tree-by-tree ET estimation possible. The Kc can be estimated using a simple linear regression obtained from NDVI values derived from the UAV imagery and Kc from field measurements as Kc (NDVI) = 4.6666NDVI-2.9277 ($R^2$=0.975, root mean square error = 0.05).

### 2.4.2 Monitoring of crop water status to implement irrigation strategies

Producers can improve water use productivity by applying a variety of irrigation strategies, including deficit irrigation. To determine the timing of irrigations, knowledge of crop water status/ crop water stress levels is required. At ground level, crop water status is generally obtained by measurement of stem water potential or crop water stress levels are inferred from leaf stomatal conductance information (Zhang et al. (2021) and references therein). Satellite-based remote sensing has been applied to assess water status in orchards for irrigation scheduling purposes using infrared thermography and various vegetative indices which reflect the status of several crop and soil characteristics (Alvino and Marino and references therein, 2017). Gerhard et al. (2019) consider thermal infrared multi-/hyperspectral and sun-induced fluorescence approaches together with classic solar-reflective (visible, near-, and shortwave infrared reflectance) hyperspectral remote sensing to be the latest state-of-the-art techniques for the detection of crop water stress, and review several challenges with regard to the use of spectral emissivity, temperature-based indices, and physically-based approaches for water-stress detection in the thermal infrared spectral domain.

Zhang et al. (2021), summarize the use of UAVs and several vegetation indices to assess the water status of orchards to improve orchard productivity and irrigation water use efficiency. Although the normalized difference red edge (NDRE) is primarily used to identify potential heterogeneities in vegetation cover, it can be employed to indicate irrigation irregularities in orchard blocks (Jorge et al., 2019). The use of UAV imagery to assess canopy temperature and crop water stress index in lieu of tree water status measurements can quantify orchard variability more efficiently compared to ground-based physiological field measurements in a limited number of trees (Gonzalez-Dugo et al., 2013). The Crop Water Stress Index is defined as the difference between air (Ta) and canopy (Tc) temperature, normalized for evaporative demand as determined using a lower limit (canopy transpiring at its potential rate) and an upper limit (non-transpiring canopy) (Gonzalez-Dugo et al., 2013; Romero-Trigueros, 2019). According to Zhang et al. (2021), the use of the CWSI is limited by the spatial resolution necessary and the site-dependent equation of the non-water-stressed baseline. The thermal response for an orchard that contains trees of different species or the same fruit species on different training systems will be affected, and to obtain reliable data representative of orchard water status, more than one set of reference values may be required. In this regard, Park et al. (2017) classed the mixed orchard into sub-regions and used edge extraction and filtering before probability modelling was applied to obtain cultivar/ training system-specific lower and higher temperature references. They calculated an adaptive CWSI, which correlated better with stem water potential and stomatal conductance measurements compared to the conventional CWSI. Zhang et al. (2021) contains an exhaustive list of UAV-acquired data-derived spectral vegetation indices (including the equations and references) used in the assessment of water stress in fruit orchards. Of these indices, the NDVI, chlorophyll and fluorescence indices (leaf level), green ratio, enhanced normalized difference vegetation index (ENDVI), normalized difference green near-infrared index (NDGNI) and Saturation (S) showed potential to indicate orchard water status. Apart from these indices, a monthly canopy volume increment correlated well with a daily water stress integral for citrus trees, while two different photochemical reflectance indices correlated with water stress in an orange orchard. According to them, NDVI calculated from UAV images showed a good correlation with ground-measured leaf area index for peach, olive and citrus, whereas canopy NDVI could serve as a water stress indicator for almond.

Radoglou-Grammatikis et al. (2020) referred to research of Katsigiannis et al. (2016) who combined UAV-based thermal and multispectral data to assess the water stress and health status of a pomegranate orchard in Greece. The ground resolution of the thermal and multispectral images was 13 cm and 4 cm, respectively. After the image processing and generation of the ortho-mosaic map, the CWSI and NDVI indices were calculated from the thermal and multispectral data, respectively. For the calculation of the CWSI index, conversion of the thermal information to temperature values was required. Based on the experimental results, the CWSI values were in the range 0.4–0.9 and 0.29–0.74 for the two flights, respectively, with the implementation of an irrigation system on the second day. The NDVI values increased overall by 25% on the second day. According to the authors, the proposed system is appropriate for supporting the irrigation systems, accompanying maintenance procedures and discriminating zones based on water stress and vegetation.

If the correlation of the vegetation indices to stem water potential is compared over research studies, CSWI and the difference between canopy temperature and ambient temperature correlated well with stem water potential, but not for all species (Zhang et al., 2021). The Transform Chlorophyll Absorption in Reflectance Index/ Optimized Soil Adjusted Vegetation Index and canopy NDVI showed a good correlation to leaf stomatal conductance for several fruit species and therefore have the potential to be applied as a single index in diverse orchards. There is scope for more research on appropriate vegetation indices to identify water status for diverse fruit species.

## 2.5 APPLICATIONS OF UAV IMAGERY ON POMEGRANATE ORCHARDS

UAV-derived imagery has been used to map and monitor agricultural fields, including pomegranate orchards. Katsigiannis et al. (2016) assessed the effectiveness of an autonomous multi-sensor UAV system in providing crop water and crop health information in a pomegranate orchard. The UAV platform used in this study was a Vulcan hexacopter with a Wookong flight controller, flown at an altitude of 100 m above ground. The sensors were multispectral and thermal infrared cameras. The acquired images were processed in Agisoft Photoscan Professional software to produce orthomosaics. The raw radiometric figures were converted to surface temperature using FLIR Systems transformation equations. The acquired images were used to compute the crop water stress index (CWSI) and the Normalized Difference Vegetation Index (NDVI). The CWSI values changed by 20-30% after irrigation and remained the same where the irrigation system had failed, demonstrating the data's sensitivity to crop water changes. Since the UAV data were collected over two consecutive days, the NDVI values did not exhibit any significant changes; however, there was a stark contrast between the NDVIs of the orchard and those of the surrounding environment.

Niu et al. (2021) used UAV images to develop a tree-level evapotranspiration estimation method in a pomegranate orchard. The UAV system was a Hover mounted with a Rededge M multispectral camera, flown at midday, 60 m above the ground, with a total of seven flights between May and October 2019. The study correlated NDVI derived from UAV images and crop coefficients derived from weighing lysimeters and weather data. The correlation between NDVI and crop coefficients was 0.89. Individual tree-level evapotranspiration was estimated with a coefficient of determination of 0.91 and an MAE of 0.39 mm. Niu et al. (2022) further investigated the feasibility of using UAV-based NDVI for estimating crop coefficients and evapotranspiration of pomegranate orchards. The UAV platform used in this study was a Hover equipped with a Pixhawk flight controller, GPS, and telemetry antennas, flown at 60 m aboveground, biweekly at noon during the growing season. The UAV was mounted with a Rededge M Camera, which collects multispectral images in five wavebands, including Blue, Green, Red, Near-infrared, and Red edge. The collected images were orthomosaicked in Metashape (Agisoft). The study found a strong correlation between crop coefficients and NDVI, with simple linear regression and Stochastic Configuration Networks achieving $R^2$ values of 0.975 (RMSE = 0.05) and 0.995 (RMSE = 0.046), respectively.

Zhao et al. (2018) evaluated the performance of deep learning methods in the segmentation of UAV-acquired pomegranate orchard images. The sensors used in this study were Survey2 Mapir and ELPH110HS Canon. The study found that Mask R-CNN achieved average precisions of 38.4 to 96.2, outperforming U-Net, which achieved average precisions of 17.9 to 68.7 in tree canopy segmentation. Niu, Wang and Chen (2022) investigated the feasibility of using a small UAV platform and Convolutional Neural Networks to reliably infer individual tree level irrigation in a pomegranate field. The orchard was subdivided into 16 blocks to assess the effect of different irrigation rates on pomegranate growth. The UAV platform was a Foxtech Hover quadcopter equipped with a Pixhawk flight controller, GPS, and telemetry antennas, flown at a height of 60 m. It was mounted with a thermal camera collecting images in the 7 to 14 microns waveband. Flights were programmed for midday for optimal atmospheric conditions and to minimize the shading effect on the images. Image processing involved extracting individual tree canopies. The coefficient of determination between the UAV-thermal data and ground-measured canopy temperature was 0.87. The CNN models achieved 87% accuracy in predicting the targeted irrigation levels.

Akca and Polat, (2022) applied semantic segmentation and Convolutional Neural Networks on UAV images to classify trees, shadows and soil in an orchard. The UAV system used in this study was a DJI Mavic 2 Pro, flown at a height of 60 m and mounted with a camera to capture digital orthophotos. The acquired images were processed with a structure-from-motion approach using Agisoft software. All the reference trees were segmented successfully with recall, precision, and overall accuracy of 97.02%, 87.44% and 88.24%, respectively. These results demonstrated that the approach used in this study is effective for tree counting using UAV-based high-resolution orthophotos.

## 2.6 ADOPTION OF DRONE TECHNOLOGY

The use of remote sensing with UAVs is not yet widely adopted by farmers (Delavarpour et al., 2021). Despite the integration of new technologies in UAVs, some factors and challenges prevent widespread usage by the greater farmer community. Although UAV technologies do not necessarily require a trained human pilot, a private pilot license is still required by law for commercial flight operations. Furthermore, for non-expert users to utilize UAVs require investment in time and money and learning new skills with

complex tools. To apply UAVs for precision farming, a huge amount of complex data is collected using various sensors. Big data analytics tools and cloud computing are required to extract information from the gathered data and display it in a manner where the information can be comprehended and utilised effectively. Data analysis and interpretation usually depend heavily on using software packages with different levels of complexity and, which are often expensive. Data analysis software must often be purchased to be used independently if the software is not open source and publicly accessible. These software packages must be installed and configured by users and require maintenance, advanced coding, or advanced data training. This may pose a challenge, especially for small farming operations that tend to have smaller budgets for advanced technologies. For agricultural producers, the economic benefits and potential return on investment gained by making use of precision agricultural technologies such as UAVs must be clear before it will be adopted by them.

Further research is required to design and implement special types of cameras and sensors on-board UAVs for remote crop and soil monitoring, and other agricultural applications in real-time scenarios. The overarching goal should be a fully automated technology service pipeline, including flight preparation and parameter setting (optimal flight height and pattern, sensor setup, etc.), flight execution (calibration of sensors, ground control measurements, and flight execution itself), and data processing, along with interpretation (Delavarpour et al., 2021). Some technologies, data collection and processing systems are part of the way to perfection but still employ non-automated human expertise at critical stages of the technological journey such as with the use of human pilots, strategic use of human quality controls (quality control checks) at the data processing stage, and agronomic and/or horticultural expertise for data interpretation.

Challenges for the application of smart farming practices in developing countries need to be addressed by applying innovative and concrete strategies from local to national levels (Mohamed et al., 2021; Nhamo et al., 2020) and by generating the necessary information to support on-farm decision making (Mabhaudi et al., 2023). Currently, farmers contract outside companies for drone services or operate their own drones (Delavarpour et al., 2021). Although cheaper commercial mini or micro drones are becoming available, there are several challenges regarding accuracy specifications. Problems that may be faced include the influence of wind, low GPS accuracy and strong drift of the navigation systems, which all may affect flight stability and image acquisition (Daponte et al., 2019). To use the UAV for precision farming, care should be taken by the user that high-quality imagery of the right quality is collected for the purpose it is intended for.

# CHAPTER 3: METHODOLOGY

## 3.1 INTRODUCTION

This section describes the study area, flight plans, UAV system, drone survey data processing strategy, field measurements and the statistical analysis approach.

## 3.2 STUDY AREA

The research was conducted at a young pomegranate orchard at Avontuur (33°07'29.7"S; 18°56'08.8"E) and at a full-bearing pomegranate orchard at Welgemoed (33°35'18.3048"S; 18°59'19.302"E), which covers an area of 6.7 and 4.9 hectares, respectively (Figure 1). Table 2 summarizes selected properties of the two pomegranate orchard water use research sites.

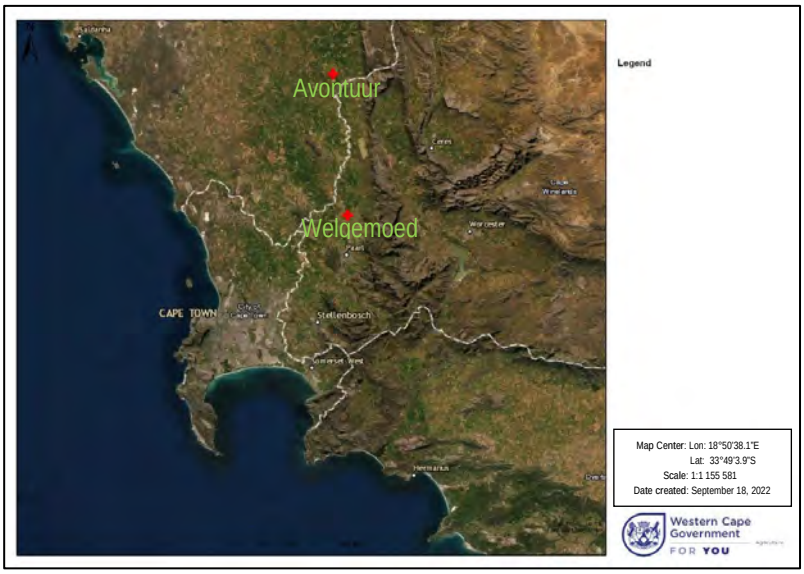


Figure 1. Location of the farms Avontuur and Welgemoed, selected for purposes of water use research for young and full bearing pomegranate orchards, respectively

Table 2. Selected properties of the two pomegranate orchard water use research sites, October 2023

| Site | Avontuur - Young | Welgemoed – Full bearing |
|---|---|---|
| Orchard row bearing | 172.32° (S7.68°E) | 71.06 (N71.06°E) |
| Year planted | 2019 | 2010 |
| Tree spacing | 2.5 m x 5 m | 2 m x 4.5 m |
| Stem diameter (mm) | c. 69 | c. 100 |
| Tree height (m) | c. 2.24 | c. 3.07 |
| Canopy width in tree row (m) | c. 2.43 | c. 2 |
| Canopy width across tree row (m) | c. 2.34 | c. 3.23 |
| Soil texture | Sandy to 0.8 m, plinthite below | Loamy sand, stone none to minimal |
| Irrigation system | Double line drip, 0.75 m spacing<br>Delivery rate 2.3 ℓ $h^{-1}$ | Double line drip, 0.75 m spacing<br>Delivery rate 2.3 ℓ $h^{-1}$ |
| Slope | Level to slight gradient | Level |

## 3.3 FLIGHT PLANS AND UAV SYSTEM

In 2023/2024 five drone surveys, representative of different pomegranate tree phenological development stages, were conducted at the young (Avontuur) and full bearing (Welgemoed) orchards (Table 3, Figure 1).

Table 3. Scheduled dates of drone surveys conducted during the 2023/2024 season

| Site | Survey | | | | |
|---|---|---|---|---|---|
| | 1 | 2 | 3 | 4 | 5 |
| Avontuur | 31/10/2023 | 15/12/2023 | 12/01/2024 | 22/02/2024 | 16/04/2024 |
| Welgemoed | 30/10/2023 | 13/12/2023 | 13/01/2024 | 23/02/2024 | 17/04/2024 |

The mapping flights were carried out using a DJI Technology© Matrice 600 drone (Figure 2) equipped with a MicaSense Red-Edge-MX multispectral camera, which acquires imagery in five wavelength bands (Table 4). A Zenmuse-XT thermal camera (not shown) was also used to acquire thermal images over the selected study areas (Figures 3 and 4). To avoid shadows from tree canopies, studies recommend solar noon as the most suitable time for UAV image acquisitions to minimize undesirable atmospheric and shadow effects on the images (Katsigiannis et al., 2016; Zhao et al., 2018; Niu et al., 2020, 2021; Niu, Wang and Chen, 2022).

Table 4. Properties of the MicaSense Red-Edge-Mx sensor

| RedEdge-MX sensor | | |
|---|---|---|
| Band Name | Center Wavelength (nm) | Bandwidth (nm) |
| Blue | 475 | 20 |
| Green | 560 | 20 |
| Red | 668 | 10 |
| Near-infrared | 840 | 40 |
| Red-Edge | 717 | 10 |


Figure 2. Multi-rotor DJI-Matrice 600 and the MicaSense RedEdge-MX sensor used to capture high-resolution imagery

Pre-flight planning included, firstly, the definition of the area of interest (AOI), which was saved as a KML or KMZ file and subsequently imported into the drone's flight planning software. Secondly, flight parameters (forward and side overlap percentages) were configured in the software to calculate the drone's survey speed. Since both cameras were used simultaneously, the camera with the smallest swath and lowest speed determined the flight parameters. These calculations determined the number of batteries required for the survey. Flight parameters were programmed as 75% overlap on both sides (forward and side), a flight height of 60 m above ground level (AGL) at take-off point and UAV ground speed of 3.4 m $s^{-1}$. This achieved a ground sample distance with a resolution of +- 4cm per pixel for multispectral and +/-5 cm for the thermal imagery. Previous studies acquired UAV images over pomegranate orchards at either 30 m, 60 m or 100 m above the ground (Katsigiannis et al., 2016; Zhao et al., 2018; Niu et al., 2021; Akca and Polat, 2022; Niu,

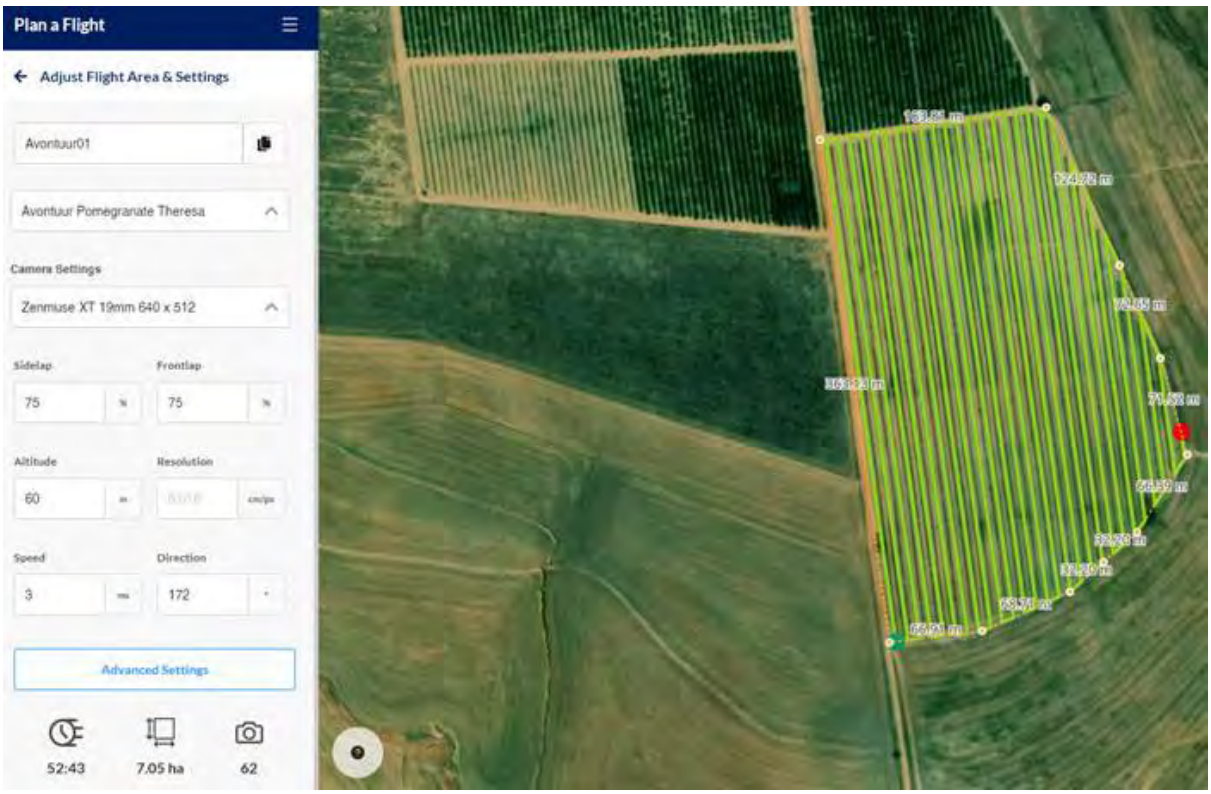


Figure 3. Flight plan for the young pomegranate orchard at Avontuur

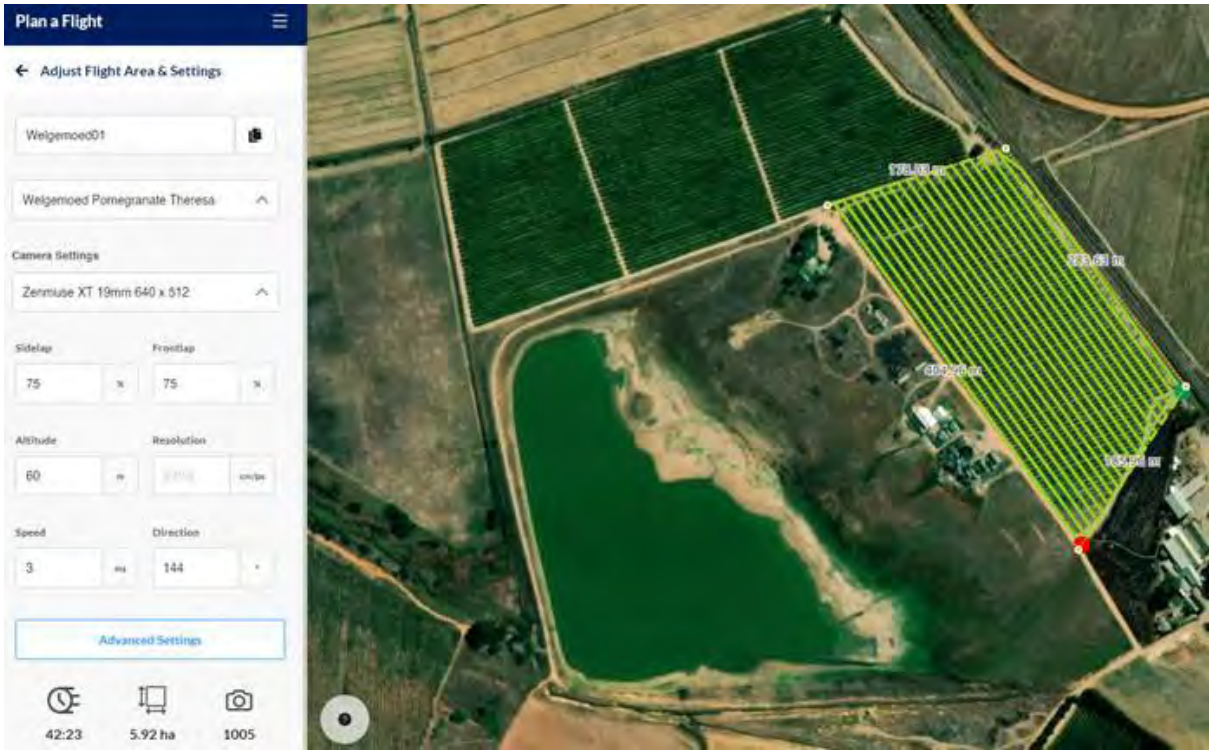


Figure 4. Flight plan for the full bearing orchard at Welgemoed

Wang and Chen, 2022). Thirdly, the KML/ KMZ file was imported into Google Earth and the Aeronautical Information Management System to secure flight permissions. The three-dimensional visualization of airspaces was conducted with the assistance of Air Traffic and Navigation Services (ATNS) of South Africa. A "Notice to Airmen" (NOTAM) was issued to inform surrounding airports of the drone operations, including details such as operation time, AOI, fly-away zones, and emergency contact information (e.g., nearest airports, hospitals, fire departments, and police). On the day of the survey, weather and environmental conditions were first evaluated. Wind speed and gusts at ground level and flying altitude were assessed to ensure they were within safe tolerances for the specific drone. Cloud cover was monitored, as it impacts the quality of the imagery. Wind conditions were carefully considered, as they affect drone performance, battery endurance, and overall safety. If conditions were considered suitable for the survey, the drone's compass and Inertial Measurement Unit (IMU) were calibrated for the survey site. The Downwelling Light Sensor 2 (DLS 2) of the multispectral camera underwent magnetometer calibration and the multispectral camera was calibrated using a Calibrated Reflectance Panel (CRP). Comprehensive safety checks were conducted on the drone and associated equipment. Before take-off, an air radio broadcast was made on the appropriate frequency to inform relevant parties of the survey. Post-flight procedures included data assessment and backup. Upon completing the flight, the image data was reviewed to ensure successful recording. The flight plan was officially closed via an air radio call. The drone and equipment were inspected again post-flight. Back at base, the data was downloaded and backed up before initiating rapid image processing, which entailed the generation of low-resolution products for quick visualization and flight verification. This was followed by full image processing as discussed in Section 3.4.

## 3.4 DRONE SURVEY DATA PROCESSING STRATEGY

Datasets collected by the UAV multispectral system consist of blue, green, red, near-infrared (NIR), RedEdge and thermal (TIR) bands. The raw images were processed using Pix4D mapper software version 4.8.4. Pixels were radiometrically corrected by using the Calibration Reflectance Panel (CRP) and the sensor measurements of irradiance from the Downwelling Light Sensor (DLS). The CRP contains unique laboratory-calibrated reflectance values that are used together with DLS data to generate surface reflectances. Within Pix4D mapper software, the following factors are taken into account: the sensor black level, the sensitivity of the sensor, sensor gain and exposure settings, and lens vignette effects to generate atmospherically corrected surface reflectance images. The values of the surface reflectance range from 0 to 1 (Munghemezulu et al., 2023). The mosaicked, orthorectified surface reflectance images can be used to generate RGB composites and to calculate vegetation indices from the Structure-of-Motion photogrammetric model (Table 5). Additional products that can be derived from UAV data include the Digital Surface Model (DSM) and Digital Terrain Model (DTM), which are crucial for crop height calculation and understanding water flow directions within the farm. Missing trees for both farms were digitized using high-resolution UAV images in QGIS software. There was no need to carry out classification tasks since the areas with missing trees were clearly visible.

Table 5. List of generated surface reflectance datasets collected and computed for each survey

| Description | Index | Formula | Related traits |
|---|---|---|---|
| Normalized Difference Vegetation Index | NDVI | (NIR-R)/(NIR+R) | Chlorophyll, LAI[1], Biomass, Yield |
| Normalized Difference Red-Edge Index | NDRE | (NIR-RE)/(NIR+RE) | Chlorophyll |
| Green Normalized Difference Vegetation Index | GNDVI | (NIR-G)/(NIR+G) | Chlorophyll, LAI, nitrogen, water content |
| Ratio Vegetation Index | RVI | NIR/R | Biomass, water content, nitrogen |
| Chlorophyll Vegetation Index | CVI | (NIR*R)/(G^2) | Chlorophyll |
| Chlorophyll Index-Red-Edge | CIRE | (NIR/RE)-1 | Chlorophyll |
| Height | H | | Crop age |
| Volume | V | | Structure |
| Temperature | T | | Crop stress |
| Spectral band: Blue | B | | |
| Spectral band: Green | G | | |
| Spectral band: Near-infrared | NIR | | |
| Spectral band: Red | R | | |
| Spectral band: Red-Edge | RE | | |

1 Leaf area index

## 3.5 FIELD MEASUREMENTS

Data were collected per survey for selected individual trees (4 sap flow, 2 soil water balance, 5 growth, 6 stem water potential) except where failure of equipment or monitoring systems or cloudy weather resulted in missing data. Weather stations, sap flow, soil water balance and micrometeorological systems automatically logged at least hourly the data required to calculate tree and orchard scale water use and crop coefficients. Manual measurements of fractional interception, tree canopy dimensions, stem water potential, physiological measurements and leaf chlorophyll content and were also conducted on the days of the surveys.

### 3.5.1 Tree measurements

Fractional interception was measured around solar noon (± 1h) on the day of each drone survey at eight trees (four sap flow, two soil water balance and two growth trees) using an Accupar LP-80 ceptometer (METER Group Inc., USA). Measurements with the 80 cm long probe were done at a constant height from the ground with the probe perpendicular to the tree row. For each side of the tree row, sequential sets of measurements were done in the tree row with the tip of the probe kept at distances of 0 m, 0.8 m and 1.6 m from the centre of the tree row. For Avontuur (tree spacing 2.5 m x 5 m) photosynthetic active radiation levels were measured in the tree row at 0 m, 0.5 m, 1 m, 1.5 m, 2 m and 2.5 m from the edge of the allocated area per tree, and for Welgemoed (tree spacing 2 m x 4.5 m) at 0, 0.4 m, 0,8 m, 1.2 m, 1.6 m and 2 m.

Leaf area index was derived from the Accupar LP-80 ceptometer and calibrated using measured canopy dimensions and actual leaf area determined *in situ* for a subset of trees (data not shown). Leaf area index was expressed per tree canopy area and orchard area allocated per tree. Tree canopy dimensions (tree height, width in the tree row and across the tree row, bottom height and width) were measured for the sap flow, soil water balance and five growth trees (n=11) on the same dates that fractional interception measurements were conducted, or within three days thereafter. From the second survey onwards, canopy dimensions were also measured for trees where stem water potential was measured (n=6).

Stem water potential was measured on the day of survey around 12h00 on six trees selected nearby the soil water balance and/ or sap flow trees. Two leaves per tree were enclosed in aluminium foil bags at least two hours before measurement and stem water potential was determined using a pressure chamber (PMS Model 1505D-EXP, PMS Instrument Company, Albany, USA). During surveys 2-5, net carbon-dioxide assimilation rate, stomatal conductance, intercellular carbon-dioxide concentration, leaf transpiration rate and leaf vapour pressure deficit measurements were also conducted on two leaves per tree for the trees selected for stem water potential measurement at 10h00, 12h00 and 14h00 using a LI-COR LI6400 XT infrared gas analyser (Lincoln, Nebraska, USA). Chlorophyll concentration was monitored during survey 1 and surveys 3-5 on ten leaves per tree representing different canopy positions (bottom to top, both sides of the tree row) using a SPAD-502 chlorophyll meter (Konica–Minolta, Inc., Osaka, Japan).

### 3.5.2 Reference evapotranspiration

An automatic weather station installed within 50 m of each orchard monitored rainfall and the necessary variables hourly (CR200/ CR300 datalogger: Campbell Scientific Inc., Logan, UT, USA) to calculate reference evapotranspiration (ETo) according to the FAO56 Penman-Monteith modified equation (Allen et al., 1998). At c. 1.2 m above the ground, wind speed and direction were measured using a wind sentry anemometer and vane (Model 03002, R.M. Young Company, Michigan, USA), temperature and relative humidity using a sensor (Hygrovue™5, Campbell Scientific Inc.) installed inside a six plate radiation shield and global solar radiation using a pyranometer (LI-200R M5, Campbell Scientific Inc.), while a Texas Electronics tipping bucket rain gauge (Model# TR-525I 6: Texas Electronics, , Dallas, TX, USA) monitored rainfall amounts. The hourly logged weather data for both stations were downloaded daily via the ARC Agromet services and was made available by email communication to the project manager.

### 3.5.3 Transpiration

Transpiration was measured using the heat ratio method (HRM) of the heat pulse velocity (HPV) sap flow technique as described by Burgess et al. (2001). In July 2023 stem diameter distribution for each orchard was determined for a subset of 30 trees and four stem diameter ranges identified for installation of the sap flow equipment in four trees (T1-T4). Equipment was installed in young

pomegranate trees from Avontuur with stem diameters at 200 mm above the ground in the range of 50-59 mm (57.3 mm), 59-67 mm (63.6 mm), 67-76 mm (72.9 mm) and 76-84 mm (82.1 mm). For the full-bearing orchard at Welgemoed sap flow equipment was installed for one tree each in the following stem diameter ranges: 72-82 mm (79.9 mm), 82-93 mm (92 mm), 93-104 mm (98.3 mm) and 104-115 mm (108.5 mm). Sap flow was monitored at four stem depths per tree to account for the radial variations in sap velocity, using one set of sensors (an upper and lower thermocouple and one heater element) per stem depth. Heat pulse velocity (cm $h^{-1}$) for each sensor set was logged hourly per site using a CR1000X logger (Campbell Scientific Inc., Logan, UT, USA) connected to a AM16/32B multiplexer. Data were downloaded via modem communication on a weekly to bi-weekly basis, while maintenance of sap flow systems (battery swop, realignment of thermocouples as required) occurred bi-weekly. Sap flow data were collected at Avontuur and Welgemoed from August 2023 until May 2024.

Sap velocity data were processed from October 2023 until May 2024 for all instrumented trees (total 8). Non-numerical (NAN) indicators or spikes occurring in recorded data were replaced by interpolating data. Where data of more than one consecutive hour was not usable, a statistical regression equation obtained between the heat pulse velocity of thermocouple sets at adjacent depths were used to estimate and replace the missing data (data not shown). The four heat pulse velocity datasets obtained per tree were corrected for the offset from zero by manually estimating the offset from data graphed for ten-day periods. The approach of Burgess et al. (2001) was followed thereafter to correct the heat pulse velocity data for wounding due to sensor implantation. Wound width and wood properties used were determined at the end of 2023/24 season. The wound width was on average 2.13 mm. The pomegranate averaged wood moisture content amounted to 69.56% and wood density was 0.93 g $cm^{-3}$. The hourly total sap flow volume ($\ell$ $tree^{-1}$) by each tree was calculated as a weighted sum of the products of the sapwood area and the sap flux density (or sap velocity) represented by the specific probe. The weights are the sapwood areas represented by each probe. Sapwood area was determined by injecting trees with methylene blue dye and taking and inspecting stem core samples after a period of three days. The hourly sap flow volume values were accumulated from 01h00 to midnight to obtain a daily sap flow value. The daily sap flow values of the four trees were weighted to obtain orchard-level transpiration, considering the frequency of the stem size distribution ranges identified for the orchard. Orchard level transpiration was calculated as:

$$T\_Young\ orchard = (0.367 \times T1) + (0.2 \times T2) + (0.1 \times T3) + (0.333 \times T4) \quad [Eq.\ 1]$$

$$T\_Full\ bearing\ orchard = (0.1 \times T1) + (0.333 \times T2) + (0.133 \times T3) + (0.433 \times T4) \quad [Eq.\ 2]$$

Where T = Transpiration in $\ell$ $d^{-1}$ or mm $d^{-1}$ and T1-T4 refer to transpiration of the four respective trees.

Transpiration coefficients were calculated as the ratio of T to ETo.

### 3.5.4 Soil water balance

Soil water content was monitored in the tree row and work row using CS650 soil water content reflectometers (Campbell Scientific Inc., Logan, UT, USA). Sensors were installed for one dripper line secured at 300 mm from the tree row at a position directly below the dripper nearest to the tree (c. 30 cm from the tree) as well as midway to the next dripper within the area allocated to the tree (c. 67 cm from the tree). Another set of sensors was installed in a position representative of the work row (c. 2.25 m from the tree row) with the rods of the sensors parallel to but centred on a dripper positioned next to the tree neighbouring the one which was instrumented in the tree row.

A set of four sensors was installed per position in different soil depth increments identified (Table 6) with the goal to measure water use for the tree root zone representatively, and to monitor if leaching of water occurs beyond the root zone. The CS650 sensors were installed perpendicularly to the dripper line and diagonally over the soil depth increment to be instrumented. To prevent damage of equipment by orchard traffic, the topmost sensors in the work rows were installed horizontally at 200 mm depth. Where an impermeable layer occurred below the root zone, sensors were also installed horizontally above it. Irrigation applied was monitored using Multi-Jet flow meters (Arad Ltd., Dalia, Israel) connected to a CR1000X data logger (Campbell Scientific Inc., Logan, UT, USA).

Table 6 Soil depth increments for installation of CS650 sensors

| Site | Installation ID | Soil depth increment (mm) | | | |
|---|---|---|---|---|---|
| Avontuur | SWB1 | 0-200 | 200-500 | 500-900 | 900-1050 |
| | SWB2 | 0-200 | 200-600 | 600-900 | 900-1200 |
| Welgemoed | SWB3 | 0-300 | 300-600 | 600-900 | 900-1150 |
| | SWB4 | 0-330 | 330-660 | 660-1050 | 1050-1250 |

The soil water balance calculations to obtain evapotranspiration for the full surface for the young orchard (SWB1 and SWB2) and the full bearing orchard (SWB3 and SWB4) were conducted using *in situ* calibrated volumetric soil water content of the CS650 sensors. At Avontuur, high stone content (c. 30%) occurring deeper than about 500 mm effectively prevented gravimetric sampling for calibration purposes and the CS650 factory calibration was therefore used for sensors installed in the two deepest soil layers.

The full surface evapotranspiration of the orchard was calculated as follows:

$$ET_{FS} = ET_{TR} + ET_{WR} \quad \text{[Eq. 1]}$$

where:

$ET_{FS}$ = full surface evapotranspiration of the orchard (mm)

$ET_{TR}$ = evapotranspiration out of the tree row fraction of the orchard (mm per orchard area)

$ET_{WR}$ = evapotranspiration out of the work row fraction of the orchard (mm per orchard area)

Evapotranspiration from the volume of soil under the tree row was determined as follows:

$$ET_{TR} = \Delta SWC_{TR} + I + P - \Delta SWC_{900} \quad \text{[Eq. 2]}$$

where:

$ET_{TR}$ = evapotranspiration out of the tree row fraction of the orchard (mm)

$\Delta SWC_{TR}$ = change in soil water content in the tree row

I = Irrigation applied (mm per tree row area)

P = rainfall (mm)

$\Delta SWC_{900+}$ = change in soil water content in the soil layer below the 900 mm depth (1050 mm for SWB4)

The fraction of ET from the work row volume of soil water was calculated according to the following soil water balance equation:

$$ET_{WR} = \Delta SWC_{WR} + P - \Delta SWC_{900+} \quad \text{[Eq. 3]}$$

where:

$ET_{WR}$ = evapotranspiration out of the work row fraction of the orchard (mm)

P = rainfall (mm)

$\Delta SWC_{900+}$ = change in soil water content in the soil layer below the 900 mm depth (1050 mm for SWB4)

The evapotranspiration losses from the tree row and work row, respectively, was converted to volume before expressing it as mm per full orchard surface area.

Crop coefficients (Kc) were calculated according to Allen et al. (1998) as the ratio of ETc to ETo for the tree row, work row and full orchard surface, respectively.

### 3.5.5 Micrometeorological methods

A surface renewal (SR) system was employed full time in the young orchard at Avontuur and an eddy covariance (EC) system in the full bearing orchard at Welgemoed. The SR system was tested and calibrated at the ARC Infruitec-Nietvoorbij Irrigation laboratory in Stellenbosch before installation on 25 November 2022 at Avontuur. The system was positioned approximately in the middle of the young pomegranate orchard and took into account the positioning of the soil water balance and sap flow installations. Components of the SR system installed at 1.2 m above the tree canopies include fine wire temperature sensors (FW 003), a net radiometer (NR Lite-Kipp and Zonen), pyranometer (SR-Apogee) and a 3D Sonic Anemometer (R.M. Young). Data were logged by a CR1000 data logger and downloaded on a bi-weekly to monthly basis using a direct connection to a laptop or other data downloading device. Equipment

installed below the ground in the tree row included two Hukseflux Heat Flux Plates at 2.5 cm depth and two Tcav soil temperature sensors at 6 cm depth.

An EC tower was installed from 21-24 September 2022 at a distance of 75 m from the road in the middle of the Welgemoed orchard and 150 m away from the netted area at the bottom end of the orchard. The height of the instruments was 1 m above the canopy, except for the NR Lite radiation sensor (Rn) mounted at c. 8 m above the ground. The instruments installed included the IRGASON (measures $H_2O$ and $CO_2$ fluxes); pyranometer (solar radiation); EC100 $CO_2$ and $H_2O$ Processing unit and CR3000 data logger (data processing and programming). A temperature and relative humidity sensor was installed at the canopy level. Equipment installed at ground level in the tree row included a Hukseflux Heat Flux Plate 2.5 cm below the ground, two Tcav soil temperature sensors 6 cm below the ground and a CS616 Soil water content sensor 8 cm below the ground. The system used a solar power system, but after the theft of the solar panel, batteries were swapped every week. The data were collected using direct connections to a laptop or other data downloading devices.

The data from both the EC and SR systems were imported and analysed in Excel using the simplified form of the energy balance equation. The evapotranspiration, which is represented by latent heat (LE), was calculated as a residual from net radiation (Rn), sensible heat (H) and the ground heat flux (G). The main difference between the systems is that sensible heat for the SR system was measured using a fine wire thermocouple, and the EC system measured the turbulent fluxes in the atmosphere. Crop coefficients (Kc) for the two research sites were calculated according to Allen et al. (1998) as the ratio of orchard scale measured ETc to ETo.

## 3.6 STATISTICAL ANALYSIS

Simple linear regressions were conducted between all data and indices derived from drone images for selected individual trees to individual tree data measured in orchards for a) orchards combined (young and full bearing), b) per orchard (five surveys combined) and c) per survey per orchard (individual trees combined). Secondly, linear regressions were conducted at orchard scale – i.e. orchard averaged values of all individual tree data derived from drone images compared to averaged ground measured tree dimensions or orchard upscaled transpiration or orchard level evapotranspiration, also for a) orchards combined and b) per orchard (five surveys combined). Regression models were considered significant at 95% level of confidence (p=0.05).

Data derived from the drone images included reflectance of the blue, green, red, NIR, RedEdge and thermal bands and drone estimated tree height and volume. The indices calculated from the drone image data included, in addition to NDVI, NDRE, GNDVI, RVI, CVI and CIRE (refer Table 5). Ground measured data included individual tree height, across row width, in row width, tree volume, fractional interception, leaf area index (ceptometer, tree canopy area based, orchard), transpiration and soil water balance derived evapotranspiration. For regressions on orchard scale orchard averages of the tree dimensions, transpiration upscaled to orchard level and evapotranspiration measured at orchard level by the micrometeorological techniques were used.

# CHAPTER 4: FIELD SURVEYS

## 4.1 INTRODUCTION

Field surveys included conducting the drone flights (Figure 5) as well as ground measurements in the orchard (Figure 6) while automatic weather stations, sap flow and micrometeorological systems monitored weather and water use variables hourly (Figure 7).


Figure 5. Drone preparation for flight by the drone pilot and assistant (a & b) in the young pomegranate orchard and the drone ready for take-off during flowering in October 2023 (c) and after fruit set when fruit were enclosed in brown paper bags in December 2023 (d)


Figure 6. Fractional interception (a), tree canopy dimensions (b), stem water potential (c) and LI6400XT photosynthesis and stomatal conductance measurements were conducted during drone surveys

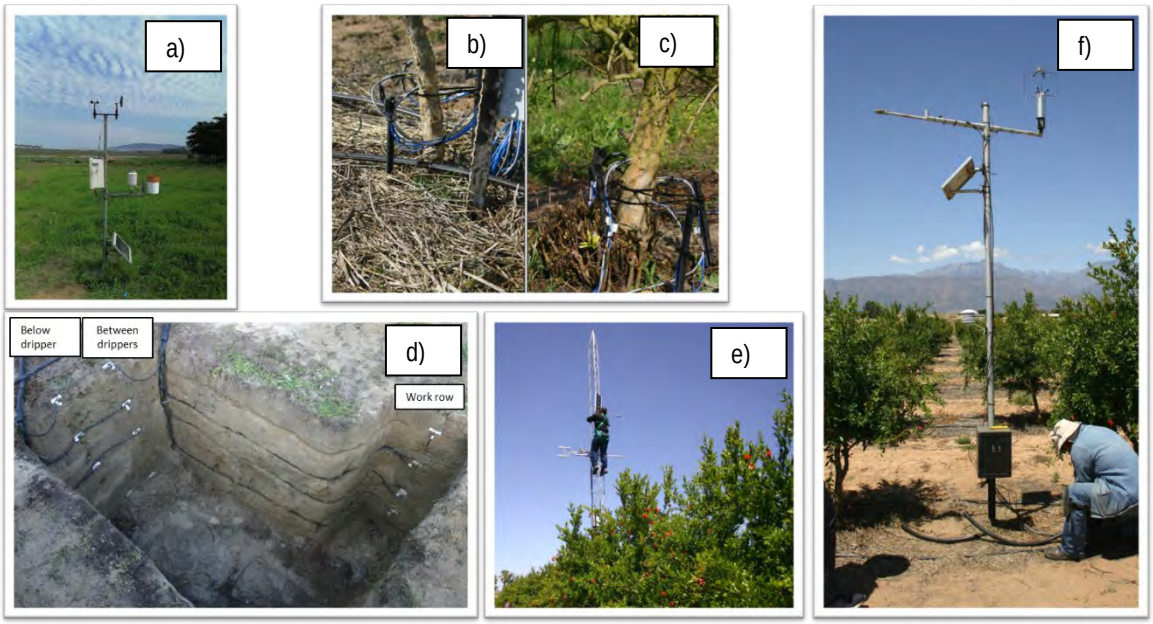


Figure 7. On days of drone surveys an automatic weather station monitored variables for calculation of reference evapotranspiration (a); sap flow equipment installed in young (b) and full bearing (c) pomegranate trees measured transpiration; soil water content was measured for soil water balance monitoring (d), eddy covariance e) and surface renewal systems (f) determined orchard level evapotranspiration

## 4.2 MULTISPECTRAL AND THERMAL IMAGES

Rapid processed multispectral and thermal orthomosaic images are presented for drone surveys 1-5 for Avontuur (Figures 8-10) and Welgemoed (Figures 11 and 12).

a)

b)

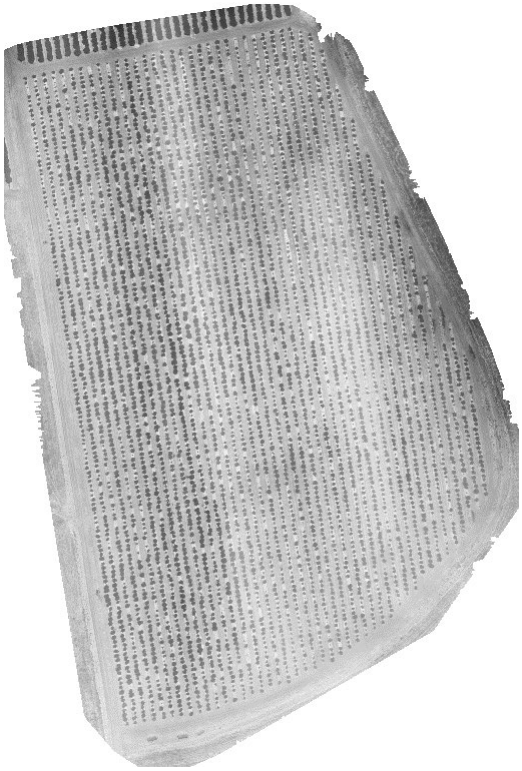

c)

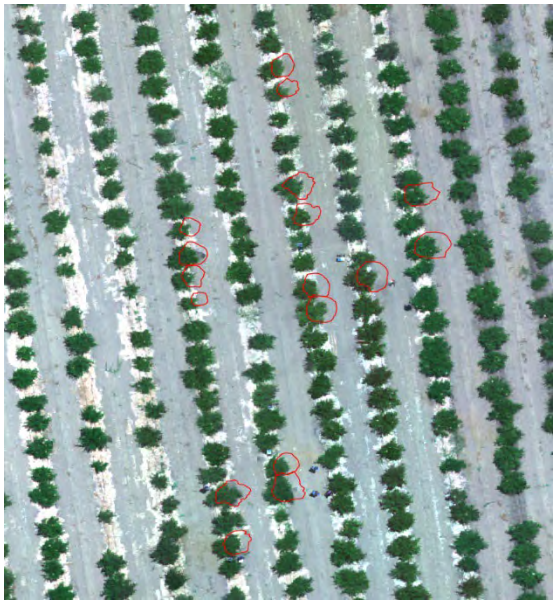

Figure 8. Avontuur (young pomegranate orchard) a) rapid multispectral orthomosaic and b) rapid thermal drone orthomosaic image on 31 October 2023. The positions of trees selected for water use or canopy dimension measurements are indicated as small red circles overlayed on the multi-spectral drone image (c).

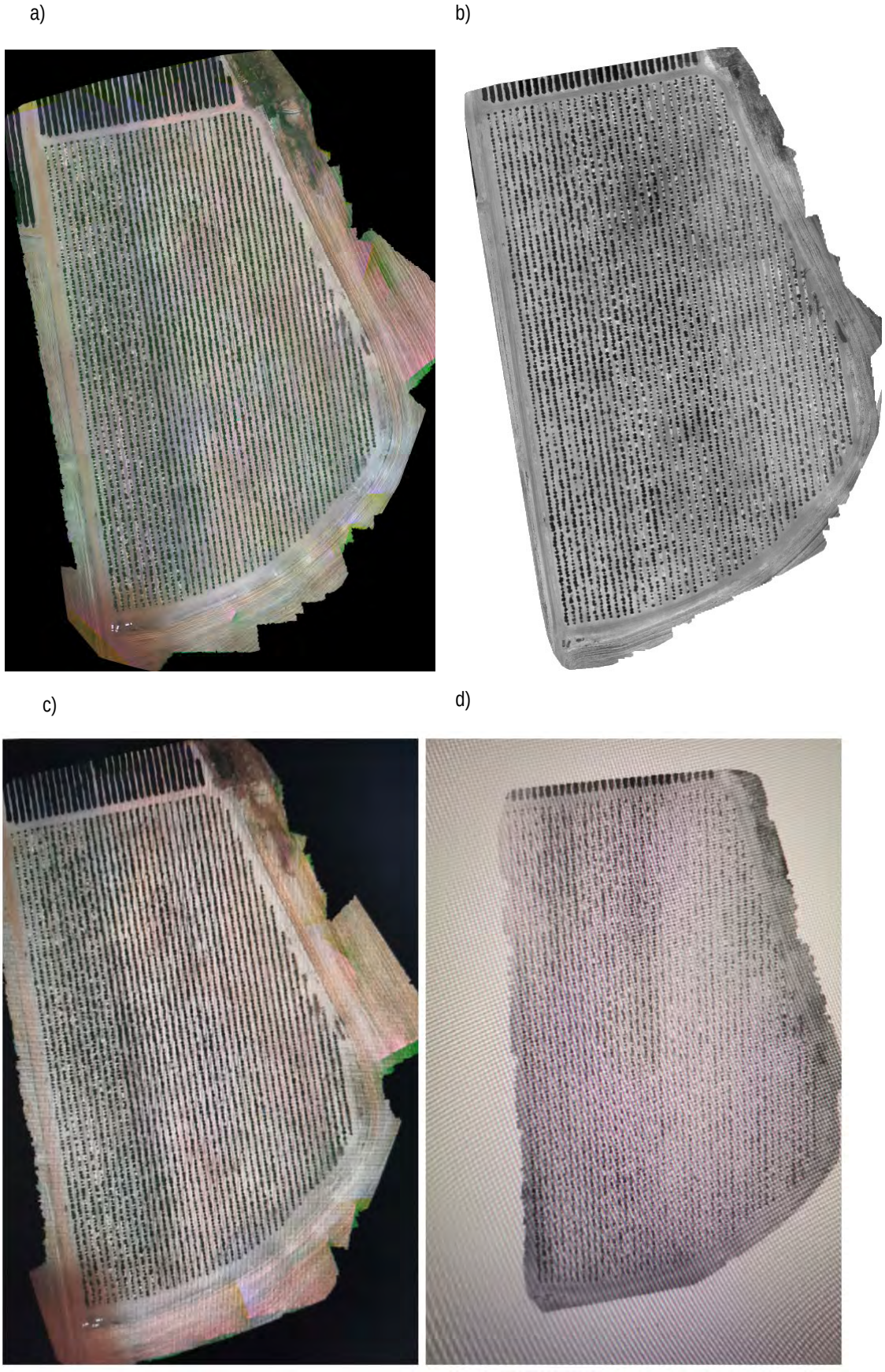


Figure 9. Avontuur (young pomegranate orchard) rapid multispectral orthomosaic (a, c) and rapid thermal drone orthomosaic (b, d) images on 15 December 2023 (a, b) and 12 January 2024 (c, d)

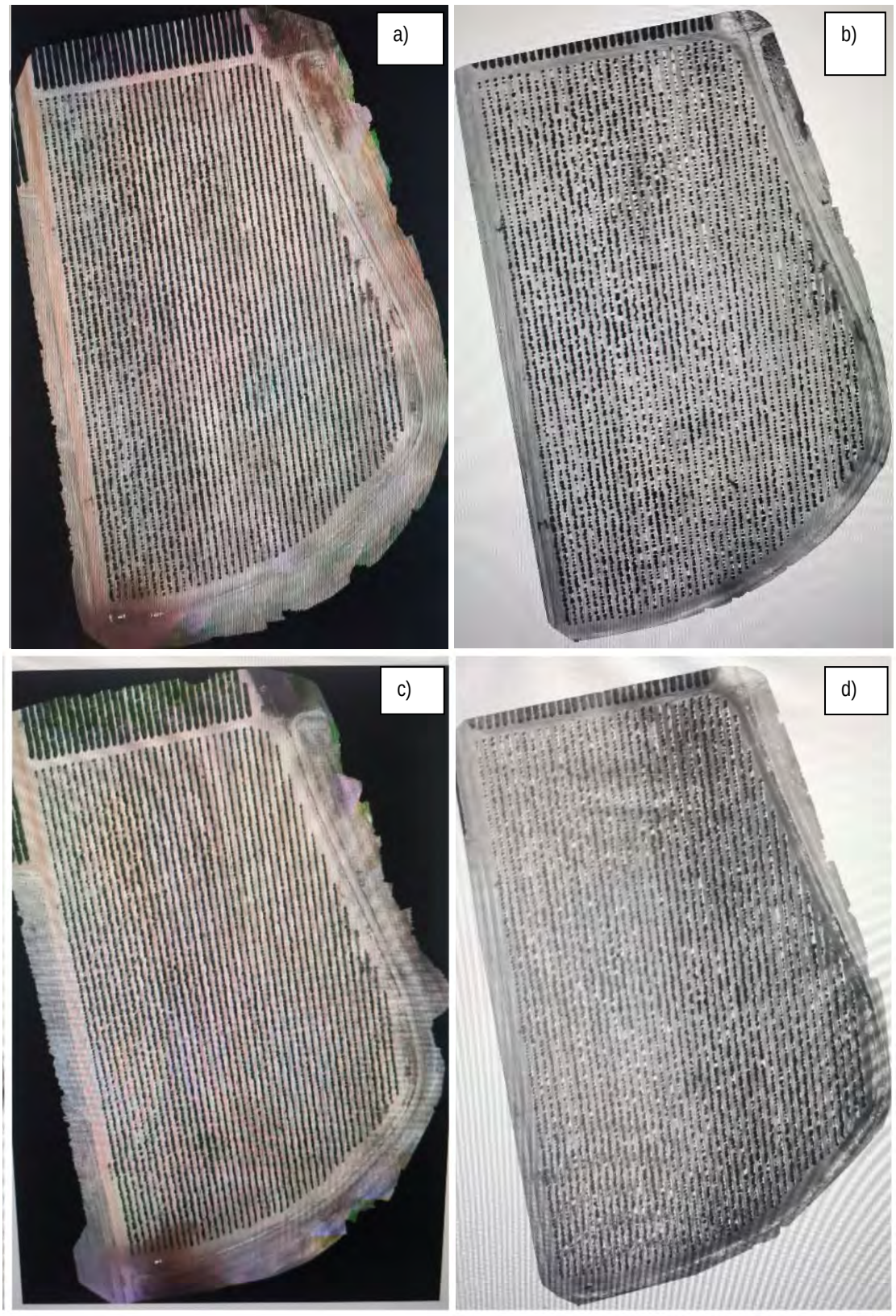


Figure 10. Avontuur (young pomegranate orchard rapid multispectral drone orthomosaic image (a, c) and rapid thermal orthomosaic (b, d) on 23 February (a, b) and 17 April (c, d) 2024

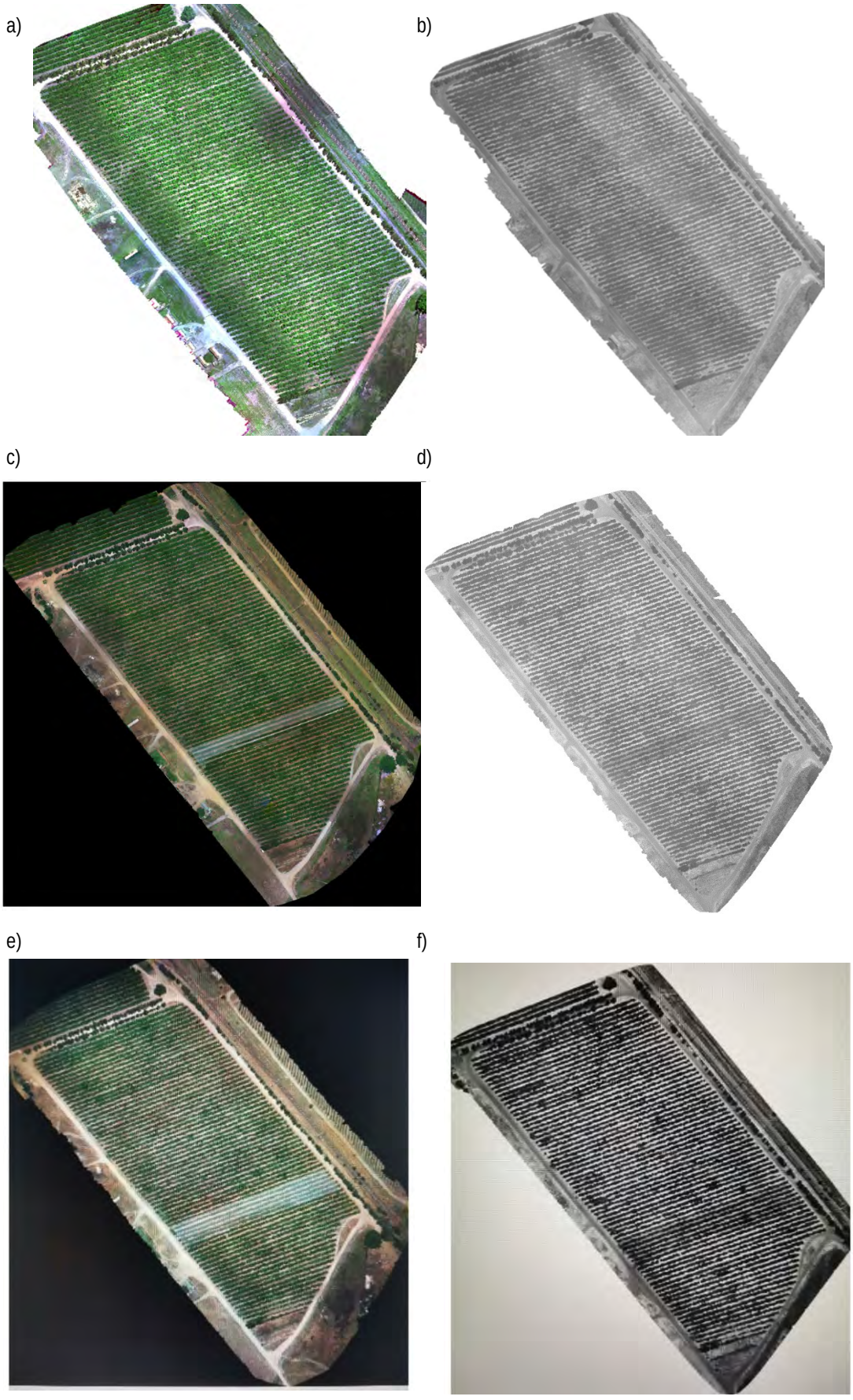


Figure 11. Welgemoed (full bearing pomegranate orchard) rapid multispectral orthomosaic (a, c, e) and rapid thermal drone orthomosaic (b, d, f) images on 30 October 2023 (a, b), 13 December 2023 (c, d) and 13 January 2024 (e, f)

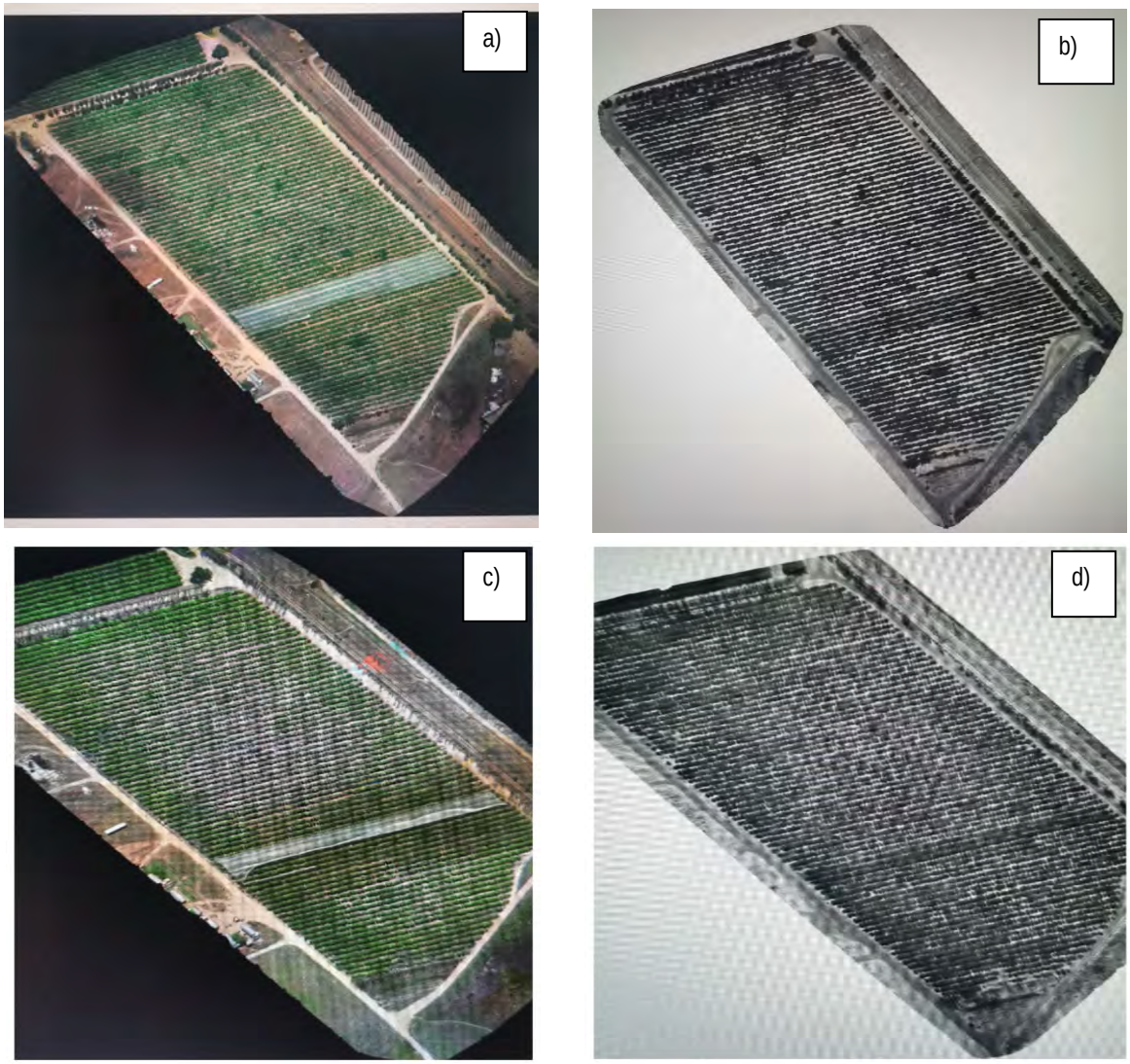


Figure 12. Welgemoed (full bearing pomegranate orchard) rapid multispectral drone orthomosaic (a, c) and rapid thermal orthomosaic (b, d) images on 24 February 2024 (a, b) and 21 April 2024 (c, d)

## 4.3 ORCHARD MAPS OF DRONE IMAGE DERIVED VARIABLES (SELECTED SURVEYS)

Processed data were supplied for each survey in Excel format for preselected trees (sap flow, soil water balance, growth, stem water potential, once-off stress experiment) as well as in Excel format and in map format per RGB band/ vegetative index per orchard. The processed data included the following spectral bands or indices: blue, green, red, NIR, RedEdge, NDVI (Normalized Difference Vegetation Index), NDRE (Normalized Difference Red Edge Index), GNDVI (Green Normalized Difference Vegetation Index), RVI (Ratio Vegetation Index), CVI (Chlorophyll vegetation index), CIRE (Chlorophyll index – Red edge), Height, Volume and Thermal infrared (TIR). Maps were also supplied, indicating DTM contours (Figures 13 and 14).

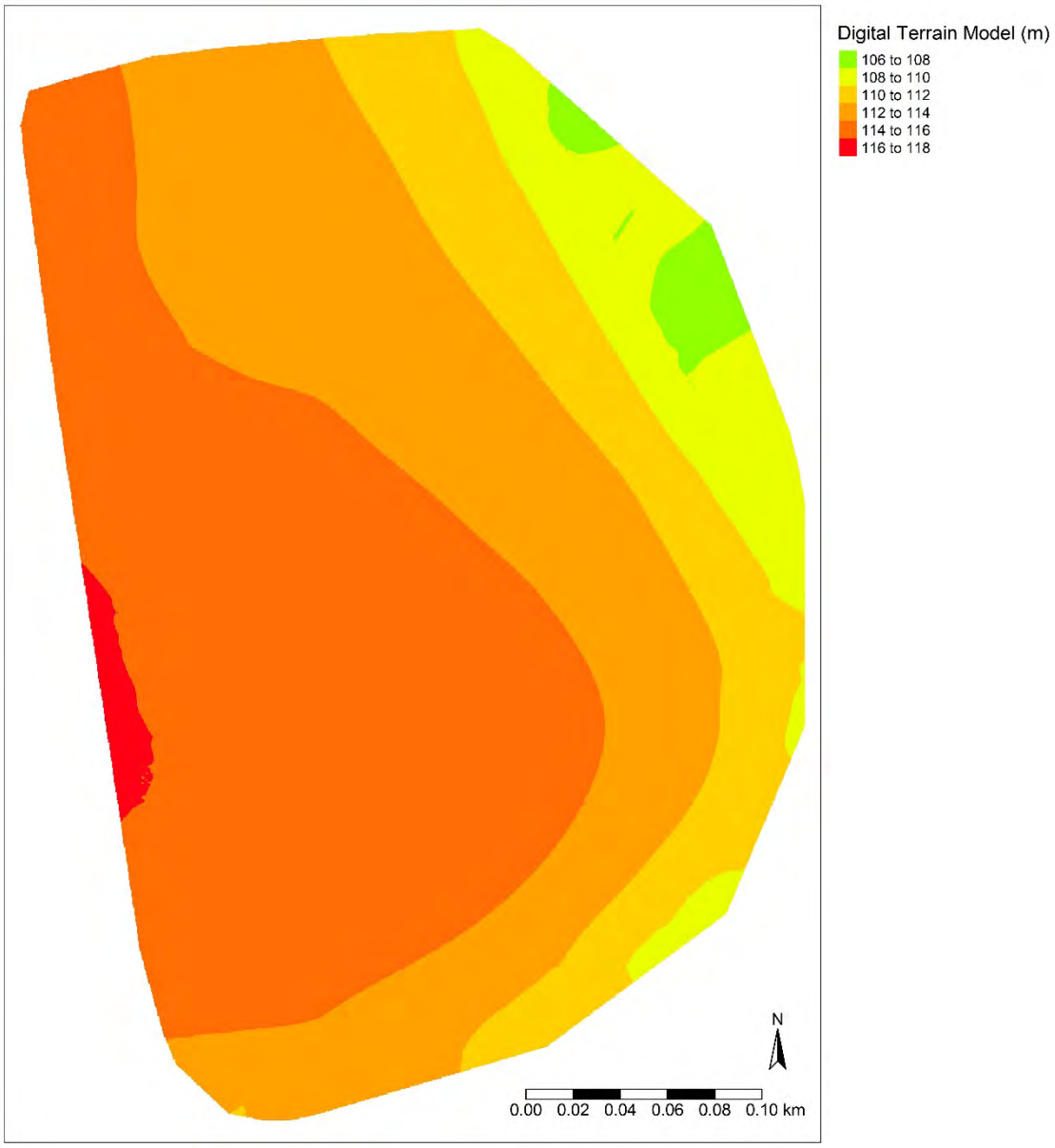


Figure 13. Avontuur digital terrain model derived from drone imagery for 31 October 2023

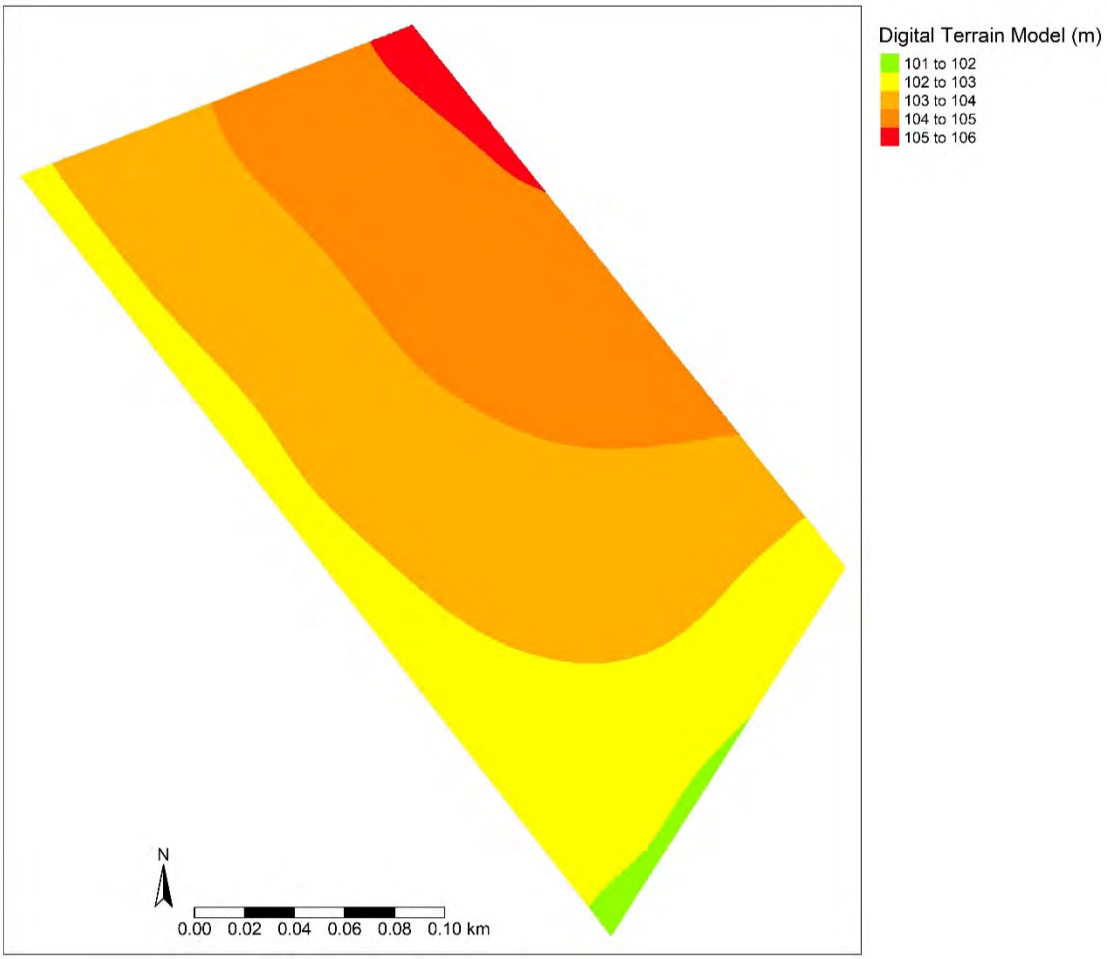


Figure 14. Welgemoed digital terrain model derived from drone imagery for 31 October 2023

According to Figure 13, the selected experimental trees at Avontuur are all located in the 114-116 m above sea level contour. At Welgemoed the experimental trees are within the 104-105 m above sea level contour, but a few trees may be located in the 103-104 m above sea level contour (Figure 14). The maps regarding the different multispectral image spectral bands and indices are in total 28 per survey and the variance of the variables presented in the maps was reported for all surveys in Chapter 8. In this deliverable only a few maps are included as examples to indicate the variation in height (Figures 15 and 18), NDVI (Figures 16 and 19) and temperature (Figures 17 and 20) in the orchard as determined on 31 and 30 October 2023 for Avontuur (Figures 15-17) and Welgemoed (Figures 18-20), respectively. The maximum height range for the young orchard was 2.5-3 m (Figure 15) and for the full bearing orchard 2-4 m (Figure 18). For Welgemoed, heights exceeding 4 m are most likely wind breaks located at the bottom end of the orchard. The maximum NDVI range for the young orchard was 0.85-0.9 (Figure 16) and for the full bearing orchard between 0.9 and 1.0 (Figure 19). Temperatures end October of more than 70°C at Avontuur is most likely due to mulch, which covers the soil where trees died (Figure 17). The maximum temperature range at Welgemoed end October was between 60°C and 70°C, but the temperatures for most parts of the orchard was between 20°C and 40°C. (Figure 20). It appears as if some of the higher temperatures occurred in the work row area between tree rows.

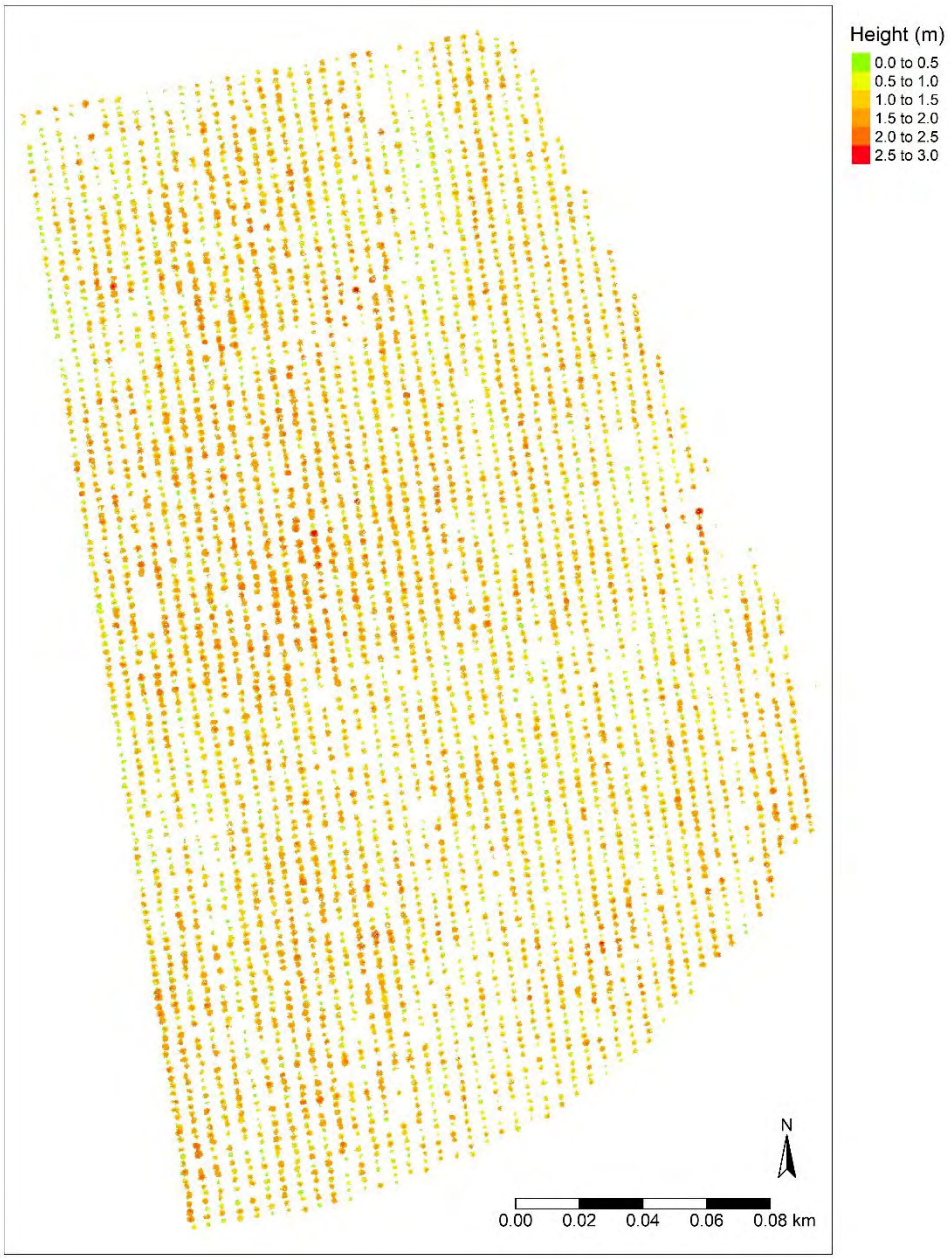


Figure 15. Young orchard (Avontuur) tree height modelled from multispectral drone imagery for 31 October 2023

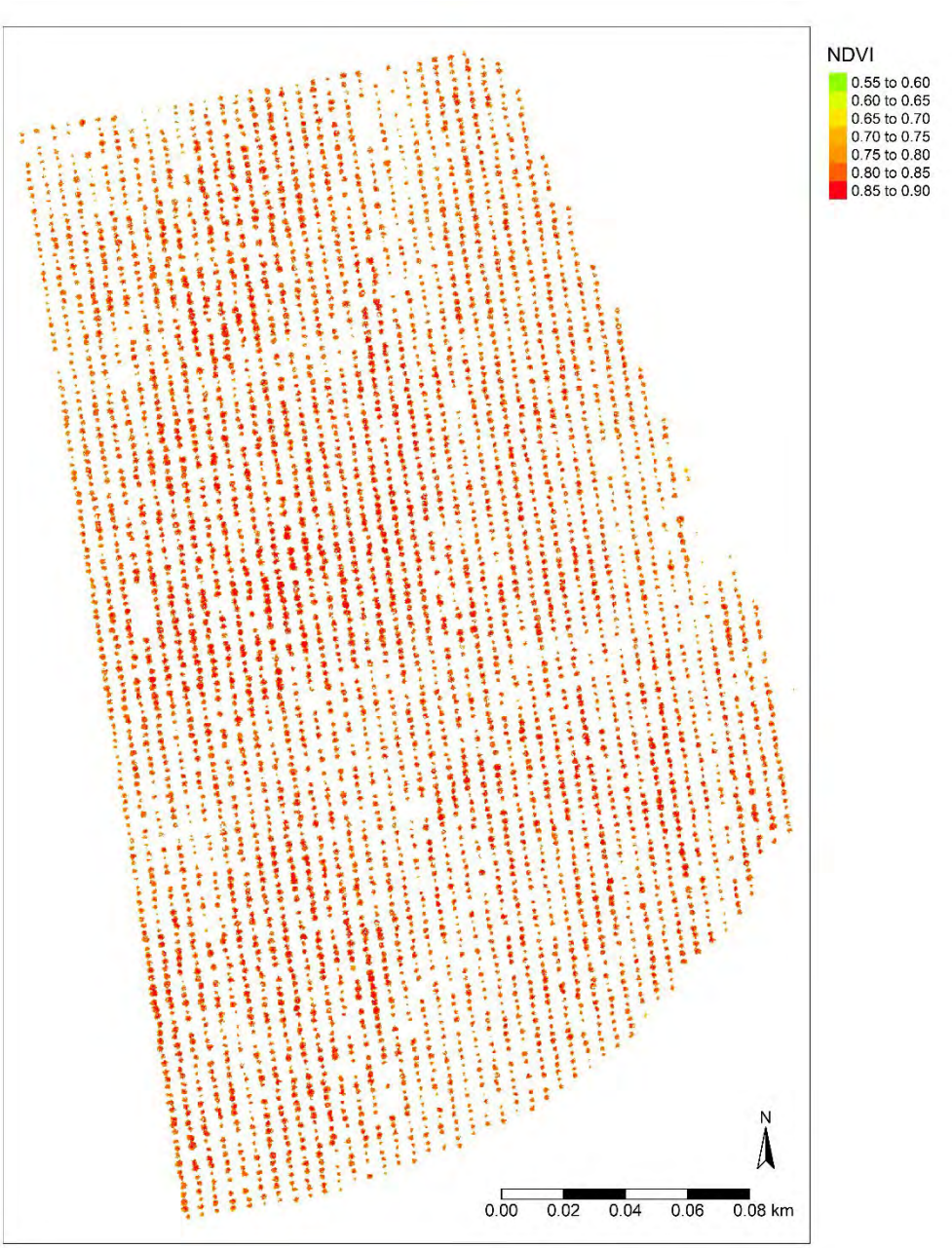


Figure 16. Young orchard (Avontuur) NDVI modelled from multispectral drone imagery for 31 October 2023

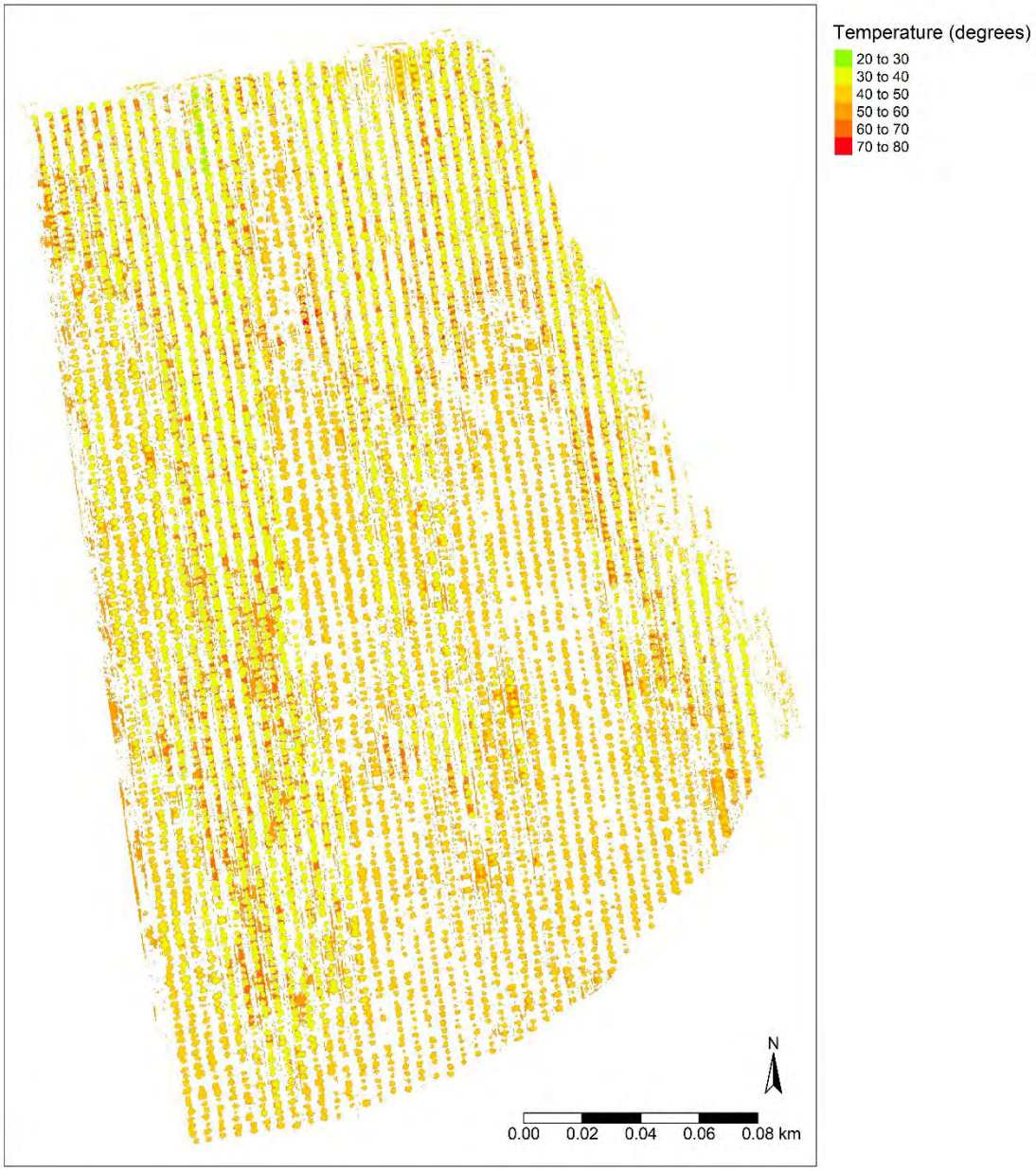


Figure 17. Young orchard (Avontuur) temperature obtained from thermal drone imagery for 31 October 2023

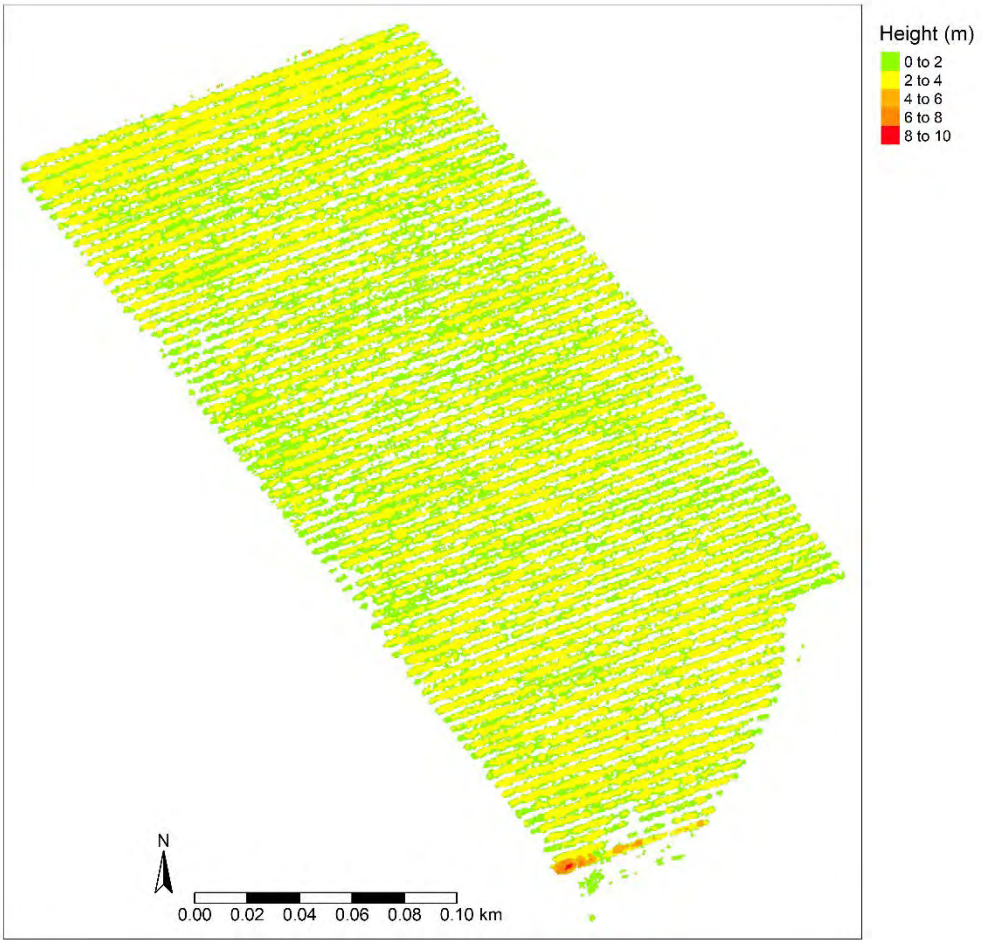


Figure 18. Full bearing orchard (Welgemoed) tree height modelled from multispectral drone imagery for 30 October 2023

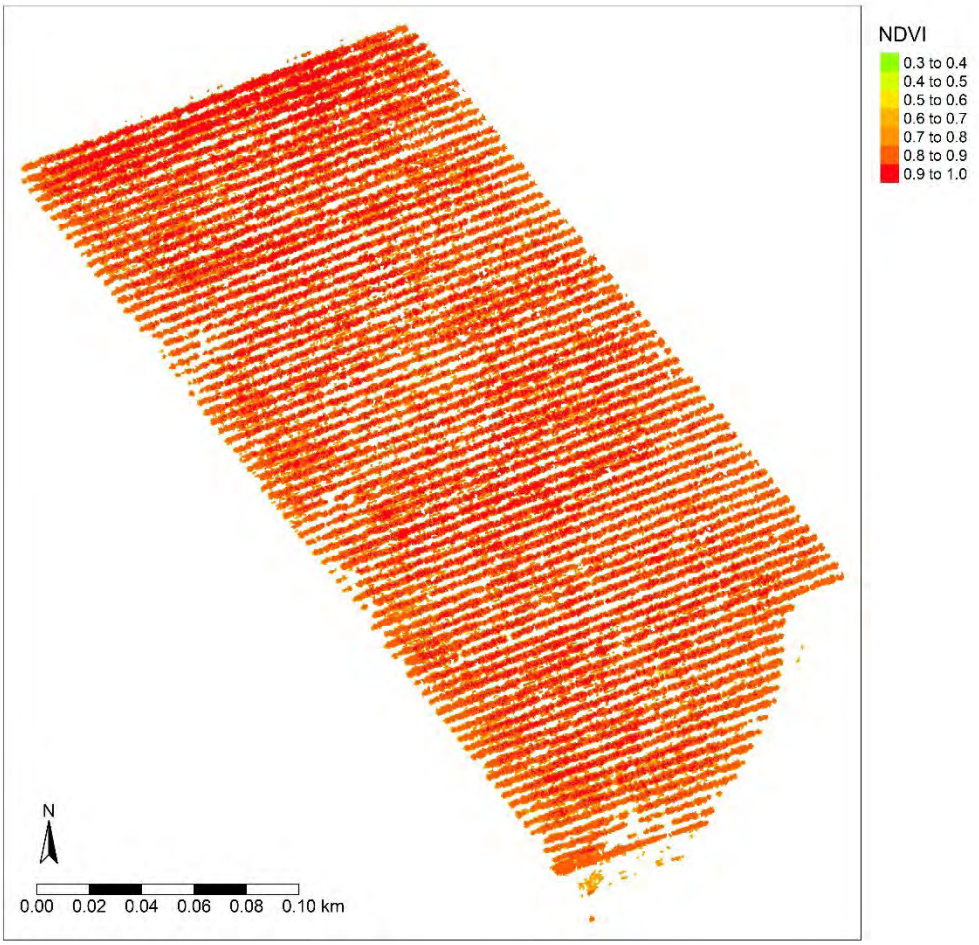


Figure 19. Full bearing orchard (Welgemoed) NDVI modelled from multispectral drone imagery for 30 October 2023

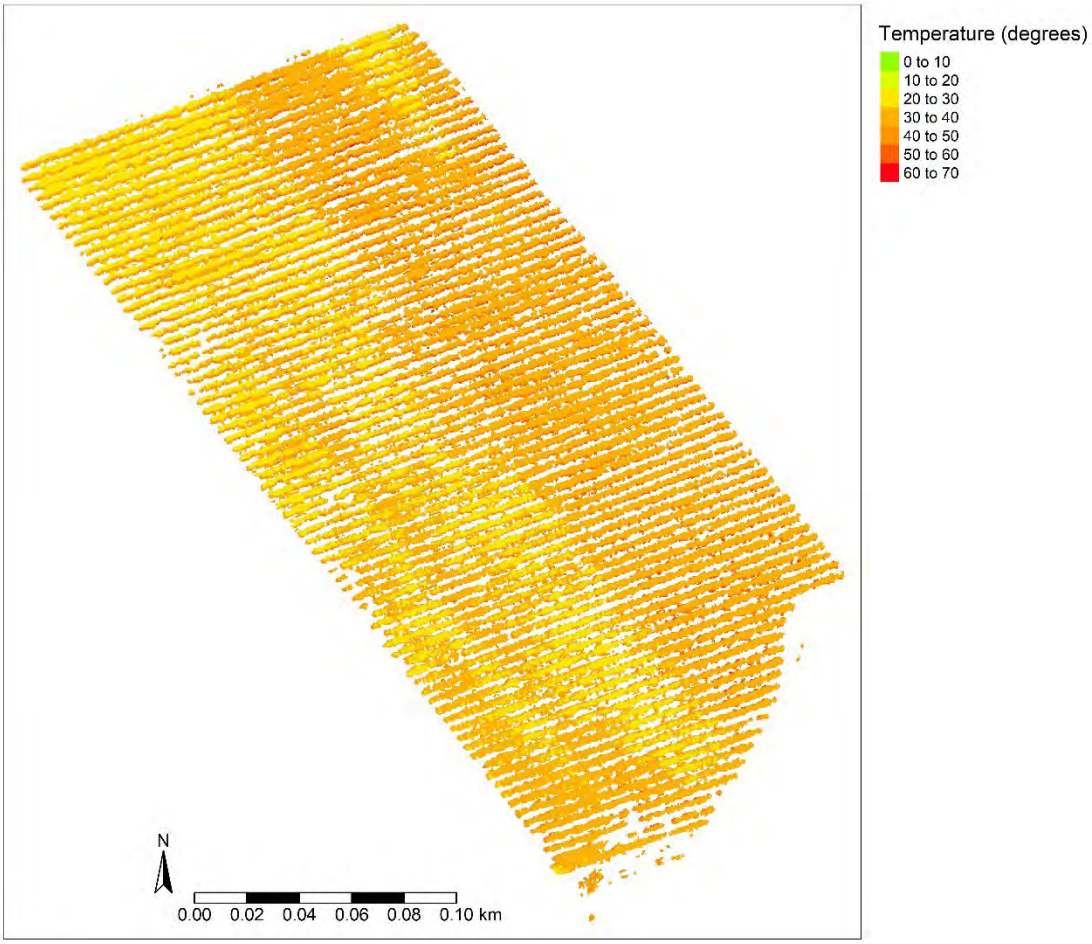


Figure 20. Full bearing orchard (Welgemoed) temperature modelled from thermal drone imagery for 30 October 2023

# CHAPTER 5: COMPARISON OF MULTISPECTRAL IMAGE SPECTRAL BANDS, INDICES, TREE GEOMETRIC DIMENSIONS AND THERMAL INFRARED TEMPERATURE TO IN-FIELD MEASURED TREE CANOPY PROPERTIES

## 5.1 INTRODUCTION

Tree canopy properties such as height, fractional interception (FI) and leaf area index (LAI) can indirectly be related to crop coefficients for purposes of irrigation scheduling (Pereira et al., 2020). Drone technology was previously successfully used to obtain fractional vegetation cover, plant height, leaf area index or canopy temperature of trees in forests and orchards (Birdal et al., 2017; Gonzalez-Dugo et al., 2013; Islami et al., 2021; Liu et al., 2021; Mahmud et al., 2023), including pomegranate trees (Zhang et al., 2017). This chapter explores the potential of multispectral drone image derived spectral bands, tree geometric properties, vegetation indices and thermal infrared temperature to estimate various ground measured pomegranate tree canopy properties for orchards varying in canopy size in the Western Cape, South Africa.

## 5.2 METHODOLOGY

In 2023/2024 five drone surveys were conducted at the young (Avontuur, 33°07'29.7"S; 18°56'08.8"E) and full bearing (Welgemoed, 33°35'18.3048"S; 18°59'19.302"E) cv. 'Wonderful' pomegranate orchards (Table 2, Figure 1, Refer to Chapter 3 regarding methodology and UAV system details). The surveys were piloted at solar noon (±1 hour) about two months after bud break during canopy development (October 2023), after most fruit set was completed (December 2023), at full canopy (January 2024), during ripening (February 2024) and after harvest (April 2024). On the day of the survey, or within three days thereafter, individual tree height, across row width, in row width and canopy bottom height and width were measured. These measurements were conducted in October 2024 on trees selected for sap flow, soil water balance and growth monitoring (n=11), but from December 2023 six stem water potential trees were added to the number of trees measured (n=17). Tree volume was calculated from the tree geometrical measurements assuming a general ellipsoid tree form. Fractional interception was measured for eight trees around solar noon on the day of the survey using an Accupar LP-80 ceptometer (refer to chapter 3 for detailed methodology), with LAI being a modelled output of the instrument. Tree canopy area-based LAI (Tr-LAI) and orchard LAI (OLAI) was calculated by calibrating the ceptometer LAI (CP-LAI) estimates using *in situ* measured leaf area data for six selected trees per site (data not shown). The estimated leaf area was expressed over the calculated tree canopy area and the full area allocated per tree per orchard.

Multispectral and thermal drone images were processed using Pix4D mapper software (Version 4.8.4). Pixels were radiometrically corrected by using a calibration reflectance panel and downwelling light sensor measurements of irradiance. Simple linear regressions were conducted between all data and indices derived from drone images for selected individual trees to individual tree data measured in orchards. Regressions were also conducted at orchard scale – i.e. orchard averaged values of all individual tree data derived from drone images compared to averaged ground measured tree dimensions, FI and leaf area indices. Regression models were considered to be significant at 95% level of confidence ($p = 0.05$). Data variables derived from the drone images included reflectance of the blue, green, red, NIR, RedEdge and TIR bands and drone estimated tree height and volume. The indices calculated from the drone image data included, in addition to NDVI, NDRE, GNDVI, RVI, CVI and CIRE. For regressions on orchard scale orchard averages of the tree height, width in the tree row, width across the tree row, tree volume, FI and of the various leaf area indices, respectively, were used.

## 5.3 RESULTS AND DISCUSSION

Ground measured tree height, canopy width across the tree row and in the tree row, tree volume, FI and LAI (CP-LAI, Tr-LAI and OLAI), respectively, was compared to the multispectral drone image derived spectral bands, indices, tree geometric dimensions and infrared temperature from the thermal images using a simple linear regression, of which the coefficients of determination and Pearson

p-values were summarized in Appendix A: Tables 9-21. Results are firstly presented for linear regressions between data derived from drone images for a limited number of selected individual trees to individual tree data measured in orchards for a) orchards combined (young and full bearing, Appendix A: Table 9), b) per orchard (five surveys combined, Appendix A: Tables 10 and 11) and c) per survey per orchard (individual trees per survey combined, Appendix A: Tables 12-19). Secondly results are presented for linear regressions at orchard scale – i.e. orchard averaged values of all individual tree data derived from drone images compared to averaged ground measured tree dimensions, also for a) orchards combined (Appendix A: Table 20) and b) per orchard (five surveys combined, Appendix A: Table 21).

### 5.3.1 Individual tree level

If individual tree data of the five surveys for both sites are combined for the 2023/2024 season there were numerous significant correlations, but most of these relationships had poor coefficients of determination, i.e. between <0.0001 and 0.526 (Appendix A: Table 9). The tree height, canopy width across and in the tree row, tree volume, CP-LAI and Tr-LAI related best to drone image determined tree height ($R^2$ values between 0.09-0.53). Although FI had the best linear regression relationship with CVI ($R^2$ = 0.39), higher CVI values related to low FI values at the young orchard and vice versa at the full bearing orchard, resulting in a negative regression trend (data not shown). This reflected the greater sensitivity of CVI to chlorophyll compared to biomass, as CVI is more typically used to describe tree health and to identify nutrient deficiencies (Vincini and Frazzi, 2011).

Drone-derived variables that had significant linear regression relationships at a 5% significance level with all the tree geometric dimensions, FI and CP-LAI included the red spectral band, NDVI, RVI, CVI, drone-estimated tree height and volume (Appendix A: Table 9). Drone estimated tree height was also significantly related to Tr-LAI, but with a very low coefficient of determination (<0.09). The OLAI was not significantly related to any of the drone image-derived variables. The positive linear regression relationships between measured tree height, across row width, tree volume, FI and CP-LAI with drone (UAV) image-derived tree height for individual tree data of orchards combined are indicated in Figures 21-23. Actual tree volume related better to drone estimated tree height than to drone estimated tree volume (Figure 22) even when a non-linear trend was fitted to the latter data ($R^2$ = 0.22).

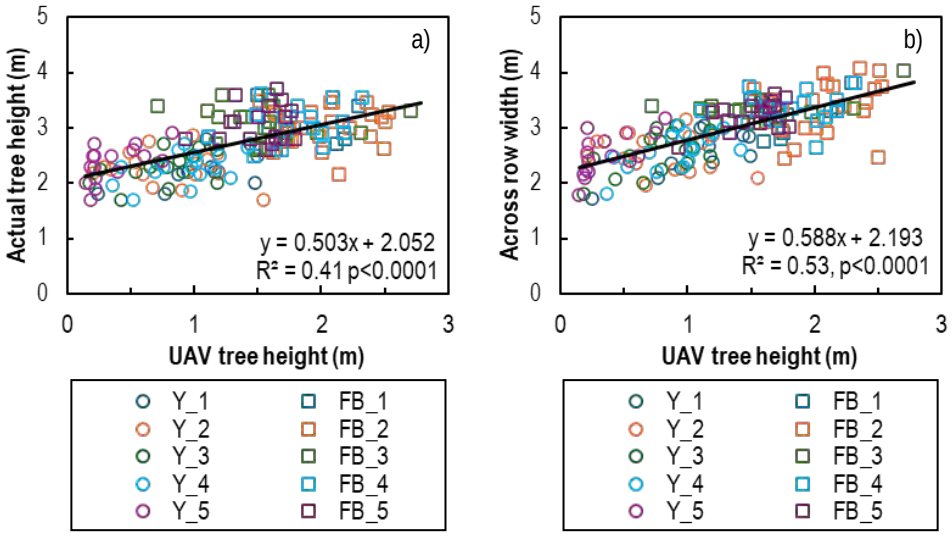


Figure 21. Comparison of linear regression relationships of a) actual tree height and b) across row canopy width with tree height derived from images of five drone (UAV) surveys conducted during 2023/2024 on young (Y) and full bearing (FB) cultivar 'Wonderful' pomegranate trees

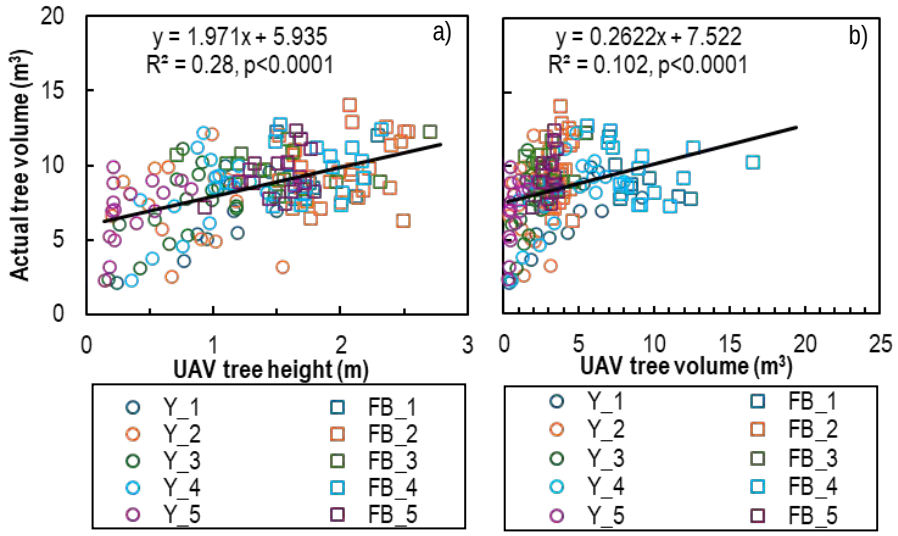


Figure 22. Comparison of linear regression relationships between actual tree volume with a) tree height and b) volume derived from images of five drone (UAV) surveys conducted during 2023/2024 on young (Y) and full bearing (FB) cultivar 'Wonderful' pomegranate trees

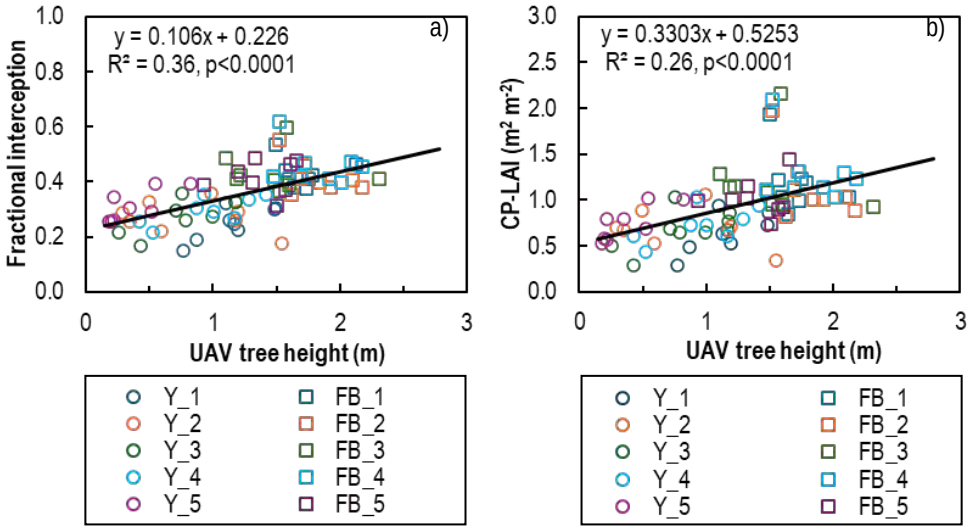


Figure 23. Comparison of linear regression relationships of a) fractional light interception and b) Accupar LP-80 modelled leaf area index (CP-LAI), respectively, with tree height derived from images of five drone (UAV) surveys conducted during 2023/2024 on young (Y) and full bearing (FB) cultivar 'Wonderful' pomegranate trees

At site level, tree height, FI and the three LAI versions were not significantly related at a 5% significance level to any of the drone image-derived variables (Appendix A: Tables 10 and 11). The FI was thought to be related to NDVI at a 10% significance level ($p = 0.089$), with a very poor coefficient of determination ($R^2 = 0.07$). Drone estimated tree height was significantly related to across tree row canopy width at both sites and in the tree row canopy width and tree volume at the young orchard, with $R^2$-values ranging from 0.079 to 0.138. Drone estimated canopy volume was significantly but poorly correlated with tree row canopy width, in the tree row canopy width and tree volume, only at the young orchard ($R^2$-values between 0.126 and 0.15).

At survey level most of the coefficients of determination at a 5% significance level were low and ranged from 0.255 to 0.662 for across row canopy width, 0.275 to 0.78 for in row canopy width (Appendix A: Tables 12 and 13), 0.25 to 0.481 for tree height, 0.241 to 0.645 for tree volume (Appendix A: Tables 14 and 15), 0.527 to 0.867 for FI and 0.516 to 0.818 for CP-LAI (Appendix A: Tables 16 and 17), 0.507 to 0.845 for Tr-LAI and 0.507 to 0.824 for OLAI (Appendix A: Tables 18 and 19). For the young orchard (Avontuur), not one of

the drone-derived spectral bands or indices was consistently significantly correlated to the various tree canopy measurements, FI or LAI over all five surveys. However, drone-estimated tree height and volume had significant regression relationships for all surveys except the one in December 2023 with across and within row canopy width ($p < 0.01$, Appendix A: Tables 12 and 13) and FI ($p < 0.05$, Appendix A: Tables 16 and 17).

Several drone image-derived indices (NDVI, NDRE, GNDVI, RVI, CVI, CIRE) had significant linear regression relationships with across-row canopy width, in-row canopy width and tree volume during December 2023, with $R^2$-values ranging between 0.255 and 0.553 (Appendix A: Tables 12-15). For this survey, the best statistically significant relationships across row canopy width, in row canopy width and tree volume, respectively, was with CVI and the $R^2$-values were 0.553, 0.465; 0.505. There were no significant statistical relationships of any of the drone image-derived spectral bands or indices with FI for December 2023 (Appendix A: Tables 16 and 17). The regression relationships between in row canopy width and drone image derived tree height or volume for the last survey in April 2024 were significant only at a 10% significance level ($p=0.095$, Appendix A: Table 13), whereas that between measured tree volume and these variables were just outside the 5% significance level ($p=0.052$, Appendix A: Table 15). If the 10% level of significance (which is more representative of natural variability in agricultural plots) is accepted, in row canopy width and measured tree volume can be estimated from drone estimated tree height and volume except for December 2023.

If this lower level of accuracy is acceptable, measured tree height can also be estimated for all surveys except December from drone estimated tree height, given that the p-values for the linear regression relationships ranged from 0.018 to 0.079 (Appendix A: Table 15). Actual tree height can also be estimated with greater accuracy using RedEdge from January until April (survey 3-5) or the red spectral band early (October, survey 1) or later (February, April, surveys 4 and 5) in the season. Compared to using drone estimated height and volume to obtain FI, the latter can also be estimated with greater accuracy early in the season (October) using the red, blue and green spectral bands, before harvest in February using RedEdge and in April after harvest using the green spectral band or CVI index (Appendix A: Tables 16 and 17). The drawback is that the latter relationships were not consistent over the season.

There were significant linear regression relationships between CP-LAI, Tr-Lai and OLAI, respectively, and the green spectral band for the first (beginning of the season), fourth (before harvest) and fifth (after harvest) survey ($R^2$ values between 0.52 and 0.73, 0.59 and 0.63, 0.53 and 0.7, respectively, Appendix A: Tables 16-19). In addition, CP-LAI related significantly during the first and fourth surveys to RedEdge ($R^2$ = 0.516 and 0.818), whereas Tr-LAI and OLAI were only related significantly at the 5% significance level during the fourth survey ($R^2$ values 0.845 and 0.824, respectively). At a 10% significance level, Tr-LAI and OLAI were significantly related to RedEdge during three surveys (surveys 1, 3 and 4, Appendix A: Table 19) and CP-LAI during four surveys (surveys 1, 3-5, Appendix A: Table 17). The CP-LAI related significantly at a 5% significance level to drone estimated tree height only during the last survey (Appendix A: Table 17), whereas Tr-LAI and OLAI related significantly during the first and last survey ($R^2$-values > 0.5, Appendix A: Table 19). At a 10% significance level, Tr-LAI related significantly to drone estimated tree height during four surveys ($R^2$-values 0.397 - 0.6) and CP-LAI and OLAI only during Surveys 1, 3 and 5 (Appendix A: Tables 17 and 19). Drone estimated tree volume related at a 5% significance level to CP-LAI, Tr-LAI, and OLAI only during the first and the last survey (Appendix A: Tables 16-19). At a 10% significance level, drone-estimated tree volume was related significantly to all these variables during four surveys (Surveys 1, 3-5) with $R^2$ values ranging between 0.39 and 0.62. The CP-LAI, Tr-LAI and OLAI can also be estimated from the blue ($R^2$ = 0.68, 0.66,0.67) or red ($R^2$ = 0.8, 0.77, 0.8) spectral bands early in the season (October) or late in the season from GNDVI ($R^2$ = 0.56, 0.51,0.55) or CVI ($R^2$=0.69, 0.63, 0.69).

For the full bearing trees at Welgemoed at survey level, the coefficients of determination for across-row canopy width ranged between 0.27 and 0.42 (Appendix A: Table 12). Across row canopy width can be estimated at a 5% significance level from linear regression relationships with the blue spectral band in survey 1 and from drone-estimated height or volume in surveys 3 and 5. Tree height was only significantly correlated with TIR during survey 1 in October 2023 ($R^2$ = 0.48) and CVI during survey 4 before harvest ($R^2$ = 0.26) (Appendix A: Table 14). Likewise, tree volume was poorly ($R^2$ = 0.24) but significantly correlated at the 5% significance level only with the green spectral band during survey 4 (Appendix A: Tables 14 and 15). At a 10% significance level, tree volume was also related to drone estimated tree volume during the first survey and to RedEdge and CVI during the fourth survey (Appendix A: Table 15). The FI rendered a significant correlation only to TIR during survey 4 ($R^2$ = 0.59) (Appendix A: Table 16). The CP-LAI, Tr-LAI and OLAI related significantly at a 5% significance level to drone estimated tree volume during survey 1 ($R^2$ = 0.65) and to TIR during survey 4 ($R^2$ = 0.68) (Appendix A: Tables 16 and 18). At a 10% significance level CP-LAI related to both these drone-derived variables during the first and the fourth survey ($R^2$ values between 0.39 and 0.65) (Appendix A: Tables 16 and 17).

### 5.3.2 Orchard level

Simple linear regressions of orchard-averaged measured tree variables with orchard-averaged multispectral drone image estimated variables for orchards combined resulted in significant regression relationships at a 5% significance level for all ground-measured tree-related variables, except for OLAI, with drone-estimated tree height (Appendix A: Table 20, Figure 24). Measured tree height, across row canopy width, tree volume, FI, CP-LAI and OLAI related significantly to CVI at a 5% significance level, but except for FI, the regression relationships were poorer compared to those with drone-estimated tree height (Figure 25). Ceptometer LAI was the only ground-measured tree variable that related significantly to drone-estimated tree volume, with an $R^2$ of 0.4. According to Figure 24, tree height, across row width and volume, FI and CP-LAI related positively to and can be estimated relatively well from the orchard averaged values of drone estimated tree height (Figure 24a-e). However, Tr-LAI had a poorer regression relationship and decreased with increasing drone-estimated tree height (Figure 24f). The negative relationship is due to the young orchard having higher actual leaf area coverage per canopy area than the full-bearing orchard, despite the latter having taller trees. Although one would expect a larger leaf area for taller trees with larger volume, the training and pruning, wood fraction, as well as the vigour of trees, may affect the resultant leaf area per tree volume. The LAI modelled from the Accupar LP-80 ceptometer (Figure 24d) is based on FI measurements representing the allocated area per tree. The canopy area-based LAI was derived from a calibration of CP-LAI data with actual measured leaf and canopy areas (data not shown). Based on these results, drone-derived tree height is not recommended for the estimation of Tr-LAI for other pomegranate orchards. The standard error of the estimate for the regression relationships of tree height and FI with drone estimated tree height was 0.193 m and 0.045, respectively, and for FI with CVI, 0.042. It must be noted, though, that for most of the regression relationships between tree canopy properties and drone-estimated tree height, there was a lack of continuous data along the trendline (Figure 24).

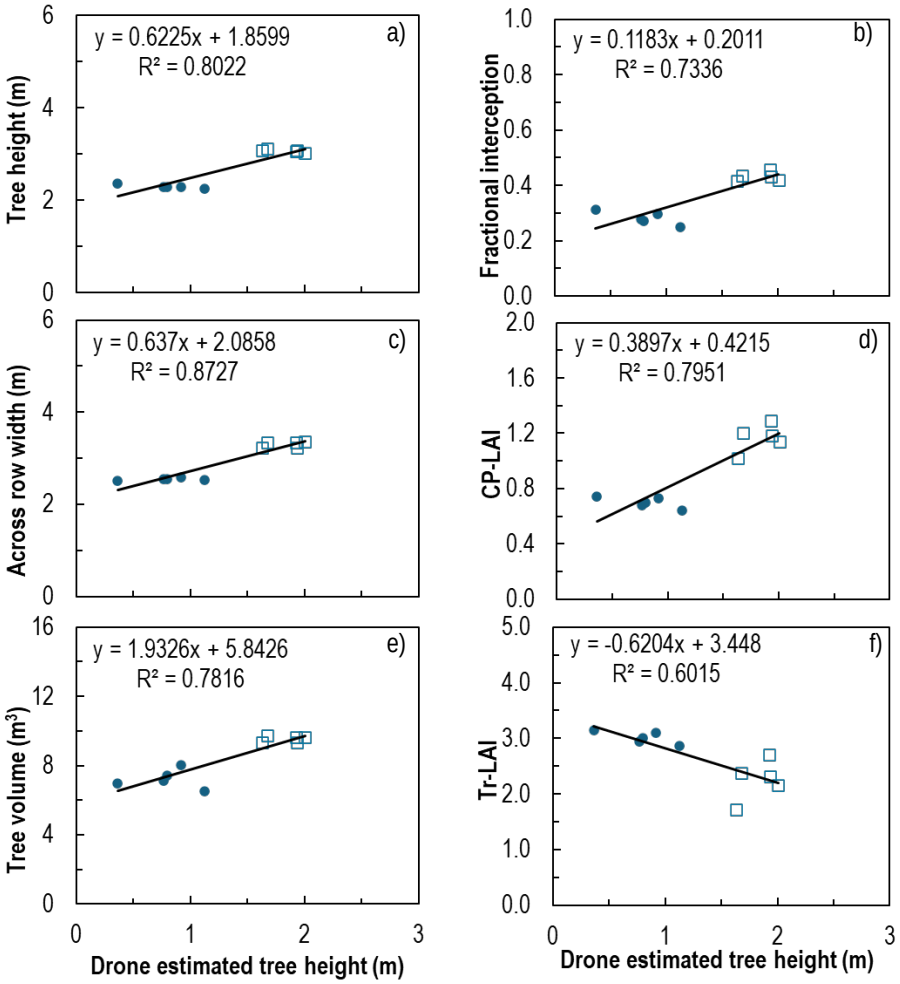


Figure 24. Simple linear regressions of orchard averaged measured a) tree height, b) fractional light interception, c) across row canopy width, d) ceptometer leaf area index (CP-LAI), e) calculated tree volume and f) tree canopy area based leaf area index (Tr-LAI) with orchard averaged multispectral drone image estimated tree height. Data are from drone surveys and field measurements conducted for young (circle markers) and full-bearing (square markers) cultivar 'Wonderful' pomegranate orchards over the 2023/2024 season.

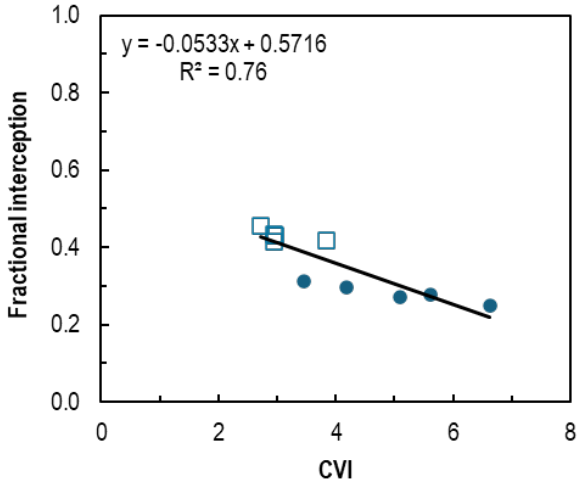


Figure 25. Simple linear regression of orchard averaged Accupar LP-80 ceptometer measured fractional light interception with averaged multispectral drone image estimated tree height. Data are from drone surveys and field measurements for young and full bearing cultivar 'Wonderful' pomegranate orchards conducted over the 2023/2024 season.

With regard to orchard averaged tree canopy dimensions per orchard, tree height of the young orchard related significantly at a 5% significance level to all the drone-derived variables except for NIR, CVI, drone estimated tree volume and TIR (Appendix A: Table 21). The coefficients of determination ranged between 0.89 and 0.993. Tree height was the best and increased with blue spectral band reflectance (Figure 26a), whereas tree height decreased with NDVI (Figure 26d). The standard error of the estimate for tree height with the blue spectral band was small, namely 0.004 m. It increased to 0.013 m if NDVI was used to estimate tree height. The negative trend with NDVI can partially be explained by a decrease in NIR reflection measured in April after harvest (Figure 26c), while red reflectance simultaneously increased substantially compared to summer (Figure 26b), most likely due to the aging of leaves.

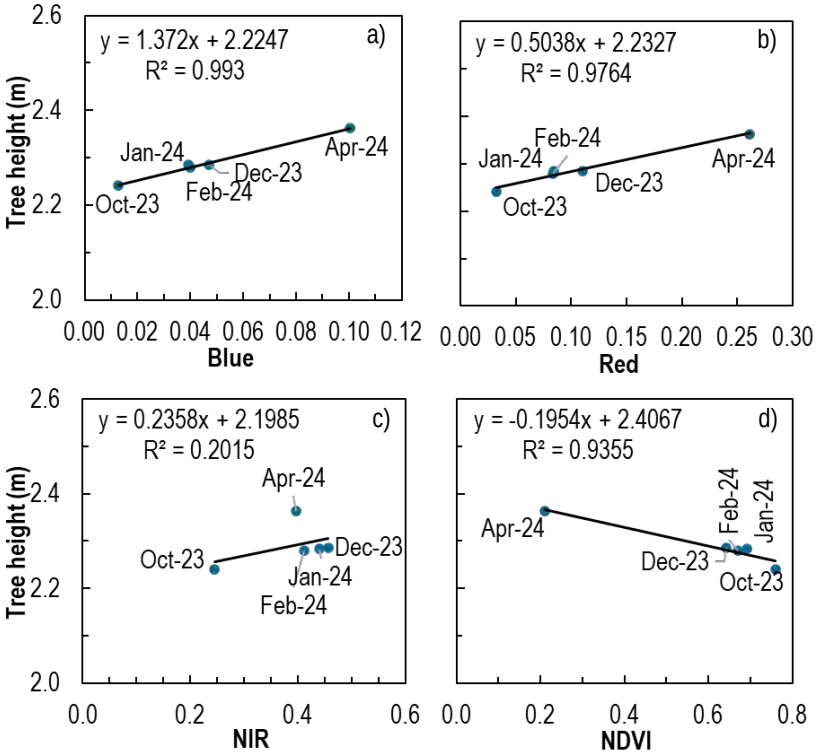


Figure 26. Simple linear regressions of orchard averaged measured tree height with orchard averaged multispectral drone image derived blue (a), red (b) and near-infrared (NIR) spectral band reflectance and the NDVI (d, Normalized Difference Vegetation Index), respectively. Data are averages of field measurements conducted during five drone surveys for the young cultivar 'Wonderful' pomegranate orchard over the 2023/2024 season.

The FI and various measured LAI variables were related at a 5% significance level only to CVI, with coefficients of determination exceeding 0.94 (Appendix A: Table 21). The linear regression trends for all variables were negative and FI and the LAI variables all increased with decreasing CVI as the season progressed from October to April (Figure 27). The CVI, indicative of tree canopy chlorophyll content (Vincini and Frazzi, 2011), is calculated from the NIR, red and green spectral bands (refer Table 5). The negative trend of FI with CVI may partially be related to the tendency of NIR to decrease from December until April (Figure 28a), whereas FI in general tended to increase over the whole season with reflectance of the green and red spectral bands, albeit at a lower significance level (Appendix A: Table 21, Figure 28b and c). Factors that may affect the orchard reflectance profile include red flowers in October and the brown paper bags used to cover developing fruit to prevent sunburn in the period from December until shortly before harvest in March. The standard error of the estimate for FI and Tr-LAI with CVI was 0.007 and 0.015, respectively. This error for Tr-LAI from the young orchard data is much smaller compared to the standard error of the estimate of 0.316 obtained for estimates from the regression relationship of Tr-LAI with drone-estimated tree height for data of the two orchards combined. For the regression relationship between OLAI and CVI, the standard error of the estimate was 0.01.

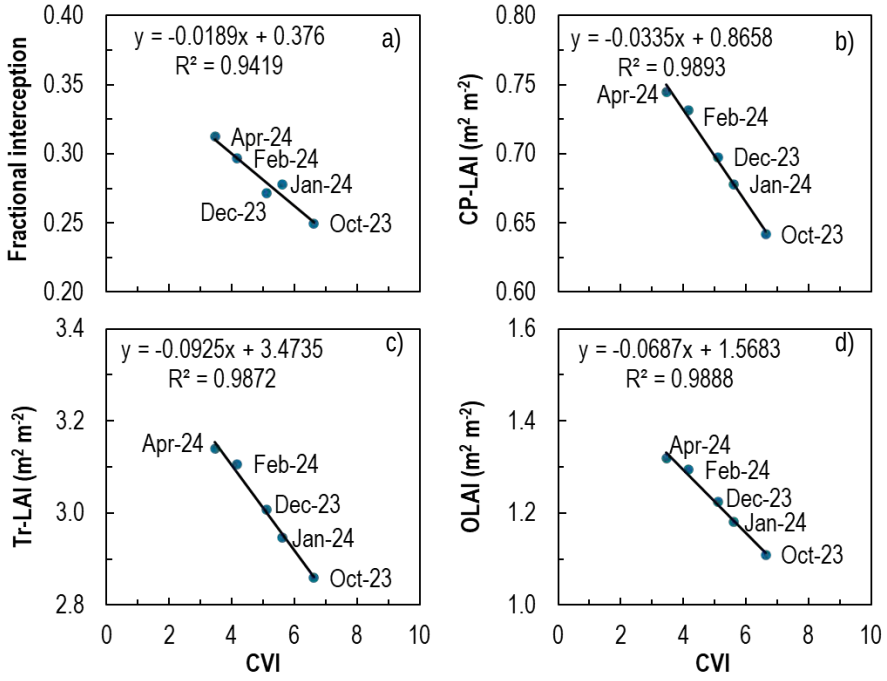


Figure 27. Simple linear regressions of orchard averaged measured a) fractional light interception, b) ceptometer leaf area index (CP-LAI), c) tree canopy area based leaf area index (Tr-LAI) and f) orchard leaf area index (OLAI) with orchard averaged multispectral drone image estimated chlorophyll vegetation index (CVI). Data are from drone surveys and field measurements conducted for the young cultivar 'Wonderful' pomegranate orchard over the 2023/2024 season.

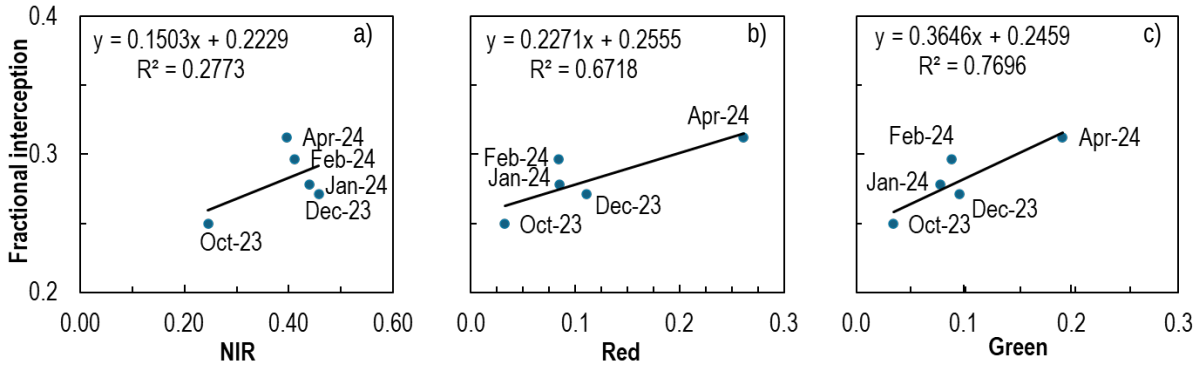


Figure 28. Simple linear regressions of orchard averaged measured fractional interception (n=8) with orchard averaged multispectral drone image derived near-infrared (a, NIR), red (b) and green (c) spectral band reflectance, respectively. Data are from field measurements conducted during five drone surveys for the young cultivar 'Wonderful' pomegranate orchard over the 2023/2024 season.

Another option could be to estimate FI and OLAI from the green or RedEdge spectral bands. The p-values for FI just exceeded 0.05, whereas that for OLAI was about 0.08 (Appendix A: Table 21). Their coefficients of determination, however, were not as high as that for CVI, but they had a positive regression relationship with FI and OLAI, increasing with RedEdge reflection from the beginning towards the end of the season (Figure 28C, Figure 29). The standard error of the estimate for FI and OLAI from RedEdge or green spectral reflectance was similar and amounted to 0.013 and 0.054 for the two respective variables.

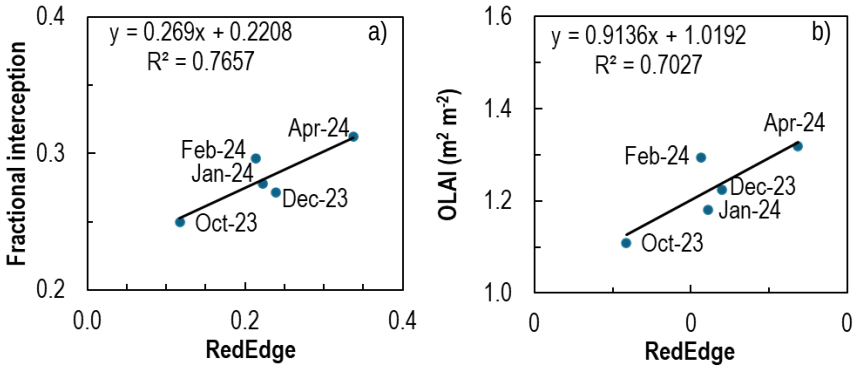


Figure 29. Simple linear regressions of orchard averaged measured a) fractional interception (n=8) and b) orchard leaf area index (OLAI) with orchard averaged multispectral drone image derived RedEdge spectral band reflectance. Data are from field measurements conducted during five drone surveys for the young cultivar 'Wonderful' pomegranate orchard over the 2023/2024 season.

The FI and various LAI variables were not significantly related to NDVI even at a 10% significance level, with $R^2$ values that ranged between 0.531 and 0.635 (Appendix A: Table 21).The poor and/ or negative regression relationships of NDVI with tree FI (similar to the relationship of tree height with NDVI, Figure 26d) is in contrast with research of Zhang et al. (2017) who concluded – based on data for individual trees – that NDVI is a robust indicator of pomegranate tree canopy ground cover. Some of the variability in our results may be related to seasonal effects induced by phenological changes, while the saturation of vegetation indices could have been affected by soil background reflectance, leaf properties (e.g. leaf chlorophyll and dry matter content) and canopy structures (Tian et al., 2025). Using data of all surveyed trees for each of the five surveys, tree height was estimated for the young orchard from the regression relationship with the blue spectral band reflectance (Figure 26a) and FI and OLAI from the regression relationships with RedEdge spectral band reflectance (Table 7, Figure 29). Mean tree height increased over the season from 2.24 m at the end of October 2023 to 2.33 m by mid-April 2024. Minimum and maximum tree height at the end of the season were 2.25 m and 2.44 m, respectively. Mean FI increased from 0.25 to 0.29 over the season, with a minimum of 0.24 and a maximum of 0.34. Mean OLAI increased from 1.13 to 1.26 $m^2$ $m^{-2}$ from end of October until mid-April, with a minimum of 1.08 and a maximum of 1.42 $m^2$ $m^{-2}$, respectively, over the season. The minimum values for FI and OLAI estimated from the regression relationship with CVI were negative for April (data not shown), which indicated that additional data should be collected to enlarge the range of data collected and to verify the regression relationships. According to Gao et al. (2024), the separation of chlorophyll and LAI has been a difficult problem in the field of quantitative remote sensing.

Table 7. Maximum (Max), minimum (Min) and mean (±standard deviation or STDev) of tree specific height, fractional light interception (FI) and orchard leaf area index (OLAI) estimated from the regression relationships of height with the blue and FI and OLAI with RedEdge spectral band reflectance derived from drone imagery for the five-year old cultivar 'Wonderful' pomegranate orchard for selected dates during the 2023/24 season

| Date | Tree height (m) | | | | Fractional light interception | | | | OLAI ($m^2$ $m^{-2}$) | | | | n |
|---|---|---|---|---|---|---|---|---|---|---|---|---|---|
| | Min | Max | Mean | STDev | Min | Max | Mean | STDev | Min | Max | Mean | STDev | |
| 31/10/2023 | 2.24 | 2.26 | 2.24 | 0.001 | 0.24 | 0.27 | 0.25 | 0.002 | 1.10 | 1.17 | 1.13 | 0.006 | 4829 |
| 15/12/2023* | 2.25 | 2.33 | 2.26 | 0.004 | 0.25 | 0.31 | 0.27 | 0.004 | 1.13 | 1.32 | 1.20 | 0.014 | 4946 |
| 12/01/2024 | 2.25 | 2.29 | 2.26 | 0.004 | 0.26 | 0.30 | 0.27 | 0.004 | 1.15 | 1.28 | 1.19 | 0.015 | 4921 |
| 22/02/2024 | 2.24 | 2.45 | 2.29 | 0.023 | 0.24 | 0.34 | 0.28 | 0.009 | 1.08 | 1.42 | 1.23 | 0.032 | 5173 |
| 16/04/2024 | 2.25 | 2.44 | 2.33 | 0.031 | 0.25 | 0.33 | 0.29 | 0.010 | 1.13 | 1.39 | 1.26 | 0.034 | 5173 |

For the full bearing orchard only orchard averaged across row canopy width related significantly at a 5% level to orchard averaged TIR (Appendix A: Table 21, Figure 29).

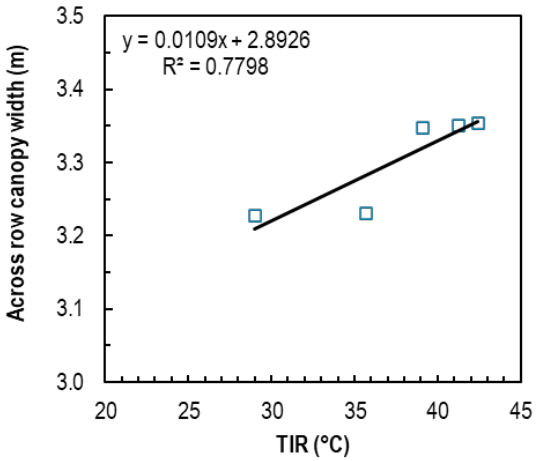


Figure 30. Simple linear regression of orchard averaged measured across row canopy width with orchard averaged thermal drone image derived thermal infrared temperature for the full bearing cultivar 'Wonderful' pomegranate orchard over the 2023/2024 season.

## 5.4 CONCLUSION

If both levels of statistical significance and all five surveys are considered for simple linear regressions of selected individual trees, drone image estimated tree height and volume appear to be the variables that relate most frequently to the ground-measured tree variables, especially at the young orchard. There were no good, significant regression relationships between the drone image-derived variables and in-field measured tree properties for the full bearing orchard, probably due to a lack of variation in the properties of the trees required for strong linear regression relationships. At the individual tree level, for data of orchards combined, drone estimated tree height had significant regression relationships with all tree canopy properties except for OLAI ($R^2$ values between 0.09 and 0.53). The coefficients of determination for all measured canopy properties with drone image-derived tree height were higher than those with each of all the other drone image-derived variables, except for FI, which had a better regression relationship with CVI.

At orchard level, for data from orchards combined, orchard-averaged tree height, across row width, tree volume, FI and CP-LAI related relatively well to orchard-averaged drone-estimated tree height, with $R^2$-values ranging between 0.73 and 0.87. Reliability of these regression models could be improved by the collection of more data to address a paucity of data points existing in the mid-range between that available for the young and the full bearing orchard of the current research. Unexpectedly, there were no significant linear regression relationships at a 95% confidence level of the orchard averaged canopy dimensions, FI or LAI variables with NDVI, except for tree height of the young orchard, which increased with decreasing NDVI. The variability in NDVI was partially ascribed to a decrease in NIR from summer to fall, simultaneous with a general increase in red spectral band reflectance over the season.

Using orchard-averaged ground-measured and drone image-derived data improved the regression relationships considerably, especially for the young orchard considered on its own. For the young orchard, the orchard averaged blue spectral band reflectance was the best suited to estimate the orchard averaged tree height. Although CVI had the best regression relationship with FI and the LAI variables ($R^2$ values > 0.94), it appeared to be more sensitive to chlorophyll changes in the canopy than to changes in FI and LAI, with the latter variables increasing with decreasing CVI. Although the regression relationships of FI and LAI with the RedEdge spectral band had $R^2$ values of only 0.77 and 0.7, respectively, it was due to the positive regression relationships preferred to provide FI and OLAI estimates. Tree height, FI and OLAI are important input parameters to estimate crop coefficients as an alternative if crop coefficients cannot be acquired directly from regression relationships with drone image-derived variables. The full bearing orchard only had one significant regression relationship at a 5% significance level, i.e., between orchard averaged across tree row canopy width and TIR ($R^2$ =0.78). Poor relationships of orchard averaged FI and LAI variables with NDVI were perplexing. Some of the variability in

NDVI may be related to seasonal effects induced by phenological changes, while the saturation of vegetation indices could have been affected by changes in soil background reflectance, leaf properties and canopy structures over the season.

A collection of additional data sets representative of more growing seasons and/or more pomegranate orchards varying in canopy cover is required to validate or improve regression relationships between the drone image-derived spectral bands, indices, tree geometric dimensions and thermal infrared temperature with tree height, FI and LAI. It is recommended to collect in the future more detailed information on soil background reflectance, leaf and tree structure properties over the growing season to assist in the identification of the most appropriate vegetation indices to estimate tree height, FI and LAI. The fusion of morphological (canopy height, canopy cover and canopy volume) and vegetation indices for more accurate estimation of LAI over the season can also be investigated.

# CHAPTER 6: COMPARISON OF MULTISPECTRAL IMAGE SPECTRAL BANDS, VEGETATION INDICES AND THERMAL INFRARED TEMPERATURE TO IN-FIELD MEASURED TREE PHYSIOLOGICAL PARAMETERS

## 6.1 INTRODUCTION

To schedule irrigation properly, information is required on when, where and how much to irrigate. The decision of when to irrigate is generally based on soil water depletion levels in the root zone or on thermal-based stress indices (O'Shaughnessy and Rush, 2012). The thresholds triggering irrigation are usually correlated to plant physiological measurements such as stem water potential (SWP) and leaf stomatal conductance ($g_s$), which indicate actual tree water status and plant stress levels (Zhang et al., 2021). Liu et al. (2025) managed to estimate citrus $g_s$ from multimodal information derived from a UAV combined with an optimized machine learning algorithm, providing valuable support for precision irrigation and field management decisions. The objective of this chapter is to identify the drone image-derived spectral bands and vegetation indices that present the highest correlation for the estimation of SWP, leaf chlorophyll content and selected plant physiological variables for individual pomegranate trees and on orchard scale.

## 6.2 METHODOLOGY

In 2023/2024 five drone surveys were conducted using a multispectral DJI Technology© Matrice 600 drone equipped with a MicaSense Red-Edge-MX multispectral camera and Zenmuse-XT thermal camera at the young (Avontuur, 33°07'29.7"S; 18°56'08.8"E) and full bearing (Welgemoed, 33°35'18.3048"S; 18°59'19.302"E) cv. 'Wonderful' pomegranate orchards (Table 2, Figure 1). The surveys were completed at solar noon (±1 hour) during canopy development about two months after bud break (October 2023), after most fruit set was completed (December 2023), at full canopy (January 2024), during ripening (February 2024) and after harvest (April 2024). Stem water potential was measured on the day of the survey, around 12h00 on six trees nearby and of comparable size to the two soil water balance and/ or four sap flow trees. Two leaves per tree were enclosed in aluminium foil bags at least two hours before measurement and SWP was determined using a pressure chamber (PMS Model 1505D-EXP, PMS Instrument Company, Albany, USA).

Chlorophyll concentration was monitored during survey 1 at four sap flow, two soil water balance and five growth monitoring trees on ten leaves per tree representing different canopy positions (bottom to top, both sides of the tree row) using a SPAD-502 chlorophyll meter (Konica–Minolta, Inc., Osaka, Japan). During surveys 3-5 chlorophyll content was also measured for the SWP trees. During surveys 2-5, physiological measurements were also conducted on two leaves per tree for the trees selected for SWP measurement at 10h00, 12h00 and 14h00 using a LI-COR LI6400XT infrared gas analyser (Lincoln, Nebraska, USA). The physiological variables monitored included net carbon dioxide assimilation rate ($A_n$), stomatal conductance ($g_s$) and leaf transpiration rate ($Tr_L$).

Multispectral and thermal drone images were processed using Pix4D mapper software (Version 4.8.4). Pixels were radiometrically corrected by using a calibration reflectance panel and downwelling light sensor measurements of irradiance. Simple linear regressions were conducted between all data and indices derived from drone images for selected individual trees to individual tree data measured in orchards. Regressions were also conducted at orchard scale – i.e. orchard averaged values of all individual tree data derived from drone images compared to averaged ground measured tree SWP, leaf chlorophyll content and physiological variables as measured by the LI6400XT infrared gas analyser. Regression models were considered to be significant at 95% level of confidence (p=0.05). Data variables derived from the drone images included reflectance of the blue, green, red, NIR, RedEdge and TIR bands. The indices calculated from the drone image data included, in addition to NDVI, NDRE, GNDVI, RVI, CVI and CIRE. For regressions on orchard scale orchard averages of midday SWP, leaf chlorophyll content as well as $A_n$, $g_s$, and $Tr_L$, respectively, were used. Regressions for the physiological variables were done for measurements conducted at 10h00, 12h00 and 14h00, depending on data availability.

## 6.3 RESULTS AND DISCUSSION

Linear regression results are presented in Appendix B at the individual tree level for orchards combined (Tables 22 and 23), for the young and full bearing orchards separately (Tables 24-27) and then per survey per orchard (Table 28). Orchard averaged data regression results are presented for both orchards combined in Tables 29 and 30 and for orchards individually in Tables 31-34.

### 6.3.1 Individual tree level

For orchards combined, midday SWP did not relate significantly to any of the drone image-derived variables at a 95% confidence level (Appendix B: Tables 22 and 23). Chlorophyll content related significantly to CVI, and very poorly, but significantly at a 95% confidence level to CIRE ($R^2$ <0.04) and GNDVI ($R^2$ < 0.05). The chlorophyll content tended to increase with CVI despite a lot of variation from data points for the young orchard from survey 4 in February before harvest (Figure 31). The CVI and chlorophyll content tended to be higher at the young compared to the full-baring orchard, which agrees with in-field observations that leaves of the young orchard were greener in comparison to those of the full-baring orchard. The $A_n$ related the best at 10h00 to NIR reflectance and CVI, with $R^2$ values being less than 0.57 (Appendix B: Tables 22 and 23). The $A_n$ tended to increase with NIR spectral band reflectance (Figure 32a).

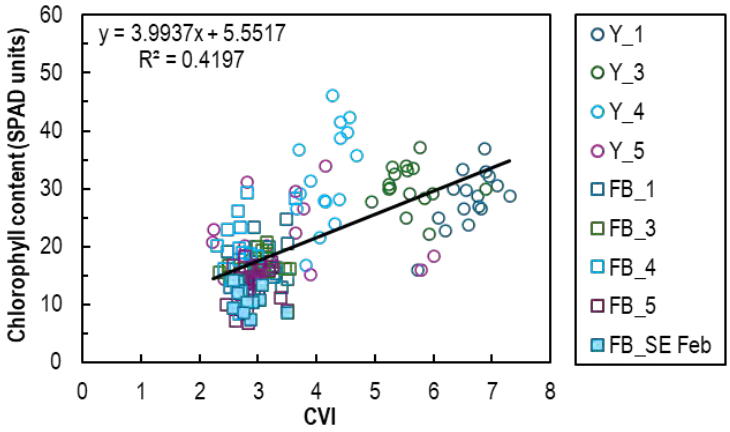


Figure 31. Simple linear regression of chlorophyll content (measured using a SPAD 502 meter) with Chlorophyll Vegetation Index (CVI) for individual tree data available from drone surveys and field measurements conducted for young and full bearing cultivar 'Wonderful' pomegranate orchards over the 2023/2024 season. FB_SE Feb refers to a stress experiment conducted on selected trees in February 2024.

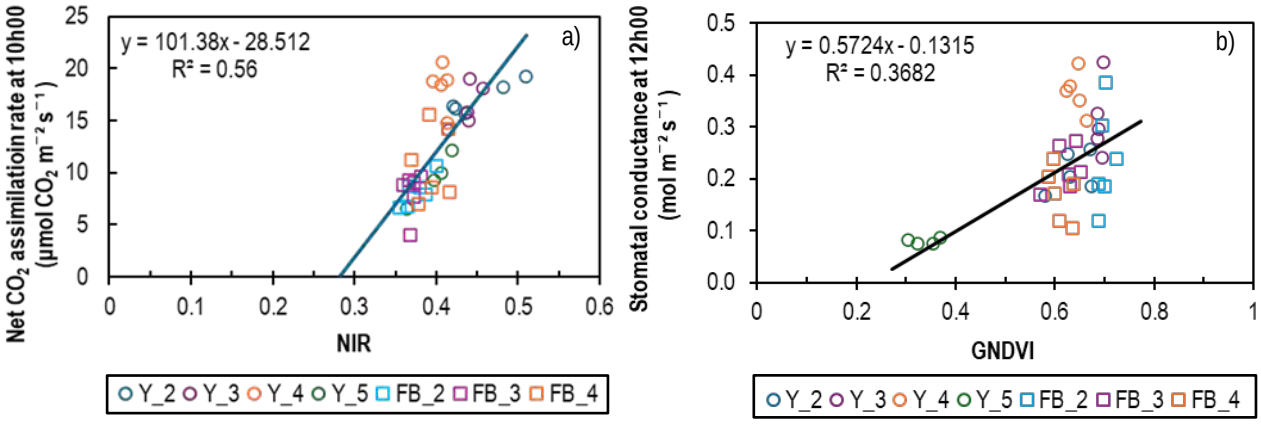


Figure 32. Simple linear regressions of a) net carbon dioxide ($CO_2$) assimilation rate at 10h00 to the drone image derived near-infrared (NIR) spectral band and b) stomatal conductance at 12h00 to the Green Normalized Difference Vegetation Index (GNDVI) for individual tree data available from selected drone surveys and field measurements conducted for young (Y) and full bearing (FB) cultivar 'Wonderful' pomegranate orchards over the 2023/2024 season

At 12h00, $A_n$ related somewhat poorer, but also significantly to NIR ($R^2$ = 0.134) and CVI ($R^2$ = 0.189), whereas it was not related to any of the drone image-derived variables at 14h00 (Appendix B: Tables 22 and 23). Stomatal conductance was related during all three time slots significantly and the best to GNDVI ($R^2$ values of between 0.318 - 0.368), NDRE ($R^2$ values of between 0.273 and 0.34) and CIRE ($R^2$ values of between 0.252 and 0.349). It was during all three time slots to a lesser extent, but also significantly, related to the blue, green, red and RedEdge spectral bands and to NDVI, CVI and TIR. The $g_s$ was also significantly related to NIR at 12h00 and 14h00 and to RVI at 10h00 and 12h00. If all time slots are considered, the best regression relationship was between $g_s$ at 12h00 and GNDVI. Although $g_s$ had a positive regression relationship with GNDVI, there was a paucity of data mid-range, and the regression model is therefore not very reliable (Figure 32b). Leaf transpiration rate was at the three time slots significantly related to almost all drone-derived variables, with $R^2$ values ranging between 0.239 and 0.584 (Appendix B: Tables 22 and 23). Exceptions were the NIR spectral band, which did not relate significantly to $Tr_L$ in any of the time slots and CVI, which was not related at 10h00 or 12h00. The best regression relationships were obtained for $Tr_L$ at 10h00 with RVI ($R^2$=0.584) and NDVI ($R^2$=0.582), respectively. Mid-range data for the $Tr_L$ and NDVI regression relationship were absent (data not shown), while the data points were distributed well along the trendline for the relationship between $Tr_L$ and RVI (Figure 33).

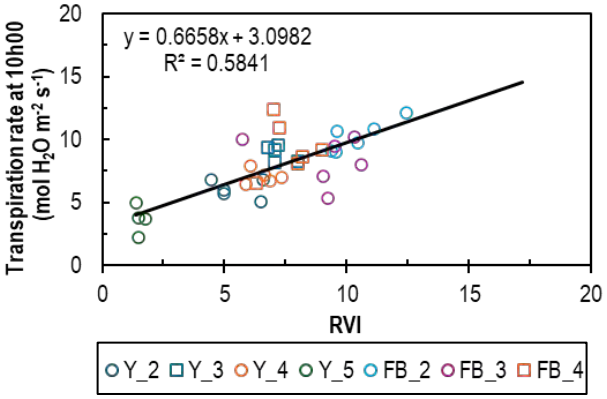


Figure 33. Simple linear regression of leaf transpiration rate with RVI for individual tree data available from selected drone surveys and field measurements conducted for young (Y) and full bearing (FB) cultivar 'Wonderful' pomegranate orchards over the 2023/2024 season

For the young orchard considered on its own, midday SWP had significant linear regression relationships at a 5% significance level with the blue, green, red, and RedEdge spectral bands, NDVI, NDRE, GNDVI and RVI (Appendix B: Tables 24 and 25). The coefficients of determination were low – probably due to lack of variability in SWP between trees irrigated similarly at the same site – and ranged between 0.173 and 0.267 (Appendix B: Table 24). The best regression relationship was with RVI (Figure 34), which has a good correlation to biomass and water content (refer Table 5). Stem water potential tended to decrease with increasing RVI.

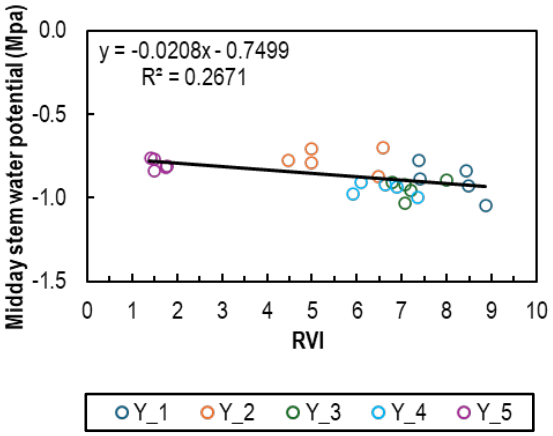


Figure 34. Simple linear regression of midday stem water potential with drone image derived ratio vegetation index (RVI) for data available from drone surveys and field measurements conducted for young cultivar 'Wonderful' pomegranate orchard over the 2023/2024 season

Chlorophyll content related significantly at a 95% confidence level with all the drone derived variables except for NIR, with $R^2$ values ranging between 0.075 and 0.282 (Appendix B: Tables 24 and 25). It related the best to and tended to increase with CIRE, having a coefficient of determination of 0.282 (Figure 35). However, lower chlorophyll content data collected during survey 5 in April were grouped at the one end of the regression line and the data for October, January and February at the other end (surveys 1, 3 and 4). More data will have to be collected to confirm this regression relationship.

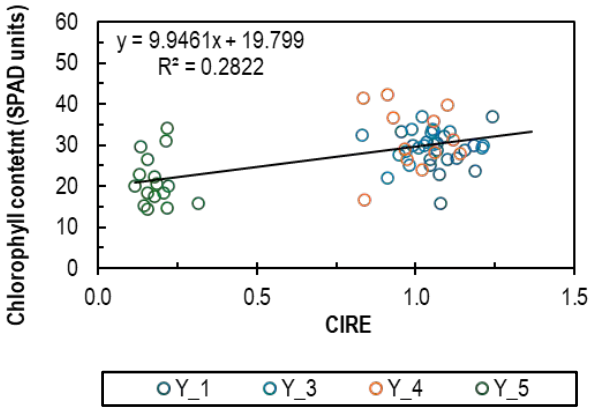


Figure 35. Simple linear regression of chlorophyll content (measured using a SPAD 502 meter) with CVI (chlorophyll vegetation index) for data available from drone surveys and field measurements conducted for young cultivar 'Wonderful' pomegranate orchard over the 2023/2024 season

The young orchard $A_n$ at 10h00 related significantly ($p < 0.05$) to all drone-derived variables, with the best relationships being with NDRE, CIRE, GNDVI and NDVI, with coefficients of determination of 0.703, 0.698, 0.667 and 657, respectively (Appendix B: Tables 24 and 25). At 12h00, $A_n$ related significantly to all drone variables except for NIR, CVI and TIR, with the best relationship with the blue and red spectral bands ($R^2$ values between 0.4 and 523). The significant linear regression relationships $A_n$ had at 10h00 with NDRE, CIRE, GNDVI and NDVI worsened significantly at 12h00. At 14h00, $A_n$ related significantly only to blue, red and RedEdge reflectance, with the best relationship with the latter ($R^2$=0.232, Appendix B: Table 24). If all time slots are considered for $A_n$, measurements at 10h00 had the best significant relationship with NDRE (Figure 36a). The $A_n$ at 10h00 ranged between 14.1 and 20.6 µmol $CO_2$ $m^{-2}$ $s^{-1}$ for surveys conducted from October until February and decreased by mid-April (survey 5) to between 6.6 and 12.1 µmol $CO_2$ $m^{-2}$ $s^{-1}$.

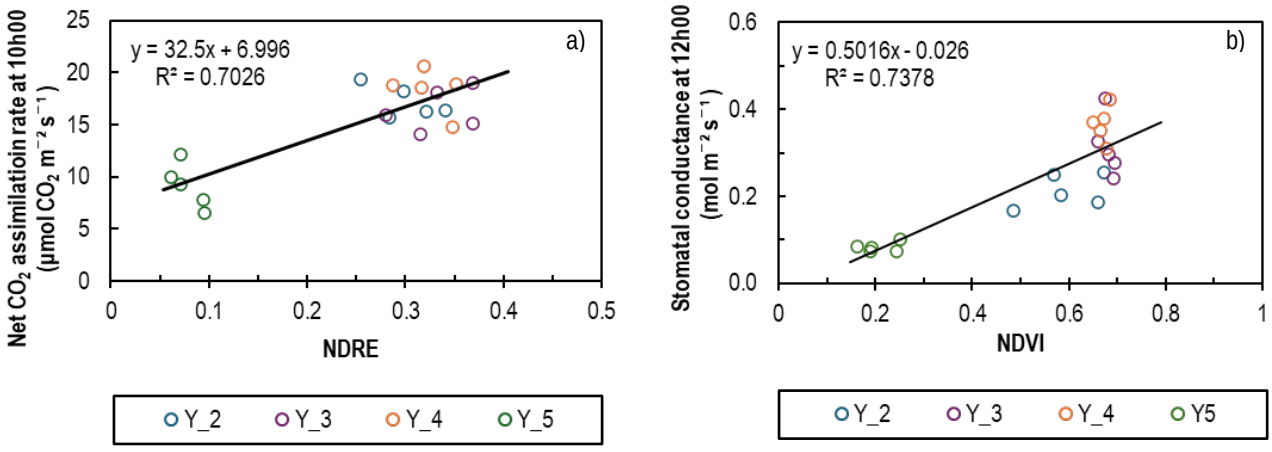


Figure 36. Simple linear regressions of a) net carbon-dioxide ($CO_2$) assimilation rate at 10h00 with drone image derived Normalized Difference Red Edge Index (NDRE) and b) stomatal conductance at 12h00 with Normalized Difference Vegetation Index (NDVI) for data available from midday drone surveys and field measurements conducted for young cultivar 'Wonderful' pomegranate orchards over the 2023/2024 season

The $g_s$ in all time slots were significantly related to all drone-derived variables except for NIR, which was not significant in any time slot (Appendix B: Table 25). The best relationship for $g_s$ at 10h00 was with RVI, NDVI and the green band reflectance with $R^2$ values

ranging between 0.6 and 0.65 (Appendix B: Table 24). At 12h00, the relationship for $g_s$ with NDVI and RVI improved with $R^2$ values increasing to around 0.73. However, $g_s$ at 12h00 related slightly better to the red spectral band ($R^2$=0.726) compared to green ($R^2$ = 0.683), whereas it was the other way round at 10h00. At 14h00, the drone-derived variables that related best to $g_s$ remained the same as at 12h00, but the coefficients of determination were lower compared to those at 12h00 (Appendix B: Table 24). If $g_s$ at all time slots are considered, $g_s$ at 12h00 had the best linear regression relationship with NDVI, and $g_s$ increased with NDVI (Figure 36b). Canopy NDVI previously showed a good correlation to leaf $g_s$ for several fruit tree species (Zhang et al., 2021). The individual tree midday $g_s$ reached a maximum of 0.425 mol $m^{-2}$ $s^{-1}$ mid-season and before harvest (surveys 3 and 4) and decreased to a minimum of 0.074 mol $m^{-2}$ $s^{-1}$ in April after harvest. Likewise, NDVI decreased from a maximum value of 0.68 mid-season (January 2024) to a minimum 0.16 in mid-April 2024. Similar to $g_s$, $Tr_L$ was significantly related to all drone-derived variables in all time slots except for NIR, which was not significant in any time slot (Appendix B: Table 24). The $T_{rL}$ related the best to RVI ($R^2$ values of 0.731-0.844), GNDVI ($R^2$ values of 0.698-0.851), NDRE ($R^2$ values of 0.673-0.866) and NDVI ($R^2$ values of 0.679-0.861), with the highest coefficients of determination concentrated around 12h00. Considering all time slots, the best regression relationship was between $Tr_L$_12 and NDRE (Figure 37). Leaf transpiration rate was distinctly lower in April (survey 5) compared to the rest of the season. The minimum and maximum leaf transpiration rates was 2.6 and 10.9 mol $H_2O$ $m^{-2}$ $s^{-1}$, respectively. The TIR related less well to $Tr_L$, but significantly at a 5% significance level with $R^2$ values ranging between 0.517 and 0.72 over the three timeslots (Appendix B: Table 24).

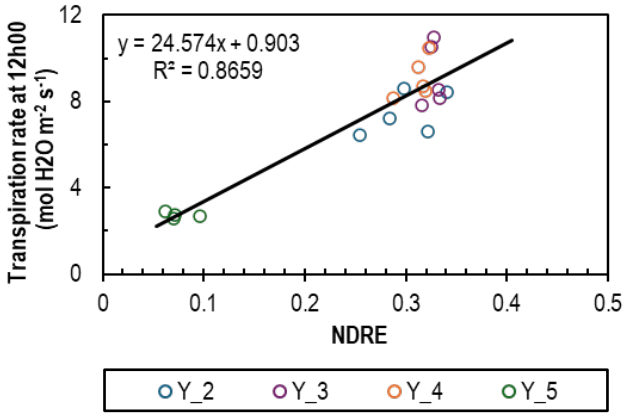


Figure 37. Simple linear regression of leaf transpiration rate at 12h00 with Normalized Difference Red Edge Index (NDRE) for data available from drone surveys and field measurements conducted for the young cultivar 'Wonderful' pomegranate orchard over the 2023/2024 season

For the full bearing compared to the young orchard, the linear regression relationships between the physiological variables and the drone image-derived variables were, in general, poorer (Appendix B: Tables 24-27). Midday SWP related significantly but poorly to NIR and the red spectral band ($R^2$ values of ≤0.201), whereas predawn SWP of selected trees from a localised water stress experiment in the orchard, related better to NIR ($R^2$ = 0.464) compared to the measurements at midday (Appendix B: Tables 26 and 27, Figure 38). Chlorophyll content related significantly but very poorly to TIR and RVI, with coefficients of determination of less than 0.1 (Appendix B: Table 26).

The $A_n$ related significantly only to NIR at 10h00, tending to increase with NIR while ranging from 4 to 15.6 µmol $CO_2$ $m^{-2}$ $s^{-1}$ over the four surveys (Figure 39a). The $g_s$ related significantly only at 12h00 and only to RVI and GNDVI, with $R^2$ values of 0.274 and 0.176, respectively. The $g_s$ tended to increase with increasing RVI, with $g_s$ values ranging between 0.08 and 0.386 mol $m^{-2}$ $s^{-1}$ (Figure 39b). Leaf level transpiration related significantly at 10h00 to TIR, and at 12h00 to the green spectral band, NDVI, NDRE, GNDVI, RVI and CIRE, with coefficients of determination of less than 0.36. At 14h00, $Tr_L$ had significant regression relationships with the green spectral band, GNDVI, RVI and TIR. If all time slots are considered, the best relationship between $Tr_L$ and drone image-derived variables was obtained for $Tr_L$ at 14h00 with RVI, with a coefficient of determination of 0.45 (Figure 40). The transpiration rate varied between 3.3 and 10.9 mol $H_2O$ $m^{-2}$ $s^{-1}$ while the RVI ranged between 5 and 12.5.

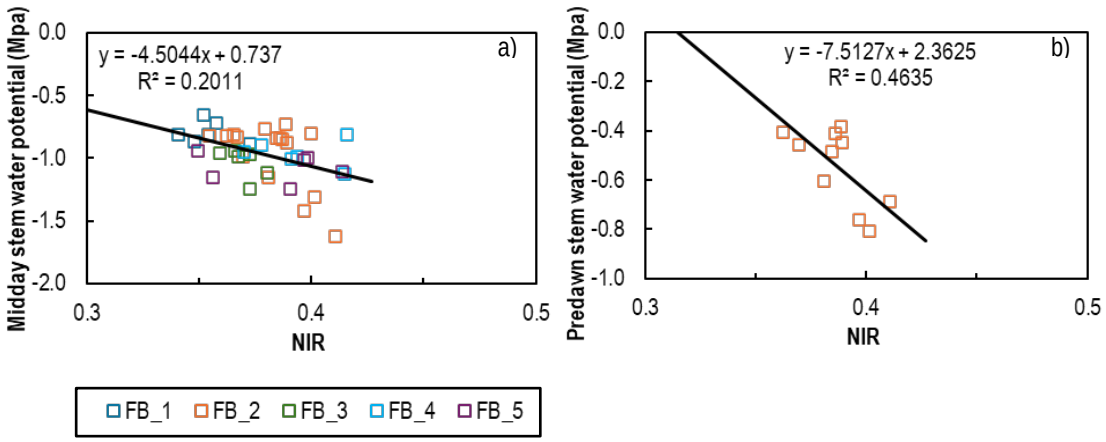


Figure 38. Simple linear regression of a) midday stem water potential and b) predawn stem water potential with drone image estimated near-infrared (NIR) spectral band reflectance for data available from drone surveys and field measurements conducted for the full bearing cultivar 'Wonderful' pomegranate orchard over the 2023/2024 season. Midday stem water potential beyond -1.25 MPa was for selected trees that were water stressed in December 2024.

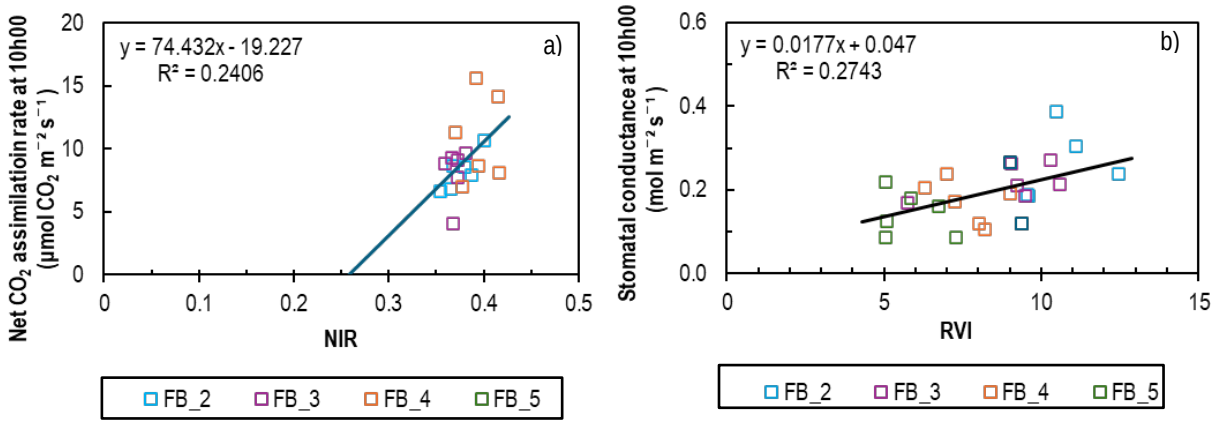


Figure 39. Simple linear regression of a) net carbon-dioxide assimilation rate with drone image estimated near-infrared (NIR) spectral band reflectance and b) stomatal conductance at 10h00 with Ratio Vegetation Index (RVI) for data available from drone surveys and field measurements conducted for the full bearing cultivar 'Wonderful' pomegranate orchard over the 2023/2024 season

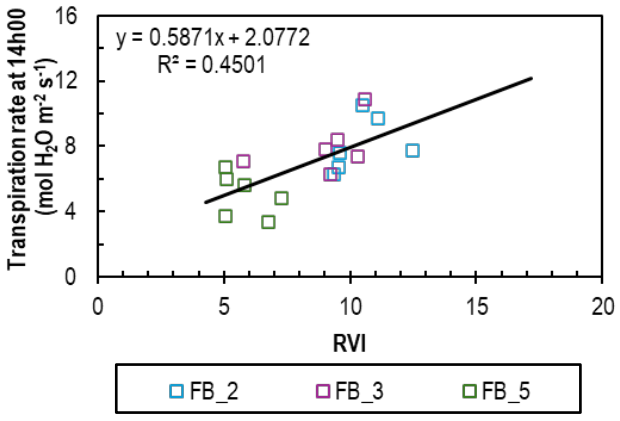


Figure 40. Simple linear regressions of leaf transpiration rate at 14h00 with drone image derived Ratio Vegetation Index (RVI) using data available from drone surveys and field measurements conducted for the full bearing cultivar 'Wonderful' pomegranate orchard over the 2023/2024 season

The coefficients of determination for the linear regressions between plant physiological parameters and drone image-derived variables for the individual trees per site per survey were summarized in Appendix B: Table 28. Although there were several linear regression relationships significant at the 95% confidence level, there was not a single drone variable that related to the same physiological variable for all surveys conducted per orchard. Although the research tried to standardize conditions by conducting drone surveys and physiological measurements under full sun conditions, environmental conditions changed over the season and canopy reflection properties may have changed with phenological phases, as was found for trees in a mixed deciduous-evergreen forest (Tian et al., 2025). This may partially explain the variability in the regression results (Appendix B: Table 28).

### 6.3.2 Orchard level

On an orchard scale, for data of both orchards combined, orchard orchard-averaged midday SWP over the 2023/2024 season did not relate significantly to any drone image-derived variables (Appendix B: Tables 29 and 30). Leaf chlorophyll content measured in SPAD units related significantly at a 5% level only to CVI with an $R^2$ of 0.61, where the trend was strongly affected by data originating from the young orchard (Figure 41). The chlorophyll content tended to increase with increasing CVI. Orchard averaged $A_n$ related, as for individual full bearing trees (Table 26, Figure 39a), significantly at a 5% significance level only to NIR at 10h00 (Appendix B: Table 29 and 30, Figure 42).

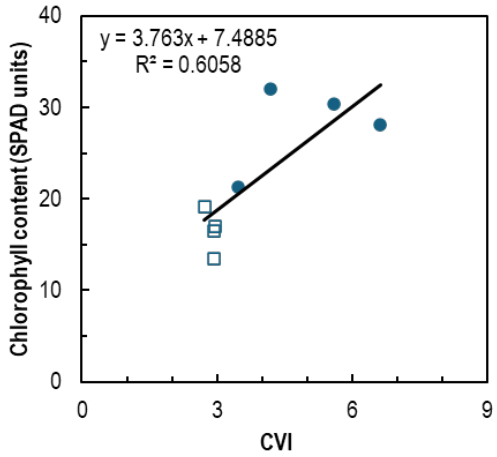


Figure 41. Simple linear regression of orchard averaged chlorophyll content with orchard averaged chlorophyll vegetation index (CVI) using data available from drone surveys and field measurements conducted for the young (circle markers) and full bearing (square markers) cultivar 'Wonderful' pomegranate orchards over the 2023/2024 season

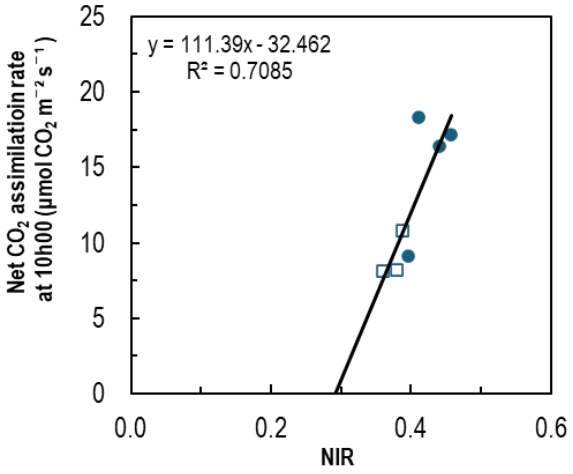


Figure 42. Simple linear regression of orchard averaged net $CO_2$ assimilation rate at 10h00 with orchard averaged near-infrared (NIR) spectral band reflectance, using data available from drone surveys and field measurements conducted for the young (circle markers) and full bearing (square markers) cultivar 'Wonderful' pomegranate orchards over the 2023/2024 season

Stomatal conductance related at a 5% significance level significantly only at 12h00 to GNDVI, CIRE and NDRE with the respective $R^2$ values being 0.54, 0.51 and 0.5 (Appendix B: Tables 29 and 30). The $g_s$, which ranged between 0.113 and 0.269 mol $m^{-2}$ $s^{-1}$ around 12h00, tended to increase with the vegetation indices, with the highest stomatal conductance measured in January and February (Figure 43). The latter values tended to be more outlying for the regression relationships with CIRE and NDRE than with GNDVI.

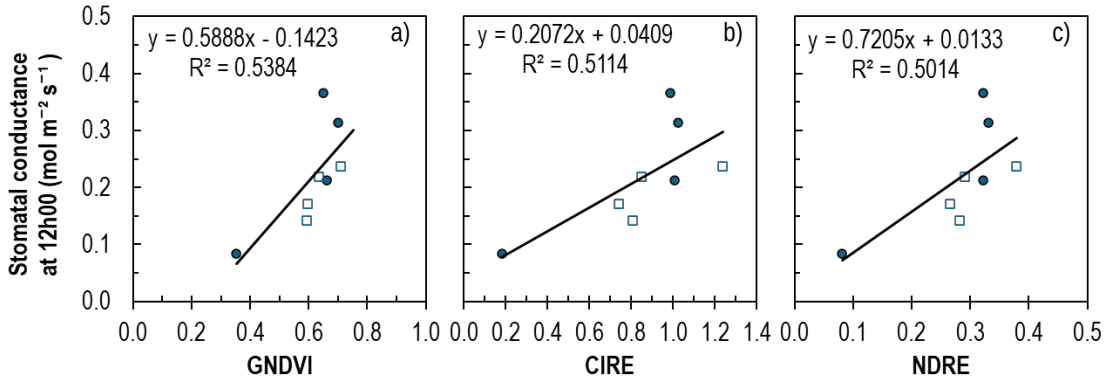


Figure 43. Comparison of simple linear regressions of orchard averaged leaf stomatal conductance at 12h00 with a) Green Normalized Difference Vegetation Index (GNDVI), b) Chlorophyll index – Red edge (CIRE) and c) Normalized Difference Red Edge Index (NDRE) using data available from drone surveys and field measurements conducted for the young (circle markers) and full bearing (square markers) cultivar 'Wonderful' pomegranate orchards over the 2023/2024 season

Orchard averaged leaf transpiration rate at 10h00 and 12h00 related significantly at a 5% significance level to all drone-derived spectral bands and vegetation indices except for NIR, CVI and CIRE (Appendix B: Tables 29 and 30). It was significantly related to CIRE only at 12h00. Orchard averaged leaf transpiration rate at 14h00 related significantly only with the green spectral band, NDRE, GNDVI, CIRE and TIR, with poorer regression relationships compared to earlier in the day. The best regression relationship for orchard orchard-averaged leaf transpiration rate was with RVI and GNDVI at midday (Figure 44a and b), whereas it was significantly related to NDVI, but with a lower coefficient of determination (Figure 44c). The minimum and maximum transpiration rate amounted to 2.9 and 10.6 mol $H_2O$ $m^{-2}$ $s^{-1}$, respectively, for the 12h00 timeslot.

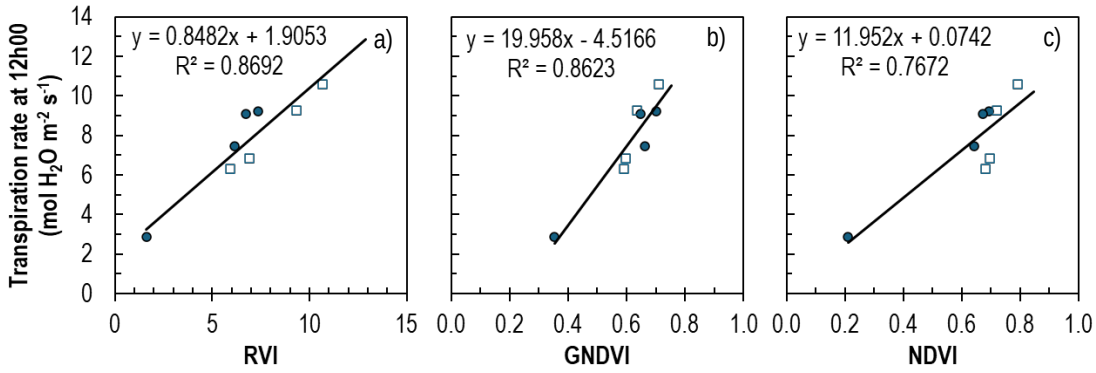


Figure 44. Comparison of simple linear regressions of orchard averaged leaf transpiration rate at 12h00 with a) Ratio Vegetation Index (RVI), b) Green Normalized Difference Vegetation Index (GNDVI) and c) Normalized Difference Vegetation Index (NDVI) using data available from drone surveys and field measurements conducted for the young (circle markers) and full bearing (square markers) cultivar 'Wonderful' pomegranate orchards over the 2023/2024 season

At the young orchard, neither orchard averaged midday SWP nor leaf chlorophyll content was related significantly to any drone image-derived variables (Appendix B: Tables 31 and 32). Orchard averaged net $CO_2$ assimilation at 10h00 related significantly to all the orchard averaged drone image-derived variables except for NIR, CVI and TIR. The coefficients of determination for all of these regression relationships exceeded 0.94, but the blue, red and RedEdge spectral bands had the best distribution of data points along the trendline (Figure 45). The vegetation indices had fairly similar values for the different months during summer, which concentrated data points together at one end of the regression relationship against the value measured in fall on the other end (data not shown). The An at 10h00 decreased with increasing blue, red and RedEdge spectral reflectance towards the end of the season. It is expected that red spectral band reflectance may increase as chlorophyll degrades towards the end of the season (Broge and Leblanc, 2000).

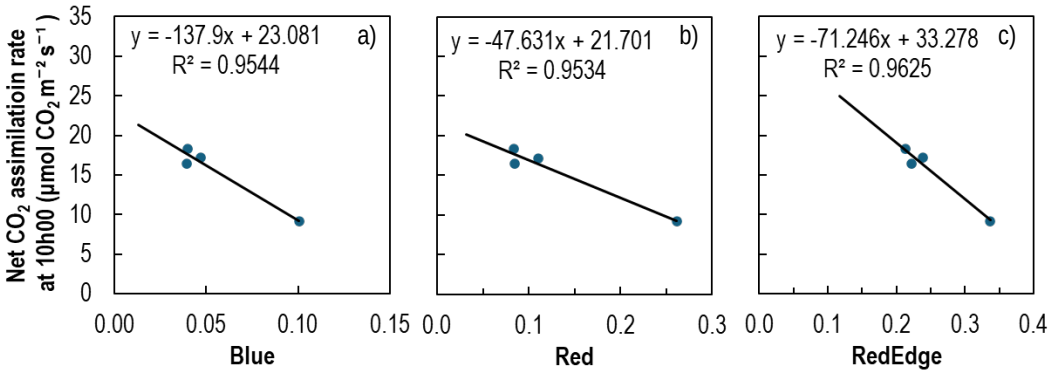


Figure 45. Comparison of simple linear regressions of orchard averaged net carbon-dioxide ($CO_2$) assimilation at 10h00 with orchard averaged a) blue, b) red and c) RedEdge spectral band reflectance using data available from drone surveys and field measurements conducted for the young cultivar 'Wonderful' pomegranate orchard over the 2023/2024 season

Orchard averaged $g_s$ at the young orchard was significantly related to the blue, RedEdge and red spectral band reflectance and to RVI at 12h00 and 14h00, but only at a lower significance level ($p<0.1$, Appendix B: Tables 31 and 32). The linear regression between $g_s$ at 12h00 and RedEdge spectral reflectance resulted in a coefficient of determination of 0.88 at a p-value of 0.06, whereas a non-linear trend improved the regression relationship markedly (Figure 46). The orchard averaged $g_s$, which was the highest in February shortly before harvest, decreased with increasing RedEdge spectral reflection (Figure 46a) and increased with RVI towards fall (Figure 46b).

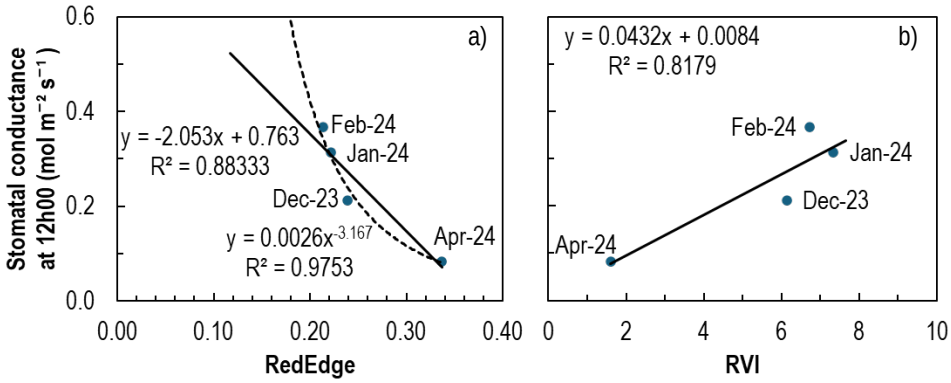


Figure 46. Comparison of simple linear and non-linear regression trends of orchard averaged stomatal conductance at 12h00 with orchard averaged drone image derived a) RedEdge spectral band reflectance and b) Ratio Vegetation Index (RVI), using data available from drone surveys and field measurements conducted for the young cultivar 'Wonderful' pomegranate orchard over the 2023/2024 season

Orchard averaged $Tr_L$ at 12h00 related significantly at a 5% significance level to all drone image derived variables except for NIR, CVI and TIR, with the best regression relationship being with the RedEdge and red spectral bands and RVI ($R^2 > 0.98$) (Appendix B: Tables 31 and 32, Figure 47). Leaf level transpiration at 14h00 related significantly at a 5% significance level only to RedEdge spectral band reflectance and RVI, with lower coefficients of determination compared to at 12h00 (Appendix B: Tables 31 and 32). The orchard averaged $Tr_L$ at the young orchard decreased at 12h00 or 14h00 with increasing RedEdge or Red spectral band reflectance (Figure 47a and b) and increased with RVI (Figure 47c), with the lowest transpiration rates occurring in fall.

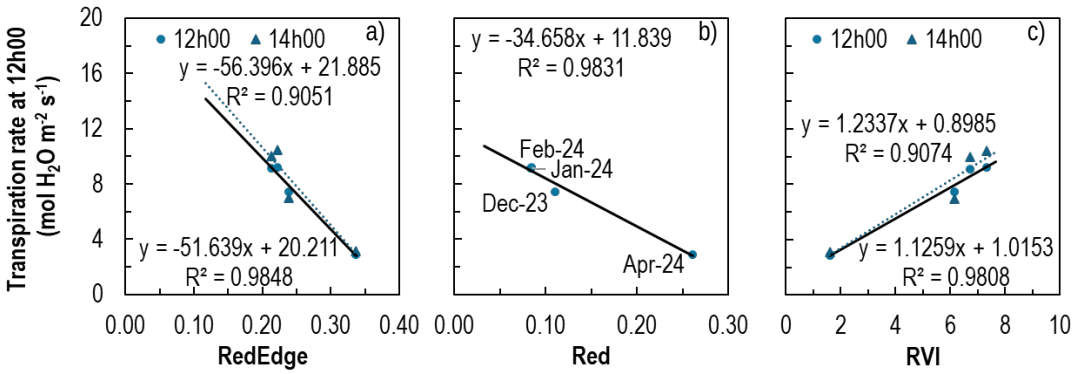


Figure 47. Comparison of simple linear regressions of orchard averaged leaf transpiration rate at 12h00 (circle markers, solid line) and 14h00 (triangular markers, dotted line) with orchard averaged a) RedEdge and b) red spectral band reflectance, respectively, and c) Ratio Vegetation Index (RVI), using data available from drone surveys and field measurements conducted for the young cultivar 'Wonderful' pomegranate orchard over the 2023/2024 season

At the full bearing orchard, orchard averaged SWP did not relate significantly to any drone image-derived variables at a 5% significance level, but it related significantly to NDVI at a p-level of 0.062 (Appendix B: Tables 33 and 34, Figure 48). Stem water potential decreased from -0.8 MPa to -1.08 MPa as NDVI decreased from 0.85 to 0.68 from the beginning to the end of the season. The leaf chlorophyll content was significantly related to NIR and increased with increasing NIR spectral reflection (Figure 49). The chlorophyll content increased from October to February and was the lowest in April, during autumn. With regard to $CO_2$ assimilation, only $A_n$ at 14h00 related significantly to and decreased with increasing RVI (Figure 50a). Orchard averaged stomatal conductance and leaf transpiration rate at 12h00 both increased with RVI (Figure 50b and c) as in the case for the young orchard (Figures 44a and 47c). The orchard averaged $Tr_L$ at 14h00 for the full bearing orchard related significantly to TIR with a coefficient of determination of 0.988. The transpiration rate increased with increasing TIR temperatures between 29°C and 41°C, but the regression relationship was based on only three datapoints, with two of them grouped closely together (data not shown). More data needs to be collected before this relationship can be considered for estimation of leaf transpiration rates for the full bearing orchard.

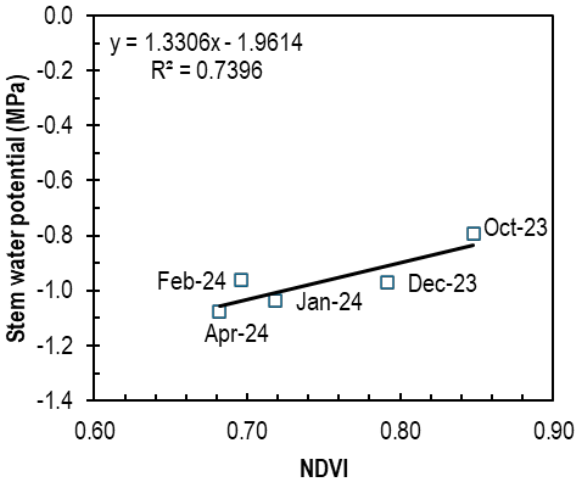


Figure 48. Simple linear regression of stem water potential with Normalized Difference Vegetation Index (NDVI) for data available from drone surveys and field measurements conducted for full bearing cultivar 'Wonderful' pomegranate orchard over the 2023/2024 season

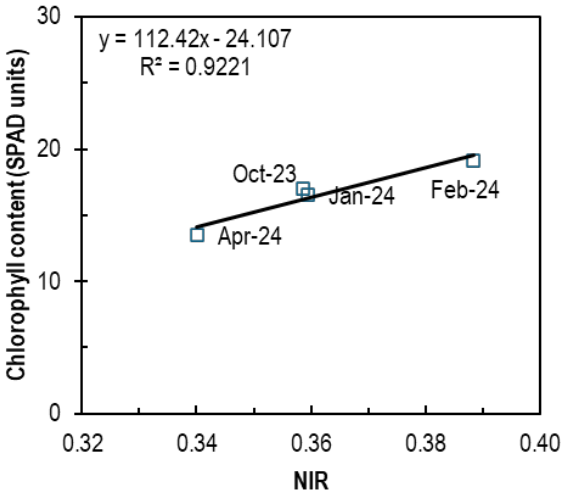


Figure 49. Simple linear regression of chlorophyll content (measured using a SPAD 502 meter) with near-infrared (NIR) spectral reflectance for data available from drone surveys and field measurements conducted for full bearing cultivar 'Wonderful' pomegranate orchard over the 2023/2024 season

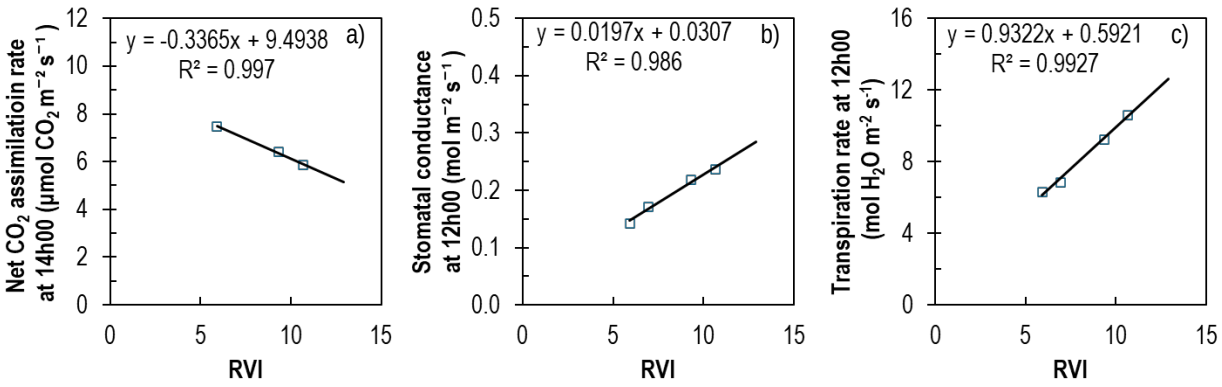


Figure 50. Comparison of simple linear regressions of orchard averaged net $CO_2$ assimilation rate at 14h00 and stomatal conductance and transpiration rate at 12h00 with orchard averaged Ratio Vegetation Index (RVI), using data available from drone surveys and field measurements conducted for the full bearing cultivar 'Wonderful' pomegranate orchard over the 2023/2024 season

## 6.4 CONCLUSIONS

With regard to comparison of drone image derived variables to individual tree plant physiological parameters, there were several linear regression relationships significant at a 95% confidence level, with coefficients of determination ranging between 0.104 and 0.584 for data of orchards combined, and the $R^2$ value increased in some cases up to 0.866 where orchards were considered on their own. However, in most cases, there was a clear paucity of mid-range data to strengthen the regression relationships. This was more frequently the case for individual tree data for orchards combined and for the young orchard considered on its own. In most cases, there was a clear distinction between data collected after harvest and that derived from the surveys done in summer.

Regressions using orchard-averaged data for orchards combined rendered $R^2$ values of between 0.5 and 0.87. When regressions were conducted for the orchard averaged data of individual orchards, the coefficients of determination were, in general, higher, i.e., between 0.74 – 0.997. In some cases, data from orchards combined may render significant regression relationships at a 95% confidence level, whereas it will not necessarily be significant for both orchards at the individual orchard level (e.g. stem water potential and chlorophyll content).

Individual tree midday stem water potential data of orchards combined were not significantly related to any drone image-derived variables, whereas it related poorly, but significantly, with a negative correlation to RVI at the young ($R^2$ = 0.27) and NIR at the full bearing orchard ($R^2$ = 0.2). Predawn stem water potential at the full bearing orchard related better to NIR, with a coefficient of determination of 0.46. Orchard averaged midday stem water potential was not related significantly to any drone image-derived variables at a 95% confidence level for the data of orchards combined, nor for the young or full-bearing orchards considered individually. Data for the young orchard lacked a clear trend in stem water potential over the season. However, at the full bearing orchard midday stem water potential tended to decrease with decreasing NDVI as the season progressed, albeit at a lower significance level (p = 0.062).

Leaf chlorophyll content data for orchards combined related significantly to CVI, with $R^2$ values of 0.42 and 0.61 for regressions based on individual tree and orchard averaged data, respectively. However, regression relationships based on individual tree data were, in general, poor for the individual orchards ($R^2$ values of 0.28 or less), with no consistent drone image-derived variable that resulted in the best regression relationship (CIRE for the young / TIR for the full bearing). Based on orchard averaged data, there was no significant regression relationship for the young orchard, but a highly significant one for the full bearing orchard ($R^2$ = 0.92) in which leaf chlorophyll content increased with NIR spectral reflection.

With regard to leaf physiological parameters, for data of orchards combined, $A_n$ at 10h00 related significantly to NIR based on individual tree data ($R^2$ = 0.56) as well as orchard averaged data ($R^2$ = 0.71). For the individual orchards, there was once again variation in the drone image-derived variables, which resulted in the best regression relationships. Based on individual tree data, $A_n$ at 10h00 related the best to NDRE for the young orchard ($R^2$ = 0.7), whereas at the full bearing orchard, NIR was the best related variable ($R^2$ = 0.24). For orchard averaged data $A_n$ at 10h00 related best to RedEdge spectral reflectance for the young orchard ($R^2$ = 0.96), while at the full bearing orchard only $A_n$ at 14h00 related significantly to RVI ($R^2$ = 0.997).

Stomatal conductance at 12h00 for data of orchards combined related significantly to GNDVI based on individual tree data ($R^2$ = 0.37) as well as orchard averaged data ($R^2$ = 0.54). At the individual tree level at the young orchard, the $g_s$ at 12h00 related significantly the best to NDVI ($R^2$ = 0.74), but at the full bearing orchard $g_s$ at 10h00 related the best to RVI ($R^2$ = 0.27). Based on orchard averaged data, $g_s$ at 12h00 related at the young orchard best to RedEdge spectral reflectance ($R^2$ = 0.88) or RVI ($R^2$ = 0.82) at the full bearing orchard to RVI ($R^2$ = 0.993).

Based on individual tree data for orchards combined, $Tr_L$ at 10h00 related significantly to RVI ($R^2$ = 0.58), whereas amongst regressions based on orchard averaged data for orchards combined, $Tr_L$ at 12h00 related the best to RVI ($R^2$ = 0.87), In contrast with that found for individual tree data of orchards combined, the time and drone image derived variables that $Tr_L$ related to the best changed for the individual orchards. For the young orchard, $Tr_L$ related at 12h00 the best to NDRE ($R^2$ = 0.87), and for the full bearing orchard at 14h00 to RVI ($R^2$ =0.45). The time and drone variable resulting in the best regression relationship of TrL with orchard averaged data for orchards combined remained similar for the individual orchards, with TrL at 12h00 giving the best relationship with either RVI or RedEdge spectral reflectance for the young orchard ($R^2$ = 0.98) and with RVI at the full bearing orchard ($R^2$ = 0.993).

Stem water potential, leaf chlorophyll content and tree physiological variables such as $A_n$, $g_s$ and $Tr_L$ are not only affected as environmental conditions change, but are also affected by phenological changes in the crop over time and as leaves age. This may explain the variability in the relationships obtained between the physiological and drone image-derived variables for individual or orchard-averaged data for orchards and surveys combined or considered separately. It is considered important to collect more detailed soil, leaf and canopy data related to electromagnetic wave reflectance and scattering of radiation to understand and confirm the relationships found between the drone image-derived variables and the physiological variables measured in this research. The use of machine learning to identify appropriate algorithms to estimate physiological variables accurately from drone image-derived variables is strongly recommended for further research.

# CHAPTER 7: COMPARISON OF DRONE MULTISPECTRAL IMAGE-DERIVED SPECTRAL BANDS, TREE GEOMETRIC PROPERTIES, VEGETATIVE INDICES AND THERMAL INFRARED TEMPERATURE TO TREE WATER USE

## 7.1 INTRODUCTION

Efficient irrigation management relies to a great extent on the timely availability of precise information about crop evapotranspiration (ETc) (Pôças et al., 2020). In this regard, methods are being progressively developed to apply very high-resolution UAV imagery for precision ETc monitoring and it can be estimated using satellite remote sensing-based UAV evapotranspiration (ET) estimation methods (Nieto et al. and references therein, 2019) or, alternatively, ETc can be estimated using the widely adopted single or dual crop coefficient (approach, combined with Penman-Monteith reference evapotranspiration (Allen et al., 1998). Research on the application of remote sensing data to assess single (Kc) and basal (Kcb) crop coefficients has been ongoing for more than 30 years (Pôças et al., 2020). Niu et al. (2020) found a strong correlation between the NDVI and the crop coefficient (Kc) at the individual pomegranate tree level. They conducted research in California, which related NDVI derived from high spatial resolution multispectral UAV imagery of a 12-year-old pomegranate orchard to Kc values determined from ET using weighing lysimeters and ETo derived from weather data (Niu et al., 2021). The purpose of this chapter is therefore to follow the more simplistic approach and to relate multispectral and thermal drone image-derived variables to Western Cape pomegranate tree water use, but measured on different scales (i.e. individual tree as well as orchard level). The intention is to use statistically significant regression relationships to estimate water use directly, or indirectly by using crop coefficients and reference evapotranspiration and thereby provide information to improve irrigation scheduling.

## 7.2 METHODOLOGY

A multispectral DJI Technology© Matrice 600 drone outfitted with a MicaSense Red-Edge-MX multispectral camera and Zenmuse-XT thermal camera was used to conduct five drone surveys during the 2023/2024 season at the young (Avontuur, 33°07'29.7"S; 18°56'08.8"E) and full bearing (Welgemoed, 33°35'18.3048"S; 18°59'19.302"E) cv. 'Wonderful' pomegranate orchards (Table 1, Figure 1). The surveys were conducted around solar noon (±1 hour) about two months after bud break during canopy development (October 2023), after most fruit set was completed (December 2023), at full canopy (January 2024), during ripening (February 2024) and after harvest (April 2024). Multispectral and thermal drone images were processed using Pix4D mapper software (Version 4.8.4). Pixels were radiometrically corrected by using a calibration reflectance panel and downwelling light sensor measurements of irradiance. Weather stations, sap flow, soil water balance and micrometeorological systems (surface renewal at the young orchard, eddy covariance at the full bearing orchard) automatically logged at least hourly the data required to calculate tree and orchard scale water use and crop coefficients (Refer to chapter 3 for further details on methodology).

Simple linear regressions were conducted between all data and indices derived from drone images for selected individual trees to individual tree data measured in orchards (sap flow, soil water balance). Regressions were also conducted at orchard scale – i.e. orchard averaged values of all individual tree data derived from drone images compared to orchard upscaled transpiration and orchard scale ETc measured by micrometeorological systems (surface renewal at the young orchard, eddy covariance at the full bearing orchard). The ratio of transpiration and ETc, respectively, to ETo was also related to the drone-derived variables. Regression models were considered significant at 95% level of confidence (p=0.05). Data variables derived from the drone images included reflectance of the blue, green, red, near-infrared, RedEdge and thermal infrared bands and drone-estimated tree height and volume. The indices calculated from the drone image data included, in addition to NDVI, NDRE, GNDVI, RVI, CVI and CIRE.

## 7.3 RESULTS AND DISCUSSION

### 7.3.1 Individual tree level

Comparison of data for all surveys at the young and full bearing orchard combined for selected individual trees indicated that transpiration had significant linear regression relationships with all the drone image derived variables at a statistical significance level of 5% ($p<0.05$) except for CVI, which had a p-value of 0.129 (Appendix C: Table 35). The T:ETo ratio correlated at a 5% significance level with drone estimated tree height ($R^2 = 0.37$), volume ($R^2 = 0.25$), CVI ($R^2 = 0.23$) and RVI ($R^2 = 0.12$) and at a 10% level with NIR ($R^2 = 0.08$). Transpiration and the T:ETo ratio related best to drone estimated tree height (Figure 51a and b). Fitting a non-linear regression relationship to drone estimated tree height for the variables increased the $R^2$ values to 0.52 and 0.40 for transpiration and the T:ETo ratios, respectively (data not shown). Transpiration was related second-best to RVI ($R^2 = 0.457$), but the coefficient of determination of the ratio of transpiration to ETo with RVI was only 0.12 (Figure 52 a and b). Linear regression relationships of transpiration with NDVI and NDRE were poorer than expected, with $R^2$ values of 0.37 and 0.28, respectively (Appendix C: Table 35).

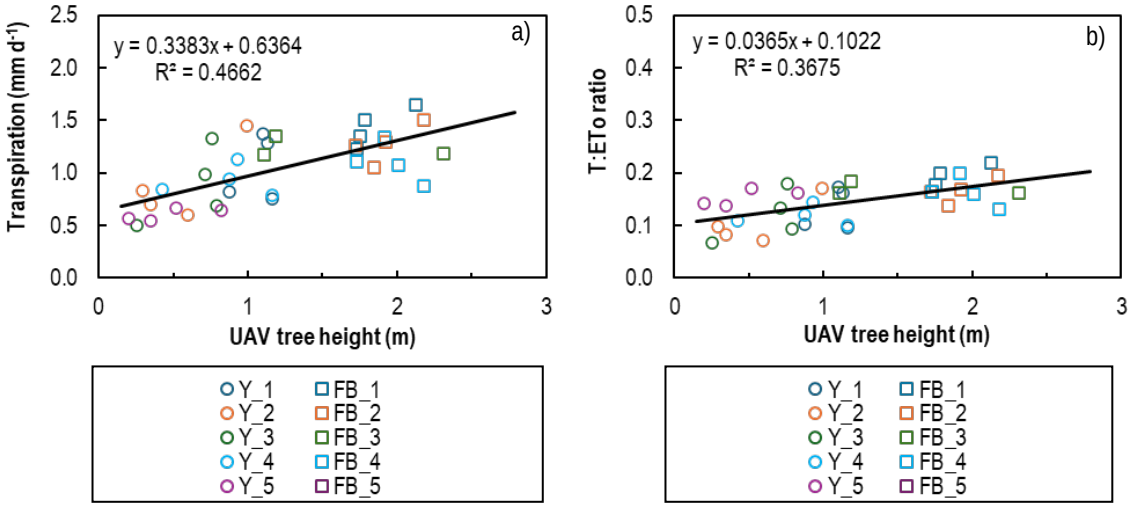


Figure 51. Comparison of sap flow derived tree transpiration (T) and the ratio thereof to reference evapotranspiration (ETo) to drone (UAV) estimated tree height for data of five drone surveys conducted during 2023/2024 on young (Y) and full bearing (FB) cultivar 'Wonderful' pomegranate trees. Transpiration data was only available for three trees for the full bearing orchard for survey 3 and none for survey 5.

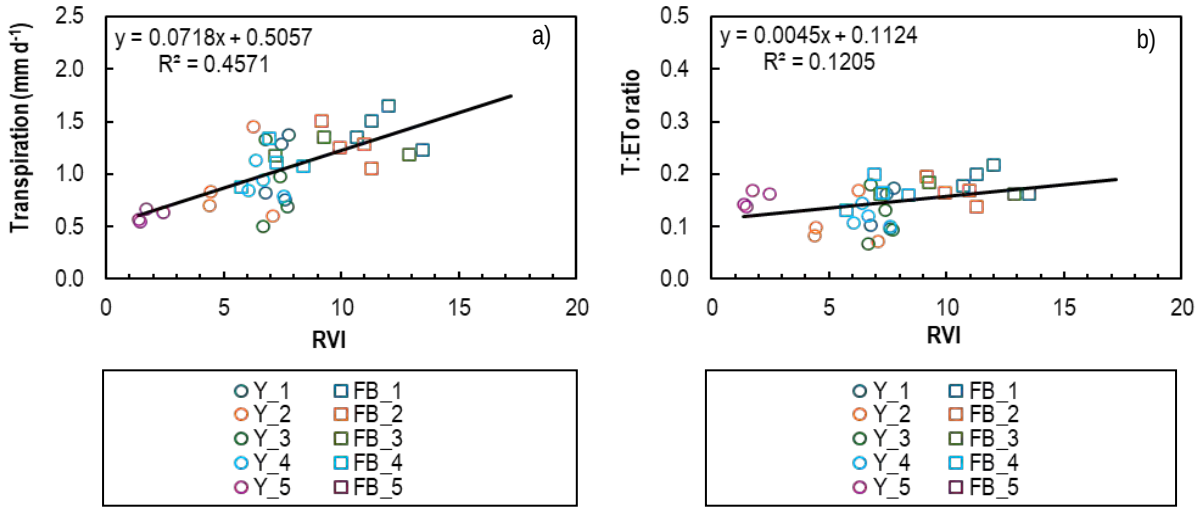


Figure 52. Comparison of sap flow derived tree transpiration (T) and the ratio thereof to reference evapotranspiration (ETo) to drone image derived Ratio Vegetation Index (RVI) for data of five drone surveys conducted during 2023/2024 on young (Y) and full bearing (FB) cultivar 'Wonderful' pomegranate trees. Transpiration data was only available for three trees for the full bearing orchard for survey 3 and none for survey 5.

Soil water balance estimated water use from the tree row and at full surface level correlated the best with the RedEdge (Figure 53a and b) and NIR spectral bands (Figure 54a and b) or with CVI (Figure 55a and b), with $R^2$ values of between 0.78 and 0.91 (Appendix C: Table 35). Soil water balance estimated water use from the work row and the ratio thereof to ETo related significantly at a 95% significance level only to drone estimated tree volume (Figure 56a and b; Appendix C: Table 35). It was significantly related to NDVI and NDRE at a lower significance level ($0.05<p<0.1$). The ratio of tree row ETc to ETo was significantly related to reflectance from the blue, green and RedEdge spectral bands (Figure 57 a, b and c), but there were no significant linear regression relationships between the ratio of orchard ETc to ETo and any of the drone derived variables (Appendix C: Table 35).

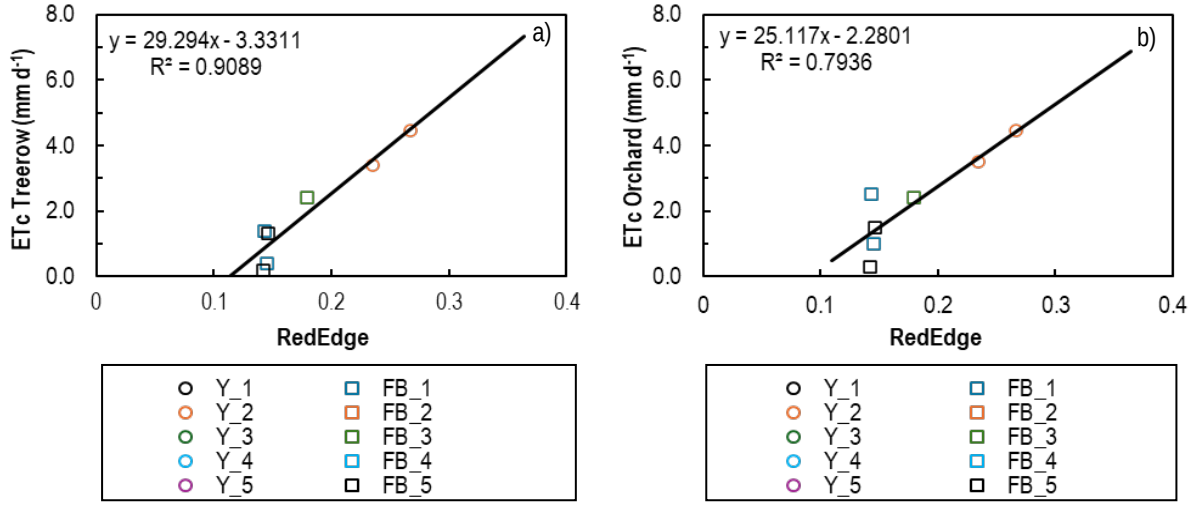


Figure 53. Comparison of soil water balance determined tree row evapotranspiration (ETc) and orchard level evapotranspiration (ETc Orchard) to drone image derived RedEdge spectral band reflectance for selected drone surveys conducted during 2023/2024 on young (Y) and full bearing (FB) cultivar 'Wonderful' pomegranate trees

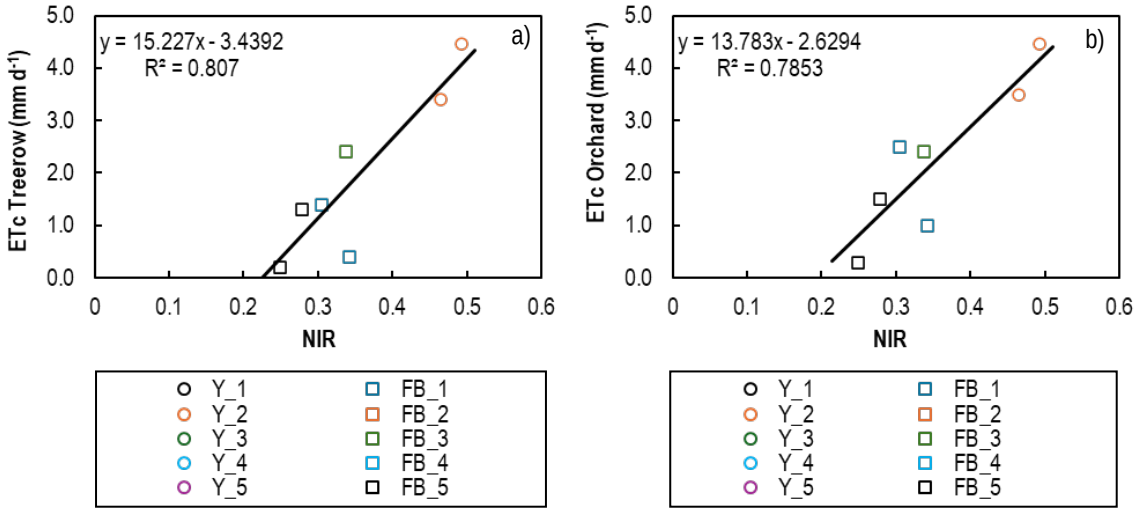


Figure 54. Comparison of soil water balance determined tree row evapotranspiration (ETc) and orchard level evapotranspiration (ETc Orchard) to drone image derived near-infrared (NIR) spectral band reflectance for selected drone surveys conducted during 2023/2024 on young (Y) and full bearing (FB) cultivar 'Wonderful' pomegranate trees

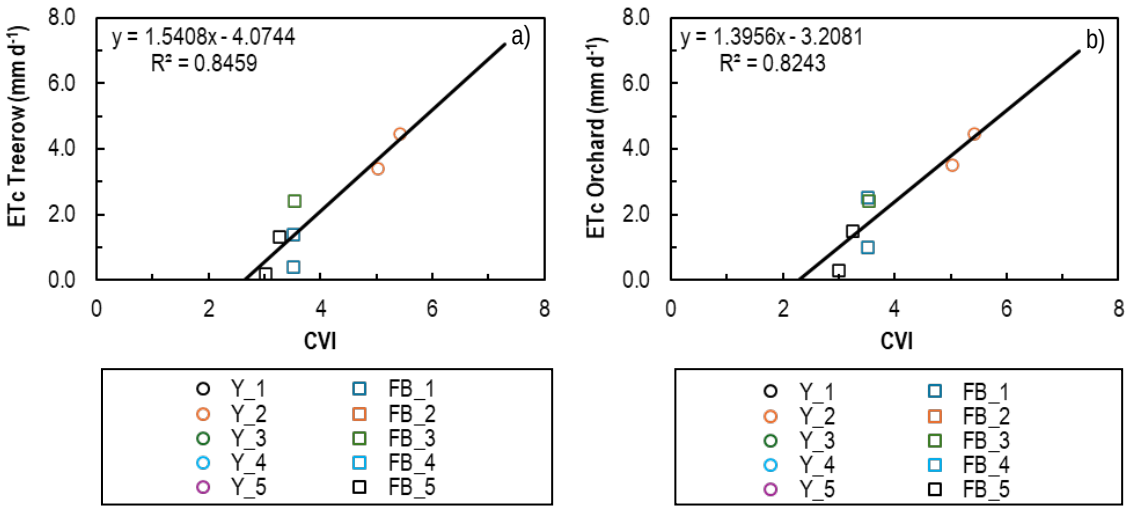


Figure 55. Comparison of soil water balance determined tree row evapotranspiration (ETc) and orchard level evapotranspiration (ETc Orchard) to drone image derived chlorophyll vegetation index (CVI) for selected drone surveys conducted during 2023/2024 on young (Y) and full bearing (FB) cultivar 'Wonderful' pomegranate trees

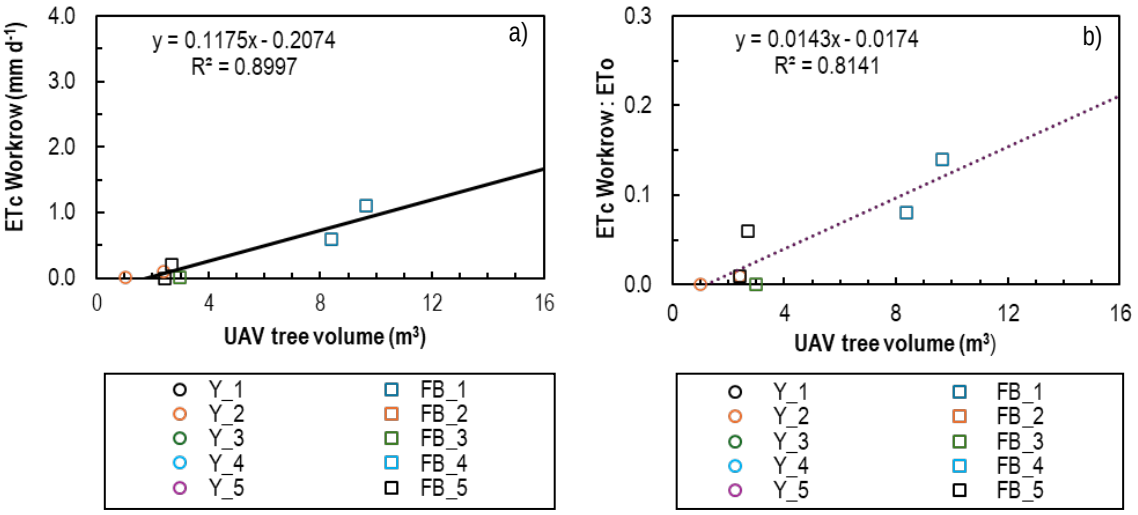


Figure 56. Comparison of soil water balance determined work row evapotranspiration (ETc) and the ratio thereof to reference evapotranspiration (ETo) to drone image estimated tree volume for selected drone surveys conducted during 2023/2024 on young (Y) and full bearing (FB) cultivar 'Wonderful' pomegranate trees

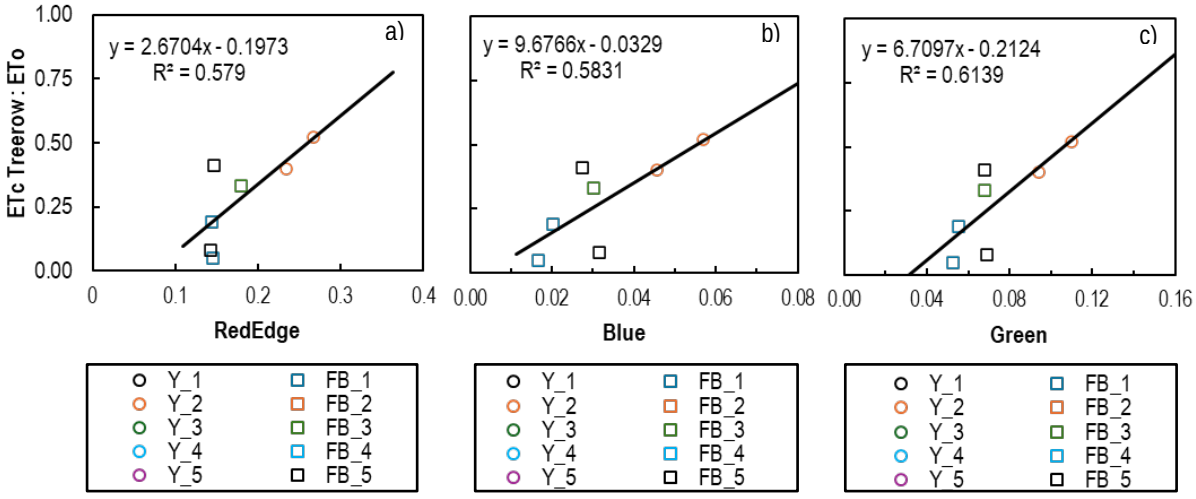


Figure 57. Comparison of the ratio of soil water balance determined tree row evapotranspiration (ETc) to reference evapotranspiration (ETo) to drone image derived RedEdge, blue and green reflectance for selected drone surveys conducted during 2023/2024 on young (Y) and full bearing (FB) cultivar 'Wonderful' pomegranate trees

At site level (combining all surveys per orchard), transpiration of the young orchard was significantly related to all drone-derived variables at a 95% confidence level except for NIR, CVI and CIRE (Appendix C: Tables 36 and 37). It related best to drone estimated tree height and RedEdge spectral band reflectance (Figure 58a and b,) whereas the $R^2$ values were only about 0.2 for the linear regression relationships with NDVI and NDRE (Appendix C: Table 36).

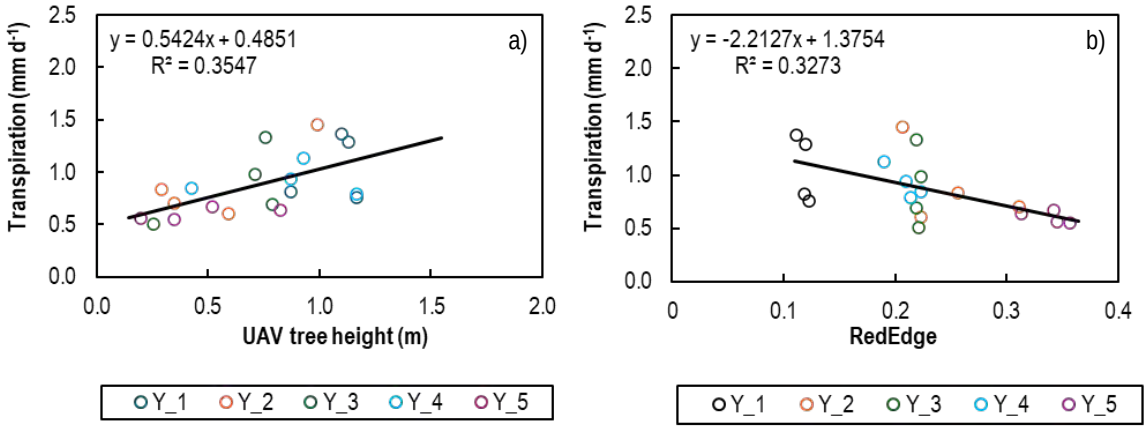


Figure 58. Comparison of sap flow derived tree transpiration to drone estimated tree height (a) and RedEdge spectral reflectance (b) for data of five surveys conducted during 2023/2024 for four young cultivar 'Wonderful' pomegranate trees

Transpiration of the full bearing orchard was related to the GNDVI and the green spectral band only at a lower significance level (Appendix C: Tables 36 and 37, Figure 59a and b). The ratio of transpiration to ETo was not significantly related to any of the drone-derived variables at any of the sites. Frequent drip irrigation, especially in young orchards, affected equilibrium conditions required in the soil for soil water balance estimates of ETc. In situ calibration of the soil water content sensors (data not shown) did not improve the availability of ETc data from the soil water balance. Only two data points were considered reliable for the young orchard, which resulted in the $R^2$ values of 1 as indicated in Table 36 (Appendix C). At the full bearing orchard, no significant regression relationships were identified that could aid in irrigation scheduling of the orchard. The significant relationship of ETc from the work row to drone estimated tree volume found for the full bearing orchard ($R^2$=0.9, p=0.013, Appendix C: Tables 36 and 37) was already apparent in Figure 56 where data of the two orchards were combined. It must be noted that the regression relationships between the limited soil water balance estimated ETc datasets available and the drone-derived variables are fragmented and do not represent the whole season (i.e. all five surveys).

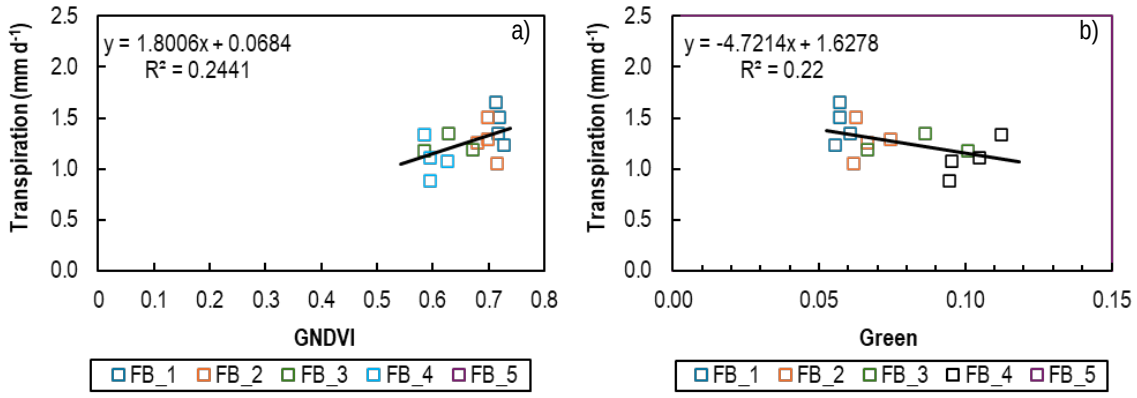


Figure 59. Comparison of sap flow derived tree transpiration to drone estimated Green Normalized Difference Vegetation Index (GNDVI) (a) and green spectral reflectance (b) for data of five surveys conducted during 2023/2024 for full bearing cultivar 'Wonderful' pomegranate trees

At survey level, transpiration and the ratio thereof to ETo were only significantly related to NIR and RedEdge spectral band reflectance during the fourth survey at the full bearing site (Appendix C: Tables 38 and 39, Figures 60 and 61). Transpiration of the young orchard and the ratio thereof to ETo was also only related during the fourth survey to NIR and RedEdge at a lower significance level with p-values of 0.053 and 0.086, respectively. The coefficients of determination for these regression relationships though, were above 0.83. Soil water balance-derived ETc data were too limited to use for survey-level regression purposes and were therefore not tabulated.

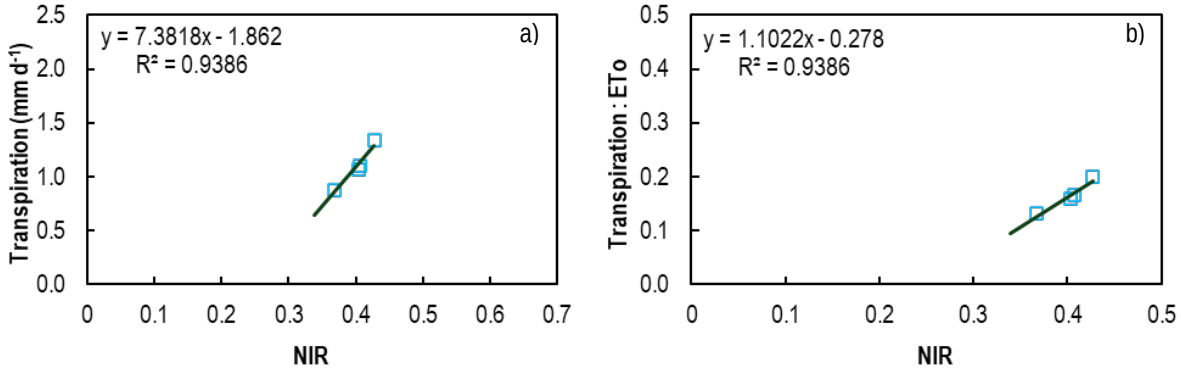


Figure 60. Comparison of a) sap flow derived tree transpiration and b) the ratio thereof to reference evapotranspiration (ETo) to drone image derived near-infrared (NIR) spectral band reflectance for data of the survey conducted during February 2024 for full bearing cultivar 'Wonderful' pomegranate trees

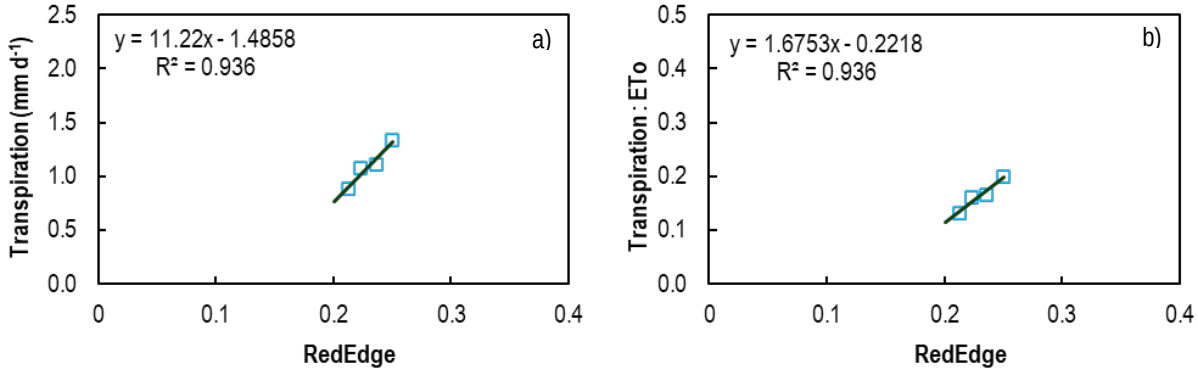


Figure 61. Comparison of a) sap flow derived tree transpiration and b) the ratio thereof to reference evapotranspiration (ETo) to drone image derived RedEdge spectral band reflectance for data of the survey conducted during February 2024 for full bearing cultivar 'Wonderful' pomegranate trees

### 7.3.2 Orchard level

For sites combined, simple linear regressions of orchard upscaled tree transpiration with orchard averaged multispectral drone image estimated variables resulted in significant regression relationships at a 5% significance level with blue, green, red and RedEdge spectral band reflectance, NDVI, NDRE, GNDVI, RVI, CIRE and drone estimated tree height, with coefficients of variation ranging between 0.517 and 0.916 (Appendix C: Table 40). The best regression relationship was obtained with RVI ($R^2$ = 0.92, $SE_{est}$ = 0.061 mm $d^{-1}$, Figure 62a), whereas that with NDVI resulted in a coefficient of determination of 0.71 ($SE_{est}$ = 0.112; Figure 62b). Transpiration ranged in a narrow band between 0.8 and 1.4 mm per day and increased with increasing RVI (Figure 77a). Orchard transpiration also tended to increase with increasing drone estimated tree height and the standard error of the estimate amounted to 0.114 ($R^2$ = 0.7, data not shown).

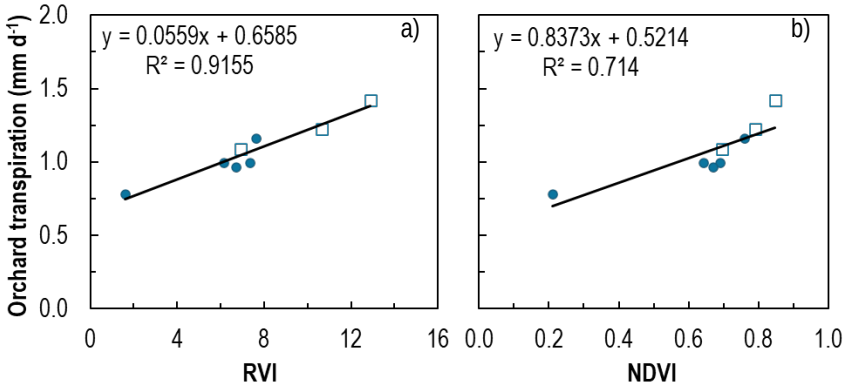


Figure 62. Comparison of orchard upscaled transpiration with orchard averaged drone image derived a) Ratio Vegetation Index (RVI) and b) NDVI (Normalized Difference Vegetation Index) for drone surveys conducted in 2023/2024 in the young (circle markers) and full bearing (square markers) cultivar 'Wonderful' pomegranate orchards

Orchard level ETc for orchards combined ranged between 1 and 4.6 mm and related significantly only at a 10% significance level to the orchard averaged RVI ($R^2$ = 0.42, p = 0.081, Appendix C: Table 40, Figure 63a), for which estimates had a standard error of 0.956. The poor regressions with drone-derived variables were due to one outlying value originating from January for the full bearing orchard and also to data from October 2023 from the young orchard (Figure 63a and b). If the outlying values greater than 2 standard deviations are removed, the regression relationship of ETc with RVI becomes significant at a 95% confidence level, the coefficient of determination improves to 0.772 (p-value of 0.021) and the standard error of the estimate decreases to 0.622 (data not shown). The ETo at the experimental sites was related significantly to several orchard-averaged multispectral drone image estimated variables, including the green spectral band reflectance and NDRE, GNDVI, CIRE and TIR (Appendix C: Table 40). The best regression relationships were with GNDVI and TIR (Figure 64).

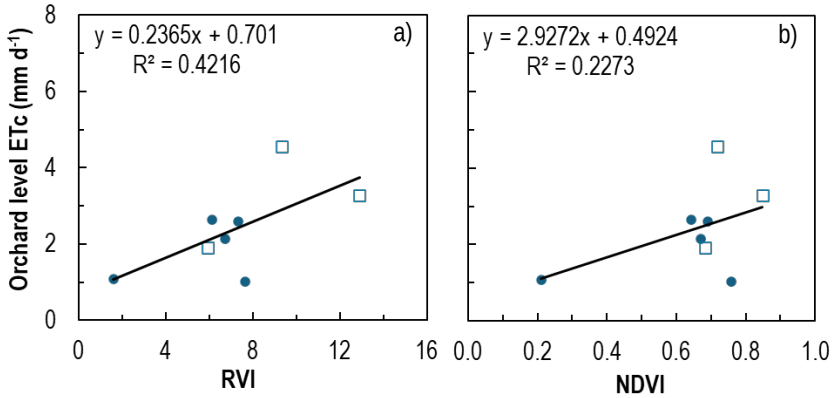


Figure 63. Comparison of orchard upscaled evapotranspiration (ETc) with orchard averaged drone image derived a) Ratio Vegetation Index (RVI) and b) NDVI (Normalized Difference Vegetation Index) for drone surveys conducted in 2023/2024 in the young (circle markers) and full bearing (square markers) cultivar 'Wonderful' pomegranate orchards

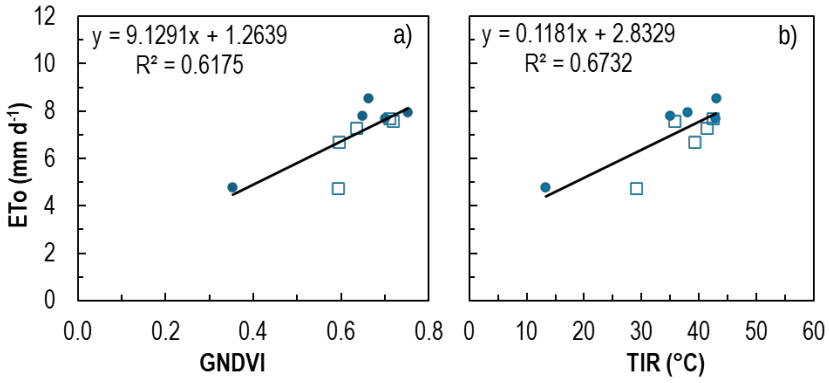


Figure 64. Comparison of automatic weather station reference evapotranspiration (ETo) with orchard averaged drone image derived a) GNDVI (Green Normalized Difference Vegetation Index) and b) thermal infrared temperature. Data were combined for the young (circle markers) and full bearing (square markers) cultivar 'Wonderful' pomegranate orchards (n = 10).

There were no significant linear regression relationships between the ratio of orchard upscaled transpiration to ETo and any of the orchard averaged multispectral drone image estimated spectral band reflectance variables or vegetative indices at a 95% confidence level (Appendix C: Tables 40 and 41). For data of orchards combined, the ratio of orchard upscaled transpiration to ETo related significantly at the 10% significance level to drone estimated tree height ($p = 0.087$) and volume ($p = 0.071$) with $R^2$ values 0.41 and 0.45, respectively, with a standard error of the estimate of about 0.02 (Appendix C: Table 40, Figure 65a and b). Poor and/ or lack of significant orchard upscaled transpiration regression relationships with the drone image-derived variables for the young orchard may be attributed to data originating from either October 2023 or April 2024 (data not shown).

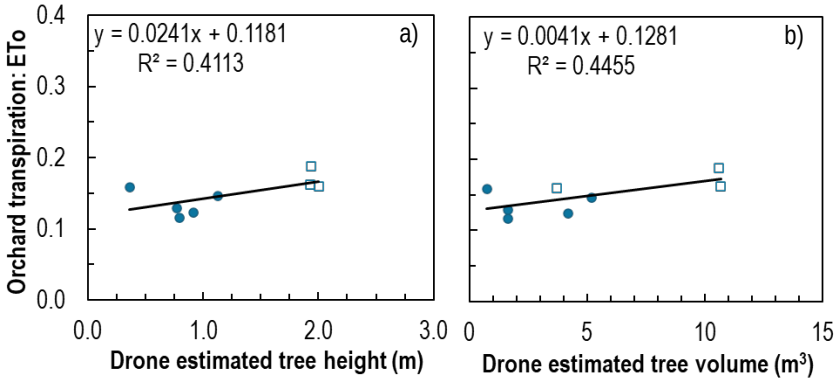


Figure 65. Comparison of the orchard upscaled transpiration to reference evapotranspiration (ETo) ratio with orchard averaged drone image derived a) tree height and b) tree volume. Data were combined for the young (circle markers) and full bearing (square markers) cultivar 'Wonderful' pomegranate orchards (n = 8).

There were also no significant linear regression relationships between the ratio of orchard level evapotranspiration to ETo and any of the orchard averaged multispectral drone image estimated spectral band reflectance variables or vegetative indices at a 5% significance level for data of orchards combined (Appendix C: Table 40). In this case, the ETc:ETo ratio was significantly related at a 10% significance level to CVI ($p = 0.061$) and drone estimated tree height ($p = 0.075$). However, the relationship with CVI did not seem reasonable and only the data for the regression relationship with drone estimated tree height is presented, wherein the ETc:ETo ratio increased with tree height (Figure 66). The standard error of the estimate of ETc:ETo ratio for the regression relationship with drone-estimated tree height is 0.12 and it will therefore not be possible to estimate the ratio accurately. As in the case of the ETc data, outlying values from October 2023 for the young and for January 2024 for the full bearing orchard resulted in the poor regression relationships (Figures 63 and 66).

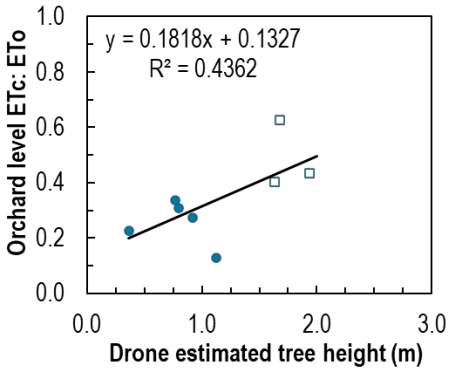


Figure 66. Comparison of the orchard level evapotranspiration to reference evapotranspiration (ETo) ratio with orchard averaged drone image-derived tree height. Data were combined for the young (circle markers) and full-bearing (square markers) cultivar 'Wonderful' pomegranate orchards (n = 8).

Orchard upscaled transpiration for the young orchard related significantly at a 95% confidence level to the blue, green, red and RedEdge spectral band reflectance and to NDVI, GNDVI, RVI, CVI and drone estimated tree height (Appendix C: Table 41). Transpiration at the full bearing orchard related significantly only to NIR spectral reflection and only at a 10% significance level (p = 0.093, data not shown). Transpiration at the young orchard related best to RedEdge amongst spectral bands and better to drone estimated tree height than to any of the vegetative indices (Appendix C: Table 41). Orchard upscaled transpiration decreased with increasing RedEdge spectral reflectance and increased with drone-estimated tree height (Figure 67a and b). The standard error of the estimate for these linear regression relationships was 0.03 and 0.048 mm for the RedEdge spectral band and drone-estimated tree height, respectively. The standard error of the estimate from the regression relationship of transpiration with NDVI was 0.068 mm ($R^2$ = 0.81, data not shown).

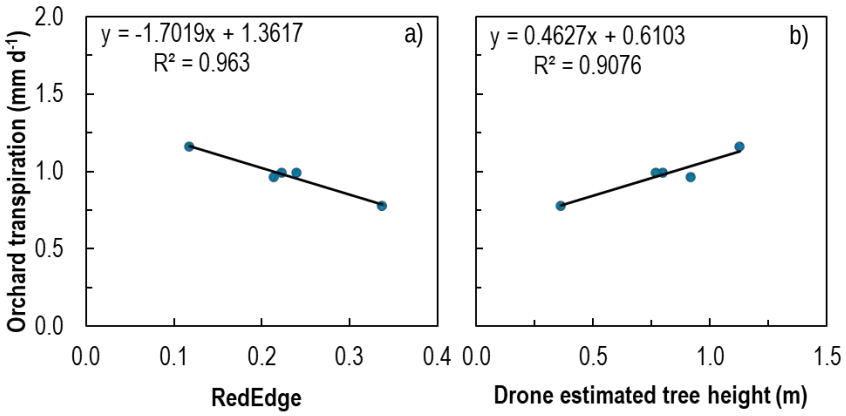


Figure 67. Regression relationships of orchard upscaled transpiration with orchard averaged drone image derived a) RedEdge spectral band reflectance and b) estimated tree height for drone surveys conducted in 2023/2024 in the young cultivar 'Wonderful' pomegranate orchard

Orchard level ETc of the young orchard did not relate significantly at a 95% or even a 90% confidence level to any of the drone image-derived variables (Appendix C: Table 41). Data surveyed early in the season (October 2023) was frequently identified as an outlying value, which prevented potential significant regression relationships of orchard level ETc with the drone image-derived variables. For the full bearing orchard, there were, except for an excellent regression relationship with TIR, no other significant linear regression relationships between orchard level ETc and any of the drone-derived variables. This is probably due to the variation between orchard orchard-averaged data available for only three surveys. Orchard level ETc increased from 1.9 to 4.6 mm $d^{-1}$ with TIR ranging between 29 and 41.2°C (Figure 68).

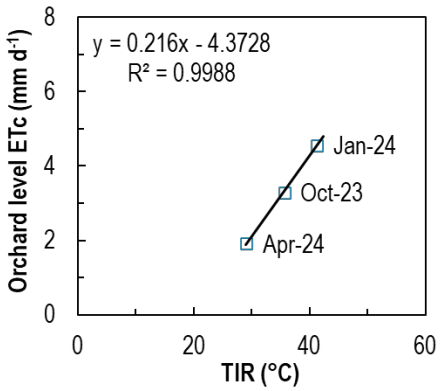


Figure 68. Regression relationship of orchard level evapotranspiration (ETc) with the orchard averaged drone image derived thermal infra-red temperature (TIR) for drone surveys conducted in 2023/2024 in the full bearing cultivar 'Wonderful' pomegranate orchard

Reference evapotranspiration at the young orchard related significantly to NDVI, NDRE, CVI, CIRE and TIR, with no significant regression relationships for the full bearing orchard at a 95% confidence level (Appendix C: Table 41). The ETo at the full bearing site though, was significantly related to TIR at a 7% significance level and to RVI. At the young orchard, ETo increased with CIRE (Figure 69a). The ETo at both sites increased with TIR, but the slopes of the trendlines differed (Figure 69b).

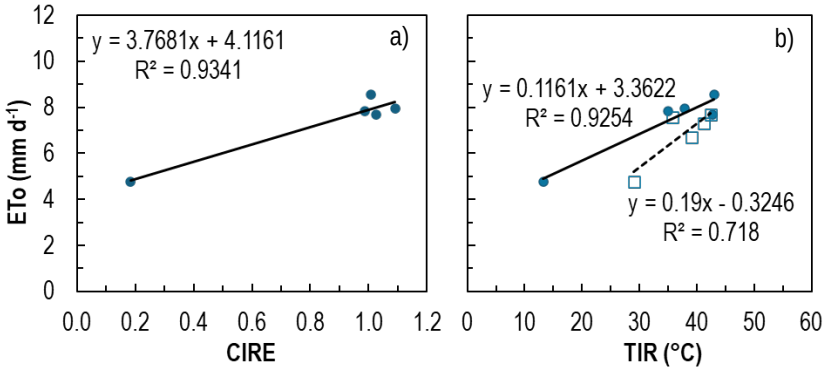


Figure 69. Comparison of the reference evapotranspiration (ETo) with orchard averaged drone image derived a) Chlorophyll Index – RedEdge (CIRE) and b) thermal infrared temperature (TIR). Data for the young and full bearing cultivar 'Wonderful' pomegranate orchards are indicated as circles and squares, respectively.

The orchard upscaled transpiration:ETo ratio was not significantly related to any of the drone-derived variables at a 5% or 10% significance level for both orchards at the individual level (Appendix C: Table 41). For the young orchard lack of significant relationships was caused by outlying datapoints originating either from October 2023 or April 2024, depending on which drone variable was related (data not shown). Orchard level ETc:ETo was significantly related to NIR for the young bearing orchard at a 95% confidence level, with no significant regression relationships for the full bearing orchard with any of the drone image-derived variables. The lack of significant relationships for the full bearing orchard may be due to limited data points available for regression analysis (n=3). The orchard level ETc:ETo ratio for the young orchard ranged between 0.13 and 0.34 and increased with increasing NIR (Figure 70). The ETc:ETo ratio and can be estimated from NIR with an error of 0.03.

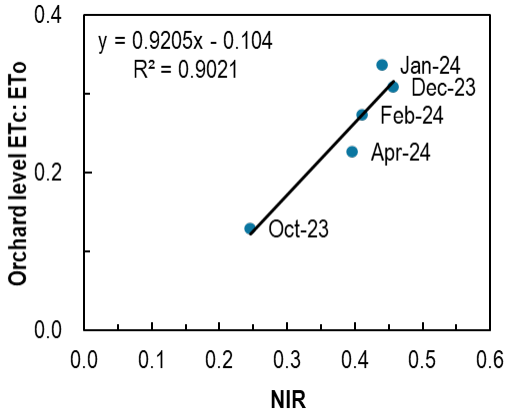


Figure 70. Comparison of the orchard level evapotranspiration to reference evapotranspiration (ETo) ratio with orchard averaged drone image derived near-infrared spectral band reflectance for drone surveys conducted in 2023/2024 in the young cultivar 'Wonderful' pomegranate orchard

Tree specific estimates of transpiration from the regression relationship between transpiration and RedEdge spectral reflectance for the five-year-old orchard (Figure 67a) indicated that the mean transpiration for the orchard about two months into in the development stage was 1.16 mm $d^{-1}$, with a maximum per tree of 1.21 mm $d^{-1}$ (Table 8). The estimated transpiration was fairly similar later during canopy development, at full canopy stage and before harvest in December, January and February, respectively, being on average 1 mm $d^{-1}$, but reachjng maximum values of between 1.13- and 1.24-mm $d^{-1}$ for some tree positions. The transpiration values decreased slightly in the period after harvest.

Tree specific estimates of the ETc:ETo ratio (Kc) from the regression relationship between ETc:ETo ratio and NIR (Figure 70) resulted in a mean crop coefficient of 0.13 about two months after bud break, with minimum and maximum values of 0.06 and 0.17, respectively (Table 8). When the canopy was already well developed (December) or fully developed (January and February), the mean Kc amounted to 0.29, with maximum values ranging between 0.41 and 0.49 at some tree positions. Very low Kc minimum values most likely indicate positions of poorly established trees in the orchard with minimal growth and/ or that the regression relationship still needs improvement in accuracy. The Kc decreased after harvest to 0.22, with a maximum value of 0.35 estimated for the orchard. The large difference between the mean and maximum Kc values indicates variability between trees in the orchard and water resources might be saved if precision irrigation is applied.

Table 8. Maximum, minimum and mean of tree specific transpiration or the ratio of crop evapotranspiration (ETc) to reference evapotranspiration (ETo) estimated from the regression relationships of these variables with RedEdge and near-infrared reflectance, respectively, derived from drone imagery for the five-year old cultivar 'Wonderful' pomegranate orchard for selected dates during the 2023/24 season

| Date | Transpiration (mm $d^{-1}$) | | | | ETc:ETo ratio | | | | |
|---|---|---|---|---|---|---|---|---|---|
| | Minimum | Maximum | Mean | STDev | Minimum | Maximum | Mean | STDev | n |
| 31/10/2023 | 1.08 | 1.21 | 1.16 | 0.011 | 0.06 | 0.17 | 0.13 | 0.013 | 4829 |
| 15/12/2023* | 0.80 | 1.15 | 1.03 | 0.027 | 0.15 | 0.49 | 0.30 | 0.027 | 4946 |
| 12/01/2024 | 0.88 | 1.13 | 1.04 | 0.028 | 0.15 | 0.41 | 0.30 | 0.028 | 4921 |
| 22/02/2024 | 0.61 | 1.24 | 0.97 | 0.059 | 0.02 | 0.49 | 0.28 | 0.042 | 5173 |
| 16/04/2024 | 0.67 | 1.16 | 0.92 | 0.064 | 0.01 | 0.35 | 0.22 | 0.035 | 5173 |

STDev – Standard deviation

## 7.4 CONCLUSIONS

At ***individual tree level***, for ***orchards combined***, *transpiration* related best to drone-estimated tree height or RVI ($R^2$ values around 0.46). The *ratio of transpiration to ETo* related significantly at a 95% confidence level the best to drone estimated tree height ($R^2$ = 0.367). The linear regression relationships of transpiration and transpiration:ETo ratio with NDVI was poor ($R^2$ = 0.37) and not significant, respectively. Soil water balance determined *ETc* related well at tree row and orchard level especially to RedEdge spectral reflectance and CVI ($R^2$ values of between 0.79 and 0.9), with no significant linear regression relationships for either water use indicator with NDVI. The *ETc:ETo ratio* in the tree row related significantly to the green, blue and RedEdge spectral band reflectance ($R^2$ values between 0.58 - 0.615), with no significant regression relationships between the ETc:ETo ratio at orchard level and any of the drone image-derived variables.

***Individual tree*** *transpiration* data of ***surveys combined*** for the *young orchard* related best to drone estimated tree height and RedEdge spectral band reflectance ($R^2$ values ≤ 0.355), whereas the regression relationship to NDVI was poorer ($R^2$ = 0.208). Individual tree *transpiration* at the *full bearing orchard* and the *transpiration: ETo ratio at both sites* were not significantly related to any of the drone-derived variables at a 5% significance level. Soil water balance-based *ETc* datasets were limited and did not render significant regression relationships that could aid in irrigation scheduling of the orchards. ***At the survey level*** at the *full bearing site*, regressions significant at a 95% confidence level were limited to that between *transpiration* and the *ratio thereof to ETo* with NIR and RedEdge spectral band reflectance, respectively, during the fourth survey. Soil water balance-derived *ETc* data were too limited to use for survey-level regression purposes.

The regression relationships between pomegranate tree water use and drone image-derived variables improved from individual tree towards orchard orchard-averaged scale. At the ***orchard averaged level***, for ***sites combined***, *orchard upscaled tree transpiration* related at a 5% significance level linearly the best to and increased with orchard averaged RVI ($R^2$ = 0.92, $SE_{est}$ = 0.061 mm $d^{-1}$). Regressions of orchard transpiration with NDVI and drone-estimated tree height resulted in coefficients of determination of 0.71 and 0.7, respectively, at a similar significance level, with standard error of the estimates around 0.11 mm $d^{-1}$. Micrometeorological system determined *orchard level ETc* for sites combined related significantly only to RVI at a 10% significance level ($R^2$ value of 0.42) with a large standard error of the estimate, i.e. 0.956. The poor regression relationships with the drone-derived variables were mostly due to an outlying value originating from January 2024 for the full bearing orchard, but in some cases one from October 2023 for the young orchard as well. For data of orchards combined, the *ratio of orchard transpiration to ETo* related significantly only to drone estimated tree height and volume at a 10% significance level ($R^2$ values 0.41 and 0.45, respectively), with a standard error of the estimate of about 0.2 for both variables. The *ratio of orchard level ETc to ETo* related significantly at the 10% significance level, reasonably only to drone estimated tree height with an $R^2$ values of 0.44, but the standard error of the estimate was 0.12, which is too large to allow accurate estimates of the ratio.

***Orchard upscaled transpiration*** *data for the* ***young orchard*** considered on its own, related linearly the best to the orchard averaged RedEdge spectral band reflectance ($R^2$ = 0.96, standard error of the estimate 0.03), whereas NDVI comparatively correlated poorer ($R^2$ = 0.811) while the standard error of the estimated transpiration increased to 0.068. There were no significant relationships at a 95% confidence level between *orchard upscaled transpiration of the* ***full bearing orchard*** and any drone image-derived variables at site level, most likely due to the variability of the limited data set available. There were no significant relationships between ***orchard-level ETc*** *of the* ***young orchard*** and the drone image-derived variables even at a 90% confidence level. For the ***full bearing orchard,*** *orchard level ETc* can be estimated from a linear regression relationship with TIR based on a limited number of datapoints ($R^2$ = 0.999), with no other significant regression relationships between orchard level ETc and other drone-derived variables, probably due to the variation of a limited dataset. Furthermore, there were no significant regression relationships for the ***young or full bearing orchards*** between the ***orchard upscaled transpiration:ETo ratio*** and any drone image-derived variables at a 5% significance level. However, the ***orchard level ETc:ETo ratio for the young orchard*** can be estimated from NIR at a %5 significance level with a standard error for the ETc:ETo estimate of 0.03. There were no significant regression relationships for the ***full bearing orchard level ETc:ETo ratio*** with any of the drone image-derived variables, probably due to limited data points available for regression analysis.

Estimation of transpiration and especially the ETc:ETo ratio for the five-year-old orchard from the regression relationships with RedEdge and NIR spectral band reflectance, respectively, indicated the presence of large variability in the orchard, which will benefit from application of precision irrigation. The estimated orchard mean transpiration (±standard error) for summer amounted to 1.01(±0.02) mm $d^{-1}$, but individual tree position transpiration could reach a maximum of 1.24 mm $d^{-1}$. The estimated orchard mean Kc

during summer was 0.29, which could increase by almost 70% for individual trees. If you irrigate according to the mean, underirrigation will be inevitable for some trees in the orchard, which might affect the orchard canopy development goals or productivity negatively. On the other hand, overirrigation could result in loss of precious water resources and expensive fertilizers beyond the root zone.

A collection of additional data sets in different orchards and/ or over more seasons is required to increase the database and to validate statistically significant regression relationships to enable reliable estimation of orchard-level transpiration, ETc and crop coefficients from drone image-derived variables for pomegranate orchards varying in canopy size.

# CHAPTER 8: ESTIMATING TREE WATER USE FROM IN-FIELD MEASURED TREE PROPERTIES

## 8.1 INTRODUCTION

Allen and Pereira (2009) used ground cover and crop height or LAI data to define a crop density coefficient that was used to directly estimate Kc and Kcb values for purposes of irrigation scheduling for a variety of annual and perennial crops (Pereira et al., 2020). The current research on pomegranate orchard water use poses the opportunity to relate ground-measured tree properties to transpiration, evapotranspiration, and the ratios thereof to ETo.

## 8.2 METHODOLOGY

In 2023/2024 data on tree geometrical properties, light interception and water use data were collected on five days representative of different pomegranate tree phenological development stages at the young (Avontuur) and full bearing (Welgemoed) cultivar 'Wonderful' pomegranate orchards (Refer to Chapter 3 for details on methodology). Tree properties (tree height, width in the tree row, width across the tree row, tree bottom height) were measured for the same individual trees where sap flow (4), soil water balance (2), growth (5) and stem water potential (6) were measured. Measurements for stem water potential trees only started from December 2023. Tree volume was calculated from tree dimensions, whereas ceptometer modelled LAI data (CP-LAI) was derived from the Accupar LP-80 measurements. Canopy area-based LAI (Tr-LAI) and orchard LAI (OLAI) were derived from the ceptometer measured data, canopy dimensions and *in situ* calibration of the LP-80 to enable leaf area estimates (Refer Chapter 5). Weather stations, sap flow, soil water balance and micrometeorological systems automatically logged at least hourly the data required to calculate tree and orchard scale water use and crop coefficients (Refer to Chapter 3 for details of methodology).

Simple linear regressions were conducted between water use and tree properties for individual trees in orchards and at orchard scale. Orchard averaged values of ground measured tree dimensions (tree height, width in the tree row, width across the tree row, tree volume), fractional interception (FI) and leaf area indices were compared to orchard upscaled transpiration and orchard level evapotranspiration (ETc) determined by micrometeorological methods (surface renewal and eddy covariance). Regression models were considered significant at a 95% level of confidence (p=0.05).

## 8.3 RESULTS AND DISCUSSION

Linear regression results are first presented at individual tree level for orchards combined and for the young and full bearing orchards separately (Table 40) and then per survey per orchard (Tables 41 and 42). Orchard averaged data results are presented for both orchards combined (Table 43) and individually (Tables 44 and 45).

### 8.3.1 Individual tree level

For selected trees of orchards combined, transpiration related significantly but poorly to tree height, across row width, in row width, tree volume, FI and ceptometer-based LAI, with $R^2$ values ranging from 0.151 to 0.463 (Table 42). Transpiration is related only to Tr-LAI and OLAI at a lower significance level, with p-values greater than 0.06. The transpiration to ETo ratio related better than transpiration to tree height, across row width, FI and CP-LAI (Figures 71-74) and was also significantly related at a 95% significance level to OLAI (Table 42).

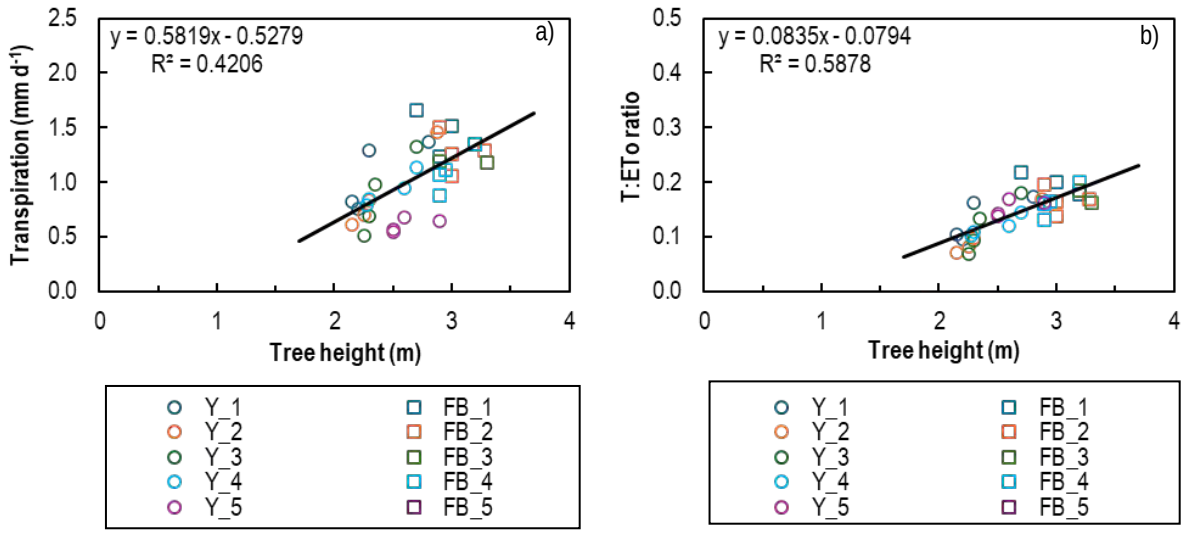


Figure 71. Comparison of a) sap flow derived tree transpiration (T) and b) the ratio thereof to reference evapotranspiration to measured individual tree height data for five drone surveys conducted during 2023/2024 for young and full bearing cultivar 'Wonderful' pomegranate trees

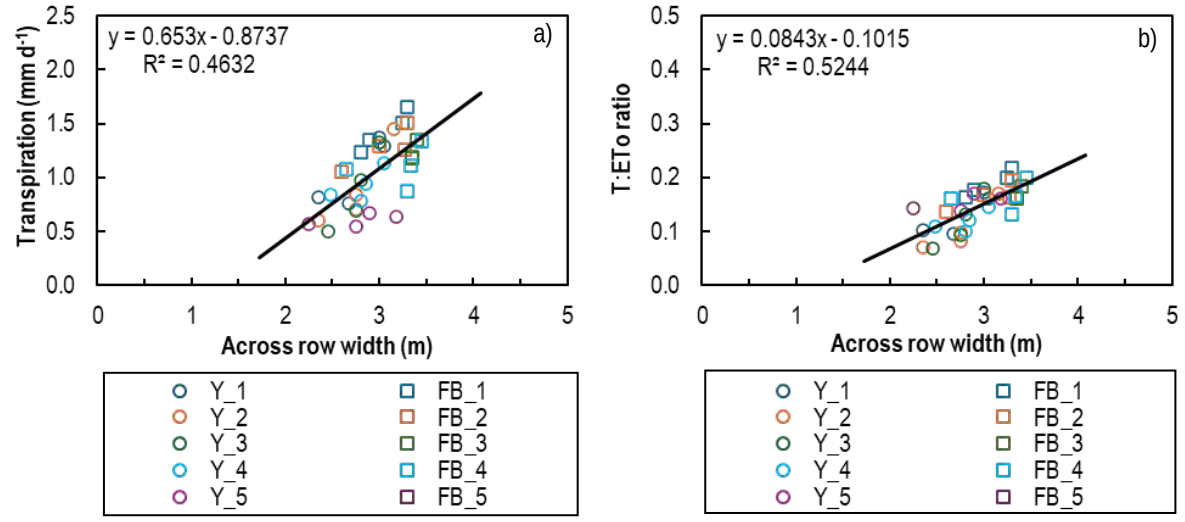


Figure 72. Comparison of a) sap flow derived tree transpiration (T) and b) the ratio thereof to reference evapotranspiration (ETo) to measured individual tree across row canopy width data for five drone surveys conducted during 2023/2024 for young and full bearing cultivar 'Wonderful' pomegranate trees

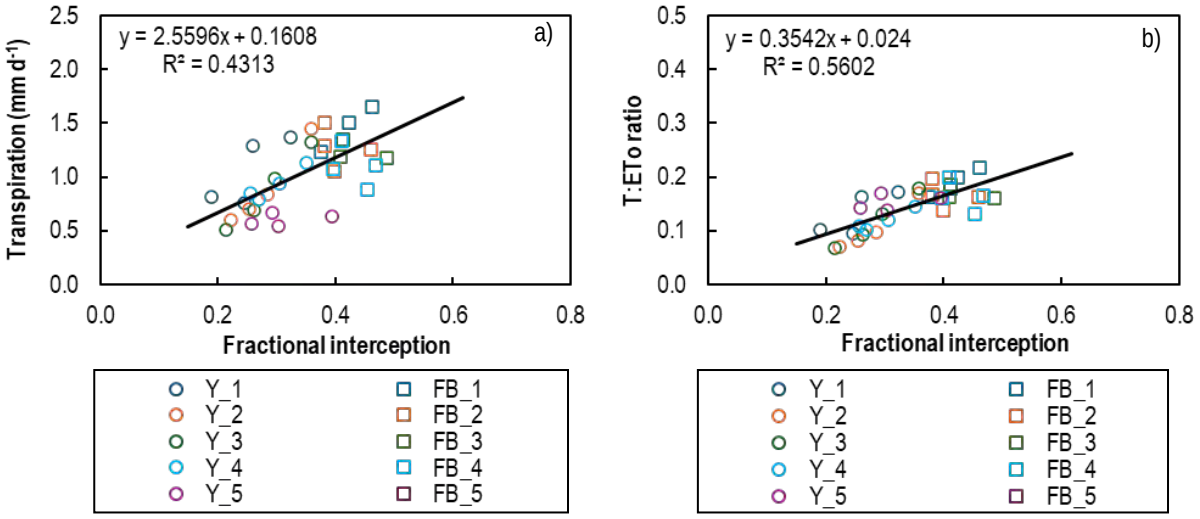


Figure 73. Comparison of a) sap flow derived tree transpiration (T) and b) the ratio thereof to reference evapotranspiration (ETo to measured individual tree fractional interception data for five drone surveys conducted during 2023/2024 for young and full bearing cultivar 'Wonderful' pomegranate trees

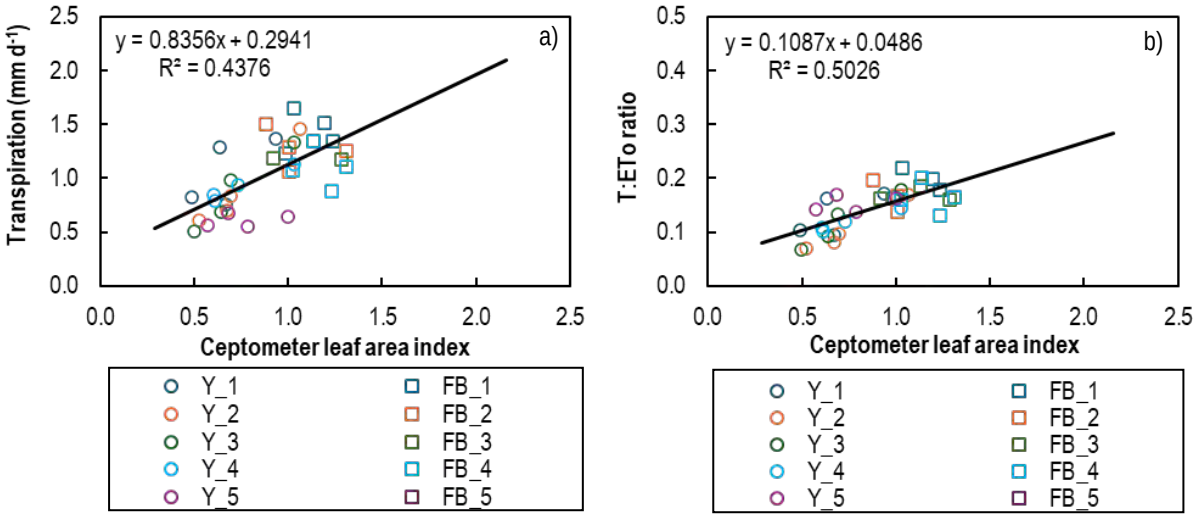


Figure 74**.** Comparison of a) sap flow derived tree transpiration (T) and b) the ratio thereof to reference evapotranspiration (ETo) to ceptometer measured individual tree leaf area index data for five drone surveys conducted during 2023/2024 for young and full bearing cultivar 'Wonderful' pomegranate trees

Transpiration of selected trees in the young orchard related significantly to all the tree canopy related variables measured, but the best to calculated tree volume ($R^2$ = 0.538, Table 42, Figures 75 and 76). It unexpectedly had the poorest correlations with tree height (Figure 75a, $R^2$ = 0.23) and FI (Figure 76a, $R^2$ = 0.238). The transpiration of the full bearing orchard did not relate significantly to any of the canopy dimensions, FI or leaf area indices. At survey level, for the young orchard, selected tree transpiration or the ratio thereof to ETo was not significantly related to any of the tree variables measured during the first or the fifth survey (Tables 43 and 44). It related consistently significantly to FI and the three leaf area indices, with $R^2$ values exceeding 0.91 during drone surveys 2, 3 and 4 conducted during summer (Figure 77). Transpiration and the ratio thereof to ETo related significantly to tree height only during survey 2 ($R^2$ = 0.99) and to tree volume during survey 2 and 3 with the coefficient of determination being 0.91 and 0.98, respectively (Tables 43 and 44). For the full bearing orchard, transpiration and the ratio thereof to ETo were only significantly related to FI during the first survey and to across row canopy width during survey 1 and 3 (Tables 43 and 44, Figures 75 and 76). Lack of significant regression relationships has previously been explained by the absence of variation in canopy dimensions in and a limited dataset for the full bearing orchard.

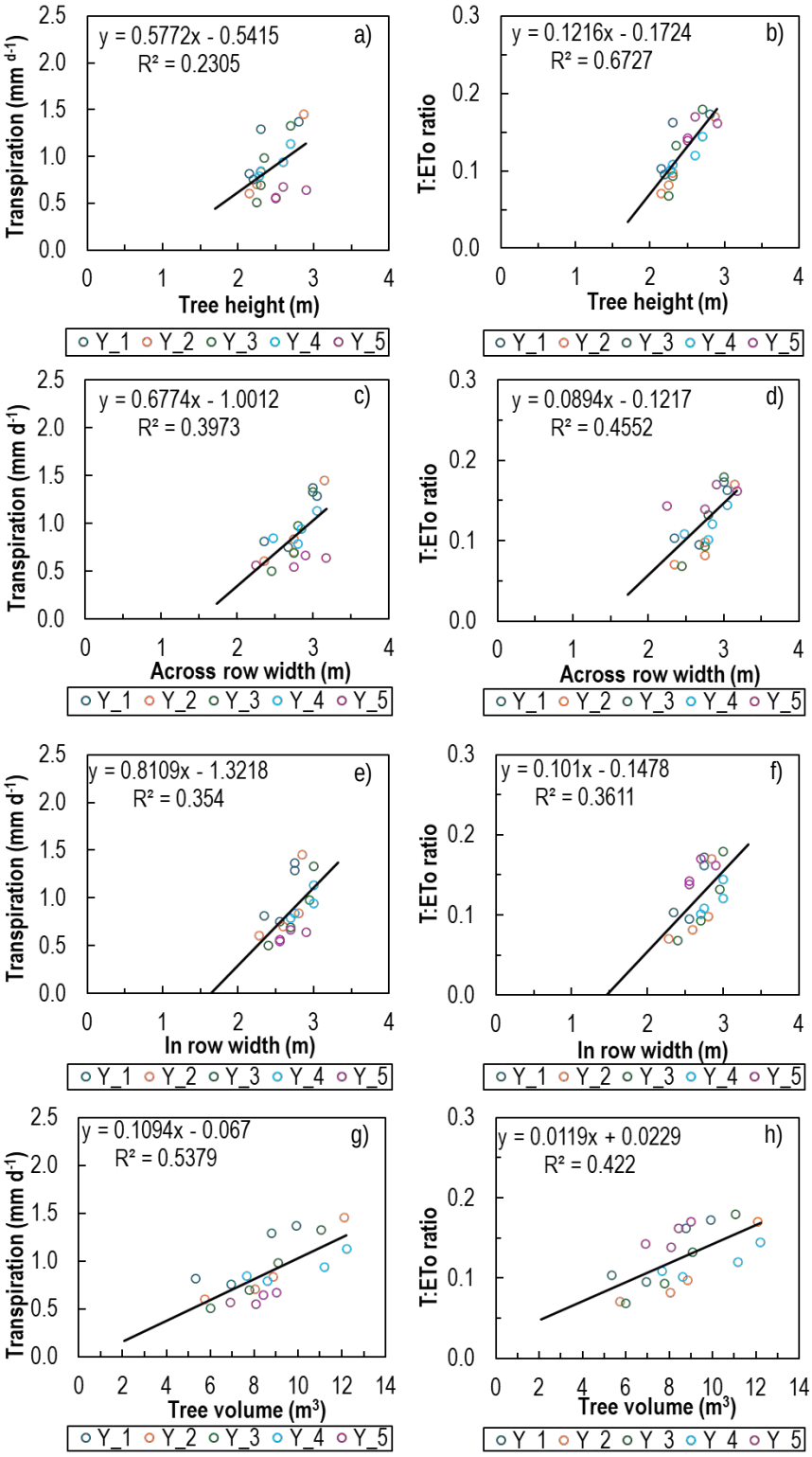


Figure 75**.** Comparison of sap flow derived tree transpiration (T, a, c, e, g) and the ratio thereof to reference evapotranspiration (ETo, b, d, f, h) to measured individual tree height (a, b), across row canopy width (c, d), in row canopy width (e, f) and tree volume (g, h) data for five drone surveys conducted during 2023/2024 for young cultivar 'Wonderful' pomegranate trees

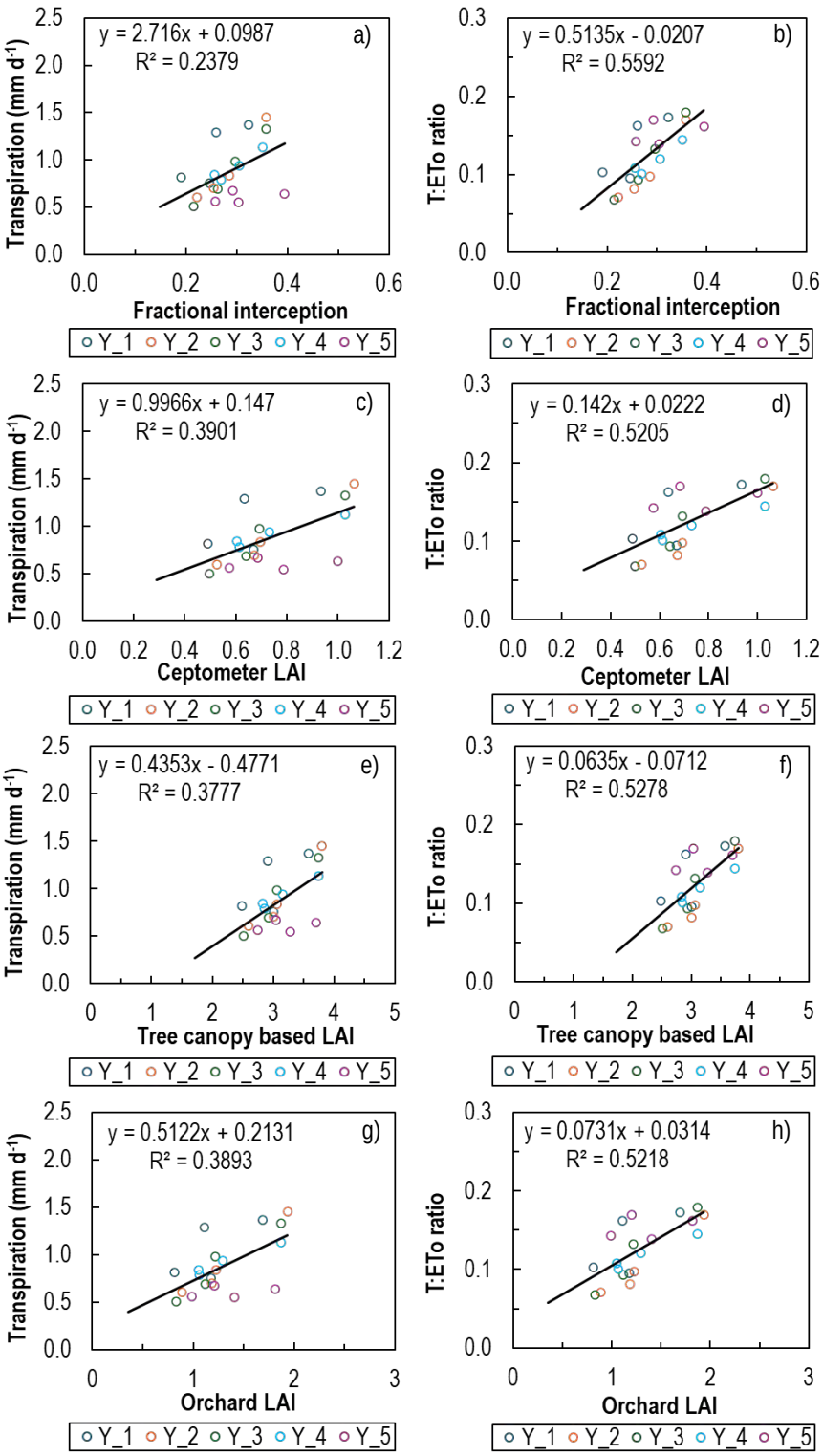


Figure 76. Comparison of sap flow derived tree transpiration (T, a, c, e, g) and the ratio thereof to reference evapotranspiration (ETo, b, d, f, h) to measured individual tree fractional interception (a, b), ceptometer leaf area index (c, d), tree canopy area based leaf area index (e, f) and orchard leaf area index (g, h) data for five drone surveys conducted during 2023/2024 for young cultivar 'Wonderful' pomegranate trees

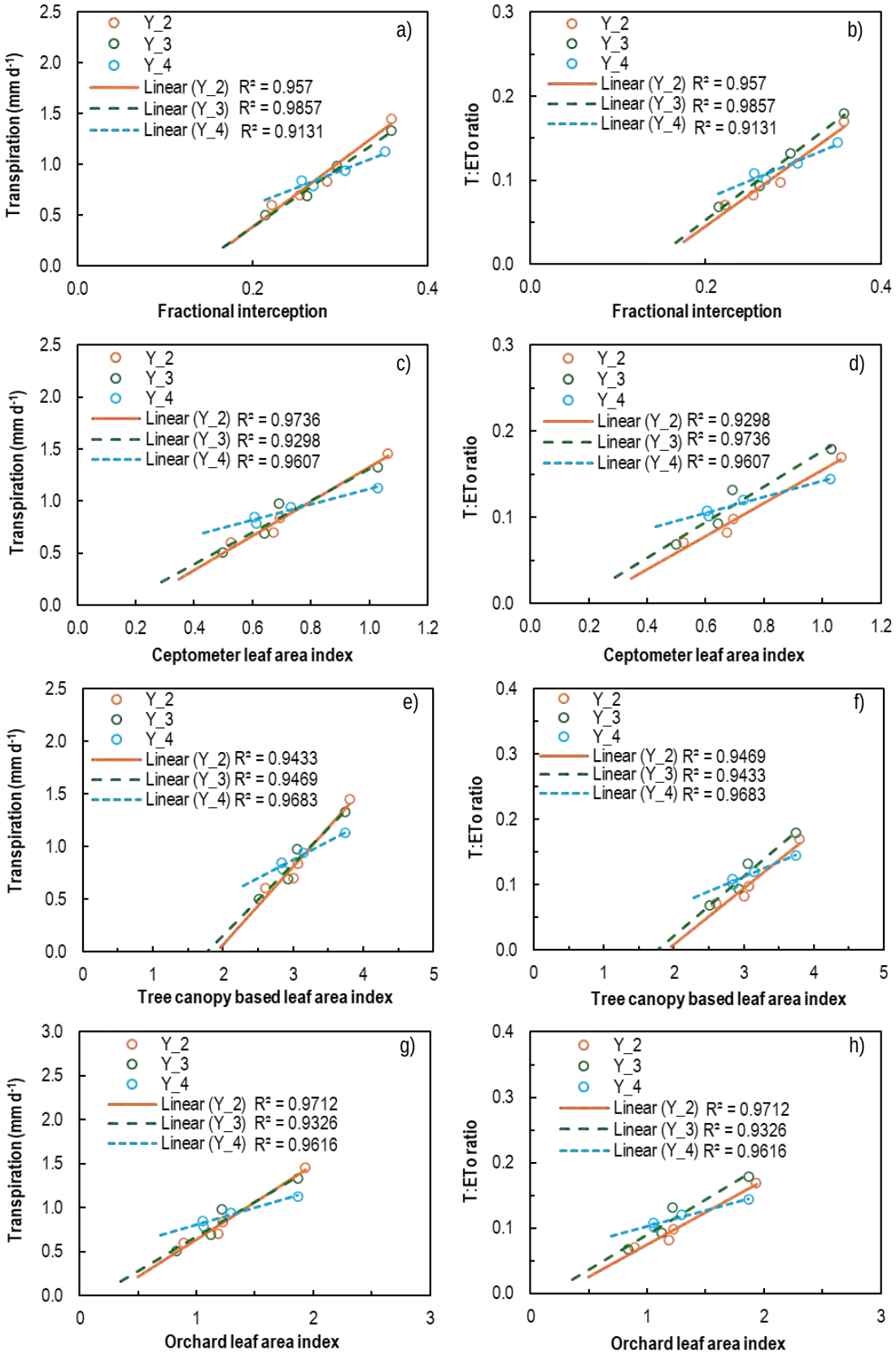


Figure 77. Comparison of sap flow derived tree transpiration (T, a, c, e, g) and the ratio thereof to reference evapotranspiration (ETo, b, d, f, h) to measured individual tree fractional interception (a, b), ceptometer based leaf area index (LAI, c, d), tree canopy based LAI (e, f) and orchard LAI (g, h) on selected days during December 2023 (Y2), January 2024 (Y3) and February 2024 (Y4) for the young cultivar 'Wonderful' pomegranate trees at Avontuur

### 8.3.2 Orchard level

Orchard upscaled transpiration for orchards combined related significantly at a 95% significance level only to orchard averaged Tr-LAI with a coefficient of determination of 0.72 (Appendix D: Table 45). Orchard level ETc for orchards combined was significantly, but poorly related to tree volume and CP-LAI at a 5% significance level. Other site-specific factors probably affected transpiration and orchard-level ETc to a greater extent than the variables mentioned above, resulting in atypical regression trends or data distribution patterns when data of orchards were combined (data not shown).

The ratio of orchard upscaled transpiration to ETo and orchard level ETc:ETo ratio was significantly linearly related at a 5% significance level to tree height, FI and CP-LAI, respectively (Appendix D: Table 45, Figure 78). The respective ratios increased with increasing tree height, FI and ceptometer based LAI, but additional data is required mid-range to improve the regressions and to validate it. In addition to these variables, the orchard level ETc:ETo ratio related significantly to across row width and tree volume at a 5% significance level, with $R^2$ values of 0.72 and 0.78, respectively (Table 45, Figure 79). However, the standard error of the estimated ETc:ETo ratio based on the data of orchards combined for the abovementioned variables ranged between 0.076 and 0.09, which is quite high.

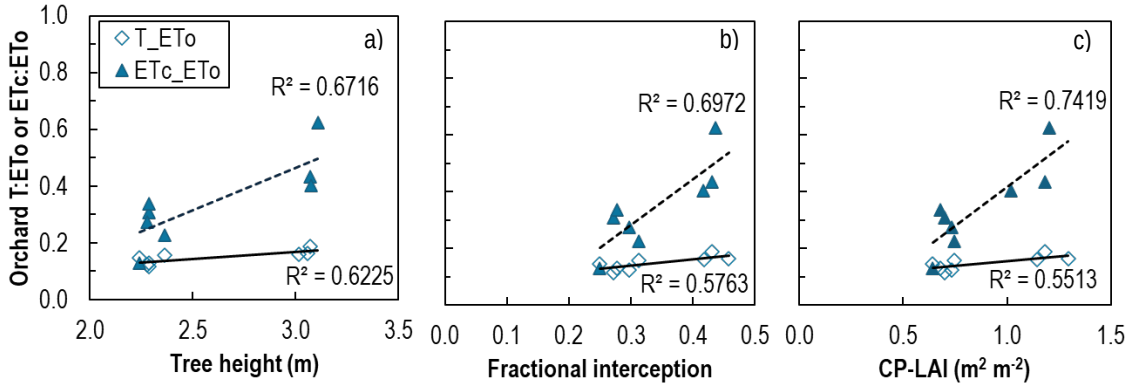


Figure 78. Comparison of the relationship between the ratio of orchard upscaled transpiration (T, diamond markers) or orchard level evapotranspiration (ETc, triangle markers) to reference evapotranspiration (ETo), respectively, with orchard averaged a) tree height, b) fractional interception and c) ceptometer based leaf area index (CP-LAI) for available data from five drone surveys conducted during the 2023/2024 season at the young and full bearing cultivar 'Wonderful' pomegranate orchards

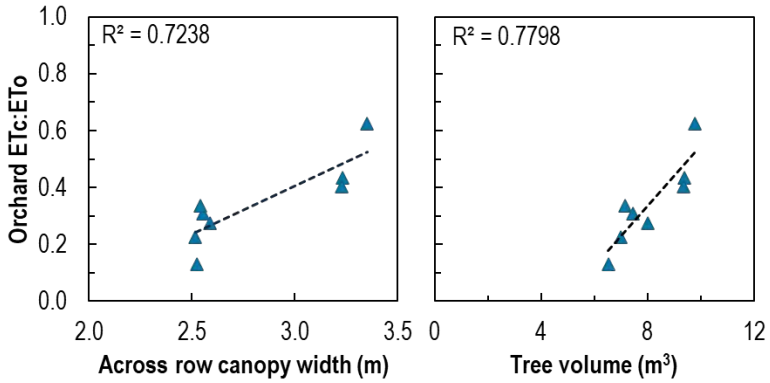


Figure 79. Comparison of the relationship between the ratio of orchard scale evapotranspiration (ETc) to reference evapotranspiration (ETo) with orchard averaged a) across row canopy width and b) tree volume for available data from five drone surveys conducted during the 2023/2024 season at the young and full bearing cultivar 'Wonderful' pomegranate orchards

Orchard upscaled transpiration for the young orchard considered on its own related significantly at a 5% significance level to tree height, FI, CP-LAI, Tr-LAI and OLAI (Appendix D: Tables 46 and 47, Figures 80 and 81). Orchard averaged data resulted, as in the case where data for orchards were combined for orchard transpiration vs Tr-LAI, in a negative correlation of transpiration with not only tree height and FI (Figure 80), but also with the various LAI variables (Figure 81). Since tree height increased over the season (data not shown), it could be that the effect of atmospheric evaporative demand or factors such as stomatal control and/ or leaf aging surpassed that of the tree canopy properties on the already low transpiration rates, resulting in these apparently illogical trends. There were no significant relationships between orchard upscaled transpiration or orchard level ETc, respectively, with ETo (Appendix D: Table 46). Data from October 2023 appeared to be an outlying value, which added to variability (data not shown). There were no significant regression relationships of orchard upscaled transpiration at the full bearing orchard with any of the other field-measured variables. Orchard ETc or the ratio of transpiration or ETc, respectively, to ETo, was not significantly related to any of the field measured canopy properties for the orchards considered separately, with the exception of the orchard level transpiration:ETo ratio for the full-bearing orchard across row width and tree volume. However, these regression relationships had only three data points, which were not evenly distributed and the regression relationships were not considered reliable (data not shown).

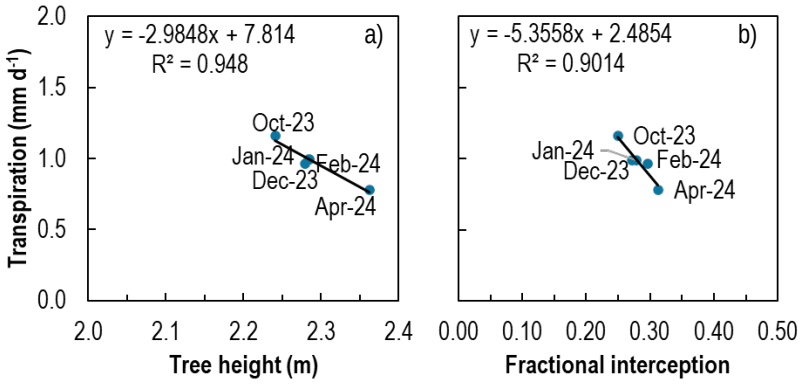


Figure 80. Comparison of the linear regression relationships orchard level upscaled transpiration to orchard averaged a) tree height and b) fractional interception for data from five drone surveys conducted during the 2023/2024 season at the young cultivar 'Wonderful' pomegranate orchard

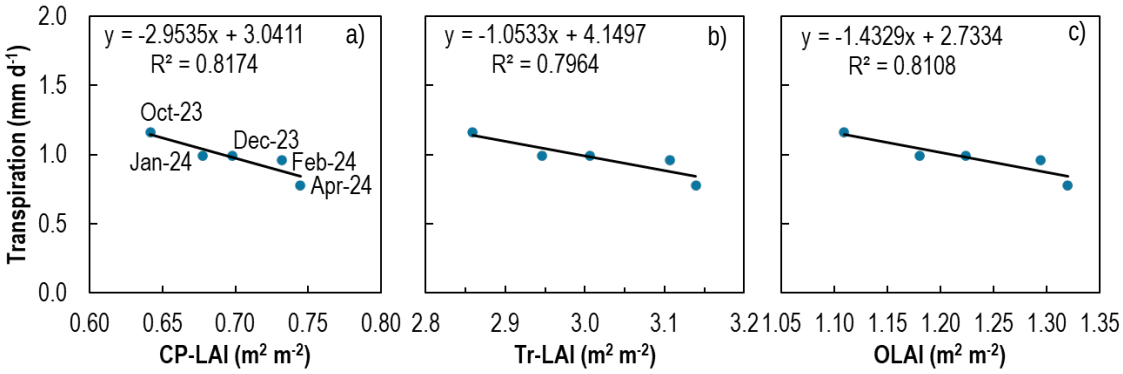


Figure 81. Comparison of the linear regression relationships of orchard level upscaled transpiration to orchard averaged a) ceptometer derived leaf area index (CP-LAI), tree canopy area based leaf area index (Tr-LAI) and c) orchard leaf are index (OLAI) data from five drone surveys conducted during the 2023/2024 season at the young cultivar 'Wonderful' pomegranate orchard

## 8.4 CONCLUSIONS

The regression relationships between measured tree water use and tree geometric properties of the young and full-bearing pomegranate orchards were poorer than expected. For individual tree data of both orchards combined, transpiration and its ratio to ETo related best to tree height, across row canopy width, FI and CP-LAI, with the highest coefficient of determination reaching only 0.588. At the individual orchard level, only the young orchard acquired significant linear regression relationships, with a limited dataset hampering proper evaluation for the full bearing orchard. Transpiration in the young orchard related significantly to all the tree canopy-related variables measured, but the best to calculate tree volume ($R^2$ = 0.538) and unexpectedly the poorest to tree height ($R^2$ = 0.23) and FI ($R^2$ = 0.238). Transpiration of the individual trees in the young orchard was not related to any tree geometric properties early in the season and after harvest, but it related well to and increased with FI and LAI after most of the fruit set in December 2023, at full canopy development stage in January 2024 and shortly before harvest in February 2024 ($R^2$ values> 0.9). For the full bearing orchard, transpiration and the ratio thereof to ETo were only significantly related to FI early in the season during October 2023 and to across row canopy width during October 2023 and January 2024. Lack of significant regression relationships for the full bearing orchard can be explained by the absence of variation in canopy dimensions and a limited dataset.

For data of orchards combined, the ratio of orchard upscaled transpiration to ETo as well as ETc:ETo were significantly linearly related at a 5% significance level to tree height, FI and CP-LAI. The respective ratios increased with increasing tree height, FI and ceptometer-based LAI, but additional data are required mid-range to improve the regressions and to validate it. The orchard level ETc:ETo ratio was also significantly related to across row width and tree volume at a 5% significance level with $R^2$ values of about 0.73. The standard error of the ETc:ETo estimates from the above variables were between 0.076 and 0.9, which is considered too high to estimate the ratio accurately.

There were no significant regression relationships of orchard upscaled transpiration at the full bearing orchard with other tree canopy measured variables. The orchard ETc or the ratio of transpiration or ETc to ETo, respectively, was not significantly related to any of the field-measured canopy properties for the orchards considered separately. The exception was the orchard upscaled transpiration:ETo ratio for the full bearing orchard, but due to the limited number of data points, regression relationships across row width and tree volume were not considered reliable. Several anomalous significant regression relationships were obtained between orchard upscaled transpiration and selected tree canopy variables for the orchards combined and for the young orchard on its own. A collection of additional datasets are recommended to improve regression relationships and to resolve atypical linear regression trends found for transpiration with tree height, FI and LAI at orchard scale.

# CHAPTER 9: ORCHARD HOMOGENEITY FOR TWO ORCHARDS VARYING IN CANOPY COVER

## 9.1 INTRODUCTION

Quantification of orchard homogeneity supply supplementary information on the orchard properties underlying the single seasonal water use values obtained via sap flow and micrometeorological methods that will be made available for decision support and policy making in the water sector. In this chapter orchard homogeneity of a young and a full bearing orchard was evaluated using drone image derived spectral bands, indices, tree geometric dimensions and TIR.

## 9.2 METHODOLOGY

In 2023/2024 five drone surveys, representative of different pomegranate tree phenological development stages, were conducted at the young (Avontuur) and full bearing (Welgemoed) cultivar 'Wonderful' pomegranate orchards (Refer to Chapter 3 for details on methodology and UAV). Drone flights were scheduled for October 2023 (early season), December 2023 (development), January (full canopy), February (before harvest) and April 2024 (post-harvest). Orchard averaged multispectral band reflectance values (blue, green, near-infrared, red, RedEdge), selected spectral vegetation indices (NDVI, NDRE, GNDVI, RVI, CVI, CIRE) and drone image-derived geometric traits (tree height, tree volume) and TIR were used to determine the tree homogeneity of orchards. Spectral profiles were used to compare the reflection of different spectral bands by the orchards over the season. Histograms visualize the size distribution of individual tree canopy characteristics determined using drone technology for each characteristic in each orchard. The histograms (b) indicate the normal distribution, average and standard deviation of data per survey per orchard. The data distribution according to the boxplot (a) indicates the minimum, lower quartile (25th percentile), median, upper quartile (75th percentile), and maximum. Seasonal variation for each canopy characteristic was obtained for each orchard by combining the averages obtained from each survey done from October 2023 until April 2024. SAS software (Version 9.4, SAS Institute Inc, Cary, USA) and XLStat (Lumivero, 2024) were used to conduct statistical analysis.

## 9.3 RESULTS AND DISCUSSION

### 9.3.1 Spectral profile dynamics

For all five surveys at both sites the highest reflectance was in the NIR band, followed by RedEdge (Figure 82). For healthy vegetation, NIR reflectance of up to 50% can be expected (Gibson, 2000). At the young orchard the blue, green, red and RedEdge reflectance tended to increase gradually from October 2023 to April 2024, whereas the NIR was the lowest in October, peaked during summer and decreased again in April 2024 (Figure 82a). For the full bearing orchard the blue, green, red and RedEdge reflectance was similar for October, December and January and increased slightly during February, after which it decreased towards the end of the season in April 2024 (Figure 82b). According to Gibson (2000, in Kumar), a 10% reflection in the green band is typical for healthy crops. The canopies of both pomegranate orchards approached this value only near the end of the season (Figure 82).

The NIR, green and RedEdge reflectance was higher in the full bearing orchard compared to that in the young orchard during survey 1 in October 2023 (Figure 83a). The NIR reflectance reached its maximum in December 2023 and was higher in the young orchard (0.44) compared to that in the full bearing orchard (0,4) (Figure 83b). The NIR was considerably higher in the young orchard compared to the full bearing one in January (Figure 83c), which might indicate temporary stressed conditions in the full bearing orchard. The NIR reflection was almost comparable for the two orchards in February shortly before harvest (Figure 83d). In April 2024 the blue, red and RedEdge reflectance of the young orchard exceeded that of the full bearing orchard and the NIR became somewhat less (Figure 83e). Plant stress may increase reflectance in the blue and red bands and reduce reflectance in the NIR band, whereas denser canopies may have higher infrared reflection compared to sparse canopies (Gibson, 2000).

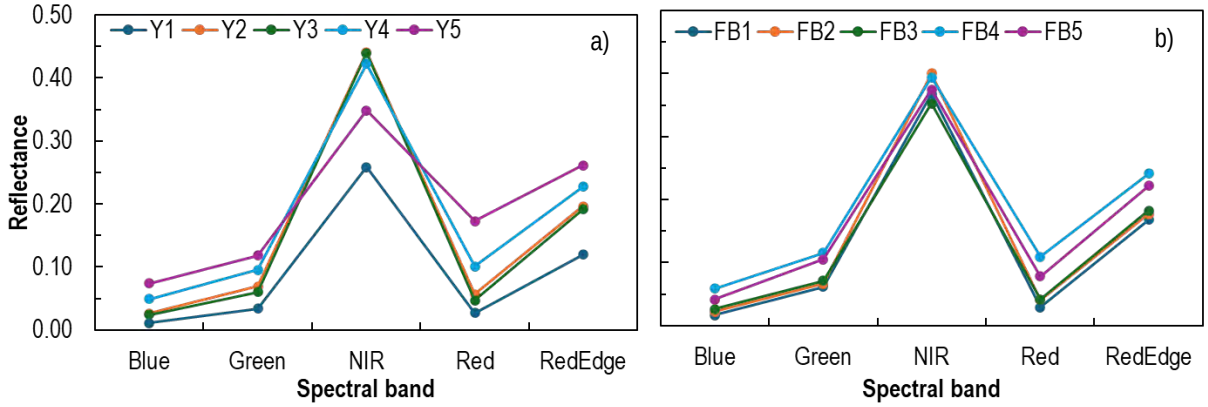


Figure 82. Comparison of spectral profiles of an a) young (Y) and b) full bearing (FB) orchard for five drone surveys conducted during the 2023/2024 growing season

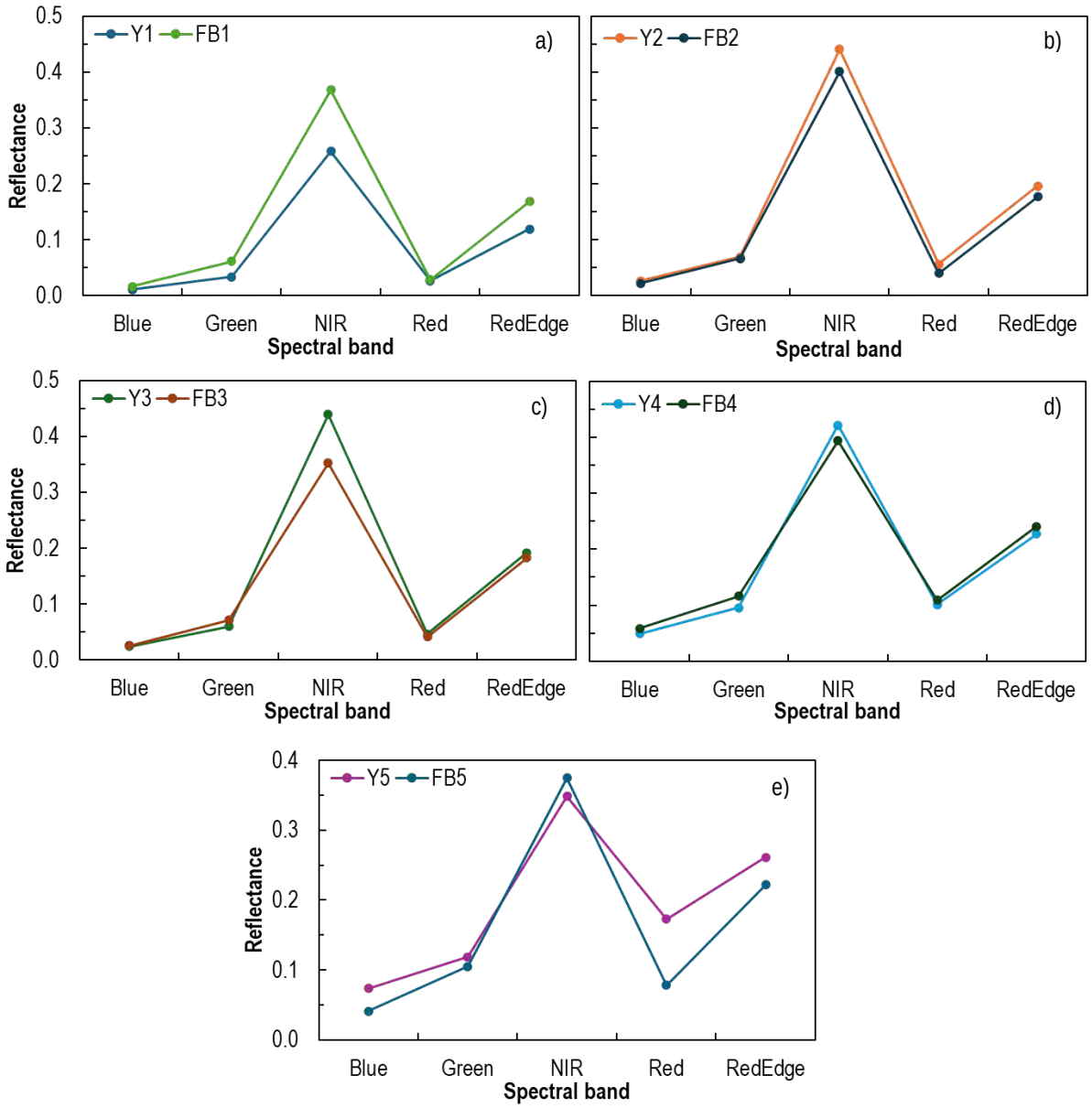


Figure 83. Comparison of spectral profiles derived from multispectral images of drone surveys conducted during a) October 2023, b) December 2023, c) January 2024, d) February 2024 and e) April 2024 for a young (Y) and full bearing (FB) cultivar 'Wonderful' pomegranate orchard at Avontuur and Welgemoed, respectively

### 9.3.2 Variation in tree canopy characteristics

Variation in individual tree canopy characteristics determined for the five drone surveys conducted over the 2023/2024 growing season is displayed in box plots and histograms to visualize the data distribution of each characteristic for each orchard (Appendix E: Figures 86-99). A summary of statistics included in the boxplot is also provided in Table 48 in Appendix E. Each histogram indicates in the legend the average and standard deviation of the specific spectral band, index, or canopy characteristic depicted per survey and orchard (Appendix E: Figures 86b-99b). Reflectance in the blue band ranged between 0.09 and 0.279 (Appendix E: Table 48). It was comparable for the two orchards from October until February (Appendix E: Figure 86a). The reflectance increased at both orchards towards February before harvest, but in April, after harvesting, it still increased at the young orchard while it decreased at the full bearing orchard. Reflectance in the green spectral band ranged between 0.019 and 0.31 (Appendix E: Table 48). It was initially lower in October in the young orchard, but comparable to that of the full-bearing orchard for the rest of the season (Appendix E: Figure 87a). Reflectance in the green band increased in February and April compared to earlier in the season for both orchards. Reflectance in the red spectral band ranged between 0.016 and 0.343 (Appendix E: Table 48). It followed the same trends as the blue, but the mean reflectance values were somewhat higher compared to those for blue (Appendix E: Figures 86a and 88a, Table 48). Increased reflectance in the blue and red bands might indicate some form of stress that interrupts normal tree growth and productivity (Gibson, 2000). Values for the near-infrared (NIR) band ranged between 0.127 and 0.643. It was low at the young orchard in October, but increased to about 0.44 during the summer months, whereafter it decreased to 0.35 (Appendix E: Figure 89a, Table 48). The NIR reflectance for the full bearing orchard had a variable pattern and the mean ranged between 0.35 and 0.4 for all five surveys. The NIR reflection of the young orchard probably reflects the active development of the canopy and, nearer to the end of the season, senescence of leaves, whereas the full bearing orchard canopy does not change much in size and density over the season. Mean NIR reflectance was overall much higher compared to the blue, green and red spectral bands (Appendix E: Table 48), which is expected for healthy plants (Gibson, 2000). RedEdge reflection ranged between 0.07 and 0.442 (Appendix E: Figure 90, Table 48). It followed a similar pattern to that of the blue, green and red bands (Appendix E: Figures 86a-88a). RedEdge at the young orchard reached a maximum of 0.26 in April, whereas it reached a maximum of 0.24 for the full bearing orchard in February (Appendix E: Table 48).

With regard to drone image-derived spectral band indices, NDVI ranged between 0.05 and 0.855 for the young and 0.156 and 0.914 for the full bearing orchard (Appendix E: Figure 91a, Table 48). The mean NDVI at the young orchard remained between 0.107 and 0.81 during October until January, after which it decreased to 0.63 in February shortly before harvest. It decreased further to 0.35 during April 2024. At the full bearing orchard mean NDVI decreased gradually from 0.85 in October 2023 to 0.79 in January 2024. Hereafter, it decreased to 0.6 shortly before harvest in February and tended to increase again, reaching 0.67 in April. The NDVI, NDRE, GNDVI and CIRE displayed more or less similar trends for the two orchards, although the values for the indices differed (Appendix E: Figures 91a, 92a, 93a, 96a, Table 48). The RVI, which represents biomass, water content and nitrogen (Table 5), also tended to have the same trend as the abovementioned for the young orchard, but for the full bearing orchard the index decreased from October to December 2023 and January 2024 and then steeply towards February and April, which had similar values (Figure 94a). The RVI of the full bearing orchard tended to be higher than that for the young orchard until January 2024. The CVI did not display any particular trend over the season for both orchards, although it was slightly higher for the young orchard compared to the full bearing one (Figure 95a). Furthermore, there was an exceptionally high value with a large deviation from the median in April 2024 for the young orchard.

Tree height estimated from the drone images appeared not to vary a lot over the season, but it distinguished clearly between the heights of the young and the full-bearing orchards (Appendix E: Figure 97a). Estimated tree height ranged between 0.6102 and 0.982 for the young orchard and 1.59 and 2.04 m for the full bearing orchard over the season (Appendix E: Table 48). Especially for the full bearing orchard, though, one would not expect a lower median during January and February when full canopy size has been achieved

(Figure 97a). LIDAR is recommended as a better way to obtain tree height data. Unfortunately, it was beyond the scope of this project to make use thereof. The same comments apply to drone-estimated tree volume, which reached a maximum of 4.55 $m^3$ for the young and 10.85 $m^3$ for the full bearing orchard (Figure 98a). The thermal infrared temperature appeared to be comparable for the young orchard for the first three surveys (October and December 2023, January 2024), with a slight drop in temperature during February and a steep drop in April 2024 (Figure 99a). At the full bearing orchard, the thermal infrared temperature increased from October toward January and decreased toward February and April. Mean thermal infrared temperature during the five surveys ranged between 23.9°C and 47.4°C for the young orchard and between 32.2°C and 47.6°C for the full bearing orchard.

With regard to seasonal variation, there seemed to be no differences between orchards with regard to the seasonal averaged spectral band reflection, apart from larger standard errors for the young orchard (Figure 84). Amongst vegetative indices, the CVI was the only variable that differed significantly between the two orchards, with that for the young orchard being more than double that for the full bearing orchard (Figure 85). This is the only vegetation index that confirmed in-field observations that the leaves in the full-bearing orchard were less green compared to those in the young orchard. The seasonal averaged CVI for the young orchard remained higher compared to that of the full bearing one even if the data of the fifth survey containing a high outlying value was omitted from the seasonal average, indicating that the leaves of the young orchard were overall in a healthier state than that in the full bearing one. The seasonal averaged TIR for the young and full bearing orchards was 40.9 (±4.87)°C and 40.3 (±3.25)°C, respectively, making the two sites appear very similar in terms of temperature.

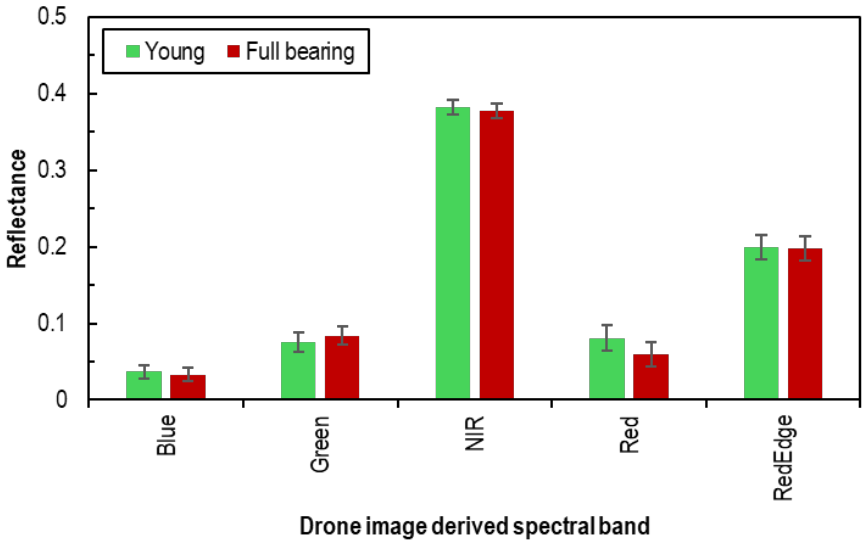


Figure 84. Seasonal mean reflectance (± standard error) for different drone multispectral image derived spectral bands for the young (green bars) and full bearing (Red bars) cultivar 'Wonderful' orchards. Means were derived from data of five drone surveys conducted over the 2023/2024 growing season.

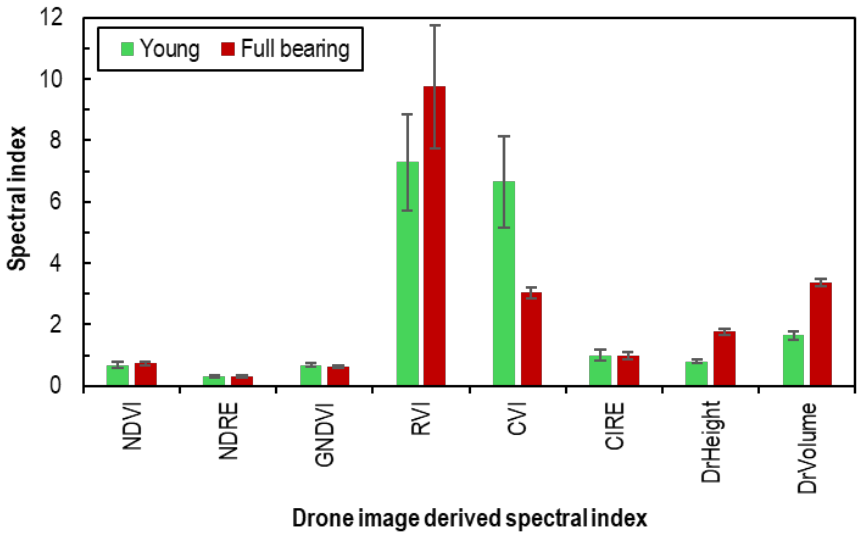


Figure 85. Seasonal mean spectral index (± standard error) for different drone multispectral image derived spectral indices for the young (green bars) and full bearing (Red bars) cultivar 'Wonderful' orchards. Means were derived from data of five drone surveys conducted over the 2023/2024 growing season.

## 9.4 CONCLUSIONS

Spectral profiles provided valuable insight into the changes in spectral band reflectance at selected crop development stages and highlighted the main differences between the young and the full-bearing orchard in two production areas. The dynamics of the NIR, red and blue bands are especially useful to determine differences in reflection that might be related to differences in canopy development or stress-induced chlorophyll degradation. According to the seasonal means, there were no differences in spectral band reflectance between orchards. Amongst the vegetation indices, CVI was significantly higher for the young compared to the full bearing orchard, indicating higher chlorophyll content of the canopies. Drone-estimated tree height and volume were also significantly different between the two orchards. Drone estimated tree height ranged between 0.675 m and 0.982 m for the young orchard and 1.59 m and 2.04 m for the full bearing orchard, whereas drone estimated tree volume reached a maximum of 4.55 $m^3$ for the young and 10.85 $m^3$ for the full bearing orchard.

# CHAPTER 10: CONCLUSIONS & RECOMMENDATIONS

## 10.1 CONCLUSIONS

Drone-technology derived attributes for individual pomegranate trees can, based on the existing dataset, not be related accurately to in-field measured tree dimensions and light interception, but it is possible for selected tree properties on orchard scale.

- Linear regressions using individual tree data for orchards combined, orchards on their own or phenological growth stages (surveys) separately did not render regression models for a single specific drone image-derived variable that could be used to estimate the canopy tree dimensions, fractional interception or LAI over the whole season. Factors contributing to the poor regression relationships could include variation in spectral reflectance between soils and/ or trees of orchards, within orchards as well as between phenological growth stages, and specifically for the full bearing orchard, lack of variation in the canopy properties of the trees required for strong linear regression relationships. Amongst the multispectral and thermal drone image-derived variables, drone image-estimated tree height and volume related most frequently significantly via linear regression to in-field measured tree canopy properties of individual selected trees, especially at the young orchard. At individual tree level, for data of orchards combined, drone estimated tree height rendered the best significant regression relationships with all tree canopy properties except for OLAI (which was not significantly related) and FI (which related better to CVI), with $R^2$ values ranging between 0.09 and 0.53.

- Regression relationships improved where orchard averaged data from the various drone surveys were used, compared to those based on individual tree data. For data of the young and full bearing orchard combined, orchard averaged drone estimated tree height related significantly at a 95% confidence level to orchard averaged tree height, across row width, tree volume, fractional interception and ceptometer based leaf area index ($R^2$-values ranging between 0.73 and 0.87), but with a relatively high standard error of the estimate for tree height and FI. Reliability and accuracy of these regression models could possibly be improved by the collection of more data to address a paucity of mid-range data points.

- .For the young orchard, the orchard averaged blue spectral band reflectance was the best suited to estimate orchard averaged tree height with a low standard error of the estimate. It was recommended to rather estimate FI and OLAI from regression relationships with RedEdge spectral band reflectance instead of using the regression relationship with CVI, which correlated better, but appeared to be sensitive to seasonal chlorophyll content changes.

- Tree height, FI and OLAI are important input parameters to estimate crop coefficients as an alternative if crop coefficients cannot be acquired directly from regression relationships with drone image derived variables., Poor, atypical or lack of significant relationships of orchard averaged tree height, FI and LAI variables with NDVI was partially ascribed to NDVI variability, which may be related to phenological changes or changes over the season in soil background reflectance, leaf properties and canopy structures.

With regard to relating drone image derived variables to individual tree plant physiological parameters (stem water potential, leaf chlorophyll content, $A_n$, $g_s$ and $Tr_L$) there were several linear regression relationships significant at a 95% confidence level, with maximum coefficients of determination for data of orchards combined being 0.58 and 0.87 where orchards were considered on their own. In most cases, additional data points are required mid-range to strengthen and validate the regression relationships. Using orchard-averaged data rendered $R^2$ values of up to 0.87 and 0.997 for orchards combined and for individual orchards, respectively.

- For stem water potential data of orchards combined, neither individual tree nor orchard-averaged midday stem water potential was significantly related to any drone image-derived variables. For orchards separately, individual tree midday stem water potential related poorly ($R^2 < 0.27$), but significantly with a negative correlation to RVI at the young and NIR at the full bearing orchard, whereas orchard averaged midday stem water potential was not related significantly to any drone image derived variables at a 95% confidence level for either orchard. Data for the young orchard lacked a clear trend in stem water potential over the season. However, the full bearing orchard averaged midday stem water potential tended to decrease with decreasing NDVI as the season progressed, albeit at a lower significance level ($R^2 = 0.74$, $p = 0.062$).

- Although leaf chlorophyll content data for orchards combined related significantly to and increased with CVI based on individual tree and orchard averaged data ($R^2$ values of 0.42 and 0.61, respectively), data distribution patterns were not convincing. Regression relationships based on individual tree data were, in general, poor for the individual orchards with no common drone image-derived variable resulting in the best regression relationships. Based on orchard-averaged data, leaf chlorophyll content for the full bearing orchard increased with NIR spectral reflection ($R^2$ = 0.92), with no significant regression relationship identified for the young orchard.
- For data of orchards combined, $A_n$ at 10h00 related significantly to and increased with NIR based on individual tree data ($R^2$ = 0.56) as well as orchard averaged data ($R^2$ = 0.71). Stomatal conductance at 12h00, for data of orchards combined, related significantly to and increased with GNDVI based on individual tree data ($R^2$ = 0.37) as well as orchard averaged data ($R^2$ = 0.54). For the individual orchards, there was for both $A_n$ and $g_s$ variation in the drone image-derived variables, which resulted in the best regression relationships.

- Based on individual tree data for orchards combined, $Tr_L$ at 10h00 related significantly to RVI ($R^2$ = 0.58), whereas amongst regressions based on orchard averaged data for orchards combined, $Tr_L$ at 12h00 related the best to RVI ($R^2$ = 0.87), Individual tree data of orchards considered separately displayed variability in terms of the $Tr_L$ time and drone image derived variables that related the best. However, orchard averaged data of the young orchard displayed the best regression relationship between TrL at 12h00 with either RVI or RedEdge spectral reflectance and at the full bearing orchard, with RVI.

Drone image-derived spectral band reflectance, tree geometric traits and spectral indices were related to actual water use and crop coefficients on tree and orchard scale, with mixed success rates at individual tree and orchard scale. Some of the regression relationships could be used to derive useful information for irrigation scheduling, but it still needs to be validated before they can be endorsed and recommended for use on farms. The regression relationships between pomegranate tree water use and drone image-derived variables improved from individual tree towards orchard averaged scale.

- Transpiration:

***At individual tree level, f***or ***orchards combined***, *transpiration* related best to drone estimated tree height or RVI ($R^2$ values around 0.46), whereas t*ranspiration* data of ***surveys combined*** for the *young orchard* related best to drone estimated tree height and RedEdge spectral band reflectance ($R^2$ values ≤ 0.355). Individual tree transpiration at the full bearing orchard did not relate significantly to any of the drone-derived variables at a 95% confidence level. Regression relationships of individual tree transpiration with NDVI for data of orchards combined or for the young orchard considered on its own were poor ($R^2$ = 0.37 and 0.208, respectively), and for the full bearing orchard, not significant. Regressions ***per survey*** were only significant at a 95% confidence level at the *full bearing site* between *transpiration* with NIR and RedEdge spectral band reflectance, respectively, during the fourth survey.

***At orchard averaged level***, for ***sites combined***, *orchard upscaled tree transpiration* related linearly at a 5% significance level the best to and increased with orchard averaged RVI ($R^2$ = 0.92, $SE_{est}$ = 0.061 mm $d^{-1}$). Regressions of orchard transpiration with NDVI and drone-estimated tree height resulted in poorer coefficients of determination (c. 0.7), with standard errors of the estimates increasing to around 0.11 mm $d^{-1}$. ***Orchard upscaled transpiration*** *data for the* ***young orchard*** considered on its own, related linearly the best to the orchard averaged RedEdge spectral band reflectance ($R^2$ = 0.96, standard error of the estimate 0.03), whereas NDVI comparatively correlated poorer ($R^2$ = 0.811) with the standard error of the estimated transpiration increasing to 0.068. There were no significant relationships at a 95% confidence level between *orchard upscaled transpiration of the* ***full bearing orchard*** and any drone image-derived variables at the site level, most likely due to the variability of the limited data set available.

- Transpiration: ETo ratio

***At individual tree level***, the *ratio of transpiration to ETo* for ***orchards combined*** related significantly at a 95% confidence level, the best to drone estimated tree height ($R^2$ = 0.367), but the linear regression relationship of the transpiration:ETo ratio with NDVI was not significant. For the data of ***surveys combined,*** the *transpiration: ETo ratio* at neither site was significantly related to any of the drone-derived variables at a 5% significance level. ***At survey level,*** regressions significant at a 95% confidence level were limited to that between *transpiration* and the *ratio thereof to ETo* with NIR and RedEdge spectral band reflectance, respectively, during the fourth survey at the *full bearing orchard.*

***At orchard averaged level,*** for data of ***orchards combined***, the ratio of orchard transpiration to ETo related significantly only to drone estimated tree height and volume at a 10% significance level ($R^2$ values 0.41 and 0.45, respectively), with a standard error of the estimate of about 0.2 for both variables. Furthermore, there were no significant regression relationships for the young or full bearing

orchards considered on their own between the orchard upscaled transpiration:ETo ratio and any drone image derived variables at a 5% significance level.

- ETc

*At individual tree level*, for ETc data of *orchards combined*, soil water balance determined *ETc* related well at tree row and orchard full surface area level especially to RedEdge spectral reflectance and CVI ($R^2$ values of between 0.79 and 0.9), with no significant linear regression relationships for either water use indicator with NDVI. For *surveys combined and at the survey level,* soil water balance-based *ETc* datasets were limited and did not render significant regression relationships that could aid in irrigation scheduling of the orchards.

*At orchard level*, for *sites combined,* micrometeorological system determined *orchard level ETc* for sites combined related significantly only to RVI at a 10% significance level ($R^2$ value of 0.42) with a large standard error of the estimate, i.e. 0.956. Outlying values originating from January 2024 for the full bearing orchard and, in some cases, October 2023 for the young orchard caused the poor regression relationships. There were no significant relationships between *orchard level ETc of the young orchard* and the drone image-derived variables even at a 90% confidence level. For the *full bearing orchard, orchard level ETc* can be estimated from a linear regression relationship with TIR based on a limited number of datapoints ($R^2$ = 0.999, n = 3), but might not be reliable.

- ETc:ETo ratio

*At individual tree level*, for *orchards combined,* the soil water balance based *ETc:ETo ratio* in the tree row related significantly to the green, blue and RedEdge spectral band reflectance ($R^2$ values between 0.58 - 0.615), with no significant regression relationships between the ETc:ETo ratio at orchard full surface level and any of the drone image derived variables. For *surveys combined and at survey level* soil water balance-derived *ETc* data were too limited to use for survey-level regression purposes.

*At orchard averaged level*, for *sites combined,* the *ratio of orchard level ETc to ETo* related significantly at the 10% significance level reasonably only to drone estimated tree height with an $R^2$ value of 0.44, but the standard error of the estimate was 0.12, which is too large to allow accurate estimates of the ratio. However, the orchard level ETc:ETo ratio for the *young orchard* can be estimated from NIR at a %5 significance level with a standard error for the estimate of 0.03. There were no significant regression relationships for the *full bearing orchard* level ETc:ETo ratio with any of the drone image-derived variables, probably due to limited data points available for regression analysis.

Estimation of transpiration and especially the ETc:ETo ratio for the five-year-old orchard from the regression relationships with RedEdge and NIR spectral band reflectance, respectively, indicated the presence of large variability in the orchard, which will benefit from the application of precision irrigation. The estimated orchard mean transpiration (±standard error) for summer amounted to 1.01(±0.02) mm $d^{-1}$, but individual tree position transpiration could reach a maximum of 1.24 mm $d^{-1}$. The estimated orchard mean Kc during summer was 0.29, which could increase by almost 70% for individual trees. If you irrigate according to the mean, underirrigation will be inevitable for some trees in the orchard, which might affect the orchard canopy development goals or productivity negatively. On the other hand, overirrigation could result in loss of precious water resources and expensive fertilizers beyond the root zone.

Collection of additional data sets in different orchards and/ or over more seasons is required to increase the database and to validate statistically significant regression relationships to enable reliable estimation of orchard-level transpiration, ETc and crop coefficients from drone image-derived variables for pomegranate orchards varying in canopy size. The poor relationships between the water use indicators and NDVI might be explained by site specific differences in the spectral profiles of the orchards researched here compared to those reported on by other researchers.

The regression relationships between measured tree water use and tree geometric properties of the young and full-bearing pomegranate orchards were poorer than expected.

- This can partially be explained by transpiration not being significantly related to any tree geometric properties early in the season and after harvest, whereas data representative of the whole season were used for the linear regressions.
- Transpiration related well to and increased with FI and LAI during the middle of December after most fruit set, at full canopy development stage in January and shortly before harvest near the end of February ($R^2$ values> 0.9).

- For the full bearing orchard, lack of significant regression relationships between transpiration and the ratio thereof to ETo with the majority of tree canopy properties can partially be explained by the absence of variation in canopy dimensions and a limited dataset, which was due to temporary malfunctioning of the sap flow and eddy covariance systems.
- The ratio of orchard upscaled transpiration to ETo as well as ETc:ETo were significantly linearly related at a 5% significance level to tree height, FI and ceptometer based LAI for data of orchards combined. Additional data are required mid-range to improve the regressions and to validate it.
- The orchard level ETc:ETo ratio was also significantly related to across row width and tree volume at a 5% significance level with $R^2$ values of about 0.73, but the standard error of the estimate was quite high for both variables and exceeded 0.075, which is considered too high to estimate the ratio accurately.

Drone technology derived tree attributes were used to determine orchard homogeneity for two orchards varying in canopy cover.

- Spectral profiles provided valuable insight on the changes in spectral band reflectance at selected crop development stages and highlighted the main differences between the young and the full-bearing orchard in two production areas.
- According to the seasonal means, there were no differences in spectral band reflectance between orchards.
- Amongst the vegetation indices, CVI was significantly higher for the young compared to the full bearing orchard – indicating higher chlorophyll content of the canopies.
- Drone estimated tree height and volume was also significantly different between the two orchards.

## 10.2 RECOMMENDATIONS

Selected drone-technology derived attributes for individual pomegranate trees were related accurately to in-field measured tree water use, tree physiology, tree dimensions, light interception and LAI. However, collection of additional data sets representative of more growing seasons and/or more pomegranate orchards varying in canopy cover is required. This is necessary to validate or improve regression relationships between the drone image-derived spectral bands, indices, tree geometric dimensions and thermal infrared temperature with tree water use variables, tree height, fractional interception, leaf area index, stem water potential, leaf level transpiration and $g_s$. It is recommended to collect, in future, more detailed information over the growing season on soil background reflectance, leaf and tree canopy structure properties, to assist in the identification of the most appropriate vegetation indices to estimate tree height, FI and LAI or to clarify why certain vegetation indices (e.g. NDVI) does not relate well. The fusion of morphological (canopy height, canopy cover and canopy volume) and vegetation indices for more accurate estimation of LAI over the season can also be investigated. The use of machine learning to identify appropriate algorithms to estimate physiological variables accurately from drone image-derived variables is strongly recommended for further research.

It is important to further explore the feasibility of extrapolating and reliably estimating orchard-level transpiration, ETc and the ETc:ETo ratio for other full-bearing and/ or young pomegranate orchards varying in canopy size. The accurate in-field measurement of fractional interception and leaf area index of orchards to aid in estimation of crop coefficients is not easily achieved and it would really aid farm and irrigation management (through estimation of crop coefficients) if these variables could be estimated accurately from drone imagery. A collection of additional datasets is also recommended to improve and/or validate significant regression relationships and to investigate and resolve atypical linear regression trends found.

Future research could expand to other pomegranate orchard sites, even outside the Western Cape. In addition, the prospects of obtaining existing drone imagery and water use data from the USDA on pomegranate orchards to relate to the current South African dataset should be investigated. It may require reprocessing of the images to be comparable to our datasets, but could potentially supplement or be used to validate our dataset, or provide explanations why NDVI did not relate well to ETc:ETo for the Western Cape orchards. Furthermore, the simplistic linear regression approach should be expanded to include non-linear regression statistical techniques, including training at centres of excellence on more advanced data analysis techniques such as machine learning.

# REFERENCES


ABOUTALEBI, M, TORRES-RUA, AF, KUSTAS, WP, NIETO, H COOPMANS, C and MCKEE, M (2018) Assessment of different methods for shadow detection in high-resolution optical imagery and evaluation of shadow impact on calculation of NDVI, and evapotranspiration. Irrigation Science 37 (1) 407-429.

ACHARYA, BS, BHANDARI, M, BANDINI, F, PIZARRO, A, PERKS, M, DEEPAK, R, JOSHI, DR and WANG, S (2021) Unmanned aerial vehicles in hydrology and water management–applications, challenges and perspectives. Water Resources Research 57 (11) e2021WR029925.

ALEXANDRIS S, PSOMIADIS E, PROUTSOS N, PHILIPPOPOULOS P, CHARALAMPOPOULOS I, KAKALETRIS G, PAPOUTSI E.-M, VASSILAKIS S and PARASKEVOPOULOS A (2021) Integrating drone technology into an innovative agrometeorological methodology for the precise and real-time estimation of crop water requirements. Hydrology 8(3) 131.

ALLEN RG and PEREIRA LS (2009) Estimating crop coefficients from fraction of ground cover and height. Irrigation Science 28:17-34.

AKCA S. and POLAT N (2022) Semantic segmentation and quantification of trees in an orchard using UAV orthophoto, Earth Science Informatics 15(4) 2265–2274.

ALLEN RG, PEREIRA LS, RAES D and SMITH, M (1998) Crop evapotranspiration-Guidelines for computing crop water requirements-FAO Irrigation and drainage paper 56. FAO, Rome, Italy. 300 (9) D05109.

ALVINO A and MARINO, S (2017) Remote sensing for irrigation of horticultural crops. Horticulturae 3(2) 40

BIRDAL AC, AYDAN U and TŰRK T (2017) Estimating tree heights with images from an unmanned aerial vehicle. Geomatics, Natural Hazards and Risk, 8(2), 1144–1156.

BROGE NH and LEBLANC E (2000) Comparing prediction power and stability of broadband and hyperspectral vegetation indices for estimation of green leaf area index and canopy chlorophyll density. Remote Sensing of Environment 76: 156-172

BURGESS SS, ADAMS MA, TURNER NC, BEVERLY CR, ONG CK, KHAN AA and BLEBY, T.M. (2001) An improved heat pulse method to measure low and reverse rates of sap flow in woody plants. Tree physiology, 21(9).589-598.

CARUSO G, ZARCO-TEJADA PJ, GONZA´LEZDUGO V, MORIONDO M, TOZZINI L, PALAI G, RALLO, G., HORNERO, A., PRIMICERIO, J. and GUCCI, R (2019) High-resolution imagery acquired from an unmanned platform to estimate biophysical and geometrical parameters of olive trees under different irrigation regimes. PlosS one 14(1): e0210804.

CHANDEL AK, KHOT L, PETERS RT, STÖCKLE CO. MANTLE, S (2022) High spatiotemporal apple crop water use mapping using drone imagery. http://treefruit.wsu.edu/article/high-spatiotemporal-apple-crop-water-use-mapping-using-drone-imagery/ Accessed 12 October 2022.

CHANDEL AK, KHOT LR, MOLAEI B, PETERS RT, STÖCKLE CO, and JACOBY PW (2021) High-resolution spatiotemporal water use mapping of surface and direct-root-zone drip-irrigated grapevines using UAS-based thermal and multispectral remote sensing. Remote Sensing 13(5) 954.

CHANDEL AK, MOLAEI B, KHOT LR, PETERS RT and STÖCKLE CO (2020) Small UAS-based multispectral and thermal infrared imagery driven energy balance driven for high-resolution evapotranspiration estimation of irrigated field crops. Drones 4(3):52-69.

CHEN A, ORLOV-LEVIN V and MERON M (2018) Applying high resolution visible channels aerial scan of crop canopy to precision irrigation management. In: The 2nd International Electronic Conference on Remote Sensing (ECRS 2018) Vol. 2, Sciforum Electronic Conference Series 22 March-5 April 2018.

COLOMINA I and MOLINA P (2014) Unmanned aerial systems for photogrammetry and remote sensing: A review. ISPRS Journal of photogrammetry and remote sensing 92 79-97.

DAPONTE P, DE VITO L, GLIELMO L, IANNELLI L, LIUZZAC D, PICARIELLO F and SILANO, G (2019) A review on the use of drones for precision agriculture. IOP Conf. Series: Earth and Environmental Science 275 (1) 012022.

DELAVARPOUR N, KOPARAN C, NOWATZKI J, BAJWA S and SUN, X (2021) A Technical Study on UAV Characteristics for Precision Agriculture Applications and Associated Practical Challenges. Remote Sensing 13 (6)1204.

DEPARTMENT OF WATER AND SANITATION (2022) Business Case for the Breede-Olifants Catchment Management Agency. https://www.dws.gov.za/IO/Docs/Business%20Case%20for%20establishment%20of%20Breede%20Olifants%20Catchment%20Management%20Agency%202021%20V1.pdf. Accessed 5 May 2025.

DUCHEMIN B, HADRIA R, ERRAKI S, BOULET G, MAISONGRANDE P, CHEHBOUNI A, ESCADAFAL R,

EZZAHAR J, HOEDJES J.C.B, KHARROU MH and KHABBA S (2006) Monitoring wheat phenology and irrigation in Central Morocco: On the use of relationships between evapotranspiration, crops coefficients, leaf area index and remotely-sensed vegetation indices. Agricultural Water Management 79(1)1-27.

ER-RAKI S, CHEHBOUNI A, GUEMOURIA N, DUCHEMIN B, EZZAHAR J and HADRIA, R., (2007) Combining FAO-56 model and ground-based remote sensing to estimate water consumptions of wheat crops in a semi-arid region. Agricultural water management 87(1)41-54.

EZENNE GI, JUPP L, MANTELA, SK and TANNERA JL (2019) Current and potential capabilities of UAS for crop water productivity in precision agriculture. Agricultural Water Management 218158-164.

FERNÁNDEZ JE., ALCON, F, DIAZ-ESPEJO A, HERNANDEZ-SANTANA, V and CUEVAS MV (2020) Water use indicators and economic analysis for on-farm irrigation decision: A case study of a super high density olive tree orchard. Agricultural Water Management 237 (106074):1-13.

GAO S, YAN K, LIU J, PU J, ZOU D, QI J, MU X and YAN G (2024) Assessment of remote-sensed vegetation indices for estimating forest chlorophyll concentration. Ecological Indicators, Volume 162, 112001.

GAUTAM D and PAGAY V (2021) A review of current and potential applications of remote sensing to study the water status of horticultural crops. Agronomy 10 (1) 140

GAUTAM D, OSTENDORF, B and PAGAY V (2021) Estimation of grapevine crop coefficient using a multispectral camera on an unmanned aerial vehicle. Remote Sensing13(13) 2639.

GERHARDS M, SCHLERF M, MALLICK K and UDELHOVEN, T. (2019) Challenges and future perspectives of multi-/hyperspectral thermal infrared remote sensing for crop water-stress detection: A review Remote Sensing. 11(10), 1240:1-24.

GIBSON PJ (2000) Introductory Remote Sensing- Principles and Concepts. Routledge, London.

GONZALEZ-DUGO V, ZARCO-TEJADA P, NICOLÁS E, NORTES PA, ALARCÓN JJ, INTIGLIO DS and FERERES E (2013) Using high resolution UAV thermal imagery to assess the variability in the water status of five fruit tree species within a commercial orchard. Precision Agriculture 14 660-678.

ISLAMI MM, RUSLONO T, SETIAWAN Y, RAHADIAN A, HUDJIMARTSU SA, and PRASETY LB (2021). Height, diameter and tree canopy cover estimation based on unmanned aerial vehicle (UAV) imagery with various acquisition height. Media Konservasi 26(1): 17-27.

JORGE J, VALLBÉ, M and SOLER, JA (2019) Detection of irrigation inhomogeneities in an olive grove using the NDRE vegetation index obtained from UAV images, European Journal of Remote Sensing 52(1)169-177.

JACKSON R.D, IDSO SB, REGINATO RJ, PINTER PJ (1981). Canopy temperature a Crop Water Stress Indicator. Water resources. research 17 (4) 1133-1138.

KATSIGIANNIS P, MISOPOLINOS LN, LIAKOPOULOS V, ALEXANDRIDIS T, ZALIDIS G (2016) An autonomous multi-sensor UAV system for reduced-input precision agriculture applications, 24th Mediterranean Conference on Control and Automation, MED 60–64 IEEE.

KAMIENSKIC, SOININEN J-P, TAUMBERGER M, DANTAS R., TOSCANO A, CINOTTI TS, MAIA RF and NETO AT (2019) Smart water management platform: IoT-based precision irrigation for agriculture. Sensors 19(2), 276

KATSIGIANNIS P, MISOPOLINOS L. LIAKOPOULOS V, ALEXANDRIDIS TK and ZALIDIS, G (2016) An autonomous multi-sensor UAV system for reduced-input precision agriculture applications, In: 2016 24th Mediterranean Conference on Control and Automation (MED) 60–64.

KNOX J.W, KAY, MG, and WEATHERHEAD EK (2012) Water regulation, crop production, and agricultural water management – Understanding farmer perspectives on irrigation efficiency. Agricultural Water Management 108 3-8.

LIU Q, WU Z, CUI N, ZHENG S, JIANG S, WANG Z, GONG D, WANG Y, ZHAO L, WEI R (2025) Estimating stomatal conductance of citrus orchard based on UAV multi-modal information in Southwest China. Agricultural Water Management 307 (2025) 109253

LIU S, JIN X, WANG CNS, CHENG XYM, SHAO M, WANG Z, TUOHUTI N, BAI Y AND LIU Y (2021) Estimating leaf area index using unmanned aerial vehicle data: shallow vs. deep machine learning algorithms. PLANT PHYSIOLOGY 187: 1551–1576.

MAHMUD MS, HE L, HEINEMANN P, CHOI D, ZHU H (2023) Unmanned aerial vehicle based tree canopy characteristics measurement for precision spray applications. Smart Agricultural Technology 4 (2023) 100153 :https://doi.org/10.1016/j.atech.2022.100153

MATESE A, BARALDI R, BERTON A, CESARACCIO C, DI GENNARO SF, DUCE P, FACINI O, MAMELI MG, PIGA A and ZALDEI A (2018). Estimation of water stress in grapevines using proximal and remote sensing methods. Remote Sensing, 10(1) 114.

MUNGHEMEZULU, C, MASHABA-MUNGHEMEZULU, Z, RATSHIEDANA, P.E, ECONOMON, E, CHIRIMA, G. and SIBANDA, S (2023) Unmanned aerial vehicle (UAV) and spectral datasets in South Africa for precision agriculture. Data 8(6) 98.

MATESE A, BARALDI R, BERTON A, CESARACCIO C, DI GENNARO SF, DUCE P, FACINI O, MAMELI MG, PIGA A and ZALDEI A (2018). Estimation of water stress in grapevines using proximal and remote sensing methods. Remote Sensing, 10(1) 114.

MUNGHEMEZULU C, MASHABA-MUNGHEMEZULU Z, RATSHIEDANA, PE, ECONOMON E, CHIRIMA G and SIBANDA S (2023) Unmanned aerial vehicle (UAV) and spectral datasets in South Africa for precision agriculture. Data 8(6) 98.

MABHAUDI T, SIBANDA M, CLULOW A, GOKOOL S, CHIMONYO VGP, MUTANGA O, ODINDI J, MAGIDI J and NAIKEN V. (2023) Using drones to monitor crop health, water stress, and crop water requirements for improving crop water productivity in the context of precision agriculture in smallholder croplands. Water Research Commission Report No. 2971/1/23.

MOHAMED ES, BELAL AA, ABD-ELMABOD SK, EL-SHIRBENY MA, GAD A and ZAHRAN, MB (2021) Smart farming for improving agricultural management. The Egyptian Journal of Remote Sensing and Space Sciences 24 (3) 971–981.

NIETO H, KUSTAS WP, TORRES-RÚA A, ALFIERI JG, GAO F, ANDERSON MC, WHITE WA, SONG L, DEL MAR ALSINA M, PRUEGER JH, MCKEE M, ELARAB M and MCKEE L.G (2019) Evaluation of TSEB turbulent fluxes using different methods for the retrieval of soil and canopy component temperatures from UAV thermal and multispectral imagery Irrigation Science. 37(3) 389–406.

NIU H, HOLLENBECK D, ZHAO T, WANG D and CHEN Y (2000) Evapotranspiration estimation with small UAVS in precision agriculture. Sensors 20 (22) 6427.

NIU H, WANG D AND CHEN YQ (2021) Estimating Crop Coefficients Using Linear and Deep Stochastic Configuration Networks Models and UAV-Based Normalized Difference Vegetation Index (NDVI). 2020 International Conference on Unmanned Aircraft Systems (ICUAS) Athens, Greece. September 1-4.

NIU H, ZHAO T, WEI J, WANG D and CHEN YQ (2021) Reliable tree-level evapotranspiration estimation of pomegranate trees using lysimeter and UAV multispectral imagery. In: 2021 IEEE Conference on Technologies for Sustainability (SusTech) . 1-6 IEEE, (April).

NIU H, WANG D and CHEN YQ (2022) Tree-level irrigation inference using UAV thermal imagery and convolutional neural networks. In: 2022 International Conference on Unmanned Aircraft Systems (ICUAS) 1586–1591.

NIU H, ZHAO T, WANG D and CHEN YQ (2022) Estimating Evapotranspiration of Pomegranate Trees Using Stochastic Configuration Networks (SCN) and UAV Multispectral Imagery, Journal of Intelligent and Robotic Systems: Theory and Applications., 104(4) 66.

ORTEGA-FARÍAS S, ORTEGA-SALAZAR S, POBLETE T, POBLETE-ECHEVERRÍA C, ZÚÑIGA M, SEPÚLVEDA-REYES D, KILIC A and ALLEN R (2017) Estimation of olive evapotranspiration using multispectral and thermal sensors placed aboard an unmanned aerial vehicle. In: Girona J & Marsal J (Eds.) *8th International Symposium on Irrigation of Horticultural Crops* (pp. 1-8). (Acta Horticulturae; Vol. 1150). International Society for Horticultural Science.

O'SHAUGHNESSY SA and RUSH C (2012) Precision Agriculture: Irrigation In: Encyclopaedia of Agriculture and Food Systems4 521-535.

PARK S, RYU D, FUENTESS, CHUNG H, O'CONNELL M and KIM J (2021) Mapping very-high-resolution evapotranspiration from unmanned aerial vehicle (UAV) imagery. ISPRS International Journal of Geo-Information. 10 (4) 211.

PEREIRA LS, PAREDESA P, F. MELTON, F. JOHNSON, L, T. WANG, T, LÓPEZ-URREAD, R, CANCELAE, JJ, ALLEN, RG (2020) Prediction of crop coefficients from fraction of ground cover and height. Background and validation using ground and remote sensing data. Agricultural Water Management 241:106197.

PEREIRA LS, PAREDES P, MELTON F, JOHNSON L, MOTOA= M and WANG T (2021) Prediction of crop coefficients from fraction of ground cover and height: Practical application to vegetable, field and fruit crops with focus on parameterization. Agricultural Water Management *252* 106663.

PÔÇAS I, CALERA A, CAMPOS I and CUNHA M (2020) Remote sensing for estimating and mapping single and basal crop coefficients: A review on spectral vegetation indices approaches. Agricultural Water Management 233106081.

POMASA (2024) Pomegranate producers Association of South Africa: Industry overview. POMASA, 258 Main Street, Paarl, South Africa.

RADOGLOU-GRAMMATIKIS P, SARIGIANNIDIS P, LAGKAS T and MOSCHOLIOS I (2020) A compilation of UAV applications for precision agriculture. Computer Networks 172 107148.

ROMERO-TRIGUEROS C, GAMBIN JMB, TORTOSA PAN CABAÑERO JJA, and NICOLÁS EN (2019) Determination of crop water stress index by infrared thermometry in grapefruit trees irrigated with saline reclaimed water combined with deficit irrigation. Remote Sensing. 11 (7) 757

TIAN X, JIA X, DA Y, LIU J and GE W (2025) Evaluating the sensitivity of vegetation indices to leaf area index variability at individual tree level using multispectral drone acquisitions. Agricultural and Forest Meteorology, Volume 364,110441.

VINCINI M AND FRAZZI E (2011) Comparing narrow and broad-band vegetation indices to estimate leaf chlorophyll content in planophile crop canopies. Precision Agric 12:334–344

WANNIARACHCHI S and SARUKKALIGE R (2022) A review on evapotranspiration estimation in agricultural water management: past, present and future. Hydrology 9, 123.

WESTERN CAPE DEPARTMENT OF ENVIRONMENTAL AFFAIRS AND DEVELOPMENT PLANNING. (2018) Western Cape Sustainable Water Management Plan 2017 – 2022. Towards a new norm for water resilience. March 2018.
https://www.westerncape.gov.za/eadp/files/atoms/files/WC%20Sustainable%20Water%20Management%20Plan%202018_1.pdf. Accessed July 13, 2021.

WILLIAMS L and AYARS J. Grapevine water use and the crop coefficient are linear functions of the shaded area measured beneath the canopy. Agriculture and Forest Meteorology. 132 (3-4) 201-211.
ZHANG C, VALENTE J, KOOISTRA L, GUO Land WANG W (2021) Orchard management with small unmanned aerial vehicles: A survey of sensing and analysis approaches. Precision agriculture 22 (6) 2007-2052.
ZHANG Y, HAN W, NIU X. and LI G (2019a) Maize crop coefficient estimated from UAV-measured multispectral vegetation indices. Sensors 19(23) 5250.
ZHANG L, ZHANG H, NIU Y and HAN W (2019b) Mapping maize water stress based on UAV multispectral remote sensing. Remote Sensing 11(6) 605.
ZHANG H, WANG D, AYARS JE and PHENE CJ (2017). Biophysical response of young pomegranate trees to surface and sub-surface drip irrigation and deficit irrigation. Irrigation Science 35(5), 425-435.
ZHAO T, YANG Y, NIU H, WANG D and CHEN YQ (2018) Comparing U-Net convolutional networks with fully convolutional networks with mask R-CNN in the performances of pomegranate tree canopy segmentation, In: Multispectral, Hyperspectral, and Ultraspectral Remote Sensing Technology, Techniques and Applications VII, 10780.210-218 SPIE.

# APPENDIX A: SUMMARY OF COEFFICIENTS OF DETERMINATION AND PEARSON p-VALUES OF LINEAR REGRESSIONS OF MEASURED TREE CANOPY PROPERTIES WITH DRONE IMAGE DERIVED VARIABLES

Table 9. Comparison of coefficients of determination ($R^2$) of simple linear regressions of multispectral drone image derived spectral bands, indices, tree geometric dimensions or thermal infrared temperature with measured or calculated tree canopy dimensions, fractional interception and leaf area index (LAI) of selected individual trees for orchards combined over the 2023/2024 season. Pearson p-values (p) are indicated in the bottom part of the table. Bold black text indicates indices which related significantly to the measured parameters at a **significance level of 5% (p≤0.05) and bold red italicized text at a significance level of 10% (0.05<p≤0.1).** Increased green colour intensity indicates increasing $R^2$ values.

| Tree Property | SI | Drone image spectral band or index | | | | | | | | | | | | | |
|---|---|---|---|---|---|---|---|---|---|---|---|---|---|---|---|
| | | Blue | Green | NIR | Red | RedEdge | NDVI | NDRE | GNDVI | RVI | CVI | CIRE | Dr_Height | Dr_Volume | TIR |
| Tree_height | $R^2$ | 0.095 | 0.032 | 0.045 | 0.120 | 0.061 | 0.111 | 0.026 | 0.007 | 0.162 | 0.307 | 0.017 | 0.412 | 0.120 | 0.019 |
| Across row width | $R^2$ | 0.120 | 0.051 | 0.031 | 0.149 | 0.074 | 0.149 | 0.047 | 0.023 | 0.217 | 0.278 | 0.036 | 0.526 | 0.171 | 0.058 |
| In row width | $R^2$ | 0.116 | 0.055 | 0.054 | 0.119 | 0.086 | 0.117 | 0.048 | 0.027 | 0.142 | 0.147 | 0.039 | 0.203 | 0.033 | 0.022 |
| Tree_volume | $R^2$ | 0.046 | 0.016 | 0.006 | 0.065 | 0.026 | 0.064 | 0.020 | 0.006 | 0.094 | 0.168 | 0.014 | 0.275 | 0.102 | 0.032 |
| Fractional interception | $R^2$ | 0.036 | 0.007 | 0.029 | 0.061 | 0.020 | 0.053 | 0.003 | 0.001 | 0.121 | 0.385 | <0.0001 | 0.364 | 0.160 | 0.003 |
| Ceptometer LAI | $R^2$ | 0.043 | 0.015 | 0.017 | 0.065 | 0.023 | 0.063 | 0.008 | 0.002 | 0.131 | 0.242 | 0.003 | 0.257 | 0.111 | 0.016 |
| Tree canopy-based LAI | $R^2$ | 0.039 | 0.020 | 0.028 | 0.044 | 0.042 | 0.036 | 0.024 | 0.006 | 0.030 | 0.048 | 0.020 | 0.088 | 0.020 | 0.001 |
| Orchard LAI | $R^2$ | <0.0001 | <0.0001 | 0.000 | 0.001 | 0.001 | 0.001 | 0.001 | 0.001 | 0.012 | 0.026 | 0.003 | 0.017 | 0.013 | 0.003 |
| Tree_height | p | <0.0001 | 0.022 | 0.006 | <0.0001 | 0.001 | <0.0001 | 0.039 | 0.270 | <0.0001 | <0.0001 | *0.096* | <0.0001 | <0.0001 | *0.078* |
| Across row width | p | <0.0001 | 0.004 | 0.024 | <0.0001 | 0.000 | <0.0001 | 0.005 | *0.051* | <0.0001 | <0.0001 | 0.015 | <0.0001 | <0.0001 | 0.002 |
| In row width | p | <0.0001 | 0.002 | 0.003 | <0.0001 | 0.000 | <0.0001 | 0.005 | 0.037 | <0.0001 | <0.0001 | 0.011 | <0.0001 | 0.020 | *0.055* |
| Tree_volume | p | 0.006 | 0.103 | 0.324 | 0.001 | 0.039 | 0.001 | *0.074* | 0.320 | <0.0001 | <0.0001 | 0.130 | <0.0001 | <0.0001 | 0.022 |
| Fractional interception | p | *0.091* | 0.456 | 0.132 | 0.027 | 0.206 | 0.040 | 0.653 | 0.799 | 0.002 | <0.0001 | 0.932 | <0.0001 | 0.000 | 0.652 |
| Ceptometer LAI | p | *0.064* | 0.287 | 0.255 | 0.023 | 0.181 | 0.025 | 0.422 | 0.712 | 0.001 | <0.0001 | 0.633 | <0.0001 | 0.003 | 0.257 |
| Tree canopy-based LAI | p | *0.078* | 0.216 | 0.139 | *0.063* | *0.069* | *0.091* | 0.171 | 0.485 | 0.125 | *0.052* | 0.209 | 0.008 | 0.210 | 0.796 |
| Orchard LAI | p | 0.961 | 0.934 | 0.865 | 0.810 | 0.794 | 0.762 | 0.734 | 0.843 | 0.327 | 0.155 | 0.641 | 0.251 | 0.305 | 0.617 |

SI – Statistical indicator, NIR – Near-infrared, NDVI - Normalized Difference Vegetation Index, NDRE - Normalized Difference Red Edge Index, GNDVI -Green Normalized Difference Vegetation Index, RVI - Ratio Vegetation Index, CVI - Chlorophyll vegetation index, CIRE - Chlorophyll index – Red edge, Dr_Height – drone image estimated tree height, Dr_Volume – drone image estimated tree volume, TIR – thermal infrared temperature.

Table 10. Comparison of coefficients of determination ($R^2$) of simple linear regressions of multispectral drone image derived spectral bands, indices, tree geometric dimensions or thermal infrared temperature with measured or calculated tree canopy dimensions, fractional interception and leaf area index (LAI) of individual trees per orchard over the 2023/2024 season. Bold text indicates indices which related significantly to the measured parameters at a significance level of 5% ($p \leq 0.05$). Y refer to the young orchard at Avontuur and FB to the full bearing orchard at Welgemoed. Increased green colour intensity indicates increasing $R^2$ values.

| Site | Tree property | Drone image spectral band or index | | | | | | | | | | | | | |
|---|---|---|---|---|---|---|---|---|---|---|---|---|---|---|---|
| | | Blue | Green | NIR | Red | RedEdge | NDVI | NDRE | GNDVI | RVI | CVI | CIRE | Dr_Height | Dr_Volume | TIR |
| Y | Tree_height | 0.007 | 0.006 | 0.001 | 0.005 | 0.003 | 0.010 | 0.010 | 0.012 | 0.005 | 0.002 | 0.009 | 0.032 | 0.021 | 0.010 |
| FB | Tree_height | 0.004 | 0.011 | 0.001 | 0.005 | 0.011 | 0.001 | 0.009 | 0.007 | 0.004 | 0.016 | 0.010 | <0.0001 | 0.004 | 0.002 |
| Y | Across row width | 0.000 | 0.001 | <0.0001 | 0.003 | 0.000 | 0.002 | 0.000 | 0.000 | 0.005 | 0.003 | <0.0001 | **0.138** | **0.150** | 0.005 |
| FB | Across row width | 0.000 | 0.001 | 0.021 | <0.0001 | 0.005 | 0.004 | 0.000 | 0.002 | 0.008 | 0.000 | 0.000 | 0.079 | 0.000 | 0.030 |
| Y | In row width | 0.003 | 0.003 | 0.005 | 0.000 | 0.004 | 0.000 | 0.002 | 0.003 | 0.001 | 0.033 | 0.003 | **0.113** | **0.126** | 0.001 |
| FB | In row width | - | - | - | - | - | - | - | - | - | - | - | - | - | - |
| Y | Tree_volume | <0.0001 | <0.0001 | 0.002 | 0.001 | <0.0001 | 0.000 | <0.0001 | 0.000 | 0.003 | 0.024 | <0.0001 | **0.111** | **0.136** | 0.006 |
| FB | Tree_volume | <0.0001 | 0.003 | 0.013 | 0.000 | 0.005 | 0.002 | <0.0001 | <0.0001 | 0.001 | 0.002 | <0.0001 | 0.034 | 0.003 | 0.006 |
| Y | Fractional interception | 0.073 | 0.045 | 0.006 | 0.058 | 0.057 | 0.074 | 0.071 | 0.061 | 0.044 | 0.024 | 0.070 | 0.016 | 0.036 | 0.063 |
| FB | Fractional interception | 0.006 | 0.015 | 0.001 | 0.004 | 0.016 | 0.001 | 0.022 | 0.014 | 0.000 | 0.072 | 0.025 | 0.009 | 0.001 | 0.009 |
| Y | Ceptometer LAI | 0.016 | 0.003 | 0.001 | 0.010 | 0.006 | 0.020 | 0.017 | 0.011 | 0.009 | 0.000 | 0.017 | 0.039 | 0.056 | 0.008 |
| FB | Ceptometer LAI | 0.000 | 0.006 | 0.038 | <0.0001 | 0.023 | 0.010 | 0.003 | 0.001 | 0.012 | 0.034 | 0.005 | 0.014 | 0.000 | 0.034 |
| Y | Tree canopy-based LAI | 0.020 | 0.007 | <0.0001 | 0.015 | 0.010 | 0.023 | 0.020 | 0.015 | 0.010 | 0.003 | 0.021 | 0.036 | 0.061 | 0.010 |
| FB | Tree canopy-based LAI | 0.000 | 0.006 | 0.038 | <0.0001 | 0.023 | 0.010 | 0.003 | 0.001 | 0.012 | 0.034 | 0.005 | 0.014 | 0.000 | 0.034 |
| Y | Orchard LAI | 0.017 | 0.004 | 0.000 | 0.012 | 0.007 | 0.021 | 0.018 | 0.012 | 0.009 | 0.000 | 0.018 | 0.038 | 0.057 | 0.009 |
| FB | Orchard LAI | 0.000 | 0.006 | 0.038 | <0.0001 | 0.023 | 0.010 | 0.003 | 0.001 | 0.012 | 0.034 | 0.005 | 0.014 | 0.000 | 0.034 |

NIR – Near-infrared, NDVI - Normalized Difference Vegetation Index, NDRE - Normalized Difference Red Edge Index, GNDVI -Green Normalized Difference Vegetation Index, RVI - Ratio Vegetation Index, CVI - Chlorophyll vegetation index, CIRE - Chlorophyll index – Red edge, Dr_Height – drone image estimated tree height, Dr_Volume – drone image estimated tree volume, TIR – thermal infrared temperature.

Table 11. Comparison of Pearson p-values (p) of simple linear regressions between multispectral drone image derived spectral bands, indices, tree geometric dimensions or thermal infrared temperature with measured or calculated tree canopy dimensions, fractional interception and leaf area index (LAI) of individual trees per orchard over the 2023/2024 season. Bold **black text indicates indices which related significantly to the measured parameters at a significance level of 5% (p≤0.05) and** bold red italicized text at a significance level of 10% **(0.05<p≤0.1). Y refer to the young orchard at Avontuur and FB to the full bearing orchard at Welgemoed.**

| Site | Tree property | Drone image spectral band or index | | | | | | | | | | | | | |
|---|---|---|---|---|---|---|---|---|---|---|---|---|---|---|---|
| | | Blue | Green | NIR | Red | RedEdge | NDVI | NDRE | GNDVI | RVI | CVI | CIRE | Dr_Height | Dr_Volume | TIR |
| Y | Tree_height | 0.480 | 0.499 | 0.823 | 0.553 | 0.648 | 0.384 | 0.402 | 0.357 | 0.561 | 0.735 | 0.408 | 0.124 | 0.217 | 0.388 |
| FB | Tree_height | 0.544 | 0.328 | 0.746 | 0.519 | 0.317 | 0.769 | 0.366 | 0.431 | 0.572 | 0.239 | 0.355 | 0.947 | 0.579 | 0.657 |
| Y | Across row width | 0.854 | 0.798 | 0.946 | 0.661 | 0.872 | 0.716 | 0.920 | 0.869 | 0.529 | 0.635 | 0.985 | 0.001 | 0.001 | 0.546 |
| FB | Across row width | 0.842 | 0.801 | 0.172 | 0.978 | 0.525 | 0.538 | 0.919 | 0.713 | 0.414 | 0.895 | 0.848 | 0.008 | 0.893 | 0.104 |
| Y | In row width | 0.663 | 0.664 | 0.541 | 0.928 | 0.601 | 0.898 | 0.717 | 0.638 | 0.760 | 0.119 | 0.654 | 0.003 | 0.002 | 0.845 |
| FB | In row width | - | - | - | - | - | - | - | - | - | - | - | - | - | - |
| Y | Tree_volume | 0.979 | 0.960 | 0.690 | 0.767 | 0.968 | 0.852 | 0.939 | 0.879 | 0.619 | 0.181 | 0.996 | 0.004 | 0.001 | 0.514 |
| FB | Tree_volume | 0.984 | 0.625 | 0.286 | 0.875 | 0.492 | 0.674 | 0.943 | 0.979 | 0.762 | 0.642 | 0.996 | *0.083* | 0.641 | 0.473 |
| Y | Fractional interception | *0.091* | 0.187 | 0.631 | 0.133 | 0.138 | *0.089* | *0.097* | 0.123 | 0.192 | 0.345 | *0.098* | 0.442 | 0.243 | 0.118 |
| FB | Fractional interception | 0.636 | 0.446 | 0.829 | 0.703 | 0.432 | 0.890 | 0.357 | 0.471 | 0.897 | *0.093* | 0.333 | 0.566 | 0.888 | 0.556 |
| Y | Ceptometer LAI | 0.441 | 0.721 | 0.889 | 0.530 | 0.633 | 0.385 | 0.423 | 0.525 | 0.565 | 0.946 | 0.420 | 0.221 | 0.141 | 0.585 |
| FB | Ceptometer LAI | 0.934 | 0.641 | 0.229 | 0.998 | 0.345 | 0.537 | 0.723 | 0.882 | 0.507 | 0.256 | 0.677 | 0.461 | 0.906 | 0.256 |
| Y | Tree canopy-based LAI | 0.382 | 0.602 | 0.957 | 0.456 | 0.541 | 0.350 | 0.378 | 0.449 | 0.537 | 0.753 | 0.377 | 0.242 | 0.123 | 0.533 |
| FB | Tree canopy-based LAI | 0.934 | 0.641 | 0.229 | 0.998 | 0.345 | 0.537 | 0.723 | 0.882 | 0.507 | 0.256 | 0.677 | 0.461 | 0.906 | 0.256 |
| Y | Orchard LAI | 0.423 | 0.689 | 0.906 | 0.508 | 0.608 | 0.372 | 0.408 | 0.502 | 0.553 | 0.895 | 0.406 | 0.228 | 0.139 | 0.569 |
| FB | Orchard LAI | 0.934 | 0.641 | 0.229 | 0.998 | 0.345 | 0.537 | 0.723 | 0.882 | 0.507 | 0.256 | 0.677 | 0.461 | 0.906 | 0.256 |

NIR – Near-infrared, NDVI - Normalized Difference Vegetation Index, NDRE - Normalized Difference Red Edge Index, GNDVI -Green Normalized Difference Vegetation Index, RVI - Ratio Vegetation Index, CVI - Chlorophyll vegetation index, CIRE - Chlorophyll index – Red edge, Dr_Height – drone image estimated tree height, Dr_Volume – drone image estimated tree volume, TIR – thermal infrared temperature.

Table 12. Comparison of coefficients of determination ($R^2$) of simple linear regressions of multispectral drone image derived spectral bands, indices, tree geometric dimensions or thermal infrared temperature with canopy width across the tree row and in the tree row, respectively, for individual trees from five surveys conducted over the 2023/2024 season for the young (Y, green gradient colour) and full bearing (FB, red gradient colour) pomegranate orchards at Avontuur and Welgemoed, respectively. Bold text indicates indices with significant potential to model the measured parameters at a significance level of 5% ($p \leq 0.05$). Increased colour intensity indicates increasing $R^2$ values.

| Site | Survey | Tree property | Drone image spectral band or index | | | | | | | | | | | | | |
|---|---|---|---|---|---|---|---|---|---|---|---|---|---|---|---|---|
| | | | Blue | Green | NIR | Red | RedEdge | NDVI | NDRE | GNDVI | RVI | CVI | CIRE | Dr_Height | Dr_Volume | TIR |
| Y | 1 | Across row width | **0.367** | 0.008 | 0.230 | 0.354 | 0.060 | **0.449** | 0.278 | 0.298 | **0.392** | 0.034 | 0.249 | **0.579** | **0.662** | 0.000 |
| Y | 2 | Across row width | 0.155 | 0.105 | 0.207 | 0.125 | 0.058 | 0.270 | **0.352** | **0.336** | 0.255 | **0.553** | **0.378** | 0.027 | 0.027 | 0.147 |
| Y | 3 | Across row width | 0.000 | 0.001 | 0.004 | 0.052 | 0.008 | 0.010 | 0.003 | 0.023 | 0.113 | 0.226 | 0.000 | **0.325** | **0.325** | 0.214 |
| Y | 4 | Across row width | 0.188 | 0.185 | 0.011 | **0.375** | 0.110 | 0.149 | 0.008 | 0.035 | 0.191 | 0.108 | 0.009 | **0.409** | **0.570** | 0.072 |
| Y | 5 | Across row width | 0.060 | 0.049 | 0.001 | 0.160 | 0.054 | 0.213 | 0.133 | 0.059 | **0.264** | 0.057 | 0.148 | **0.405** | **0.405** | 0.009 |
| FB | 1 | Across row width | **0.417** | 0.000 | 0.095 | **0.338** | 0.093 | **0.357** | 0.003 | 0.154 | **0.305** | **0.387** | 0.007 | 0.216 | 0.136 | 0.022 |
| FB | 2 | Across row width | <0.0001 | 0.017 | 0.011 | 0.001 | 0.032 | 0.000 | 0.022 | 0.014 | 0.003 | 0.037 | 0.026 | 0.047 | 0.047 | 0.001 |
| FB | 3 | Across row width | 0.089 | 0.037 | 0.001 | 0.071 | 0.012 | 0.097 | 0.020 | 0.056 | 0.043 | 0.120 | 0.008 | **0.271** | **0.271** | 0.070 |
| FB | 4 | Across row width | 0.018 | **0.195** | 0.014 | 0.043 | **0.158** | 0.027 | **0.202** | **0.145** | 0.091 | 0.031 | **0.196** | 0.002 | 0.027 | 0.026 |
| FB | 5 | Across row width | 0.016 | 0.093 | 0.071 | 0.032 | 0.077 | 0.000 | 0.068 | 0.063 | 0.010 | 0.197 | 0.076 | **0.310** | **0.310** | 0.131 |
| Y | 1 | In row width | **0.490** | 0.007 | **0.368** | **0.431** | 0.106 | **0.619** | **0.414** | **0.447** | **0.547** | 0.014 | **0.376** | **0.745** | **0.780** | 0.006 |
| Y | 2 | In row width | 0.205 | 0.156 | 0.125 | 0.176 | 0.097 | 0.328 | **0.383** | **0.383** | 0.323 | **0.465** | **0.410** | 0.003 | 0.003 | 0.200 |
| Y | 3 | In row width | 0.001 | 0.011 | 0.008 | 0.025 | 0.004 | 0.019 | 0.010 | 0.009 | 0.186 | 0.200 | 0.024 | **0.451** | **0.451** | 0.090 |
| Y | 4 | In row width | **0.275** | **0.226** | 0.030 | **0.380** | 0.041 | 0.131 | 0.024 | 0.042 | 0.134 | 0.066 | 0.030 | **0.313** | **0.434** | 0.011 |
| Y | 5 | In row width | 0.006 | 0.000 | 0.088 | 0.074 | 0.087 | 0.037 | 0.020 | 0.006 | 0.063 | 0.001 | 0.026 | 0.186 | 0.186 | 0.005 |

NIR – Near-infrared, NDVI - Normalized Difference Vegetation Index, NDRE - Normalized Difference Red Edge Index, GNDVI -Green Normalized Difference Vegetation Index, RVI - Ratio Vegetation Index, CVI - Chlorophyll vegetation index, CIRE - Chlorophyll index – Red edge, Dr_Height – drone image estimated tree height, Dr_Volume – drone image estimated tree volume, TIR – thermal infrared temperature.

Table 13. Comparison of Pearson p-values (p) of simple linear regressions of multispectral drone image derived spectral bands, indices, tree geometric dimensions or thermal infrared temperature with canopy width across the tree row and in the tree row, respectively, for individual trees from five surveys conducted over the 2023/2024 season for the young (Y) and full bearing (FB) pomegranate orchards at Avontuur and Welgemoed, respectively. Bold text indicates indices with significant potential to model the measured parameters at a significance level of 5% ($p \leq 0.05$) and bold red italicized text at a significance level of 10% ($0.05 < p \leq 0.1$).

| Site | Survey | Tree Property | Drone image spectral band or index | | | | | | | | | | | | | |
|---|---|---|---|---|---|---|---|---|---|---|---|---|---|---|---|---|
| | | | Blue | Green | NIR | Red | RedEdge | NDVI | NDRE | GNDVI | RVI | CVI | CIRE | Dr_Height | Dr_Volume | TIR |
| Y | 1 | Across row width | 0.048 | 0.791 | 0.136 | *0.054* | 0.469 | 0.024 | *0.095* | *0.082* | 0.039 | 0.586 | 0.118 | 0.007 | 0.002 | 0.972 |
| Y | 2 | Across row width | 0.131 | 0.220 | *0.077* | 0.180 | 0.369 | 0.039 | 0.015 | 0.019 | 0.046 | 0.001 | 0.011 | 0.543 | 0.543 | 0.142 |
| Y | 3 | Across row width | 0.950 | 0.897 | 0.808 | 0.396 | 0.744 | 0.719 | 0.845 | 0.573 | 0.202 | *0.063* | 0.959 | 0.021 | 0.021 | *0.071* |
| Y | 4 | Across row width | *0.093* | *0.096* | 0.705 | 0.012 | 0.210 | 0.140 | 0.735 | 0.485 | *0.090* | 0.213 | 0.731 | 0.008 | 0.001 | 0.315 |
| Y | 5 | Across row width | 0.361 | 0.410 | 0.921 | 0.125 | 0.386 | *0.072* | 0.164 | 0.366 | 0.042 | 0.374 | 0.141 | 0.008 | 0.008 | 0.724 |
| FB | 1 | Across row width | 0.044 | 0.960 | 0.387 | *0.078* | 0.392 | *0.068* | 0.881 | 0.262 | *0.098* | *0.055* | 0.817 | 0.176 | 0.295 | 0.684 |
| FB | 2 | Across row width | 0.959 | 0.499 | 0.596 | 0.849 | 0.355 | 0.957 | 0.444 | 0.545 | 0.796 | 0.315 | 0.403 | 0.257 | 0.257 | 0.879 |
| FB | 3 | Across row width | 0.263 | 0.475 | 0.924 | 0.318 | 0.682 | 0.239 | 0.603 | 0.378 | 0.441 | 0.188 | 0.735 | 0.039 | 0.039 | 0.323 |
| FB | 4 | Across row width | 0.606 | *0.076* | 0.652 | 0.423 | 0.114 | 0.531 | *0.071* | 0.132 | 0.239 | 0.502 | *0.075* | 0.850 | 0.529 | 0.537 |
| FB | 5 | Across row width | 0.627 | 0.233 | 0.301 | 0.493 | 0.282 | 0.951 | 0.310 | 0.333 | 0.697 | *0.075* | 0.283 | 0.020 | 0.020 | 0.153 |
| Y | 1 | In row width | 0.016 | 0.810 | 0.048 | 0.028 | 0.328 | 0.004 | 0.033 | 0.025 | 0.009 | 0.725 | 0.045 | 0.001 | 0.000 | 0.826 |
| Y | 2 | In row width | *0.078* | 0.130 | 0.179 | 0.105 | 0.241 | 0.020 | 0.011 | 0.011 | 0.022 | 0.004 | 0.008 | 0.854 | 0.854 | *0.082* |
| Y | 3 | In row width | 0.926 | 0.700 | 0.741 | 0.557 | 0.805 | 0.607 | 0.719 | 0.734 | *0.095* | *0.082* | 0.569 | 0.004 | 0.004 | 0.259 |
| Y | 4 | In row width | 0.037 | *0.062* | 0.524 | 0.011 | 0.451 | 0.169 | 0.563 | 0.448 | 0.164 | 0.337 | 0.519 | 0.024 | 0.006 | 0.693 |
| Y | 5 | In row width | 0.774 | 0.961 | 0.266 | 0.309 | 0.267 | 0.473 | 0.599 | 0.773 | 0.349 | 0.931 | 0.552 | *0.095* | *0.095* | 0.795 |

NIR – Near-infrared, NDVI - Normalized Difference Vegetation Index, NDRE - Normalized Difference Red Edge Index, GNDVI -Green Normalized Difference Vegetation Index, RVI - Ratio Vegetation Index, CVI - Chlorophyll vegetation index, CIRE - Chlorophyll index – Red edge, Dr_Height – drone image estimated tree height, Dr_Volume – drone image estimated tree volume, TIR – thermal infrared temperature.

Table 14. Comparison of coefficients of determination ($R^2$) of simple linear regressions of multispectral drone image derived bands, indices, tree geometric dimensions or thermal infrared temperature with tree height and canopy volume, respectively, for individual trees from five surveys conducted over the 2023/2024 season for the young (Y, green gradient colour) and full bearing (FB, red gradient colour) pomegranate orchards at Avontuur and Welgemoed, respectively. Bold text indicates indices with significant potential to model the measured parameters at a significance level of 5% ($p \leq 0.05$). Increased colour intensity indicates increasing $R^2$ values.

| Site | Survey | Tree property | Drone image spectral band or index | | | | | | | | | | | | | |
|---|---|---|---|---|---|---|---|---|---|---|---|---|---|---|---|---|
| | | | Blue | Green | NIR | Red | RedEdge | NDVI | NDRE | GNDVI | RVI | CVI | CIRE | Dr_Height | Dr_Volume | TIR |
| Y | 1 | Height | 0.327 | 0.108 | 0.035 | 0.368 | 0.007 | 0.255 | 0.186 | 0.138 | 0.239 | 0.076 | 0.159 | 0.356 | 0.264 | 0.000 |
| Y | 2 | Height | 0.045 | 0.031 | 0.083 | 0.039 | 0.010 | 0.106 | 0.104 | 0.126 | 0.149 | 0.179 | 0.128 | 0.033 | 0.033 | <0.0001 |
| Y | 3 | Height | 0.036 | 0.183 | 0.044 | 0.078 | 0.351 | 0.013 | 0.045 | 0.033 | 0.172 | 0.034 | 0.085 | 0.222 | 0.222 | 0.018 |
| Y | 4 | Height | 0.162 | 0.373 | 0.120 | 0.277 | 0.468 | 0.070 | 0.098 | 0.075 | 0.226 | 0.003 | 0.130 | 0.204 | 0.164 | 0.074 |
| Y | 5 | Height | 0.250 | 0.129 | 0.144 | 0.450 | 0.410 | 0.310 | 0.376 | 0.072 | 0.293 | 0.127 | 0.369 | 0.338 | 0.338 | 0.013 |
| FB | 1 | Height | 0.009 | 0.271 | 0.238 | 0.002 | 0.153 | 0.046 | 0.074 | 0.017 | 0.040 | 0.047 | 0.086 | 0.060 | 0.154 | 0.481 |
| FB | 2 | Height | 0.005 | 0.001 | 0.002 | 0.001 | <0.0001 | 0.002 | 0.002 | 0.001 | 0.001 | <0.0001 | 0.001 | 0.017 | 0.017 | 0.032 |
| FB | 3 | Height | 0.068 | 0.131 | 0.105 | 0.070 | 0.135 | 0.054 | 0.115 | 0.120 | 0.082 | 0.007 | 0.133 | 0.028 | 0.028 | 0.003 |
| FB | 4 | Height | 0.028 | 0.070 | 0.015 | 0.014 | 0.043 | 0.029 | 0.016 | 0.029 | 0.002 | 0.255 | 0.021 | 0.068 | 0.015 | 0.099 |
| FB | 5 | Height | 0.008 | 0.009 | 0.052 | 0.002 | 0.018 | 0.091 | 0.023 | 0.040 | 0.053 | 0.021 | 0.026 | 0.027 | 0.027 | 0.099 |
| Y | 1 | Volume | 0.418 | 0.031 | 0.175 | 0.418 | 0.018 | 0.448 | 0.307 | 0.279 | 0.400 | 0.056 | 0.272 | 0.590 | 0.645 | 0.001 |
| Y | 2 | Volume | 0.153 | 0.106 | 0.195 | 0.126 | 0.052 | 0.278 | 0.327 | 0.336 | 0.282 | 0.505 | 0.358 | 0.020 | 0.020 | 0.108 |
| Y | 3 | Volume | <0.0001 | 0.001 | 0.015 | 0.034 | 0.042 | 0.002 | 0.000 | 0.017 | 0.129 | 0.130 | 0.003 | 0.359 | 0.359 | 0.134 |
| Y | 4 | Volume | 0.230 | 0.302 | 0.109 | 0.397 | 0.225 | 0.094 | <0.0001 | 0.026 | 0.169 | 0.060 | 0.000 | 0.347 | 0.484 | 0.094 |
| Y | 5 | Volume | 0.052 | 0.004 | 0.098 | 0.144 | 0.151 | 0.080 | 0.073 | 0.001 | 0.086 | 0.002 | 0.075 | 0.244 | 0.244 | 0.001 |
| FB | 1 | Volume | 0.099 | 0.117 | 0.012 | 0.114 | 0.005 | 0.054 | 0.015 | 0.030 | 0.056 | 0.063 | 0.009 | 0.002 | 0.342 | 0.146 |
| FB | 2 | Volume | 0.001 | 0.011 | 0.000 | <0.0001 | 0.014 | 0.005 | 0.031 | 0.023 | 0.000 | 0.023 | 0.036 | 0.073 | 0.073 | 0.010 |
| FB | 3 | Volume | 0.003 | 0.024 | 0.039 | 0.004 | 0.036 | 0.000 | 0.026 | 0.015 | 0.015 | 0.033 | 0.040 | 0.010 | 0.010 | 0.016 |
| FB | 4 | Volume | 0.001 | 0.241 | 0.044 | 0.003 | 0.186 | 0.001 | 0.118 | 0.116 | 0.015 | 0.232 | 0.122 | 0.041 | 0.014 | 0.083 |
| FB | 5 | Volume | 0.001 | 0.026 | 0.052 | 0.000 | 0.029 | 0.039 | <0.0001 | 0.000 | 0.005 | 0.076 | <0.0001 | 0.127 | 0.127 | 0.128 |

NIR – Near-infrared, NDVI - Normalized Difference Vegetation Index, NDRE - Normalized Difference Red Edge Index, GNDVI -Green Normalized Difference Vegetation Index, RVI - Ratio Vegetation Index, CVI - Chlorophyll vegetation index, CIRE - Chlorophyll index – Red edge, Dr_Height – drone image estimated tree height, Dr_Volume – drone image estimated tree volume, TIR – thermal infrared temperature.

Table 15 Comparison of Pearson p-values (p) of simple linear regressions of multispectral drone image derived bands, indices, tree geometric dimensions or thermal infrared temperature with tree height and canopy volume, respectively, for individual trees from five surveys conducted over the 2023/2024 season for the young (Y) and full bearing (FB) pomegranate orchards at Avontuur and Welgemoed, respectively. Bold text indicates indices with significant potential to model the measured parameters at a significance level of 5% ($p \leq 0.05$) and bold red italicized text at a significance level of 10% ($0.05 < p \leq 0.1$).

| Site | Survey | Tree property | Drone image spectral band or index | | | | | | | | | | | | | |
|---|---|---|---|---|---|---|---|---|---|---|---|---|---|---|---|---|
| | | | Blue | Green | NIR | Red | RedEdge | NDVI | NDRE | GNDVI | RVI | CVI | CIRE | Dr_Height | Dr_Volume | TIR |
| Y | 1 | Height | *0.066* | 0.324 | 0.580 | 0.048 | 0.801 | 0.113 | 0.185 | 0.260 | 0.127 | 0.412 | 0.224 | *0.053* | 0.106 | 0.954 |
| Y | 2 | Height | 0.432 | 0.514 | 0.278 | 0.466 | 0.711 | 0.217 | 0.223 | 0.178 | 0.139 | 0.102 | 0.174 | 0.501 | 0.501 | 0.978 |
| Y | 3 | Height | 0.483 | *0.098* | 0.434 | 0.294 | 0.016 | 0.670 | 0.432 | 0.499 | 0.110 | 0.493 | 0.273 | *0.066* | *0.066* | 0.624 |
| Y | 4 | Height | 0.123 | 0.012 | 0.189 | 0.036 | 0.003 | 0.320 | 0.237 | 0.306 | *0.063* | 0.831 | 0.169 | *0.079* | 0.120 | 0.308 |
| Y | 5 | Height | 0.049 | 0.172 | 0.147 | 0.004 | 0.008 | 0.025 | 0.011 | 0.315 | 0.030 | 0.176 | 0.013 | 0.018 | 0.018 | 0.678 |
| FB | 1 | Height | 0.790 | 0.123 | 0.153 | 0.892 | 0.263 | 0.551 | 0.446 | 0.722 | 0.581 | 0.547 | 0.410 | 0.496 | 0.262 | 0.026 |
| FB | 2 | Height | 0.725 | 0.849 | 0.809 | 0.893 | 0.973 | 0.811 | 0.836 | 0.871 | 0.875 | 0.988 | 0.863 | 0.498 | 0.498 | 0.351 |
| FB | 3 | Height | 0.314 | 0.154 | 0.205 | 0.306 | 0.147 | 0.368 | 0.183 | 0.174 | 0.266 | 0.753 | 0.150 | 0.520 | 0.520 | 0.843 |
| FB | 4 | Height | 0.520 | 0.305 | 0.638 | 0.651 | 0.424 | 0.514 | 0.625 | 0.516 | 0.883 | 0.039 | 0.575 | 0.310 | 0.638 | 0.220 |
| FB | 5 | Height | 0.728 | 0.711 | 0.378 | 0.861 | 0.610 | 0.238 | 0.565 | 0.443 | 0.376 | 0.578 | 0.539 | 0.525 | 0.525 | 0.218 |
| Y | 1 | Volume | 0.032 | 0.603 | 0.200 | 0.032 | 0.693 | 0.024 | *0.077* | *0.095* | 0.037 | 0.482 | *0.100* | 0.006 | 0.003 | 0.942 |
| Y | 2 | Volume | 0.134 | 0.219 | *0.087* | 0.177 | 0.394 | 0.036 | 0.021 | 0.019 | 0.034 | 0.002 | 0.014 | 0.600 | 0.600 | 0.213 |
| Y | 3 | Volume | 0.999 | 0.923 | 0.654 | 0.495 | 0.449 | 0.873 | 0.954 | 0.626 | 0.172 | 0.170 | 0.848 | 0.014 | 0.014 | 0.163 |
| Y | 4 | Volume | *0.060* | 0.027 | 0.211 | 0.009 | *0.063* | 0.249 | 0.986 | 0.547 | 0.114 | 0.361 | 0.940 | 0.016 | 0.003 | 0.247 |
| Y | 5 | Volume | 0.397 | 0.826 | 0.239 | 0.147 | 0.138 | 0.290 | 0.311 | 0.910 | 0.270 | 0.883 | 0.303 | *0.052* | *0.052* | 0.899 |
| FB | 1 | Volume | 0.375 | 0.333 | 0.763 | 0.340 | 0.846 | 0.517 | 0.740 | 0.630 | 0.509 | 0.485 | 0.794 | 0.908 | *0.076* | 0.276 |
| FB | 2 | Volume | 0.853 | 0.581 | 0.928 | 0.989 | 0.536 | 0.704 | 0.364 | 0.430 | 0.953 | 0.432 | 0.326 | 0.156 | 0.156 | 0.608 |
| FB | 3 | Volume | 0.841 | 0.569 | 0.466 | 0.825 | 0.481 | 0.939 | 0.551 | 0.648 | 0.651 | 0.498 | 0.455 | 0.712 | 0.712 | 0.641 |
| FB | 4 | Volume | 0.931 | 0.045 | 0.419 | 0.849 | *0.084* | 0.888 | 0.178 | 0.181 | 0.643 | *0.050* | 0.170 | 0.435 | 0.648 | 0.261 |
| FB | 5 | Volume | 0.894 | 0.535 | 0.380 | 0.956 | 0.511 | 0.449 | 0.982 | 0.950 | 0.793 | 0.286 | 0.974 | 0.160 | 0.160 | 0.159 |

NIR – Near-infrared, NDVI - Normalized Difference Vegetation Index, NDRE - Normalized Difference Red Edge Index, GNDVI -Green Normalized Difference Vegetation Index, RVI - Ratio Vegetation Index, CVI - Chlorophyll vegetation index, CIRE - Chlorophyll index – Red edge, Dr_Height – drone image estimated tree height, Dr_Volume – drone image estimated tree volume, TIR – thermal infrared temperature.

Table 16. Comparison of coefficients of determination ($R^2$) of simple linear regressions of multispectral drone image derived bands, indices, tree geometric dimensions or thermal infrared temperature with fractional interception (FI) and ceptometer derived leaf area index (CP-LAI), respectively, for individual trees from five surveys conducted over the 2023/2024 season for the young (Y, green gradient colour) and full bearing (FB, red gradient colour) pomegranate orchards at Avontuur and Welgemoed, respectively. Bold text indicates indices with significant potential to model the measured parameters at a significance level of 5% ($p \leq 0.05$). Increased colour intensity indicates increasing $R^2$ values.

| Site | Survey | Tree property | Drone image spectral band or index | | | | | | | | | | | | | |
|---|---|---|---|---|---|---|---|---|---|---|---|---|---|---|---|---|
| | | | Blue | Green | NIR | Red | RedEdge | NDVI | NDRE | GNDVI | RVI | CVI | CIRE | Dr_Height | Dr_Volume | TIR |
| Y | 1 | FI | 0.760 | 0.740 | 0.003 | 0.867 | 0.453 | 0.600 | 0.390 | 0.246 | 0.596 | 0.183 | 0.358 | 0.628 | 0.734 | 0.138 |
| Y | 2 | FI | 0.082 | 0.047 | 0.302 | 0.078 | 0.009 | 0.223 | 0.200 | 0.240 | 0.267 | 0.166 | 0.235 | 0.095 | 0.095 | 0.015 |
| Y | 3 | FI | 0.015 | 0.202 | 0.146 | 0.060 | 0.352 | 0.002 | 0.005 | 0.001 | 0.178 | 0.014 | <0.0001 | 0.527 | 0.527 | 0.171 |
| Y | 4 | FI | 0.302 | 0.511 | 0.247 | 0.408 | 0.706 | 0.040 | 0.152 | 0.036 | 0.247 | 0.007 | 0.206 | 0.534 | 0.628 | 0.090 |
| Y | 5 | FI | 0.312 | 0.676 | 0.119 | 0.420 | 0.398 | 0.263 | 0.296 | 0.540 | 0.276 | 0.653 | 0.304 | 0.584 | 0.584 | 0.192 |
| FB | 1 | FI | 0.061 | 0.119 | 0.134 | 0.034 | 0.021 | 0.001 | 0.062 | 0.001 | 0.003 | 0.000 | 0.069 | 0.014 | 0.242 | 0.159 |
| FB | 2 | FI | <0.0001 | 0.061 | 0.003 | 0.002 | 0.041 | 0.001 | 0.170 | 0.119 | 0.001 | 0.297 | 0.173 | 0.260 | 0.260 | 0.163 |
| FB | 3 | FI | 0.001 | 0.017 | 0.383 | 0.001 | 0.045 | 0.017 | 0.007 | 0.002 | 0.027 | 0.080 | 0.006 | 0.014 | 0.014 | 0.202 |
| FB | 4 | FI | 0.002 | 0.005 | 0.021 | <0.0001 | 0.008 | 0.000 | 0.024 | 0.004 | 0.001 | 0.010 | 0.040 | 0.118 | 0.290 | 0.587 |
| FB | 5 | FI | 0.001 | 0.010 | 0.093 | 0.002 | 0.045 | 0.030 | 0.000 | 0.084 | 0.148 | 0.007 | 0.005 | 0.017 | 0.017 | 0.219 |
| Y | 1 | CP-LAI | 0.679 | 0.728 | 0.027 | 0.802 | 0.516 | 0.473 | 0.294 | 0.163 | 0.483 | 0.224 | 0.270 | 0.493 | 0.546 | 0.183 |
| Y | 2 | CP-LAI | 0.095 | 0.060 | 0.239 | 0.090 | 0.014 | 0.225 | 0.188 | 0.242 | 0.258 | 0.176 | 0.218 | 0.087 | 0.087 | 0.023 |
| Y | 3 | CP-LAI | 0.001 | 0.213 | 0.270 | 0.019 | 0.423 | 0.033 | 0.029 | 0.003 | 0.100 | 0.024 | 0.006 | 0.388 | 0.388 | 0.258 |
| Y | 4 | CP-LAI | 0.165 | 0.520 | 0.405 | 0.248 | 0.818 | <0.0001 | 0.089 | 0.009 | 0.142 | 0.043 | 0.150 | 0.357 | 0.414 | 0.202 |
| Y | 5 | CP-LAI | 0.320 | 0.687 | 0.112 | 0.412 | 0.390 | 0.259 | 0.299 | 0.558 | 0.262 | 0.694 | 0.302 | 0.620 | 0.620 | 0.164 |
| FB | 1 | CP-LAI | 0.018 | 0.084 | 0.041 | 0.012 | 0.003 | 0.003 | 0.048 | 0.007 | 0.002 | 0.023 | 0.033 | 0.175 | 0.645 | 0.441 |
| FB | 2 | CP-LAI | 0.006 | 0.105 | 0.029 | 0.000 | 0.091 | 0.002 | 0.143 | 0.103 | 0.003 | 0.293 | 0.146 | 0.324 | 0.324 | 0.165 |
| FB | 3 | CP-LAI | 0.006 | 0.001 | 0.350 | 0.007 | 0.017 | 0.032 | 0.031 | 0.022 | 0.032 | 0.034 | 0.027 | 0.027 | 0.027 | 0.377 |
| FB | 4 | CP-LAI | 0.000 | 0.001 | 0.001 | <0.0001 | <0.0001 | <0.0001 | 0.014 | 0.001 | <0.0001 | 0.007 | 0.028 | 0.158 | 0.397 | 0.678 |
| FB | 5 | CP-LAI | 0.006 | 0.004 | 0.005 | 0.001 | 0.005 | 0.018 | 0.000 | 0.000 | 0.001 | 0.035 | 0.001 | 0.017 | 0.017 | <0.0001 |

NIR – Near-infrared, NDVI - Normalized Difference Vegetation Index, NDRE - Normalized Difference Red Edge Index, GNDVI -Green Normalized Difference Vegetation Index, RVI - Ratio Vegetation Index, CVI - Chlorophyll vegetation index, CIRE - Chlorophyll index – Red edge, Dr_Height – drone image estimated tree height, Dr_Volume – drone image estimated tree volume, TIR – thermal infrared temperature.

Table 17. Comparison of Pearson p-values (p) of simple linear regressions of multispectral drone image derived bands, indices, tree geometric dimensions or thermal infrared temperature with fractional interception (FI) and ceptometer derived leaf area index (CP-LAI), respectively, for individual trees from five surveys conducted over the 2023/2024 season for the young (Y) and full bearing (FB) pomegranate orchards at Avontuur and Welgemoed, respectively. Bold text indicates indices with significant potential to model the measured parameters at a significance level of 5% ($p \leq 0.05$) and bold red italicized text at a significance level of 10% ($0.05 < p \leq 0.1$).

| Site | Survey | Tree property | Drone image spectral band or index | | | | | | | | | | | | | |
|---|---|---|---|---|---|---|---|---|---|---|---|---|---|---|---|---|
| | | | Blue | Green | NIR | Red | RedEdge | NDVI | NDRE | GNDVI | RVI | CVI | CIRE | Dr_Height | Dr_Volume | TIR |
| Y | 1 | FI | 0.005 | 0.006 | 0.901 | 0.001 | *0.067* | 0.024 | *0.098* | 0.211 | 0.025 | 0.290 | 0.117 | 0.019 | 0.007 | 0.364 |
| Y | 2 | FI | 0.492 | 0.607 | 0.158 | 0.504 | 0.827 | 0.238 | 0.267 | 0.218 | 0.190 | 0.316 | 0.223 | 0.458 | 0.458 | 0.772 |
| Y | 3 | FI | 0.772 | 0.265 | 0.351 | 0.558 | 0.121 | 0.922 | 0.871 | 0.943 | 0.298 | 0.784 | 0.982 | 0.042 | 0.042 | 0.308 |
| Y | 4 | FI | 0.158 | 0.046 | 0.211 | *0.088* | 0.009 | 0.634 | 0.339 | 0.654 | 0.210 | 0.846 | 0.259 | 0.040 | 0.019 | 0.470 |
| Y | 5 | FI | 0.150 | 0.012 | 0.403 | *0.082* | *0.093* | 0.194 | 0.163 | 0.038 | 0.181 | 0.015 | 0.157 | 0.027 | 0.027 | 0.278 |
| FB | 1 | FI | 0.554 | 0.404 | 0.372 | 0.661 | 0.730 | 0.931 | 0.550 | 0.958 | 0.895 | 0.968 | 0.531 | 0.781 | 0.216 | 0.328 |
| FB | 2 | FI | 0.999 | 0.557 | 0.898 | 0.915 | 0.632 | 0.956 | 0.311 | 0.403 | 0.939 | 0.162 | 0.306 | 0.197 | 0.197 | 0.321 |
| FB | 3 | FI | 0.950 | 0.760 | 0.102 | 0.956 | 0.613 | 0.759 | 0.844 | 0.917 | 0.696 | 0.498 | 0.856 | 0.783 | 0.783 | 0.264 |
| FB | 4 | FI | 0.924 | 0.869 | 0.733 | 0.988 | 0.838 | 0.974 | 0.717 | 0.881 | 0.944 | 0.813 | 0.635 | 0.405 | 0.169 | 0.027 |
| FB | 5 | FI | 0.945 | 0.815 | 0.463 | 0.922 | 0.616 | 0.681 | 0.981 | 0.485 | 0.346 | 0.839 | 0.866 | 0.757 | 0.757 | 0.242 |
| Y | 1 | CP-LAI | 0.012 | 0.007 | 0.698 | 0.003 | 0.045 | *0.059* | 0.165 | 0.321 | *0.056* | 0.237 | 0.187 | *0.052* | 0.036 | 0.291 |
| Y | 2 | CP-LAI | 0.457 | 0.560 | 0.219 | 0.470 | 0.780 | 0.236 | 0.283 | 0.216 | 0.199 | 0.301 | 0.244 | 0.478 | 0.478 | 0.717 |
| Y | 3 | CP-LAI | 0.945 | 0.249 | 0.187 | 0.746 | *0.081* | 0.669 | 0.689 | 0.901 | 0.446 | 0.713 | 0.855 | *0.099* | *0.099* | 0.199 |
| Y | 4 | CP-LAI | 0.319 | 0.044 | *0.090* | 0.210 | 0.002 | 0.983 | 0.474 | 0.825 | 0.357 | 0.621 | 0.344 | 0.118 | *0.085* | 0.264 |
| Y | 5 | CP-LAI | 0.144 | 0.011 | 0.418 | *0.086* | *0.098* | 0.198 | 0.161 | 0.033 | 0.194 | 0.010 | 0.158 | 0.020 | 0.020 | 0.320 |
| FB | 1 | CP-LAI | 0.752 | 0.486 | 0.631 | 0.793 | 0.893 | 0.903 | 0.601 | 0.839 | 0.909 | 0.721 | 0.665 | 0.303 | 0.016 | *0.073* |
| FB | 2 | CP-LAI | 0.858 | 0.433 | 0.686 | 0.959 | 0.469 | 0.913 | 0.357 | 0.439 | 0.891 | 0.166 | 0.350 | 0.141 | 0.141 | 0.318 |
| FB | 3 | CP-LAI | 0.856 | 0.931 | 0.122 | 0.844 | 0.755 | 0.670 | 0.677 | 0.728 | 0.672 | 0.661 | 0.696 | 0.698 | 0.698 | 0.105 |
| FB | 4 | CP-LAI | 0.975 | 0.952 | 0.929 | 0.985 | 0.993 | 0.991 | 0.778 | 0.938 | 0.988 | 0.839 | 0.692 | 0.329 | *0.094* | 0.012 |
| FB | 5 | CP-LAI | 0.854 | 0.876 | 0.868 | 0.937 | 0.868 | 0.753 | 0.974 | 0.970 | 0.936 | 0.658 | 0.956 | 0.756 | 0.756 | 0.999 |

NIR – Near-infrared, NDVI - Normalized Difference Vegetation Index, NDRE - Normalized Difference Red Edge Index, GNDVI -Green Normalized Difference Vegetation Index, RVI - Ratio Vegetation Index, CVI - Chlorophyll vegetation index, CIRE - Chlorophyll index – Red edge, Dr_Height – drone image estimated tree height, Dr_Volume – drone image estimated tree volume, TIR – thermal infrared temperature.

Table 18. Comparison of coefficients of determination ($R^2$) of simple linear regressions of multispectral drone image derived bands, indices, tree geometric dimensions or thermal infrared temperature with actual tree canopy area-based leaf area index (LAI) and actual orchard LAI, respectively, for individual trees from five surveys conducted over the 2023/2024 season for the young (Y, green gradient colour) and full bearing (FB, red gradient colour) pomegranate orchards at Avontuur and Welgemoed, respectively. Bold text indicates indices with significant potential to model the measured parameters at a significance level of 5% ($p \leq 0.05$). Increased colour intensity indicates increasing $R^2$ values.

| Site | Survey | Tree property | Drone image spectral band or index | | | | | | | | | | | | | |
|---|---|---|---|---|---|---|---|---|---|---|---|---|---|---|---|---|
| | | | Blue | Green | NIR | Red | RedEdge | NDVI | NDRE | GNDVI | RVI | CVI | CIRE | Dr_Height | Dr_Volume | TIR |
| Y | 1 | Tree canopy-based LAI | 0.664 | 0.632 | 0.012 | 0.771 | 0.407 | 0.494 | 0.279 | 0.168 | 0.490 | 0.226 | 0.252 | 0.548 | 0.583 | 0.105 |
| Y | 2 | Tree canopy-based LAI | 0.153 | 0.109 | 0.213 | 0.146 | 0.044 | 0.304 | 0.269 | 0.323 | 0.351 | 0.202 | 0.306 | 0.145 | 0.145 | 0.033 |
| Y | 3 | Tree canopy-based LAI | 0.013 | 0.242 | 0.183 | 0.056 | 0.468 | 0.004 | 0.003 | 0.001 | 0.159 | 0.029 | 0.001 | 0.435 | 0.435 | 0.205 |
| Y | 4 | Tree canopy-based LAI | 0.242 | 0.590 | 0.394 | 0.342 | 0.845 | 0.008 | 0.104 | 0.021 | 0.188 | 0.032 | 0.162 | 0.397 | 0.455 | 0.152 |
| Y | 5 | Tree canopy-based LAI | 0.296 | 0.622 | 0.099 | 0.369 | 0.345 | 0.234 | 0.264 | 0.507 | 0.240 | 0.634 | 0.269 | 0.600 | 0.600 | 0.154 |
| FB | 1 | Tree canopy-based LAI | 0.018 | 0.084 | 0.041 | 0.012 | 0.003 | 0.003 | 0.048 | 0.007 | 0.002 | 0.023 | 0.033 | 0.175 | 0.645 | 0.441 |
| FB | 2 | Tree canopy-based LAI | 0.006 | 0.105 | 0.029 | 0.000 | 0.091 | 0.002 | 0.143 | 0.103 | 0.003 | 0.293 | 0.146 | 0.324 | 0.324 | 0.165 |
| FB | 3 | Tree canopy-based LAI | 0.006 | 0.001 | 0.350 | 0.007 | 0.017 | 0.032 | 0.031 | 0.022 | 0.032 | 0.034 | 0.027 | 0.027 | 0.027 | 0.377 |
| FB | 4 | Tree canopy-based LAI | 0.000 | 0.001 | 0.001 | <0.0001 | <0.0001 | <0.0001 | 0.014 | 0.001 | <0.0001 | 0.007 | 0.028 | 0.158 | 0.397 | 0.678 |
| FB | 5 | Tree canopy-based LAI | 0.006 | 0.004 | 0.005 | 0.001 | 0.005 | 0.018 | 0.000 | 0.000 | 0.001 | 0.035 | 0.001 | 0.017 | 0.017 | <0.0001 |
| Y | 1 | Orchard LAI | 0.674 | 0.700 | 0.023 | 0.795 | 0.486 | 0.478 | 0.286 | 0.162 | 0.484 | 0.230 | 0.261 | 0.507 | 0.554 | 0.158 |
| Y | 2 | Orchard LAI | 0.104 | 0.067 | 0.236 | 0.099 | 0.018 | 0.238 | 0.202 | 0.256 | 0.274 | 0.181 | 0.233 | 0.097 | 0.097 | 0.026 |
| Y | 3 | Orchard LAI | 0.002 | 0.219 | 0.253 | 0.025 | 0.437 | 0.024 | 0.021 | 0.001 | 0.111 | 0.025 | 0.003 | 0.395 | 0.395 | 0.251 |
| Y | 4 | Orchard LAI | 0.174 | 0.531 | 0.406 | 0.260 | 0.824 | 0.000 | 0.090 | 0.010 | 0.148 | 0.042 | 0.151 | 0.362 | 0.419 | 0.196 |
| Y | 5 | Orchard LAI | 0.318 | 0.681 | 0.111 | 0.408 | 0.386 | 0.256 | 0.295 | 0.553 | 0.260 | 0.688 | 0.299 | 0.618 | 0.618 | 0.163 |
| FB | 1 | Orchard LAI | 0.018 | 0.084 | 0.041 | 0.012 | 0.003 | 0.003 | 0.048 | 0.007 | 0.002 | 0.023 | 0.033 | 0.175 | 0.645 | 0.441 |
| FB | 2 | Orchard LAI | 0.006 | 0.105 | 0.029 | 0.000 | 0.091 | 0.002 | 0.143 | 0.103 | 0.003 | 0.293 | 0.146 | 0.324 | 0.324 | 0.165 |
| FB | 3 | Orchard LAI | 0.006 | 0.001 | 0.350 | 0.007 | 0.017 | 0.032 | 0.031 | 0.022 | 0.032 | 0.034 | 0.027 | 0.027 | 0.027 | 0.377 |
| FB | 4 | Orchard LAI | 0.000 | 0.001 | 0.001 | <0.0001 | <0.0001 | <0.0001 | 0.014 | 0.001 | <0.0001 | 0.007 | 0.028 | 0.158 | 0.397 | 0.678 |
| FB | 5 | Orchard LAI | 0.006 | 0.004 | 0.005 | 0.001 | 0.005 | 0.018 | 0.000 | 0.000 | 0.001 | 0.035 | 0.001 | 0.017 | 0.017 | <0.0001 |

NIR – Near-infrared, NDVI - Normalized Difference Vegetation Index, NDRE - Normalized Difference Red Edge Index, GNDVI -Green Normalized Difference Vegetation Index, RVI - Ratio Vegetation Index, CVI - Chlorophyll vegetation index, CIRE - Chlorophyll index – Red edge, Dr_Height – drone image estimated tree height, Dr_Volume – drone image estimated tree volume, TIR – thermal infrared temperature.

Table 19. Comparison of Pearson p-values (p) of simple linear regressions of multispectral drone image derived bands, indices, tree geometric dimensions or thermal infrared temperature with actual tree canopy area-based leaf area index (LAI) and actual orchard leaf area index (OLAI), respectively, for individual trees from five surveys conducted over the 2023/2024 season for the young (Y) and full bearing (FB) pomegranate orchards at Avontuur and Welgemoed, respectively. Bold text indicates indices with significant potential to model the measured parameters at a significance level of 5% ($p \leq 0.05$) and bold red italicized text at a significance level of 10% ($0.05 < p \leq 0.1$).

| Site | Survey | Tree property | Drone image spectral band or index | | | | | | | | | | | | | |
|---|---|---|---|---|---|---|---|---|---|---|---|---|---|---|---|---|
| | | | Blue | Green | NIR | Red | RedEdge | NDVI | NDRE | GNDVI | RVI | CVI | CIRE | Dr_Height | Dr_Volume | TIR |
| Y | 1 | Tree canopy-based LAI | 0.014 | 0.018 | 0.798 | 0.004 | *0.089* | *0.052* | 0.179 | 0.314 | *0.053* | 0.234 | 0.204 | 0.036 | 0.028 | 0.433 |
| Y | 2 | Tree canopy-based LAI | 0.338 | 0.425 | 0.249 | 0.350 | 0.619 | 0.157 | 0.187 | 0.142 | 0.122 | 0.263 | 0.155 | 0.352 | 0.352 | 0.666 |
| Y | 3 | Tree canopy-based LAI | 0.790 | 0.216 | 0.290 | 0.572 | *0.061* | 0.885 | 0.893 | 0.930 | 0.327 | 0.688 | 0.951 | *0.075* | *0.075* | 0.259 |
| Y | 4 | Tree canopy-based LAI | 0.216 | 0.026 | *0.096* | 0.128 | 0.001 | 0.832 | 0.435 | 0.730 | 0.283 | 0.672 | 0.322 | *0.094* | *0.066* | 0.340 |
| Y | 5 | Tree canopy-based LAI | 0.163 | 0.020 | 0.447 | 0.110 | 0.126 | 0.225 | 0.193 | 0.048 | 0.218 | 0.018 | 0.188 | 0.024 | 0.024 | 0.336 |
| FB | 1 | Tree canopy-based LAI | 0.752 | 0.486 | 0.631 | 0.793 | 0.893 | 0.903 | 0.601 | 0.839 | 0.909 | 0.721 | 0.665 | 0.303 | 0.016 | *0.073* |
| FB | 2 | Tree canopy-based LAI | 0.858 | 0.433 | 0.686 | 0.959 | 0.469 | 0.913 | 0.357 | 0.439 | 0.891 | 0.166 | 0.350 | 0.141 | 0.141 | 0.318 |
| FB | 3 | Tree canopy-based LAI | 0.856 | 0.931 | 0.122 | 0.844 | 0.755 | 0.670 | 0.677 | 0.728 | 0.672 | 0.661 | 0.696 | 0.698 | 0.698 | 0.105 |
| FB | 4 | Tree canopy-based LAI | 0.975 | 0.952 | 0.929 | 0.985 | 0.993 | 0.991 | 0.778 | 0.938 | 0.988 | 0.839 | 0.692 | 0.329 | *0.094* | 0.012 |
| FB | 5 | Tree canopy-based LAI | 0.854 | 0.876 | 0.868 | 0.937 | 0.868 | 0.753 | 0.974 | 0.970 | 0.936 | 0.658 | 0.956 | 0.756 | 0.756 | 0.999 |
| Y | 1 | Orchard LAI | 0.012 | 0.010 | 0.718 | 0.003 | *0.055* | *0.058* | 0.172 | 0.324 | *0.055* | 0.229 | 0.195 | 0.048 | 0.034 | 0.330 |
| Y | 2 | Orchard LAI | 0.435 | 0.536 | 0.223 | 0.448 | 0.752 | 0.220 | 0.264 | 0.201 | 0.183 | 0.294 | 0.226 | 0.452 | 0.452 | 0.702 |
| Y | 3 | Orchard LAI | 0.915 | 0.242 | 0.204 | 0.709 | *0.074* | 0.712 | 0.732 | 0.934 | 0.421 | 0.710 | 0.896 | *0.095* | *0.095* | 0.206 |
| Y | 4 | Orchard LAI | 0.303 | 0.040 | *0.089* | 0.197 | 0.002 | 0.964 | 0.469 | 0.812 | 0.347 | 0.627 | 0.341 | 0.114 | *0.083* | 0.272 |
| Y | 5 | Orchard LAI | 0.146 | 0.012 | 0.420 | *0.088* | 0.100 | 0.200 | 0.164 | 0.034 | 0.196 | 0.011 | 0.161 | 0.021 | 0.021 | 0.322 |
| FB | 1 | Orchard LAI | 0.752 | 0.486 | 0.631 | 0.793 | 0.893 | 0.903 | 0.601 | 0.839 | 0.909 | 0.721 | 0.665 | 0.303 | 0.016 | *0.073* |
| FB | 2 | Orchard LAI | 0.858 | 0.433 | 0.686 | 0.959 | 0.469 | 0.913 | 0.357 | 0.439 | 0.891 | 0.166 | 0.350 | 0.141 | 0.141 | 0.318 |
| FB | 3 | Orchard LAI | 0.856 | 0.931 | 0.122 | 0.844 | 0.755 | 0.670 | 0.677 | 0.728 | 0.672 | 0.661 | 0.696 | 0.698 | 0.698 | 0.105 |
| FB | 4 | Orchard LAI | 0.975 | 0.952 | 0.929 | 0.985 | 0.993 | 0.991 | 0.778 | 0.938 | 0.988 | 0.839 | 0.692 | 0.329 | *0.094* | 0.012 |
| FB | 5 | Orchard LAI | 0.854 | 0.876 | 0.868 | 0.937 | 0.868 | 0.753 | 0.974 | 0.970 | 0.936 | 0.658 | 0.956 | 0.756 | 0.756 | 0.999 |

NIR – Near-infrared, NDVI - Normalized Difference Vegetation Index, NDRE - Normalized Difference Red Edge Index, GNDVI -Green Normalized Difference Vegetation Index, RVI - Ratio Vegetation Index, CVI - Chlorophyll vegetation index, CIRE - Chlorophyll index – Red edge, Dr_Height – drone image estimated tree height, Dr_Volume – drone image estimated tree volume, TIR – thermal infrared temperature.

Table 20. Comparison of coefficients of determination ($R^2$) of simple linear regressions of orchard averaged multispectral drone image derived spectral bands, indices, tree geometric dimensions or thermal infrared temperature with orchard averaged measured or calculated tree canopy dimensions, fractional interception (FI) and leaf area index (LAI) for orchards combined over the 2023/2024 season. Pearson p-values (p) are indicated in the bottom part of the table. Bold black text indicates indices which related significantly to the measured **parameters at a significance level of 5% ($p \leq 0.05$) and bold red italicized text at a significance level of 10% ($0.05 < p \leq 0.1$). SI refers to statistical indicator.** Increased green colour intensity indicates increasing $R^2$ values.

| Tree property | SI | Drone image spectral band or index | | | | | | | | | | | | | |
|---|---|---|---|---|---|---|---|---|---|---|---|---|---|---|---|
| | | Blue | Green | NIR | Red | RedEdge | NDVI | NDRE | GNDVI | RVI | CVI | CIRE | Dr_Height | Dr_Volume | TIR |
| Tree height | $R^2$ | 0.120 | 0.026 | 0.038 | 0.158 | 0.056 | 0.158 | 0.025 | 0.003 | 0.272 | 0.641 | 0.014 | 0.802 | 0.276 | 0.015 |
| Across row width | $R^2$ | 0.172 | 0.056 | 0.033 | 0.219 | 0.088 | 0.221 | 0.059 | 0.019 | 0.323 | 0.563 | 0.040 | 0.873 | 0.291 | 0.055 |
| Tree_volume | $R^2$ | 0.135 | 0.035 | 0.000 | 0.191 | 0.048 | 0.209 | 0.064 | 0.013 | 0.304 | 0.657 | 0.043 | 0.782 | 0.251 | 0.061 |
| Fractional interception | $R^2$ | 0.057 | 0.002 | 0.009 | 0.090 | 0.013 | 0.094 | 0.004 | 0.003 | 0.203 | 0.760 | 0.000 | 0.734 | 0.318 | 0.004 |
| Ceptometer LAI | $R^2$ | 0.097 | 0.017 | 0.012 | 0.136 | 0.033 | 0.148 | 0.021 | 0.002 | 0.284 | 0.655 | 0.010 | 0.795 | 0.404 | 0.032 |
| Tree canopy-based LAI | $R^2$ | 0.239 | 0.119 | 0.127 | 0.259 | 0.190 | 0.229 | 0.103 | 0.048 | 0.231 | 0.259 | 0.083 | 0.602 | 0.061 | 0.013 |
| Orchard LAI | $R^2$ | 0.001 | 0.020 | 0.032 | 0.001 | 0.023 | 0.007 | 0.010 | 0.021 | 0.080 | 0.412 | 0.016 | 0.254 | 0.392 | 0.016 |
| Tree height | p | 0.327 | 0.655 | 0.591 | 0.256 | 0.511 | 0.256 | 0.660 | 0.888 | 0.122 | 0.005 | 0.749 | 0.000 | 0.119 | 0.740 |
| Across row width | p | 0.233 | 0.510 | 0.615 | 0.173 | 0.404 | 0.170 | 0.500 | 0.708 | 0.086 | 0.012 | 0.582 | <0.0001 | 0.107 | 0.514 |
| Tree_volume | p | 0.297 | 0.605 | 0.977 | 0.207 | 0.544 | 0.184 | 0.482 | 0.750 | 0.099 | 0.004 | 0.564 | 0.001 | 0.140 | 0.492 |
| Fractional interception | p | 0.507 | 0.901 | 0.790 | 0.400 | 0.757 | 0.389 | 0.865 | 0.885 | 0.191 | 0.001 | 0.960 | 0.002 | 0.089 | 0.865 |
| Ceptometer LAI | p | 0.381 | 0.722 | 0.767 | 0.294 | 0.614 | 0.273 | 0.692 | 0.906 | 0.113 | 0.005 | 0.781 | 0.001 | 0.048 | 0.623 |
| Tree canopy -based LAI | p | 0.152 | 0.329 | 0.313 | 0.133 | 0.207 | 0.162 | 0.366 | 0.543 | 0.160 | 0.133 | 0.419 | 0.008 | 0.492 | 0.750 |
| Orchard LAI | p | 0.946 | 0.694 | 0.622 | 0.925 | 0.675 | 0.819 | 0.785 | 0.687 | 0.429 | 0.045 | 0.727 | 0.137 | 0.053 | 0.728 |

NIR – Near-infrared, NDVI - Normalized Difference Vegetation Index, NDRE - Normalized Difference Red Edge Index, GNDVI -Green Normalized Difference Vegetation Index, RVI - Ratio Vegetation Index, CVI - Chlorophyll vegetation index, CIRE - Chlorophyll index – Red edge, Dr_Height – drone image estimated tree height, Dr_Volume – drone image estimated tree volume, TIR – thermal infrared temperature.

Table 21. Comparison of coefficients of determination ($R^2$) of simple linear regressions between orchard averaged multispectral drone image derived spectral bands, indices, tree geometric dimensions or thermal infrared temperature with averaged measured or calculated tree canopy dimensions, fractional interception and leaf area index (LAI) per orchard over the 2023/2024 season. Pearson p-values (p) are indicated in the bottom part of the table. Bold black text indicates indices which related significantly to the measured parameters at a significance level of 5% (**p≤0.05) and bold red italicized text at a significance level of 10% (0.05<p≤0.1).** Y refer to the young orchard at Avontuur and FB to the full bearing orchard at Welgemoed. SI refers to statistical indicator. Increased green colour intensity indicates increasing $R^2$ values.

| Site | SI | Tree property | Drone image spectral band or index | | | | | | | | | | | | | |
|---|---|---|---|---|---|---|---|---|---|---|---|---|---|---|---|---|
| | | | Blue | Green | NIR | Red | RedEdge | NDVI | NDRE | GNDVI | RVI | CVI | CIRE | Dr_Height | Dr_Volume | TIR |
| Y | $R^2$ | Tree_height | 0.993 | 0.985 | 0.201 | 0.976 | 0.946 | 0.935 | 0.892 | 0.940 | 0.905 | 0.735 | 0.890 | 0.971 | 0.627 | 0.689 |
| FB | $R^2$ | Tree_height | 0.151 | 0.087 | 0.297 | 0.107 | 0.086 | 0.106 | 0.264 | 0.165 | 0.023 | 0.514 | 0.284 | 0.578 | 0.006 | 0.054 |
| Y | $R^2$ | Across row width | 0.094 | 0.072 | 0.174 | 0.147 | 0.026 | 0.195 | 0.242 | 0.123 | 0.181 | 0.035 | 0.235 | 0.126 | 0.098 | 0.182 |
| FB | $R^2$ | Across row width | 0.140 | 0.042 | 0.581 | 0.143 | 0.141 | 0.041 | 0.023 | 0.002 | 0.004 | 0.092 | 0.014 | 0.087 | 0.024 | 0.780 |
| Y | $R^2$ | Tree_volume | 0.007 | 0.013 | 0.463 | 0.000 | 0.058 | 0.008 | 0.025 | 0.000 | 0.006 | 0.275 | 0.023 | 0.002 | 0.002 | 0.026 |
| FB | $R^2$ | Tree_volume | 0.154 | 0.031 | 0.350 | 0.149 | 0.118 | 0.046 | 0.035 | 0.003 | 0.000 | 0.050 | 0.025 | 0.011 | 0.068 | 0.757 |
| Y | $R^2$ | Fractional interception | 0.742 | 0.770 | 0.277 | 0.672 | 0.766 | 0.635 | 0.596 | 0.719 | 0.599 | 0.942 | 0.606 | 0.672 | 0.311 | 0.547 |
| FB | $R^2$ | Fractional interception | 0.252 | 0.283 | 0.347 | 0.179 | 0.481 | 0.072 | 0.262 | 0.149 | 0.036 | 0.404 | 0.275 | 0.036 | 0.443 | 0.108 |
| Y | $R^2$ | Ceptometer LAI | 0.660 | 0.703 | 0.337 | 0.587 | 0.710 | 0.533 | 0.472 | 0.629 | 0.537 | 0.989 | 0.479 | 0.543 | 0.249 | 0.431 |
| FB | $R^2$ | Ceptometer LAI | 0.032 | 0.023 | 0.605 | 0.011 | 0.140 | 0.009 | 0.016 | 0.001 | 0.040 | 0.087 | 0.018 | 0.241 | 0.421 | 0.448 |
| Y | $R^2$ | Tree canopy-based LAI | 0.646 | 0.691 | 0.302 | 0.578 | 0.683 | 0.531 | 0.473 | 0.629 | 0.538 | 0.987 | 0.480 | 0.518 | 0.218 | 0.447 |
| FB | $R^2$ | Tree canopy-based LAI | 0.032 | 0.023 | 0.605 | 0.011 | 0.140 | 0.009 | 0.016 | 0.001 | 0.040 | 0.087 | 0.018 | 0.241 | 0.421 | 0.448 |
| Y | $R^2$ | Orchard LAI | 0.656 | 0.700 | 0.328 | 0.585 | 0.703 | 0.533 | 0.472 | 0.629 | 0.538 | 0.989 | 0.478 | 0.536 | 0.241 | 0.434 |
| FB | $R^2$ | Orchard LAI | 0.032 | 0.023 | 0.605 | 0.011 | 0.140 | 0.009 | 0.016 | 0.001 | 0.040 | 0.087 | 0.018 | 0.241 | 0.421 | 0.448 |
| Y | p | Tree_height | 0.000 | 0.001 | 0.448 | 0.002 | 0.005 | 0.007 | 0.016 | 0.006 | 0.013 | *0.063* | 0.016 | 0.002 | 0.110 | *0.082* |
| FB | p | Tree_height | 0.518 | 0.630 | 0.342 | 0.590 | 0.632 | 0.593 | 0.376 | 0.498 | 0.808 | 0.173 | 0.355 | 0.136 | 0.899 | 0.707 |
| Y | p | Across row width | 0.617 | 0.663 | 0.485 | 0.524 | 0.796 | 0.456 | 0.400 | 0.562 | 0.475 | 0.762 | 0.408 | 0.557 | 0.608 | 0.474 |
| FB | p | Across row width | 0.536 | 0.740 | 0.134 | 0.531 | 0.533 | 0.743 | 0.810 | 0.940 | 0.925 | 0.620 | 0.848 | 0.631 | 0.802 | 0.047 |
| Y | p | Tree_volume | 0.897 | 0.854 | 0.206 | 0.990 | 0.698 | 0.887 | 0.801 | 0.996 | 0.899 | 0.364 | 0.809 | 0.948 | 0.937 | 0.794 |
| FB | p | Tree_volume | 0.514 | 0.778 | 0.293 | 0.520 | 0.571 | 0.730 | 0.764 | 0.931 | 0.982 | 0.717 | 0.799 | 0.866 | 0.671 | *0.055* |
| Y | p | Fractional interception | *0.061* | *0.051* | 0.362 | *0.089* | *0.052* | 0.107 | 0.126 | *0.070* | 0.125 | 0.006 | 0.121 | *0.089* | 0.328 | 0.153 |
| FB | p | Fractional interception | 0.389 | 0.356 | 0.296 | 0.478 | 0.194 | 0.662 | 0.378 | 0.522 | 0.759 | 0.249 | 0.364 | 0.758 | 0.220 | 0.589 |
| Y | p | Ceptometer LAI | *0.095* | *0.076* | 0.304 | 0.131 | *0.073* | 0.161 | 0.200 | 0.109 | 0.159 | 0.000 | 0.196 | 0.156 | 0.392 | 0.229 |
| FB | p | Ceptometer LAI | 0.772 | 0.806 | 0.122 | 0.867 | 0.536 | 0.881 | 0.839 | 0.963 | 0.746 | 0.630 | 0.831 | 0.400 | 0.236 | 0.217 |
| Y | p | Tree canopy-based LAI | 0.101 | *0.081* | 0.338 | 0.136 | *0.085* | 0.163 | 0.199 | 0.109 | 0.158 | 0.001 | 0.195 | 0.170 | 0.428 | 0.217 |
| FB | p | Tree canopy-based LAI | 0.772 | 0.806 | 0.122 | 0.867 | 0.536 | 0.881 | 0.839 | 0.963 | 0.746 | 0.630 | 0.831 | 0.400 | 0.236 | 0.217 |
| Y | p | Orchard LAI | *0.097* | *0.077* | 0.313 | 0.132 | *0.076* | 0.162 | 0.200 | 0.109 | 0.158 | 0.001 | 0.196 | 0.160 | 0.401 | 0.226 |
| FB | p | Orchard LAI | 0.772 | 0.806 | 0.122 | 0.867 | 0.536 | 0.881 | 0.839 | 0.963 | 0.746 | 0.630 | 0.831 | 0.400 | 0.236 | 0.217 |

NIR – Near-infrared, NDVI - Normalized Difference Vegetation Index, NDRE - Normalized Difference Red Edge Index, GNDVI -Green Normalized Difference Vegetation Index, RVI - Ratio Vegetation Index, CVI - Chlorophyll vegetation index, CIRE - Chlorophyll index – Red edge, Dr_Height – drone image estimated tree height, Dr_Volume – drone image estimated tree volume, TIR – thermal infrared temperature.

# APPENDIX B: SUMMARY OF COEFFICIENTS OF DETERMINATION OF LINEAR REGRESSIONS OF TREE PHYSIOLOGICAL PARAMETERS WITH DRONE IMAGE DERIVED VARIABLES

Table 22. Comparison of coefficients of determination ($R^2$) of simple linear regressions of multispectral drone image derived spectral bands, indices or thermal infrared temperature with ground measured stem water potential, leaf chlorophyll content and selected physiological variables for individual trees in orchards combined over the 2023/2024 season for the young (Y) and full bearing (FB) pomegranate orchards at Avontuur and Welgemoed, respectively. Bold black text indicates indices which related significantly to the measured parameters at a **significance level of 5% ($p \leq 0.05$)**. Increased green colour intensity indicates increasing $R^2$ values.

| Tree | Drone image spectral band or index | | | | | | | | | | | |
|---|---|---|---|---|---|---|---|---|---|---|---|---|
| Property | Blue | Green | NIR | Red | RedEdge | NDVI | NDRE | GNDVI | RVI | CVI | CIRE | TIR |
| SWP | 0.029 | 0.010 | 0.002 | 0.041 | 0.008 | 0.034 | 0.013 | 0.008 | 0.013 | 0.026 | 0.010 | 0.024 |
| Chl_c | 0.003 | 0.014 | 0.020 | 0.008 | 0.001 | 0.006 | 0.019 | 0.049 | 0.006 | 0.420 | 0.035 | 0.022 |
| $A_n$_10 | 0.002 | 0.006 | 0.560 | 0.001 | 0.009 | 0.001 | 0.043 | 0.055 | 0.058 | 0.421 | 0.043 | 0.052 |
| $A_n$_12 | <0.0001 | 0.002 | 0.134 | 0.001 | 0.002 | 0.001 | 0.006 | 0.014 | 0.019 | 0.189 | 0.008 | <0.0001 |
| $A_n$_14 | 0.001 | 0.006 | 0.039 | 0.002 | 0.000 | 0.001 | 0.006 | 0.013 | 0.020 | 0.095 | 0.005 | <0.0001 |
| $g_s$_10 | 0.197 | 0.265 | 0.058 | 0.231 | 0.163 | 0.256 | 0.273 | 0.318 | 0.121 | 0.104 | 0.252 | 0.230 |
| $g_s$_12 | 0.180 | 0.289 | 0.090 | 0.190 | 0.188 | 0.222 | 0.340 | 0.368 | 0.165 | 0.213 | 0.349 | 0.232 |
| $g_s$_14 | 0.144 | 0.255 | 0.123 | 0.175 | 0.140 | 0.203 | 0.286 | 0.337 | 0.089 | 0.294 | 0.278 | 0.239 |
| $Tr_L$_10 | 0.499 | 0.509 | 0.020 | 0.540 | 0.485 | 0.582 | 0.491 | 0.489 | 0.584 | 0.001 | 0.467 | 0.479 |
| $Tr_L$_12 | 0.406 | 0.506 | 0.004 | 0.416 | 0.432 | 0.472 | 0.546 | 0.549 | 0.514 | 0.060 | 0.554 | 0.435 |
| $Tr_L$_14 | 0.256 | 0.422 | 0.060 | 0.299 | 0.284 | 0.353 | 0.446 | 0.508 | 0.314 | 0.239 | 0.449 | 0.436 |

$A_n$_10/ 12/ 14 – Net $CO_2$ assimilation rate measured at 10h00/ 12h00/ 14h00, Chl_c – Chlorophyll concentration, CIRE - Chlorophyll index – Red edge, CVI - Chlorophyll vegetation index, GNDVI -Green Normalized Difference Vegetation Index, $g_s$_10/12/14 – Stomatal conductance measured at 10h00 /12h00 /14h00, NDRE - Normalized Difference Red Edge Index, NIR – Near-infrared, NDVI - Normalized Difference Vegetation Index, RVI - Ratio Vegetation Index, SWP – Stem water potential at 12h00,. TIR – thermal infrared temperature, $Tr_L$_10/ 12/ 14 - Leaf level transpiration at 10h00/ 12h00/ 14h00

Table 23. Comparison of Pearson p-values (p) of simple linear regressions of multispectral drone image derived bands, indices or thermal infrared temperature with ground measured stem water potential, leaf chlorophyll content and selected physiological variables for individual trees in orchards combined over the 2023/2024 season for the young (Y) and full bearing (FB) pomegranate orchards at Avontuur and Welgemoed, respectively. Bold text indicates indices with significant potential to model the measured parameters at a significance level of 5% ($p \leq 0.05$) and bold red italicized text at a significance level of 10% ($0.05 < p \leq 0.1$).

| Tree | Drone image spectral band or index | | | | | | | | | | | |
|---|---|---|---|---|---|---|---|---|---|---|---|---|
| Property | Blue | Green | NIR | Red | RedEdge | NDVI | NDRE | GNDVI | RVI | CVI | CIRE | TIR |
| SWP | 0.176 | 0.423 | 0.734 | 0.107 | 0.474 | 0.139 | 0.359 | 0.473 | 0.365 | 0.195 | 0.419 | 0.222 |
| Chl_c | 0.471 | 0.139 | *0.078* | 0.259 | 0.670 | 0.356 | *0.083* | 0.006 | 0.320 | <0.0001 | 0.020 | *0.063* |
| $A_n$_10 | 0.783 | 0.655 | <0.0001 | 0.875 | 0.575 | 0.823 | 0.211 | 0.157 | 0.145 | <0.0001 | 0.211 | 0.167 |
| $A_n$_12 | 0.998 | 0.761 | 0.015 | 0.881 | 0.762 | 0.871 | 0.606 | 0.452 | 0.373 | 0.003 | 0.553 | 0.992 |
| $A_n$_14 | 0.863 | 0.641 | 0.237 | 0.776 | 0.944 | 0.843 | 0.632 | 0.500 | 0.394 | *0.059* | 0.683 | 0.996 |
| $g_s$_10 | 0.005 | 0.001 | 0.146 | 0.002 | 0.012 | 0.001 | 0.001 | 0.000 | 0.032 | 0.048 | 0.001 | 0.002 |
| $g_s$_12 | 0.004 | 0.000 | 0.048 | 0.003 | 0.003 | 0.001 | <0.0001 | <0.0001 | 0.006 | 0.002 | <0.0001 | 0.001 |
| $g_s$_14 | 0.019 | 0.001 | 0.031 | 0.009 | 0.021 | 0.005 | 0.001 | 0.000 | *0.069* | 0.000 | 0.001 | 0.002 |
| $Tr_L$_10 | <0.0001 | <0.0001 | 0.402 | <0.0001 | <0.0001 | <0.0001 | <0.0001 | <0.0001 | <0.0001 | 0.838 | <0.0001 | <0.0001 |
| $Tr_L$_12 | <0.0001 | <0.0001 | 0.687 | <0.0001 | <0.0001 | <0.0001 | <0.0001 | <0.0001 | <0.0001 | 0.109 | <0.0001 | <0.0001 |
| $Tr_L$_14 | 0.001 | <0.0001 | 0.139 | 0.000 | 0.001 | <0.0001 | <0.0001 | <0.0001 | 0.000 | 0.002 | <0.0001 | <0.0001 |

$A_n$_10/ 12/ 14 – Net $CO_2$ assimilation rate measured at 10h00/ 12h00/ 14h00, Chl_c – Chlorophyll concentration, CIRE - Chlorophyll index – Red edge, CVI - Chlorophyll vegetation index, GNDVI -Green Normalized Difference Vegetation Index, $g_s$_10/12/14 – Stomatal conductance measured at 10h00 /12h00 /14h00, NDRE - Normalized Difference Red Edge Index, NIR – Near-infrared, NDVI - Normalized Difference Vegetation Index, RVI - Ratio Vegetation Index, SWP – Stem water potential at 12h00,. TIR – thermal infrared temperature, $Tr_L$_10/ 12/ 14 - Leaf level transpiration at 10h00/ 12h00/ 14h00

Table 24. Comparison of coefficients of determination ($R^2$) of simple linear regressions of multispectral drone image derived spectral bands, indices or thermal infrared temperature with measured stem water potential, leaf chlorophyll content and selected physiological variables for individual trees in the young cultivar 'Wonderful' pomegranate orchard over the 2023/2024 season. Bold black text indicates indices which related significantly to the measured parameters at a significance **level of 5% (p≤0.05)**. Increased green colour intensity indicates increasing $R^2$ values.

| Tree | Drone image spectral band or index | | | | | | | | | | | |
|---|---|---|---|---|---|---|---|---|---|---|---|---|
| Property | Blue | Green | NIR | Red | RedEdge | NDVI | NDRE | GNDVI | RVI | CVI | CIRE | TIR |
| SWP | 0.232 | 0.202 | 0.031 | 0.265 | 0.178 | 0.237 | 0.161 | 0.173 | 0.267 | 0.015 | 0.145 | 0.062 |
| Chl_c | 0.199 | 0.195 | 0.003 | 0.217 | 0.145 | 0.239 | 0.280 | 0.230 | 0.236 | 0.075 | 0.282 | 0.251 |
| $A_n$_10 | 0.467 | 0.549 | 0.341 | 0.522 | 0.447 | 0.657 | 0.703 | 0.667 | 0.604 | 0.341 | 0.698 | 0.611 |
| $A_n$_12 | 0.409 | 0.303 | 0.064 | 0.401 | 0.386 | 0.319 | 0.227 | 0.219 | 0.261 | 0.008 | 0.199 | 0.058 |
| $A_n$_14 | 0.199 | 0.181 | 0.066 | 0.218 | 0.232 | 0.179 | 0.134 | 0.133 | 0.170 | 0.009 | 0.124 | 0.036 |
| $g_s$_10 | 0.534 | 0.605 | 0.047 | 0.585 | 0.528 | 0.610 | 0.554 | 0.595 | 0.650 | 0.293 | 0.543 | 0.361 |
| $g_s$_12 | 0.677 | 0.683 | 0.039 | 0.726 | 0.682 | 0.738 | 0.688 | 0.661 | 0.725 | 0.233 | 0.673 | 0.454 |
| $g_s$_14 | 0.595 | 0.646 | 0.025 | 0.657 | 0.634 | 0.670 | 0.634 | 0.626 | 0.666 | 0.272 | 0.623 | 0.408 |
| $Tr_L$_10 | 0.550 | 0.678 | 0.197 | 0.598 | 0.525 | 0.679 | 0.673 | 0.734 | 0.731 | 0.552 | 0.675 | 0.588 |
| $Tr_L$_12 | 0.756 | 0.818 | 0.152 | 0.798 | 0.744 | 0.861 | 0.866 | 0.851 | 0.844 | 0.494 | 0.863 | 0.720 |
| $Tr_L$_14 | 0.600 | 0.685 | 0.075 | 0.662 | 0.626 | 0.707 | 0.691 | 0.698 | 0.733 | 0.385 | 0.689 | 0.517 |

$A_n$_10/ 12/ 14 – Net $CO_2$ assimilation rate measured at 10h00/ 12h00/ 14h00, Chl_c – Chlorophyll concentration, CIRE - Chlorophyll index – Red edge, CVI - Chlorophyll vegetation index, GNDVI -Green Normalized Difference Vegetation Index, $g_s$_10/12/14 – Stomatal conductance measured at 10h00 /12h00 /14h00, NDRE - Normalized Difference Red Edge Index, NIR – Near-infrared, NDVI - Normalized Difference Vegetation Index, RVI - Ratio Vegetation Index, SWP – Stem water potential at 12h00,. TIR – thermal infrared temperature, $Tr_L$_10/ 12/ 14 - Leaf level transpiration at 10h00/ 12h00/ 14h00

Table 25. Comparison of Pearson p-values (p) of simple linear regressions of multispectral drone image derived bands, indices or thermal infrared temperature with ground measured stem water potential, leaf chlorophyll content and selected physiological variables for individual trees in the young cultivar 'Wonderful' pomegranate orchard over the 2023/2024 season at Avontuur. Bold text indicates indices with significant potential to model the measured parameters at a significance level of 5% ($p \leq 0.05$) and bold red italicized text at a significance level of 10% ($0.05 < p \leq 0.1$).

| Tree | Drone image spectral band or index | | | | | | | | | | | |
|---|---|---|---|---|---|---|---|---|---|---|---|---|
| Property | Blue | Green | NIR | Red | RedEdge | NDVI | NDRE | GNDVI | RVI | CVI | CIRE | TIR |
| SWP | 0.015 | 0.024 | 0.402 | 0.008 | 0.035 | 0.014 | 0.047 | 0.039 | 0.008 | 0.555 | *0.061* | 0.229 |
| Chl_c | 0.000 | 0.000 | 0.694 | 0.000 | 0.002 | <0.0001 | <0.0001 | <0.0001 | <0.0001 | 0.028 | <0.0001 | <0.0001 |
| $A_n$_10 | 0.001 | 0.000 | 0.007 | 0.000 | 0.001 | <0.0001 | <0.0001 | <0.0001 | <0.0001 | 0.007 | <0.0001 | <0.0001 |
| $A_n$_12 | 0.002 | 0.012 | 0.282 | 0.003 | 0.003 | 0.009 | 0.034 | 0.038 | 0.021 | 0.702 | 0.049 | 0.305 |
| $A_n$_14 | 0.049 | *0.062* | 0.274 | 0.038 | 0.031 | *0.063* | 0.112 | 0.114 | *0.071* | 0.688 | 0.128 | 0.421 |
| $g_s$_10 | 0.000 | <0.0001 | 0.356 | <0.0001 | 0.000 | <0.0001 | 0.000 | <0.0001 | <0.0001 | 0.014 | 0.000 | 0.005 |
| $g_s$_12 | <0.0001 | <0.0001 | 0.402 | <0.0001 | <0.0001 | <0.0001 | <0.0001 | <0.0001 | <0.0001 | 0.031 | <0.0001 | 0.001 |
| $g_s$_14 | <0.0001 | <0.0001 | 0.505 | <0.0001 | <0.0001 | <0.0001 | <0.0001 | <0.0001 | <0.0001 | 0.018 | <0.0001 | 0.002 |
| $Tr_L$_10 | 0.000 | <0.0001 | *0.050* | <0.0001 | 0.000 | <0.0001 | <0.0001 | <0.0001 | <0.0001 | 0.000 | <0.0001 | <0.0001 |
| $Tr_L$_12 | <0.0001 | <0.0001 | *0.089* | <0.0001 | <0.0001 | <0.0001 | <0.0001 | <0.0001 | <0.0001 | 0.001 | <0.0001 | <0.0001 |
| $Tr_L$_14 | <0.0001 | <0.0001 | 0.243 | <0.0001 | <0.0001 | <0.0001 | <0.0001 | <0.0001 | <0.0001 | 0.004 | <0.0001 | 0.000 |

$A_n$_10/ 12/ 14 – Net $CO_2$ assimilation rate measured at 10h00/ 12h00/ 14h00, Chl_c – Chlorophyll concentration, CIRE - Chlorophyll index – Red edge, CVI - Chlorophyll vegetation index, GNDVI -Green Normalized Difference Vegetation Index, $g_s$_10/12/14 – Stomatal conductance measured at 10h00 /12h00 /14h00, NDRE - Normalized Difference Red Edge Index, NIR – Near-infrared, NDVI - Normalized Difference Vegetation Index, RVI - Ratio Vegetation Index, SWP – Stem water potential at 12h00,. TIR – thermal infrared temperature, $Tr_L$_10/ 12/ 14 - Leaf level transpiration at 10h00/ 12h00/ 14h00

Table 26. Comparison of coefficients of determination ($R^2$) of simple linear regressions of multispectral drone image derived spectral bands, indices or thermal infrared temperature with measured stem water potential, leaf chlorophyll content and selected physiological variables for individual trees in the full bearing cultivar 'Wonderful' pomegranate orchard over the 2023/2024 season at Welgemoed. **Bold black text indicates indices which related significantly to the measured parameters at a significance level of 5% (p≤0.0**5). Increased green colour intensity indicates increasing $R^2$ values.

| Tree | Drone image spectral band or index | | | | | | | | | | | |
|---|---|---|---|---|---|---|---|---|---|---|---|---|
| Property | Blue | Green | NIR | Red | RedEdge | NDVI | NDRE | GNDVI | RVI | CVI | CIRE | TIR |
| SWP | 0.085 | 0.094 | 0.201 | 0.098 | 0.097 | 0.072 | 0.033 | 0.055 | 0.055 | 0.000 | 0.021 | 0.001 |
| SWP_PD | 0.012 | 0.086 | 0.464 | 0.032 | 0.251 | 0.006 | 0.009 | 0.006 | 0.121 | 0.012 | 0.017 | <0.0001 |
| Chl_c | 0.005 | 0.009 | 0.029 | <0.0001 | <0.0001 | 0.008 | 0.010 | 0.034 | 0.048 | 0.010 | 0.010 | 0.097 |
| $A_n$_10 | 0.071 | 0.187 | 0.241 | 0.059 | 0.190 | 0.036 | 0.080 | 0.113 | 0.166 | 0.086 | 0.087 | 0.056 |
| $A_n$_12 | 0.059 | <0.0001 | 0.124 | 0.035 | 0.008 | 0.040 | 0.002 | 0.006 | 0.012 | 0.006 | 0.002 | 0.005 |
| $A_n$_14 | 0.037 | 0.186 | 0.065 | 0.060 | 0.180 | 0.061 | 0.131 | 0.165 | 0.165 | 0.211 | 0.139 | 0.201 |
| $g_s$_10 | 0.016 | 0.047 | 0.168 | 0.007 | 0.055 | <0.0001 | 0.004 | 0.010 | 0.004 | 0.032 | 0.004 | 0.137 |
| $g_s$_12 | 0.103 | 0.131 | 0.017 | 0.111 | 0.077 | 0.151 | 0.128 | 0.176 | 0.274 | 0.025 | 0.135 | 0.086 |
| $g_s$_14 | 0.013 | 0.029 | 0.098 | 0.024 | 0.003 | 0.056 | 0.021 | 0.061 | 0.155 | <0.0001 | 0.022 | 0.107 |
| $Tr_L$_10 | 0.022 | 0.027 | 0.099 | 0.032 | 0.027 | 0.069 | 0.128 | 0.090 | 0.037 | 0.054 | 0.133 | 0.282 |
| $Tr_L$_12 | 0.123 | 0.222 | 0.003 | 0.135 | 0.162 | 0.186 | 0.238 | 0.285 | 0.356 | 0.107 | 0.250 | 0.147 |
| $Tr_L$_14 | 0.055 | 0.233 | 0.010 | 0.106 | 0.131 | 0.166 | 0.161 | 0.283 | 0.450 | 0.086 | 0.169 | 0.417 |

$A_n$_10/ 12/ 14 – Net $CO_2$ assimilation rate measured at 10h00/ 12h00/ 14h00, Chl_c – Chlorophyll concentration, CIRE - Chlorophyll index – Red edge, CVI - Chlorophyll vegetation index, GNDVI -Green Normalized Difference Vegetation Index, $g_s$_10/12/14 – Stomatal conductance measured at 10h00 /12h00 /14h00, NDRE - Normalized Difference Red Edge Index, NIR – Near-infrared, NDVI - Normalized Difference Vegetation Index, RVI - Ratio Vegetation Index, SWP – Stem water potential at 12h00,. TIR – thermal infrared temperature, $Tr_L$_10/ 12/ 14 - Leaf level transpiration at 10h00/ 12h00/ 14h00

Table 27. Comparison of Pearson p-values (p) of simple linear regressions of multispectral drone image derived bands, indices or thermal infrared temperature with ground measured stem water potential, leaf chlorophyll content and selected physiological variables for individual trees in the full bearing cultivar 'Wonderful' orchard over the 2023/2024 season at Welgemoed. Bold text indicates indices with significant potential to model the measured parameters at a significance level of 5% ($p \leq 0.05$) and bold red italicized text at a significance level of 10% ($0.05 < p \leq 0.1$).

| Tree | Drone image spectral band or index | | | | | | | | | | | |
|---|---|---|---|---|---|---|---|---|---|---|---|---|
| Property | Blue | Green | NIR | Red | RedEdge | NDVI | NDRE | GNDVI | RVI | CVI | CIRE | TIR |
| SWP | *0.069* | *0.055* | 0.004 | 0.049 | *0.051* | *0.094* | 0.262 | 0.144 | 0.144 | 0.928 | 0.377 | 0.835 |
| SWP_PD | 0.759 | 0.411 | 0.030 | 0.624 | 0.140 | 0.831 | 0.794 | 0.827 | 0.324 | 0.768 | 0.720 | 0.995 |
| Chl_c | 0.510 | 0.363 | 0.103 | 0.948 | 0.965 | 0.389 | 0.346 | *0.080* | 0.037 | 0.343 | 0.353 | 0.003 |
| $A_n$_10 | 0.285 | *0.073* | 0.039 | 0.332 | *0.070* | 0.449 | 0.256 | 0.172 | *0.093* | 0.237 | 0.236 | 0.344 |
| $A_n$_12 | 0.252 | 0.989 | *0.091* | 0.384 | 0.680 | 0.347 | 0.852 | 0.721 | 0.613 | 0.721 | 0.852 | 0.755 |
| $A_n$_14 | 0.444 | *0.074* | 0.306 | 0.326 | *0.079* | 0.325 | 0.139 | *0.095* | *0.094* | *0.055* | 0.128 | *0.062* |
| $g_s$_10 | 0.618 | 0.386 | *0.091* | 0.734 | 0.350 | 0.999 | 0.799 | 0.696 | 0.807 | 0.478 | 0.815 | 0.130 |
| $g_s$_12 | 0.127 | *0.083* | 0.549 | 0.111 | 0.189 | *0.060* | *0.086* | 0.042 | 0.009 | 0.457 | *0.077* | 0.165 |
| $g_s$_14 | 0.655 | 0.496 | 0.207 | 0.543 | 0.841 | 0.344 | 0.571 | 0.323 | 0.106 | 0.984 | 0.556 | 0.185 |
| $Tr_L$_10 | 0.558 | 0.512 | 0.203 | 0.478 | 0.518 | 0.293 | 0.146 | 0.227 | 0.447 | 0.352 | 0.137 | 0.023 |
| $Tr_L$_12 | *0.093* | 0.020 | 0.788 | *0.077* | *0.051* | 0.035 | 0.016 | 0.007 | 0.002 | 0.119 | 0.013 | *0.064* |
| $Tr_L$_14 | 0.351 | 0.043 | 0.700 | 0.188 | 0.140 | *0.093* | *0.099* | 0.023 | 0.002 | 0.238 | *0.090* | 0.004 |

$A_n$_10/ 12/ 14 – Net $CO_2$ assimilation rate measured at 10h00/ 12h00/ 14h00, Chl_c – Chlorophyll concentration, CIRE - Chlorophyll index – Red edge, CVI - Chlorophyll vegetation index, GNDVI -Green Normalized Difference Vegetation Index, $g_s$_10/12/14 – Stomatal conductance measured at 10h00 /12h00 /14h00, NDRE - Normalized Difference Red Edge Index, NIR – Near-infrared, NDVI - Normalized Difference Vegetation Index, RVI - Ratio Vegetation Index, SWP – Stem water potential at 12h00,. TIR – thermal infrared temperature, $Tr_L$_10/ 12/ 14 - Leaf level transpiration at 10h00/ 12h00/ 14h00

Table 28. Comparison of coefficients of determination ($R^2$) of simple linear regressions between multispectral drone image derived bands or indices and physiological variables for selected drone surveys conducted over the 2023/2024 season for individually selected trees in the young (Y, green gradient colour) and full bearing (FB, red gradient colour) cultivar 'Wonderful' pomegranate orchards at Avontuur and Welgemoed, respectively. Bold text indicates indices with significant potential to model the measured parameters at a significance level of 5% ($p \leq 0.05$). Increased colour intensity indicates increasing $R^2$ values.

| Site | Survey | Tree | Drone image spectral band or index | | | | | | | | | | | |
|---|---|---|---|---|---|---|---|---|---|---|---|---|---|---|
| | | Property | Blue | Green | NIR | Red | RedEdge | NDVI | NDRE | GNDVI | RVI | CVI | CIRE | TIR |
| Y | 1 | SWP | 0.082 | 0.619 | 0.147 | 0.124 | 0.865 | 0.032 | 0.509 | 0.378 | 0.004 | 0.602 | 0.461 | 0.222 |
| Y | 2 | SWP | 0.006 | 0.027 | 0.051 | 0.017 | 0.007 | 0.007 | 0.019 | 0.017 | 0.022 | 0.103 | 0.028 | 0.166 |
| Y | 3 | SWP | 0.205 | 0.001 | 0.025 | 0.098 | 0.102 | 0.185 | 0.772 | 0.034 | 0.112 | 0.178 | 0.834 | 0.821 |
| Y | 4 | SWP | 0.060 | 0.027 | 0.010 | <0.0001 | 0.026 | 0.006 | 0.038 | 0.053 | 0.136 | 0.163 | 0.008 | 0.497 |
| Y | 5 | SWP | 0.163 | 0.010 | 0.413 | 0.393 | 0.402 | 0.320 | 0.318 | 0.065 | 0.277 | 0.077 | 0.302 | 0.921 |
| FB | 1 | SWP | 0.143 | 0.100 | 0.047 | 0.015 | 0.234 | 0.003 | 0.590 | 0.046 | 0.001 | 0.001 | 0.598 | 0.729 |
| FB | 2 | SWP | 0.051 | 0.002 | 0.357 | 0.042 | 0.020 | 0.159 | 0.196 | 0.170 | 0.211 | 0.000 | 0.202 | 0.029 |
| FB | 3 | SWP | 0.031 | 0.045 | 0.331 | 0.004 | 0.051 | 0.000 | 0.000 | 0.011 | 0.013 | 0.026 | 0.002 | 0.019 |
| FB | 4 | SWP | 0.819 | 0.206 | 0.020 | 0.634 | 0.172 | 0.417 | 0.265 | 0.230 | 0.159 | 0.125 | 0.304 | 0.208 |
| FB | 5 | SWP | 0.038 | 0.040 | 0.032 | 0.089 | 0.041 | 0.211 | 0.061 | 0.081 | 0.178 | 0.277 | 0.065 | 0.592 |
| Y | 1 | Chl_c | 0.053 | 0.269 | 0.110 | 0.055 | 0.249 | 0.123 | 0.001 | 0.003 | 0.089 | 0.445 | 0.004 | 0.008 |
| Y | 2 | Chl_c | - | - | - | - | - | - | - | - | - | - | - | - |
| Y | 3 | Chl_c | 0.002 | 0.005 | 0.001 | 0.005 | 0.056 | 0.012 | 0.027 | 0.003 | 0.100 | 0.011 | 0.039 | 0.062 |
| Y | 4 | Chl_c | 0.002 | 0.024 | 0.000 | 0.005 | 0.034 | 0.000 | 0.075 | 0.053 | <0.0001 | 0.259 | 0.070 | 0.033 |
| Y | 5 | Chl_c | 0.015 | 0.002 | 0.009 | 0.004 | 0.001 | 0.014 | 0.006 | <0.0001 | 0.021 | 0.000 | 0.007 | <0.0001 |
| FB | 1 | Chl_c | 0.002 | 0.003 | 0.000 | 0.014 | 0.003 | 0.009 | 0.008 | 0.000 | 0.022 | 0.027 | 0.016 | 0.039 |
| FB | 2 | Chl_c | - | - | - | - | - | - | - | - | - | - | - | - |
| FB | 3 | Chl_c | 0.001 | 0.001 | 0.022 | 0.004 | 0.001 | 0.009 | 0.004 | 0.000 | 0.011 | 0.055 | 0.004 | 0.005 |
| FB | 4 | Chl_c | 0.282 | 0.060 | 0.035 | 0.238 | 0.045 | 0.086 | 0.000 | 0.007 | 0.001 | 0.093 | 0.001 | 0.063 |
| FB | 5 | Chl_c | 0.009 | 0.001 | 0.003 | 0.002 | 0.001 | 0.000 | 0.007 | 0.005 | 0.000 | 0.024 | 0.011 | 0.017 |
| Y | 2 | $A_n$_10 | 0.656 | 0.750 | 0.904 | 0.733 | 0.717 | 0.617 | 0.386 | 0.619 | 0.397 | 0.276 | 0.313 | 0.398 |
| Y | 3 | $A_n$_10 | 0.361 | 0.365 | 0.516 | 0.654 | 0.576 | 0.544 | 0.088 | 0.028 | 0.368 | 0.616 | 0.045 | 0.233 |
| Y | 4 | $A_n$_10 | 0.032 | 0.318 | 0.163 | 0.369 | 0.513 | 0.359 | 0.642 | 0.393 | 0.096 | 0.233 | 0.566 | 0.011 |
| Y | 5 | $A_n$_10 | 0.468 | 0.611 | 0.969 | 0.789 | 0.899 | 0.590 | 0.641 | 0.209 | 0.612 | 0.138 | 0.645 | 0.433 |
| FB | 2 | $A_n$_10 | 0.065 | 0.062 | 0.696 | 0.151 | 0.421 | 0.365 | 0.172 | 0.272 | 0.124 | 0.112 | 0.149 | 0.427 |

| Site | Survey | Tree Property | Drone image spectral band or index | | | | | | | | | | | |
|---|---|---|---|---|---|---|---|---|---|---|---|---|---|---|
| | | | Blue | Green | NIR | Red | RedEdge | NDVI | NDRE | GNDVI | RVI | CVI | CIRE | TIR |
| FB | 3 | $A_n$_10 | 0.189 | 0.223 | 0.039 | 0.194 | 0.183 | 0.217 | 0.265 | 0.282 | 0.274 | 0.078 | 0.308 | 0.005 |
| FB | 4 | $A_n$_10 | 0.414 | 0.078 | 0.023 | 0.407 | 0.067 | 0.194 | 0.040 | 0.040 | 0.043 | 0.001 | 0.045 | 0.625 |
| FB | 5 | $A_n$_10 | - | - | - | - | - | - | - | - | - | - | - | - |
| Y | 2 | $A_n$_12 | 0.663 | 0.734 | 0.838 | 0.713 | 0.685 | 0.597 | 0.376 | 0.625 | 0.349 | 0.461 | 0.297 | 0.444 |
| Y | 3 | $A_n$_12 | 0.004 | 0.049 | 0.145 | 0.013 | 0.233 | 0.004 | 0.390 | 0.012 | 0.245 | 0.009 | 0.450 | 0.916 |
| Y | 4 | $A_n$_12 | 0.003 | 0.061 | 0.008 | 0.390 | 0.419 | 0.656 | 0.749 | 0.076 | 0.470 | 0.014 | 0.783 | 0.348 |
| Y | 5 | $A_n$_12 | 0.471 | 0.056 | 0.027 | 0.263 | 0.125 | 0.429 | 0.336 | 0.069 | 0.369 | 0.112 | 0.314 | 0.358 |
| FB | 2 | $A_n$_12 | 0.444 | 0.296 | 0.098 | 0.263 | 0.012 | 0.311 | 0.569 | 0.791 | 0.416 | 0.006 | 0.571 | 0.003 |
| FB | 3 | $A_n$_12 | 0.747 | 0.578 | 0.152 | 0.778 | 0.606 | 0.744 | 0.664 | 0.559 | 0.729 | 0.924 | 0.682 | 0.785 |
| FB | 4 | $A_n$_12 | 0.003 | 0.228 | 0.143 | 0.032 | 0.261 | 0.008 | 0.049 | 0.070 | 0.064 | 0.013 | 0.018 | 0.065 |
| FB | 5 | $A_n$_12 | 0.008 | 0.068 | 0.098 | 0.057 | 0.116 | 0.131 | 0.176 | 0.113 | 0.155 | 0.005 | 0.204 | 0.355 |
| Y | 2 | $A_n$_14 | 0.076 | 0.155 | 0.363 | 0.140 | 0.132 | 0.076 | 0.002 | 0.067 | 0.037 | 0.005 | 0.000 | 0.000 |
| Y | 3 | $A_n$_14 | 0.003 | 0.012 | 0.001 | 0.008 | 0.002 | 0.009 | <0.0001 | 0.339 | 0.009 | 0.112 | 0.006 | 0.447 |
| Y | 4 | $A_n$_14 | 0.578 | 0.534 | 0.397 | 0.217 | 0.255 | 0.071 | 0.144 | 0.603 | 0.005 | 0.731 | 0.131 | 0.034 |
| Y | 5 | $A_n$_14 | 0.563 | 0.971 | 0.703 | 0.667 | 0.714 | 0.549 | 0.575 | 0.691 | 0.591 | 0.592 | 0.584 | 0.124 |
| FB | 2 | $A_n$_14 | 0.000 | 0.264 | 0.149 | 0.041 | 0.160 | 0.080 | 0.000 | 0.051 | 0.033 | 0.624 | 0.000 | 0.378 |
| FB | 3 | $A_n$_14 | 0.022 | 0.104 | 0.368 | 0.020 | 0.110 | 0.017 | 0.031 | 0.077 | 0.015 | 0.029 | 0.013 | 0.001 |
| FB | 4 | $A_n$_14 | - | - | - | - | - | - | - | - | - | - | - | - |
| FB | 5 | $A_n$_14 | 0.000 | 0.005 | 0.051 | 0.003 | 0.014 | 0.000 | 0.002 | 0.002 | 0.006 | 0.157 | 0.004 | 0.643 |
| Y | 2 | $g_s$_10 | 0.183 | 0.160 | 0.065 | 0.144 | 0.113 | 0.162 | 0.118 | 0.226 | 0.179 | 0.582 | 0.107 | 0.028 |
| Y | 3 | $g_s$_10 | 0.041 | 0.144 | 0.289 | 0.222 | 0.443 | 0.151 | 0.363 | 0.034 | 0.246 | 0.246 | 0.259 | 0.611 |
| Y | 4 | $g_s$_10 | 0.000 | 0.002 | 0.019 | 0.001 | 0.004 | <0.0001 | 0.048 | 0.017 | 0.066 | 0.072 | 0.039 | 0.002 |
| Y | 5 | $g_s$_10 | 0.063 | 0.099 | 0.046 | 0.116 | 0.076 | 0.144 | 0.121 | 0.295 | 0.102 | 0.267 | 0.107 | 0.738 |
| FB | 2 | $g_s$_10 | 0.760 | 0.276 | 0.155 | 0.693 | 0.023 | 0.706 | 0.879 | 0.818 | 0.808 | 0.206 | 0.884 | 0.094 |
| FB | 3 | $g_s$_10 | 0.103 | 0.028 | 0.023 | 0.038 | 0.029 | 0.029 | 0.022 | 0.018 | 0.020 | 0.022 | 0.022 | 0.172 |
| FB | 4 | $g_s$_10 | 0.246 | 0.131 | 0.137 | 0.311 | 0.137 | 0.042 | 0.002 | 0.011 | 0.000 | 0.002 | 0.001 | 0.460 |
| FB | 5 | $g_s$_10 | - | - | - | - | - | - | - | - | - | - | - | - |
| Y | 2 | $g_s$_12 | 0.266 | 0.185 | 0.106 | 0.210 | 0.239 | 0.238 | 0.422 | 0.222 | 0.127 | 0.046 | 0.424 | 0.771 |
| Y | 3 | $g_s$_12 | 0.259 | 0.153 | 0.269 | 0.490 | 0.274 | 0.335 | 0.003 | 0.192 | 0.191 | 0.672 | 0.000 | 0.257 |
| Y | 4 | $g_s$_12 | 0.101 | 0.246 | 0.322 | 0.008 | 0.032 | 0.035 | 0.005 | 0.254 | 0.109 | 0.560 | 0.027 | 0.446 |

| Site | Survey | Tree Property | Drone image spectral band or index | | | | | | | | | | | |
|---|---|---|---|---|---|---|---|---|---|---|---|---|---|---|
| | | | Blue | Green | NIR | Red | RedEdge | NDVI | NDRE | GNDVI | RVI | CVI | CIRE | TIR |
| Y | 5 | $g_s$_12 | 0.144 | 0.309 | 0.014 | 0.074 | 0.038 | 0.096 | 0.060 | 0.494 | 0.084 | 0.628 | 0.054 | 0.024 |
| FB | 2 | $g_s$_12 | 0.066 | 0.244 | 0.807 | 0.214 | 0.549 | 0.462 | 0.143 | 0.094 | 0.207 | 0.578 | 0.123 | 0.941 |
| FB | 3 | $g_s$_12 | 0.393 | 0.163 | 0.010 | 0.405 | 0.174 | 0.401 | 0.312 | 0.185 | 0.333 | 0.813 | 0.336 | 0.607 |
| FB | 4 | $g_s$_12 | 0.024 | 0.410 | 0.076 | 0.212 | 0.335 | 0.151 | 0.189 | 0.262 | 0.221 | 0.078 | 0.126 | 0.002 |
| FB | 5 | $g_s$_12 | 0.001 | 0.015 | 0.036 | 0.012 | 0.045 | 0.057 | 0.078 | 0.037 | 0.070 | 0.003 | 0.096 | 0.440 |
| Y | 2 | $g_s$_14 | 0.027 | 0.064 | 0.213 | 0.066 | 0.080 | 0.034 | 0.005 | 0.015 | 0.011 | 0.116 | 0.002 | 0.017 |
| Y | 3 | $g_s$_14 | 0.521 | 0.136 | 0.161 | 0.708 | 0.118 | 0.737 | 0.130 | 0.174 | 0.033 | 0.974 | 0.223 | 0.020 |
| Y | 4 | $g_s$_14 | 0.069 | 0.209 | 0.094 | 0.070 | 0.150 | 0.027 | 0.168 | 0.290 | 0.021 | 0.437 | 0.123 | 0.026 |
| Y | 5 | $g_s$_14 | 0.509 | 0.127 | 0.481 | 0.664 | 0.584 | 0.661 | 0.622 | 0.006 | 0.600 | 0.005 | 0.597 | 0.958 |
| FB | 2 | $g_s$_14 | 0.017 | 0.370 | 0.893 | 0.111 | 0.703 | 0.356 | 0.092 | 0.050 | 0.179 | 0.535 | 0.077 | 0.830 |
| FB | 3 | $g_s$_14 | 0.164 | 0.268 | 0.061 | 0.209 | 0.222 | 0.243 | 0.310 | 0.345 | 0.312 | 0.072 | 0.348 | 0.001 |
| FB | 4 | $g_s$_14 | - | - | - | - | - | - | - | - | - | - | - | - |
| FB | 5 | $g_s$_14 | 0.130 | 0.187 | 0.266 | 0.177 | 0.238 | 0.177 | 0.162 | 0.141 | 0.215 | 0.009 | 0.152 | 0.657 |
| Y | 2 | $Tr_L$_10 | 0.172 | 0.165 | 0.104 | 0.145 | 0.109 | 0.125 | 0.058 | 0.192 | 0.066 | 0.882 | 0.036 | 0.056 |
| Y | 3 | $Tr_L$_10 | 0.081 | 0.234 | 0.382 | 0.290 | 0.555 | 0.243 | 0.410 | 0.002 | 0.304 | 0.239 | 0.272 | 0.447 |
| Y | 4 | $Tr_L$_10 | 0.004 | 0.029 | 0.000 | 0.025 | 0.079 | 0.037 | 0.198 | 0.068 | 0.010 | 0.093 | 0.160 | 0.006 |
| Y | 5 | $Tr_L$_10 | 0.041 | 0.084 | 0.040 | 0.096 | 0.062 | 0.113 | 0.089 | 0.253 | 0.074 | 0.213 | 0.075 | 0.734 |
| FB | 2 | $Tr_L$_10 | 0.708 | 0.254 | 0.132 | 0.677 | 0.026 | 0.670 | 0.807 | 0.719 | 0.746 | 0.238 | 0.812 | 0.089 |
| FB | 3 | $Tr_L$_10 | 0.161 | 0.063 | 0.076 | 0.073 | 0.069 | 0.053 | 0.040 | 0.037 | 0.048 | 0.049 | 0.041 | 0.276 |
| FB | 4 | $Tr_L$_10 | 0.317 | 0.136 | 0.188 | 0.351 | 0.160 | 0.035 | 0.000 | 0.005 | 0.000 | 0.001 | 0.000 | 0.546 |
| FB | 5 | $Tr_L$_10 | - | - | - | - | - | - | - | - | - | - | - | - |
| Y | 2 | $Tr_L$_12 | 0.135 | 0.075 | 0.027 | 0.091 | 0.110 | 0.111 | 0.265 | 0.103 | 0.039 | 0.033 | 0.269 | 0.629 |
| Y | 3 | $Tr_L$_12 | 0.548 | 0.278 | 0.358 | 0.808 | 0.329 | 0.752 | 0.009 | 0.100 | 0.176 | 0.925 | 0.035 | 0.019 |
| Y | 4 | $Tr_L$_12 | 0.100 | 0.075 | 0.014 | 0.259 | 0.223 | 0.384 | 0.374 | 0.090 | 0.321 | 0.001 | 0.453 | 0.666 |
| Y | 5 | $Tr_L$_12 | 0.294 | 0.477 | 0.086 | 0.201 | 0.142 | 0.230 | 0.180 | 0.610 | 0.216 | 0.715 | 0.170 | 0.063 |
| FB | 2 | $Tr_L$_12 | 0.073 | 0.232 | 0.707 | 0.245 | 0.468 | 0.466 | 0.133 | 0.067 | 0.201 | 0.692 | 0.114 | 0.955 |
| FB | 3 | $Tr_L$_12 | 0.167 | 0.057 | 0.079 | 0.215 | 0.057 | 0.231 | 0.179 | 0.088 | 0.190 | 0.565 | 0.203 | 0.242 |
| FB | 4 | $Tr_L$_12 | 0.240 | 0.532 | 0.203 | 0.506 | 0.492 | 0.202 | 0.175 | 0.241 | 0.159 | 0.091 | 0.123 | 0.085 |
| FB | 5 | $Tr_L$_12 | 0.027 | 0.002 | 0.034 | 0.000 | 0.021 | 0.007 | 0.023 | 0.003 | 0.022 | 0.009 | 0.033 | 0.544 |
| Y | 2 | $Tr_L$_14 | <0.0001 | 0.004 | 0.063 | 0.006 | 0.012 | 0.001 | 0.000 | 0.002 | 0.000 | 0.378 | 0.000 | <0.0001 |

| Site | Survey | Tree Property | Drone image spectral band or index | | | | | | | | | | | |
|---|---|---|---|---|---|---|---|---|---|---|---|---|---|---|
| | | | Blue | Green | NIR | Red | RedEdge | NDVI | NDRE | GNDVI | RVI | CVI | CIRE | TIR |
| Y | 3 | $Tr_L$_14 | 0.600 | 0.177 | 0.189 | 0.753 | 0.132 | 0.803 | 0.146 | 0.113 | 0.044 | 0.936 | 0.240 | 0.050 |
| Y | 4 | $Tr_L$_14 | 0.234 | 0.368 | 0.206 | 0.202 | 0.283 | 0.114 | 0.276 | 0.456 | 0.005 | 0.504 | 0.242 | 0.014 |
| Y | 5 | $Tr_L$_14 | 0.470 | 0.134 | 0.475 | 0.636 | 0.564 | 0.620 | 0.580 | 0.009 | 0.559 | 0.008 | 0.555 | 0.945 |
| FB | 2 | $Tr_L$_14 | 0.020 | 0.353 | 0.858 | 0.128 | 0.675 | 0.368 | 0.087 | 0.050 | 0.155 | 0.543 | 0.071 | 0.867 |
| FB | 3 | $Tr_L$_14 | 0.100 | 0.205 | 0.085 | 0.129 | 0.169 | 0.148 | 0.205 | 0.252 | 0.229 | 0.021 | 0.242 | 0.014 |
| FB | 4 | $Tr_L$_14 | - | - | - | - | - | - | - | - | - | - | - | - |
| FB | 5 | $Tr_L$_14 | 0.118 | 0.179 | 0.256 | 0.162 | 0.234 | 0.160 | 0.164 | 0.136 | 0.198 | 0.002 | 0.156 | 0.597 |

$A_n$_10/ 12/ 14 – Net $CO_2$ assimilation rate measured at 10h00/ 12h00/ 14h00, Chl_c – Chlorophyll concentration, CIRE - Chlorophyll index – Red edge, CVI - Chlorophyll vegetation index, GNDVI -Green Normalized Difference Vegetation Index, $g_s$_10/12/14 – Stomatal conductance measured at 10h00 /12h00 /14h00, NDRE - Normalized Difference Red Edge Index, NIR – Near-infrared, NDVI - Normalized Difference Vegetation Index, RVI - Ratio Vegetation Index, SWP – Stem water potential at 12h00,. TIR – thermal infrared temperature, $Tr_L$_10/ 12/ 14 - Leaf level transpiration at 10h00/ 12h00/ 14h00

Table 29. Comparison of coefficients of determination ($R^2$) of simple linear regressions of orchard averaged multispectral drone image derived spectral bands, indices or thermal infrared temperature with orchard averaged measured stem water potential, leaf chlorophyll content and tree physiological variables for the young and full bearing cultivar 'Wonderful' pomegranate orchards over the 2023/2024 season at Avontuur and Welgemoed, respectively. Bold black text indicates indices which related significantly to the measured parameters at a **significance level of 5% ($p \leq 0.05$)**. Increased green colour intensity indicates increasing $R^2$ values.

| Tree | Drone image spectral band or index | | | | | | | | | | | |
|---|---|---|---|---|---|---|---|---|---|---|---|---|
| Property | Blue | Green | NIR | Red | RedEdge | NDVI | NDRE | GNDVI | RVI | CVI | CIRE | TIR |
| SWP | 0.108 | 0.065 | 0.063 | 0.153 | 0.079 | 0.096 | 0.021 | 0.017 | 0.012 | 0.075 | 0.006 | 0.045 |
| Chl_c | 0.000 | 0.027 | 0.035 | 0.001 | 0.004 | 0.001 | 0.038 | 0.077 | 0.027 | **0.606** | 0.057 | 0.047 |
| $A_n$_10 | 0.010 | 0.049 | **0.709** | 0.012 | 0.002 | 0.021 | 0.109 | 0.126 | 0.024 | 0.565 | 0.107 | 0.063 |
| $A_n$_12 | 0.012 | 0.000 | 0.374 | 0.009 | 0.015 | 0.004 | 0.017 | 0.020 | 0.034 | 0.324 | 0.023 | 0.001 |
| $A_n$_14 | 0.000 | 0.005 | 0.165 | 0.001 | 0.001 | 0.001 | 0.016 | 0.019 | 0.036 | 0.163 | 0.012 | 0.000 |
| $g_s$_10 | 0.386 | 0.451 | 0.051 | 0.415 | 0.338 | 0.400 | 0.404 | 0.463 | 0.202 | 0.151 | 0.359 | 0.323 |
| $g_s$_12 | 0.277 | 0.425 | 0.173 | 0.280 | 0.274 | 0.327 | **0.501** | **0.538** | 0.271 | 0.321 | **0.511** | 0.381 |
| $g_s$_14 | 0.228 | 0.340 | 0.213 | 0.249 | 0.186 | 0.280 | 0.386 | 0.440 | 0.137 | 0.357 | 0.371 | 0.330 |
| $Tr_L$_10 | **0.822** | **0.735** | 0.077 | **0.820** | **0.781** | **0.797** | **0.605** | **0.619** | **0.805** | 0.004 | **0.556** | **0.635** |
| $Tr_L$_12 | **0.722** | **0.841** | 0.006 | **0.698** | **0.747** | **0.767** | **0.852** | **0.862** | **0.869** | 0.092 | **0.858** | **0.745** |
| $Tr_L$_14 | 0.431 | **0.578** | 0.139 | 0.447 | 0.381 | 0.508 | **0.606** | **0.686** | 0.449 | 0.305 | **0.601** | **0.625** |

$A_n$_10/ 12/ 14 – Net $CO_2$ assimilation rate measured at 10h00/ 12h00/ 14h00, Chl_c – Chlorophyll concentration, CIRE - Chlorophyll index – Red edge, CVI - Chlorophyll vegetation index, GNDVI -Green Normalized Difference Vegetation Index, $g_s$_10/12/14 – Stomatal conductance measured at 10h00 /12h00 /14h00, NDRE - Normalized Difference Red Edge Index, NIR – Near-infrared, NDVI - Normalized Difference Vegetation Index, RVI - Ratio Vegetation Index, SWP – Stem water potential at 12h00,. TIR – thermal infrared temperature, $Tr_L$_10/ 12/ 14 - Leaf level transpiration at 10h00/ 12h00/ 14h00

Table 30. Comparison of Pearson p-values (p) of simple linear regressions of orchard averaged multispectral drone image derived bands, indices or thermal infrared temperature with orchard averaged ground measured stem water potential, leaf chlorophyll content and tree physiological variables for the young and full bearing cultivar 'Wonderful' orchards over the 2023/2024 season at Avontuur and Welgemoed, respectively. Bold text indicates indices with significant potential to model the measured parameters at a significance level of 5% ($p \leq 0.05$) and bold red italicized text at a significance level of 10% ($0.05 < p \leq 0.1$).

| Tree | Drone image spectral band or index | | | | | | | | | | | |
|---|---|---|---|---|---|---|---|---|---|---|---|---|
| Property | Blue | Green | NIR | Red | RedEdge | NDVI | NDRE | GNDVI | RVI | CVI | CIRE | TIR |
| SWP | 0.353 | 0.478 | 0.485 | 0.264 | 0.430 | 0.383 | 0.688 | 0.716 | 0.765 | 0.443 | 0.833 | 0.558 |
| Chl_c | 0.993 | 0.699 | 0.657 | 0.940 | 0.885 | 0.950 | 0.642 | 0.506 | 0.698 | **0.023** | 0.571 | 0.606 |
| $A_n$_10 | 0.828 | 0.633 | **0.018** | 0.815 | 0.926 | 0.757 | 0.470 | 0.435 | 0.741 | ***0.051*** | 0.474 | 0.588 |
| $A_n$_12 | 0.800 | 0.980 | 0.107 | 0.820 | 0.770 | 0.880 | 0.760 | 0.737 | 0.662 | 0.140 | 0.719 | 0.954 |
| $A_n$_14 | 1.000 | 0.880 | 0.366 | 0.951 | 0.951 | 0.957 | 0.788 | 0.767 | 0.684 | 0.369 | 0.813 | 0.987 |
| $g_s$_10 | 0.136 | ***0.099*** | 0.625 | 0.119 | 0.171 | 0.128 | 0.125 | ***0.093*** | 0.312 | 0.389 | 0.155 | 0.183 |
| $g_s$_12 | 0.180 | ***0.080*** | 0.306 | 0.178 | 0.183 | 0.138 | **0.049** | **0.038** | 0.186 | 0.143 | **0.046** | 0.103 |
| $g_s$_14 | 0.278 | 0.170 | 0.297 | 0.254 | 0.335 | 0.222 | 0.137 | 0.105 | 0.414 | 0.156 | 0.147 | 0.177 |
| $Tr_L$_10 | **0.005** | **0.014** | 0.546 | **0.005** | **0.008** | **0.007** | **0.039** | **0.036** | **0.006** | 0.893 | ***0.054*** | **0.032** |
| $Tr_L$_12 | **0.008** | **0.001** | 0.851 | **0.010** | **0.006** | **0.004** | **0.001** | **0.001** | **0.001** | 0.466 | **0.001** | **0.006** |
| $Tr_L$_14 | 0.109 | **0.047** | 0.410 | 0.101 | 0.139 | ***0.072*** | **0.039** | **0.021** | ***0.100*** | 0.198 | **0.041** | **0.034** |

$A_n$_10/ 12/ 14 – Net $CO_2$ assimilation rate measured at 10h00/ 12h00/ 14h00, Chl_c – Chlorophyll concentration, CIRE - Chlorophyll index – Red edge, CVI - Chlorophyll vegetation index, GNDVI -Green Normalized Difference Vegetation Index, $g_s$_10/12/14 – Stomatal conductance measured at 10h00 /12h00 /14h00, NDRE - Normalized Difference Red Edge Index, NIR – Near-infrared, NDVI - Normalized Difference Vegetation Index, RVI - Ratio Vegetation Index, SWP – Stem water potential at 12h00,. TIR – thermal infrared temperature, $Tr_L$_10/ 12/ 14 - Leaf level transpiration at 10h00/ 12h00/ 14h00

Table 31. Comparison of coefficients of determination ($R^2$) of simple linear regressions of orchard averaged multispectral drone image derived spectral bands, indices or thermal infrared temperature with orchard averaged measured stem water potential, leaf chlorophyll content and tree physiological variables for the young cultivar 'Wonderful' pomegranate orchard over the 2023/2024 season at Avontuur. **Bold black text indicates indices which related significantly to the measured parameters at a significance level of 5% ($p \leq 0.05$)**. Increased green colour intensity indicates increasing $R^2$ values.

| Tree | Drone image spectral band or index | | | | | | | | | | | |
|---|---|---|---|---|---|---|---|---|---|---|---|---|
| Property | Blue | Green | NIR | Red | RedEdge | NDVI | NDRE | GNDVI | RVI | CVI | CIRE | TIR |
| SWP | 0.305 | 0.299 | 0.044 | 0.346 | 0.272 | 0.307 | 0.256 | 0.264 | 0.376 | 0.094 | 0.242 | 0.119 |
| Chl_c | 0.602 | 0.584 | 0.014 | 0.698 | 0.411 | 0.772 | 0.818 | 0.691 | 0.786 | 0.180 | 0.811 | 0.782 |
| $A_n$_10 | **0.954** | **0.922** | 0.384 | **0.953** | **0.963** | **0.949** | **0.954** | 0.902 | **0.905** | 0.429 | **0.950** | 0.811 |
| $A_n$_12 | 0.377 | 0.325 | 0.032 | 0.405 | 0.469 | 0.333 | 0.293 | 0.244 | 0.345 | 0.001 | 0.276 | 0.099 |
| $A_n$_14 | 0.373 | 0.320 | 0.033 | 0.400 | 0.464 | 0.328 | 0.289 | 0.240 | 0.341 | 0.001 | 0.272 | 0.096 |
| $g_s$_10 | 0.697 | 0.699 | 0.060 | 0.719 | 0.736 | 0.664 | 0.601 | 0.627 | 0.742 | 0.343 | 0.585 | 0.445 |
| $g_s$_12 | 0.825 | 0.794 | 0.083 | 0.847 | 0.883 | 0.788 | 0.741 | 0.715 | 0.818 | 0.267 | 0.724 | 0.520 |
| $g_s$_14 | 0.828 | 0.802 | 0.089 | 0.849 | 0.881 | 0.792 | 0.742 | 0.725 | 0.830 | 0.296 | 0.725 | 0.531 |
| $Tr_L$_10 | 0.796 | 0.835 | 0.297 | 0.803 | 0.778 | 0.791 | 0.746 | 0.811 | 0.866 | 0.696 | 0.739 | 0.707 |
| $Tr_L$_12 | **0.976** | **0.970** | 0.310 | **0.983** | **0.985** | **0.962** | **0.934** | **0.932** | **0.981** | 0.540 | **0.925** | 0.797 |
| $Tr_L$_14 | 0.880 | 0.879 | 0.180 | 0.896 | **0.905** | 0.856 | 0.807 | 0.821 | **0.907** | 0.467 | 0.794 | 0.653 |

$A_n$_10/ 12/ 14 – Net $CO_2$ assimilation rate measured at 10h00/ 12h00/ 14h00, Chl_c – Chlorophyll concentration, CIRE - Chlorophyll index – Red edge, CVI - Chlorophyll vegetation index, GNDVI -Green Normalized Difference Vegetation Index, $g_s$_10/12/14 – Stomatal conductance measured at 10h00 /12h00 /14h00, NDRE - Normalized Difference Red Edge Index, NIR – Near-infrared, NDVI - Normalized Difference Vegetation Index, RVI - Ratio Vegetation Index, SWP – Stem water potential at 12h00,. TIR – thermal infrared temperature, $Tr_L$_10/ 12/ 14 - Leaf level transpiration at 10h00/ 12h00/ 14h00

Table 32. Comparison of Pearson p-values (p) of simple linear regressions of orchard averaged multispectral drone image derived bands, indices, tree geometric dimensions or thermal infrared temperature with orchard averaged ground measured stem water potential, leaf chlorophyll content and tree physiological variables for the young cultivar 'Wonderful' orchard over the 2023/2024 season at Avontuur. Bold text indicates indices with significant potential to model the measured parameters at a significance level of 5% ($p \leq 0.05$) and bold red italicized text at a significance level of 10% ($0.05 < p \leq 0.1$).

| Tree | Drone image spectral band or index | | | | | | | | | | | |
|---|---|---|---|---|---|---|---|---|---|---|---|---|
| Property | Blue | Green | NIR | Red | RedEdge | NDVI | NDRE | GNDVI | RVI | CVI | CIRE | TIR |
| SWP | 0.334 | 0.340 | 0.734 | 0.297 | 0.367 | 0.332 | 0.385 | 0.376 | 0.271 | 0.616 | 0.400 | 0.570 |
| Chl_c | 0.224 | 0.236 | 0.883 | 0.165 | 0.359 | 0.121 | *0.095* | 0.168 | 0.114 | 0.575 | *0.099* | 0.116 |
| $A_n$_10 | 0.023 | 0.040 | 0.380 | 0.024 | 0.019 | 0.026 | 0.023 | *0.050* | 0.049 | 0.345 | 0.025 | *0.100* |
| $A_n$_12 | 0.386 | 0.430 | 0.822 | 0.364 | 0.315 | 0.423 | 0.458 | 0.506 | 0.412 | 0.971 | 0.474 | 0.685 |
| $A_n$_14 | 0.390 | 0.434 | 0.817 | 0.368 | 0.319 | 0.427 | 0.463 | 0.510 | 0.416 | 0.975 | 0.478 | 0.690 |
| $g_s$_10 | 0.165 | 0.164 | 0.755 | 0.152 | 0.142 | 0.185 | 0.225 | 0.208 | 0.139 | 0.415 | 0.235 | 0.333 |
| $g_s$_12 | *0.092* | 0.109 | 0.712 | *0.080* | *0.060* | 0.112 | 0.139 | 0.155 | *0.096* | 0.484 | 0.149 | 0.279 |
| $g_s$_14 | *0.090* | 0.104 | 0.701 | *0.078* | *0.061* | 0.110 | 0.139 | 0.148 | *0.089* | 0.456 | 0.148 | 0.271 |
| $Tr_L$_10 | 0.108 | *0.086* | 0.455 | 0.104 | 0.118 | 0.111 | 0.136 | *0.099* | *0.069* | 0.166 | 0.140 | 0.159 |
| $Tr_L$_12 | 0.012 | 0.015 | 0.443 | 0.008 | 0.008 | 0.019 | 0.034 | 0.035 | 0.010 | 0.265 | 0.038 | 0.107 |
| $Tr_L$_14 | *0.062* | *0.062* | 0.576 | *0.053* | 0.049 | *0.075* | 0.102 | *0.094* | 0.047 | 0.316 | 0.109 | 0.192 |

$A_n$_10/ 12/ 14 – Net $CO_2$ assimilation rate measured at 10h00/ 12h00/ 14h00, Chl_c – Chlorophyll concentration, CIRE - Chlorophyll index – Red edge, CVI - Chlorophyll vegetation index, GNDVI -Green Normalized Difference Vegetation Index, $g_s$_10/12/14 – Stomatal conductance measured at 10h00 /12h00 /14h00, NDRE - Normalized Difference Red Edge Index, NIR – Near-infrared, NDVI - Normalized Difference Vegetation Index, RVI - Ratio Vegetation Index, SWP – Stem water potential at 12h00,. TIR – thermal infrared temperature, $Tr_L$_10/ 12/ 14 - Leaf level transpiration at 10h00/ 12h00/ 14h00

Table 33. Comparison of coefficients of determination ($R^2$) of simple linear regressions of orchard averaged multispectral drone image derived spectral bands, indices or thermal infrared temperature with orchard averaged measured stem water potential and tree physiological variables for the full bearing cultivar 'Wonderful' pomegranate orchard over the 2023/2024 season at Welgemoed. **Bold black text indicates indices which related significantly to the measured parameters at a significance level of 5% (p≤0.05)**. Increased green colour intensity indicates increasing $R^2$ values.

| Tree Property | Drone image spectral band or index | | | | | | | | | | | |
|---|---|---|---|---|---|---|---|---|---|---|---|---|
| | Blue | Green | NIR | Red | RedEdge | NDVI | NDRE | GNDVI | RVI | CVI | CIRE | TIR |
| SWP | 0.571 | 0.423 | 0.063 | 0.657 | 0.307 | 0.740 | 0.449 | 0.511 | 0.637 | 0.000 | 0.413 | 0.021 |
| Chl_c | 0.003 | 0.005 | **0.922** | 0.000 | 0.097 | 0.046 | 0.000 | 0.027 | 0.073 | 0.491 | 0.000 | 0.610 |
| $A_n$_10 | 0.416 | 0.717 | 0.562 | 0.436 | 0.699 | 0.436 | 0.411 | 0.549 | 0.853 | 0.398 | 0.413 | 0.853 |
| $A_n$_12 | 0.004 | 0.070 | 0.688 | 0.002 | 0.146 | 0.010 | 0.000 | 0.000 | 0.010 | 0.000 | 0.000 | 0.066 |
| $A_n$_14 | 0.482 | 0.850 | 0.959 | 0.586 | 0.509 | 0.863 | 0.646 | 0.882 | **0.997** | 0.572 | 0.651 | 0.938 |
| $g_s$_10 | 0.268 | 0.567 | 0.712 | 0.287 | 0.548 | 0.287 | 0.263 | 0.393 | 0.727 | 0.252 | 0.265 | 0.726 |
| $g_s$_12 | 0.399 | 0.653 | 0.205 | 0.486 | 0.350 | 0.769 | 0.545 | 0.783 | **0.986** | 0.478 | 0.549 | 0.797 |
| $g_s$_14 | 0.058 | 0.365 | 0.555 | 0.116 | 0.071 | 0.383 | 0.158 | 0.410 | 0.795 | 0.107 | 0.161 | 0.927 |
| $Tr_L$_10 | 0.544 | 0.247 | 0.479 | 0.523 | 0.264 | 0.523 | 0.549 | 0.410 | 0.119 | 0.561 | 0.546 | 0.120 |
| $Tr_L$_12 | 0.578 | 0.824 | 0.116 | 0.660 | 0.545 | 0.862 | 0.705 | 0.896 | **0.993** | 0.647 | 0.709 | 0.632 |
| $Tr_L$_14 | 0.203 | 0.588 | 0.766 | 0.293 | 0.225 | 0.606 | 0.351 | 0.633 | 0.941 | 0.280 | 0.355 | **0.998** |

$A_n$_10/ 12/ 14 – Net $CO_2$ assimilation rate measured at 10h00/ 12h00/ 14h00, Chl_c – Chlorophyll concentration, CIRE - Chlorophyll index – Red edge, CVI - Chlorophyll vegetation index, GNDVI -Green Normalized Difference Vegetation Index, $g_s$_10/12/14 – Stomatal conductance measured at 10h00 /12h00 /14h00, NDRE - Normalized Difference Red Edge Index, NIR – Near-infrared, NDVI - Normalized Difference Vegetation Index, RVI - Ratio Vegetation Index, SWP – Stem water potential at 12h00,. TIR – thermal infrared temperature, $Tr_L$_10/ 12/ 14 - Leaf level transpiration at 10h00/ 12h00/ 14h00

Table 34. Comparison of Pearson p-values (p) of simple linear regressions of orchard averaged multispectral drone image derived bands, indices or thermal infrared temperature with orchard averaged ground measured stem water potential, leaf chlorophyll content and tree physiological variables for the full bearing cultivar 'Wonderful' orchard over the 2023/2024 season at Avontuur. Bold text indicates indices with significant potential to model the measured parameters at a significance level of 5% ($p \leq 0.05$) and bold red italicized text at a significance level of 10% ($0.05 < p \leq 0.1$).

| Tree | Drone image spectral band or index | | | | | | | | | | | |
|---|---|---|---|---|---|---|---|---|---|---|---|---|
| Property | Blue | Green | NIR | Red | RedEdge | NDVI | NDRE | GNDVI | RVI | CVI | CIRE | TIR |
| SWP | 0.140 | 0.235 | 0.684 | *0.096* | 0.332 | *0.062* | 0.216 | 0.175 | 0.106 | 0.995 | 0.243 | 0.815 |
| Chl_c | 0.941 | 0.929 | **0.040** | 0.988 | 0.689 | 0.785 | 0.987 | 0.835 | 0.730 | 0.299 | 0.993 | 0.219 |
| $A_n$_10 | 0.554 | 0.357 | 0.461 | 0.541 | 0.370 | 0.541 | 0.557 | 0.469 | 0.250 | 0.565 | 0.556 | 0.251 |
| $A_n$_12 | 0.936 | 0.735 | 0.170 | 0.952 | 0.618 | 0.902 | 0.992 | 0.986 | 0.898 | 0.991 | 0.993 | 0.743 |
| $A_n$_14 | 0.511 | 0.253 | 0.131 | 0.445 | 0.494 | 0.241 | 0.406 | 0.223 | **0.035** | 0.454 | 0.403 | 0.160 |
| $g_s$_10 | 0.654 | 0.457 | 0.361 | 0.640 | 0.469 | 0.640 | 0.657 | 0.569 | 0.350 | 0.665 | 0.655 | 0.351 |
| $g_s$_12 | 0.368 | 0.192 | 0.548 | 0.303 | 0.408 | 0.123 | 0.262 | 0.115 | **0.007** | 0.309 | 0.259 | 0.107 |
| $g_s$_14 | 0.845 | 0.587 | 0.465 | 0.779 | 0.829 | 0.575 | 0.740 | 0.557 | 0.299 | 0.788 | 0.737 | 0.174 |
| $Tr_L$_10 | 0.472 | 0.669 | 0.513 | 0.485 | 0.656 | 0.485 | 0.469 | 0.557 | 0.776 | 0.461 | 0.470 | 0.775 |
| $Tr_L$_12 | 0.240 | *0.092* | 0.659 | 0.187 | 0.261 | *0.072* | 0.160 | *0.053* | **0.004** | 0.196 | 0.158 | 0.205 |
| $Tr_L$_14 | 0.702 | 0.444 | 0.322 | 0.636 | 0.685 | 0.432 | 0.597 | 0.414 | 0.156 | 0.645 | 0.594 | **0.031** |

$A_n$_10/ 12/ 14 – Net $CO_2$ assimilation rate measured at 10h00/ 12h00/ 14h00, Chl_c – Chlorophyll concentration, CIRE - Chlorophyll index – Red edge, CVI - Chlorophyll vegetation index, GNDVI -Green Normalized Difference Vegetation Index, $g_s$_10/12/14 – Stomatal conductance measured at 10h00 /12h00 /14h00, NDRE - Normalized Difference Red Edge Index, NIR – Near-infrared, NDVI - Normalized Difference Vegetation Index, RVI - Ratio Vegetation Index, SWP – Stem water potential at 12h00,. TIR – thermal infrared temperature, $Tr_L$_10/ 12/ 14 - Leaf level transpiration at 10h00/ 12h00/ 14h00

# APPENDIX C: SUMMARY OF COEFFICIENTS OF DETERMINATION OF LINEAR REGRESSIONS OF MEASURED TREE WATER USE PROPERTIES WITH DRONE IMAGE DERIVED VARIABLES

Table 35. Comparison of coefficients of determination ($R^2$) of simple linear regressions between multispectral drone image derived spectral bands or indices and measured tree water use, ratios of transpiration (T) or soil water balance-based evapotranspiration (ETc) to reference evapotranspiration (ETo) for selected trees in orchards combined over the 2023/2024 season. Increased colour intensity indicates increasing $R^2$ values. Pearson p-values (p) are indicated in the bottom part of the table. Black bold text indicates indices which related significantly to the me**asured parameters at a significance level of 5% and red bold italic text at a significance level of 10% (p≤0.1). SI refers to** statistical indicator.

| Water use indicator | SI | Drone index Blue | Green | NIR | Red | RedEdge | NDVI | NDRE | GNDVI | RVI | CVI | CIRE | Dr_Height | Dr_Volume | TIR |
|---|---|---|---|---|---|---|---|---|---|---|---|---|---|---|---|
| Transpiration | $R^2$ | 0.355 | 0.288 | 0.139 | 0.379 | 0.339 | 0.367 | 0.281 | 0.222 | 0.457 | 0.069 | 0.264 | 0.466 | 0.298 | 0.175 |
| T:ETo | $R^2$ | 0.024 | 0.003 | 0.084 | 0.027 | 0.024 | 0.022 | 0.000 | 0.002 | 0.121 | 0.239 | 0.000 | 0.367 | 0.249 | 0.015 |
| ETc_Treerow | $R^2$ | 0.752 | 0.778 | 0.807 | 0.801 | 0.909 | 0.318 | 0.101 | 0.006 | 0.112 | 0.846 | 0.051 | 0.505 | 0.274 | 0.354 |
| ETc_Workrow | $R^2$ | 0.415 | 0.375 | 0.073 | 0.300 | 0.227 | 0.518 | 0.499 | 0.344 | 0.250 | 0.080 | 0.383 | 0.338 | 0.900 | 0.003 |
| ETc_Orchard | $R^2$ | 0.571 | 0.608 | 0.785 | 0.659 | 0.794 | 0.172 | 0.024 | 0.055 | 0.054 | 0.824 | 0.007 | 0.368 | 0.090 | 0.380 |
| ETc:ETo_Treerow | $R^2$ | 0.583 | 0.614 | 0.423 | 0.562 | 0.579 | 0.323 | 0.133 | 0.017 | 0.214 | 0.490 | 0.064 | 0.416 | 0.420 | 0.057 |
| ETc:ETo_Workrow | $R^2$ | 0.505 | 0.455 | 0.167 | 0.399 | 0.351 | 0.521 | 0.498 | 0.227 | 0.189 | 0.165 | 0.393 | 0.371 | 0.814 | 0.069 |
| ETc:ETo_Orchard | $R^2$ | 0.364 | 0.408 | 0.363 | 0.384 | 0.427 | 0.135 | 0.020 | 0.003 | 0.113 | 0.425 | 0.002 | 0.254 | 0.158 | 0.043 |
| Transpiration | p | 0.000 | 0.001 | 0.027 | <0.0001 | 0.000 | 0.000 | 0.001 | 0.004 | <0.0001 | 0.129 | 0.002 | <0.0001 | 0.001 | 0.012 |
| T:ETo | p | 0.377 | 0.771 | *0.091* | 0.342 | 0.371 | 0.395 | 0.937 | 0.792 | 0.041 | 0.003 | 0.963 | 0.000 | 0.002 | 0.478 |
| ETc_Treerow | p | 0.012 | 0.009 | 0.006 | 0.007 | 0.001 | 0.187 | 0.487 | 0.869 | 0.463 | 0.003 | 0.627 | *0.073* | 0.228 | 0.159 |
| ETc_Workrow | p | 0.118 | 0.144 | 0.557 | 0.203 | 0.280 | *0.068* | *0.076* | 0.166 | 0.254 | 0.538 | 0.138 | 0.171 | 0.001 | 0.900 |
| ETc_Orchard | p | 0.049 | 0.039 | 0.008 | 0.027 | 0.007 | 0.354 | 0.740 | 0.614 | 0.616 | 0.005 | 0.863 | 0.148 | 0.512 | 0.140 |
| ETc:ETo_Treerow | p | 0.046 | 0.037 | 0.114 | *0.052* | 0.047 | 0.183 | 0.421 | 0.780 | 0.296 | *0.080* | 0.585 | 0.118 | 0.115 | 0.607 |
| ETc:ETo_Workrow | p | *0.073* | *0.096* | 0.363 | 0.128 | 0.161 | *0.067* | *0.076* | 0.280 | 0.330 | 0.365 | 0.132 | 0.147 | 0.005 | 0.570 |
| ETc:ETo_Orchard | p | 0.152 | 0.122 | 0.152 | 0.138 | 0.111 | 0.417 | 0.761 | 0.914 | 0.462 | 0.112 | 0.926 | 0.249 | 0.378 | 0.654 |

NIR – Near-infrared, NDVI - Normalized Difference Vegetation Index, NDRE - Normalized Difference Red Edge Index, GNDVI -Green Normalized Difference Vegetation Index, RVI - Ratio Vegetation Index, CVI - Chlorophyll vegetation index, CIRE - Chlorophyll index – Red edge, Dr_Height – drone image estimated tree height, Dr_Volume – drone image estimated tree volume, TIR – thermal infrared temperature.

Table 36. Comparison of coefficients of determination ($R^2$) of simple linear regressions between multispectral drone image derived spectral bands or indices and measured or calculated tree water use indicators for selected trees per orchard over the 2023/2024 season for the young (Y) and full bearing (FB) cultivar 'Wonderful' pomegranate orchards. Bold text indicates **indices which related significantly to the measured parameters at a significance level of 5% (p≤0.05). Increased colour intens**ity indicates increasing $R^2$ values. Transpiration was determined using sap flow and evapotranspiration derived from a soil water balance.

| Site | Water use indicator | Drone index Blue | Green | NIR | Red | RedEdge | NDVI | NDRE | GNDVI | RVI | CVI | CIRE | Dr_Height | Dr_Volume | TIR |
|---|---|---|---|---|---|---|---|---|---|---|---|---|---|---|---|
| Y | Transpiration | 0.261 | 0.282 | 0.182 | 0.272 | 0.327 | 0.208 | 0.203 | 0.206 | 0.232 | 0.082 | 0.195 | 0.355 | 0.280 | 0.206 |
| FB | Transpiration | 0.136 | 0.220 | 0.097 | 0.158 | 0.186 | 0.192 | 0.190 | 0.244 | 0.176 | 0.051 | 0.167 | 0.000 | 0.000 | 0.001 |
| Y | Transpiration : ETo[3] | 0.035 | 0.032 | 0.109 | 0.040 | 0.003 | 0.094 | 0.116 | 0.091 | 0.068 | 0.023 | 0.116 | 0.093 | 0.053 | 0.137 |
| FB | Transpiration : ETo | 0.029 | 0.036 | 0.013 | 0.045 | 0.023 | 0.074 | 0.030 | 0.053 | 0.040 | 0.001 | 0.019 | 0.001 | 0.035 | 0.003 |
| Y | ETc[4]_Treerow | 1.000 | 1.000 | 1.000 | 1.000 | 1.000 | 1.000 | 1.000 | 1.000 | 1.000 | 1.000 | 1.000 | 1.000 | 1.000 | 1.000 |
| FB | ETc_Treerow | 0.064 | 0.067 | 0.203 | 0.091 | 0.666 | 0.012 | 0.034 | 0.045 | 0.049 | 0.335 | 0.027 | 0.128 | 0.021 | 0.208 |
| Y | ETc_Workrow | 1.000 | 1.000 | 1.000 | 1.000 | 1.000 | 1.000 | 1.000 | 1.000 | 1.000 | 1.000 | 1.000 | 1.000 | 1.000 | 1.000 |
| FB | ETc_Workrow | 0.688 | 0.742 | 0.084 | 0.669 | 0.188 | 0.471 | 0.479 | 0.409 | 0.152 | 0.272 | 0.388 | 0.565 | 0.903 | 0.034 |
| Y | ETc_Orchard | 1.000 | 1.000 | 1.000 | 1.000 | 1.000 | 1.000 | 1.000 | 1.000 | 1.000 | 1.000 | 1.000 | 1.000 | 1.000 | 1.000 |
| FB | ETc_Orchard | 0.023 | 0.028 | 0.284 | 0.010 | 0.283 | 0.170 | 0.020 | 0.234 | 0.137 | 0.585 | 0.016 | 0.458 | 0.103 | 0.247 |
| Y | ETc : ETo_Treerow | 1.000 | 1.000 | 1.000 | 1.000 | 1.000 | 1.000 | 1.000 | 1.000 | 1.000 | 1.000 | 1.000 | 1.000 | 1.000 | 1.000 |
| FB | ETc : ETo_Treerow | 0.177 | 0.279 | 0.000 | 0.162 | 0.218 | 0.030 | 0.064 | 0.024 | 0.041 | 0.018 | 0.033 | 0.007 | 0.213 | 0.022 |
| Y | ETc : ETo_Workrow | 1.000 | 1.000 | 1.000 | 1.000 | 1.000 | 1.000 | 1.000 | 1.000 | 1.000 | 1.000 | 1.000 | 1.000 | 1.000 | 1.000 |
| FB | ETc : ETo_Workrow | 0.645 | 0.631 | 0.028 | 0.664 | 0.301 | 0.394 | 0.496 | 0.303 | 0.071 | 0.171 | 0.426 | 0.414 | 0.760 | 0.000 |
| Y | ETc : ETo_Orchard | 1.000 | 1.000 | 1.000 | 1.000 | 1.000 | 1.000 | 1.000 | 1.000 | 1.000 | 1.000 | 1.000 | 1.000 | 1.000 | 1.000 |
| FB | ETc : ETo_Orchard | 0.007 | 0.039 | 0.014 | 0.005 | 0.077 | 0.011 | 0.002 | 0.009 | 0.003 | 0.109 | 0.009 | 0.039 | 0.011 | 0.012 |

NIR – Near-infrared, NDVI - Normalized Difference Vegetation Index, NDRE - Normalized Difference Red Edge Index, GNDVI -Green Normalized Difference Vegetation Index, RVI - Ratio Vegetation Index, CVI - Chlorophyll vegetation index, CIRE - Chlorophyll index – Red edge, Dr_Height – drone image estimated tree height, Dr_Volume – drone image estimated tree volume, TIR – thermal infrared temperature. ETc – evapotranspiration, ETo – reference evapotranspiration.

Table 37. Comparison of Pearson p-values (p) of simple linear regressions between multispectral drone image derived spectral bands or indices and measured or calculated tree water use indicators for selected trees per orchard over the 2023/2024 season for the young (Y) and full bearing (FB) cultivar 'Wonderful' pomegranate orchards. Bold text indicates indices which related significantly to the measured parameters at a significance level of 5% (p<0.05) and bold italic text highlighted in blue a significance level of 10% (0.1>p>0.05).

| Site | Water use indicator | Drone index Blue | Green | NIR | Red | RedEdge | NDVI | NDRE | GNDVI | RVI | CVI | CIRE | Dr_Height | Dr_Volume | TIR |
|---|---|---|---|---|---|---|---|---|---|---|---|---|---|---|---|
| Y[1] | Transpiration | 0.021 | 0.016 | *0.061* | 0.018 | 0.008 | 0.043 | 0.046 | 0.044 | 0.032 | 0.222 | *0.051* | 0.006 | 0.017 | 0.044 |
| FB[2] | Transpiration | 0.177 | *0.078* | 0.259 | 0.142 | 0.108 | 0.102 | 0.105 | *0.061* | 0.119 | 0.421 | 0.130 | 0.964 | 0.952 | 0.901 |
| Y | Transpiration:ETo[3] | 0.427 | 0.453 | 0.155 | 0.399 | 0.815 | 0.188 | 0.141 | 0.197 | 0.267 | 0.526 | 0.142 | 0.191 | 0.330 | 0.108 |
| FB | Transpiration:ETo | 0.542 | 0.499 | 0.682 | 0.449 | 0.591 | 0.327 | 0.537 | 0.411 | 0.472 | 0.905 | 0.625 | 0.920 | 0.503 | 0.836 |
| Y | ETc[4]_Treerow | <0.0001 | <0.0001 | <0.0001 | <0.0001 | <0.0001 | <0.0001 | <0.0001 | <0.0001 | <0.0001 | <0.0001 | <0.0001 | <0.0001 | <0.0001 | <0.0001 |
| FB | ETc_Treerow | 0.681 | 0.674 | 0.446 | 0.621 | *0.092* | 0.859 | 0.765 | 0.731 | 0.721 | 0.306 | 0.790 | 0.554 | 0.818 | 0.440 |
| Y | ETc_Workrow | <0.0001 | <0.0001 | <0.0001 | <0.0001 | <0.0001 | <0.0001 | <0.0001 | <0.0001 | <0.0001 | <0.0001 | <0.0001 | 1.000 | <0.0001 | <0.0001 |
| FB | ETc_Workrow | *0.082* | *0.061* | 0.635 | *0.091* | 0.465 | 0.201 | 0.195 | 0.246 | 0.517 | 0.368 | 0.262 | 0.143 | 0.013 | 0.766 |
| Y | ETc_Orchard | <0.0001 | <0.0001 | <0.0001 | <0.0001 | <0.0001 | <0.0001 | <0.0001 | <0.0001 | <0.0001 | <0.0001 | <0.0001 | <0.0001 | <0.0001 | <0.0001 |
| FB | ETc_Orchard | 0.806 | 0.787 | 0.356 | 0.870 | 0.356 | 0.491 | 0.819 | 0.409 | 0.540 | 0.132 | 0.841 | 0.209 | 0.598 | 0.394 |
| Y | ETc:ETo_Treerow | <0.0001 | <0.0001 | <0.0001 | <0.0001 | <0.0001 | <0.0001 | <0.0001 | <0.0001 | <0.0001 | <0.0001 | 1.000 | <0.0001 | 1.000 | <0.0001 |
| FB | ETc:ETo_Treerow | 0.481 | 0.360 | 0.988 | 0.501 | 0.428 | 0.782 | 0.681 | 0.803 | 0.744 | 0.828 | 0.770 | 0.893 | 0.435 | 0.812 |
| Y | ETc:ETo_Workrow | <0.0001 | <0.0001 | <0.0001 | <0.0001 | <0.0001 | <0.0001 | <0.0001 | <0.0001 | 1.000 | <0.0001 | <0.0001 | <0.0001 | <0.0001 | <0.0001 |
| FB | ETc:ETo_Workrow | 0.102 | 0.108 | 0.788 | *0.093* | 0.338 | 0.257 | 0.184 | 0.336 | 0.664 | 0.489 | 0.232 | 0.241 | *0.054* | 0.984 |
| Y | ETc:ETo_Orchard | <0.0001 | 1.000 | <0.0001 | <0.0001 | <0.0001 | <0.0001 | <0.0001 | <0.0001 | <0.0001 | <0.0001 | <0.0001 | <0.0001 | 1.000 | 1.000 |
| FB | ETc:ETo_Orchard | 0.891 | 0.752 | 0.850 | 0.914 | 0.652 | 0.866 | 0.943 | 0.878 | 0.932 | 0.587 | 0.878 | 0.752 | 0.866 | 0.861 |

NIR – Near-infrared, NDVI - Normalized Difference Vegetation Index, NDRE - Normalized Difference Red Edge Index, GNDVI -Green Normalized Difference Vegetation Index, RVI - Ratio Vegetation Index, CVI - Chlorophyll vegetation index, CIRE - Chlorophyll index – Red edge, Dr_Height – drone image estimated tree height, Dr_Volume – drone image estimated tree volume, TIR – thermal infrared temperature. ETc – evapotranspiration, ETo – reference evapotranspiration.

Table 38. Comparison of coefficients of determination ($R^2$) of simple linear regressions between multispectral drone image derived bands or indices and sap flow derived transpiration and the ratio thereof to reference evapotranspiration (ETo), respectively, for five surveys conducted over the 2023/2024 season for selected trees in the young (Y, green gradient colour) and full bearing (FB, red gradient colour) cultivar 'Wonderful' pomegranate orchards at Avontuur and Welgemoed, respectively. Bold text indicates indices with significant potential to model the measured parameters at a significance level of 5% ($p \leq 0.05$). Increased colour intensity indicates increasing $R^2$ values.

| Site | Survey | Tree | Drone image spectral band or index | | | | | | | | | | | | | |
|---|---|---|---|---|---|---|---|---|---|---|---|---|---|---|---|---|
| | | Property | Blue | Green | NIR | Red | RedEdge | NDVI | NDRE | GNDVI | RVI | CVI | CIRE | Dr_Height | Dr_Volume | TIR |
| Y | 1 | Transpiration | 0.290 | 0.596 | 0.185 | 0.574 | 0.462 | 0.167 | 0.125 | 0.013 | 0.254 | 0.162 | 0.104 | 0.107 | 0.391 | 0.179 |
| Y | 2 | Transpiration | 0.090 | 0.163 | 0.733 | 0.126 | 0.298 | 0.013 | 0.013 | 0.001 | 0.024 | 0.197 | 0.007 | 0.620 | 0.620 | 0.218 |
| Y | 3 | Transpiration | 0.456 | 0.034 | 0.412 | 0.274 | 0.029 | 0.397 | 0.491 | 0.482 | 0.016 | 0.587 | 0.460 | 0.419 | 0.419 | 0.199 |
| Y | 4 | Transpiration | 0.580 | 0.155 | 0.897 | 0.240 | 0.835 | 0.726 | 0.046 | 0.615 | 0.196 | 0.001 | 0.002 | 0.003 | 0.101 | 0.851 |
| Y | 5 | Transpiration | 0.446 | 0.184 | 0.437 | 0.440 | 0.337 | 0.468 | 0.562 | 0.221 | 0.394 | 0.046 | 0.541 | 0.497 | 0.497 | 0.611 |
| FB | 1 | Transpiration | 0.073 | 0.001 | 0.394 | 0.001 | 0.001 | 0.060 | 0.340 | 0.804 | 0.120 | 0.044 | 0.483 | 0.736 | 0.769 | 0.076 |
| FB | 2 | Transpiration | 0.044 | 0.007 | 0.050 | 0.251 | 0.001 | 0.316 | 0.506 | 0.158 | 0.740 | 0.104 | 0.610 | 0.565 | 0.565 | 0.089 |
| FB | 3 | Transpiration | 0.003 | 0.000 | 0.118 | 0.006 | 0.006 | 0.005 | 0.002 | 0.005 | 0.009 | 0.116 | 0.000 | 0.154 | 0.154 | 0.852 |
| FB | 4 | Transpiration | 0.477 | 0.811 | 0.939 | 0.186 | 0.936 | 0.019 | 0.110 | 0.085 | 0.130 | 0.894 | 0.097 | 0.328 | 0.418 | 0.736 |
| FB | 5 | Transpiration | - | - | - | - | - | - | - | - | - | - | - | - | - | - |
| Y | 1 | Transpiration:ETo | 0.290 | 0.596 | 0.185 | 0.574 | 0.462 | 0.167 | 0.125 | 0.013 | 0.254 | 0.162 | 0.104 | 0.107 | 0.391 | 0.179 |
| Y | 2 | Transpiration:ETo | 0.090 | 0.163 | 0.733 | 0.126 | 0.298 | 0.013 | 0.013 | 0.001 | 0.024 | 0.197 | 0.007 | 0.620 | 0.620 | 0.218 |
| Y | 3 | Transpiration:ETo | 0.456 | 0.034 | 0.412 | 0.274 | 0.029 | 0.397 | 0.491 | 0.482 | 0.016 | 0.587 | 0.460 | 0.419 | 0.419 | 0.199 |
| Y | 4 | Transpiration:ETo | 0.580 | 0.155 | 0.897 | 0.240 | 0.835 | 0.726 | 0.046 | 0.615 | 0.196 | 0.001 | 0.002 | 0.003 | 0.101 | 0.851 |
| Y | 5 | Transpiration:ETo | 0.446 | 0.184 | 0.437 | 0.440 | 0.337 | 0.468 | 0.562 | 0.221 | 0.394 | 0.046 | 0.541 | 0.497 | 0.497 | 0.611 |
| FB | 1 | Transpiration:ETo | 0.073 | 0.001 | 0.394 | 0.001 | 0.001 | 0.060 | 0.340 | 0.804 | 0.120 | 0.044 | 0.483 | 0.736 | 0.769 | 0.076 |
| FB | 2 | Transpiration:ETo | 0.044 | 0.007 | 0.050 | 0.251 | 0.001 | 0.316 | 0.506 | 0.158 | 0.740 | 0.104 | 0.610 | 0.565 | 0.565 | 0.089 |
| FB | 3 | Transpiration:ETo | 0.003 | 0.000 | 0.118 | 0.006 | 0.006 | 0.005 | 0.002 | 0.005 | 0.009 | 0.116 | 0.000 | 0.154 | 0.154 | 0.852 |
| FB | 4 | Transpiration:ETo | 0.477 | 0.811 | 0.939 | 0.186 | 0.936 | 0.019 | 0.110 | 0.085 | 0.130 | 0.894 | 0.097 | 0.328 | 0.418 | 0.736 |
| FB | 5 | Transpiration:ETo | - | - | - | - | - | - | - | - | - | - | - | - | - | - |

NIR – Near-infrared, NDVI - Normalized Difference Vegetation Index, NDRE - Normalized Difference Red Edge Index, GNDVI -Green Normalized Difference Vegetation Index, RVI - Ratio Vegetation Index, CVI - Chlorophyll vegetation index, CIRE - Chlorophyll index – Red edge, Dr_Height – drone image estimated tree height, Dr_Volume – drone image estimated tree volume, TIR – thermal infrared temperature. ETc – evapotranspiration, ETo – reference evapotranspiration.

Table 39. Comparison of Pearson p-values (p) of simple linear regressions between multispectral drone image derived bands or indices and actual tree canopy area-based leaf area index (LAI) and actual orchard leaf area index (OLAI), respectively, for five surveys conducted over the 2023/2024 season for selected trees in the young (Y) and full bearing (FB) pomegranate orchards at Avontuur and Welgemoed, respectively. Bold text indicates indices with significant potential to model the measured parameters at a significance level of 5% ($p \leq 0.05$) and bold red italicized text at a significance level of 10% ($0.05 < p \leq 0.1$).

| Site | Survey | Tree | Drone image spectral band or index | | | | | | | | | | | | | |
|---|---|---|---|---|---|---|---|---|---|---|---|---|---|---|---|---|
| | | Property | Blue | Green | NIR | Red | RedEdge | NDVI | NDRE | GNDVI | RVI | CVI | CIRE | Dr_Height | Dr_Volume | TIR |
| Y | 1 | Transpiration | 0.462 | 0.228 | 0.570 | 0.242 | 0.321 | 0.591 | 0.647 | 0.885 | 0.496 | 0.597 | 0.678 | 0.673 | 0.375 | 0.577 |
| Y | 2 | Transpiration | 0.700 | 0.597 | 0.144 | 0.645 | 0.455 | 0.887 | 0.886 | 0.967 | 0.844 | 0.556 | 0.916 | 0.213 | 0.213 | 0.533 |
| Y | 3 | Transpiration | 0.325 | 0.815 | 0.358 | 0.477 | 0.831 | 0.370 | 0.299 | 0.306 | 0.872 | 0.234 | 0.322 | 0.353 | 0.353 | 0.554 |
| Y | 4 | Transpiration | 0.239 | 0.607 | *0.053* | 0.510 | *0.086* | 0.148 | 0.785 | 0.216 | 0.557 | 0.974 | 0.955 | 0.947 | 0.682 | *0.077* |
| Y | 5 | Transpiration | 0.332 | 0.571 | 0.339 | 0.337 | 0.419 | 0.316 | 0.250 | 0.530 | 0.372 | 0.785 | 0.264 | 0.295 | 0.295 | 0.218 |
| FB | 1 | Transpiration | 0.731 | 0.964 | 0.372 | 0.962 | 0.974 | 0.755 | 0.417 | 0.103 | 0.653 | 0.790 | 0.305 | 0.142 | 0.123 | 0.725 |
| FB | 2 | Transpiration | 0.791 | 0.915 | 0.777 | 0.499 | 0.969 | 0.438 | 0.289 | 0.603 | 0.140 | 0.677 | 0.219 | 0.248 | 0.248 | 0.701 |
| FB | 3 | Transpiration | 0.964 | 0.987 | 0.777 | 0.952 | 0.951 | 0.954 | 0.975 | 0.956 | 0.940 | 0.779 | 0.986 | 0.744 | 0.744 | 0.251 |
| FB | 4 | Transpiration | 0.309 | *0.099* | 0.031 | 0.569 | 0.033 | 0.862 | 0.669 | 0.708 | 0.639 | *0.054* | 0.688 | 0.427 | 0.353 | 0.142 |
| FB | 5 | Transpiration | - | - | - | - | - | - | - | - | - | - | - | - | - | - |
| Y | 1 | Transpiration:ETo | 0.462 | 0.228 | 0.570 | 0.242 | 0.321 | 0.591 | 0.647 | 0.885 | 0.496 | 0.597 | 0.678 | 0.673 | 0.375 | 0.577 |
| Y | 2 | Transpiration:ETo | 0.700 | 0.597 | 0.144 | 0.645 | 0.455 | 0.887 | 0.886 | 0.967 | 0.844 | 0.556 | 0.916 | 0.213 | 0.213 | 0.533 |
| Y | 3 | Transpiration:ETo | 0.325 | 0.815 | 0.358 | 0.477 | 0.831 | 0.370 | 0.299 | 0.306 | 0.872 | 0.234 | 0.322 | 0.353 | 0.353 | 0.554 |
| Y | 4 | Transpiration:ETo | 0.239 | 0.607 | *0.053* | 0.510 | *0.086* | 0.148 | 0.785 | 0.216 | 0.557 | 0.974 | 0.955 | 0.947 | 0.682 | *0.077* |
| Y | 5 | Transpiration:ETo | 0.332 | 0.571 | 0.339 | 0.337 | 0.419 | 0.316 | 0.250 | 0.530 | 0.372 | 0.785 | 0.264 | 0.295 | 0.295 | 0.218 |
| FB | 1 | Transpiration:ETo | 0.731 | 0.964 | 0.372 | 0.962 | 0.974 | 0.755 | 0.417 | 0.103 | 0.653 | 0.790 | 0.305 | 0.142 | 0.123 | 0.725 |
| FB | 2 | Transpiration:ETo | 0.791 | 0.915 | 0.777 | 0.499 | 0.969 | 0.438 | 0.289 | 0.603 | 0.140 | 0.677 | 0.219 | 0.248 | 0.248 | 0.701 |
| FB | 3 | Transpiration:ETo | 0.964 | 0.987 | 0.777 | 0.952 | 0.951 | 0.954 | 0.975 | 0.956 | 0.940 | 0.779 | 0.986 | 0.744 | 0.744 | 0.251 |
| FB | 4 | Transpiration:ETo | 0.309 | *0.099* | 0.031 | 0.569 | 0.033 | 0.862 | 0.669 | 0.708 | 0.639 | *0.054* | 0.688 | 0.427 | 0.353 | 0.142 |
| FB | 5 | Transpiration:ETo | - | - | - | - | - | - | - | - | - | - | - | - | - | - |

NIR – Near-infrared, NDVI - Normalized Difference Vegetation Index, NDRE - Normalized Difference Red Edge Index, GNDVI -Green Normalized Difference Vegetation Index, RVI - Ratio Vegetation Index, CVI - Chlorophyll vegetation index, CIRE - Chlorophyll index – Red edge, Dr_Height – drone image estimated tree height, Dr_Volume – drone image estimated tree volume, TIR – thermal infrared temperature. ETc – evapotranspiration, ETo – reference evapotranspiration.

Table 40. Comparison of coefficients of determination ($R^2$) of simple linear regressions between orchard averaged multispectral drone image derived spectral bands or indices and orchard level upscaled transpiration, measured orchard evapotranspiration, reference evapotranspiration and the ratios of transpiration and ETc to ETo for orchards combined over the 2023/2024 season. Increased green colour intensity indicates increasing $R^2$ values. Pearson p-values (p) are indicated in the bottom part of the table. Bold black text indicates indices **which related significantly to the measured parameters at a significance level of 5% ($p \leq 0.05$) and bold red italicized text at a significance level of 10% ($0.05 < p \leq 0.1$). SI refers to statistical** indicator. Transpiration was determined using sap flow and orchard evapotranspiration by surface renewal (young orchard) and Eddy covariance (full bearing orchard) techniques.

| Water use | SI | Drone image spectral band or index | | | | | | | | | | | | | |
|---|---|---|---|---|---|---|---|---|---|---|---|---|---|---|---|
| Property | | Blue | Green | NIR | Red | RedEdge | NDVI | NDRE | GNDVI | RVI | CVI | CIRE | Dr_Height | Dr_Volume | TIR |
| T_Orchard level | $R^2$ | 0.714 | 0.587 | 0.196 | 0.690 | 0.651 | 0.714 | 0.584 | 0.517 | 0.916 | 0.020 | 0.585 | 0.704 | 0.498 | 0.259 |
| ETc_Orchard level | $R^2$ | 0.104 | 0.076 | 0.068 | 0.154 | 0.029 | 0.227 | 0.144 | 0.100 | 0.422 | 0.194 | 0.127 | 0.337 | 0.064 | 0.315 |
| ETo | $R^2$ | 0.307 | 0.435 | 0.019 | 0.291 | 0.265 | 0.373 | 0.561 | 0.617 | 0.313 | 0.284 | 0.589 | 0.005 | 0.019 | 0.673 |
| T_Orchard level : ETo | $R^2$ | 0.025 | 0.000 | 0.190 | 0.020 | 0.029 | 0.018 | 0.002 | 0.008 | 0.197 | 0.381 | 0.001 | 0.411 | 0.446 | 0.078 |
| ETc_Orchard level : ETo | $R^2$ | 0.040 | 0.011 | 0.028 | 0.078 | 0.003 | 0.109 | 0.026 | 0.006 | 0.247 | 0.470 | 0.014 | 0.436 | 0.033 | 0.087 |
| T_Orchard level | p | 0.008 | 0.027 | 0.272 | 0.011 | 0.016 | 0.008 | 0.027 | 0.044 | 0.000 | 0.737 | 0.027 | 0.009 | *0.050* | 0.197 |
| ETc_Orchard level | p | 0.435 | 0.508 | 0.532 | 0.336 | 0.687 | 0.232 | 0.355 | 0.445 | *0.081* | 0.275 | 0.386 | 0.131 | 0.544 | 0.147 |
| ETo | p | *0.097* | 0.038 | 0.707 | 0.108 | 0.128 | *0.061* | 0.013 | 0.007 | *0.093* | 0.112 | 0.010 | 0.851 | 0.701 | 0.004 |
| T_Orchard level : ETo | p | 0.710 | 0.960 | 0.281 | 0.741 | 0.688 | 0.752 | 0.924 | 0.828 | 0.270 | 0.103 | 0.936 | *0.087* | *0.071* | 0.503 |
| ETc_Orchard level : ETo | p | 0.633 | 0.809 | 0.695 | 0.503 | 0.892 | 0.425 | 0.702 | 0.852 | 0.211 | *0.061* | 0.777 | *0.075* | 0.668 | 0.477 |

NIR – Near-infrared, NDVI - Normalized Difference Vegetation Index, NDRE - Normalized Difference Red Edge Index, GNDVI -Green Normalized Difference Vegetation Index, RVI - Ratio Vegetation Index, CVI - Chlorophyll vegetation index, CIRE - Chlorophyll index – Red edge, Dr_Height – drone image estimated tree height, Dr_Volume – drone image estimated tree volume, TIR – thermal infrared temperature. T – transpiration, ETc – evapotranspiration, ETo – reference evapotranspiration.

Table 41. Comparison of coefficients of determination ($R^2$) of simple linear regressions between orchard averaged multispectral drone image derived spectral bands or indices and averaged measured or calculated tree water use indicators per orchard over the 2023/2024 season. Increased green colour intensity indicates increasing $R^2$ values. Pearson p-values (p) are indicated in the bottom part of the table. Bold black text indicates indices which related significantly to the measured parameters at a significance level **of 5% (p≤0.05)** and bold red ***italicized text at a significance level of 10% (0.05<p≤0.1). SI refers to statistical indicator. Transpiration was determined*** using sap flow and orchard evapotranspiration by surface renewal (young orchard) and Eddy covariance (full bearing orchard) techniques.

| Site | SI | Water use | Drone | index | | | | | | | | | | | |
|---|---|---|---|---|---|---|---|---|---|---|---|---|---|---|---|
| | | Indicator | Blue | Green | NIR | Red | RedEdge | NDVI | NDRE | GNDVI | RVI | CVI | CIRE | Dr_Height | Dr_Volume | TIR |
| Y[1] | $R^2$ | T_Orchard level | 0.936 | 0.942 | 0.338 | 0.880 | 0.963 | 0.811 | 0.750 | 0.854 | 0.780 | 0.876 | 0.752 | 0.908 | 0.587 | 0.574 |
| FB[2] | $R^2$ | T_Orchard level | 0.881 | 0.780 | 0.979 | 0.940 | 0.775 | 0.942 | 0.660 | 0.723 | 0.943 | 0.013 | 0.611 | 0.000 | 0.008 | 0.347 |
| Y | $R^2$ | ETc_Orchard level | 0.041 | 0.046 | 0.620 | 0.082 | 0.001 | 0.175 | 0.250 | 0.157 | 0.185 | 0.001 | 0.254 | 0.008 | 0.084 | 0.463 |
| FB | $R^2$ | ETc_Orchard level | 0.002 | 0.073 | 0.800 | 0.001 | 0.001 | 0.053 | 0.009 | 0.121 | 0.255 | 0.014 | 0.012 | 0.025 | 0.001 | 0.999 |
| Y | $R^2$ | ETo | 0.740 | 0.734 | 0.000 | 0.786 | 0.543 | 0.872 | 0.928 | 0.856 | 0.825 | 0.446 | 0.934 | 0.675 | 0.241 | 0.925 |
| FB | $R^2$ | ETo | 0.266 | 0.399 | 0.346 | 0.304 | 0.187 | 0.506 | 0.391 | 0.572 | 0.673 | 0.159 | 0.395 | 0.471 | 0.077 | 0.718 |
| Y | $R^2$ | T_Orchard level : ETo | 0.193 | 0.186 | 0.325 | 0.262 | 0.054 | 0.384 | 0.484 | 0.337 | 0.361 | 0.024 | 0.487 | 0.153 | 0.003 | 0.620 |
| FB | $R^2$ | T_Orchard level : ETo | 0.411 | 0.281 | 0.864 | 0.515 | 0.276 | 0.519 | 0.170 | 0.224 | 0.521 | 0.159 | 0.133 | 0.233 | 0.329 | 0.836 |
| Y | $R^2$ | ETc_Orchard level : ETo | 0.037 | 0.032 | 0.902 | 0.011 | 0.174 | 0.001 | 0.013 | 0.000 | 0.004 | 0.090 | 0.013 | 0.101 | 0.362 | 0.109 |
| FB | $R^2$ | ETc_Orchard level : ETo | 0.194 | 0.020 | 0.405 | 0.143 | 0.185 | 0.034 | 0.098 | 0.004 | 0.013 | 0.085 | 0.092 | 0.064 | 0.143 | 0.810 |
| Y | p | T_Orchard level | 0.007 | 0.006 | 0.304 | 0.018 | 0.003 | 0.037 | *0.058* | 0.025 | 0.047 | 0.019 | *0.057* | 0.012 | 0.131 | 0.138 |
| FB | p | T_Orchard level | 0.224 | 0.311 | *0.093* | 0.157 | 0.314 | 0.154 | 0.396 | 0.353 | 0.153 | 0.927 | 0.429 | 0.987 | 0.944 | 0.599 |
| Y | p | ETc_Orchard level | 0.743 | 0.730 | 0.114 | 0.640 | 0.959 | 0.483 | 0.391 | 0.509 | 0.470 | 0.955 | 0.387 | 0.889 | 0.637 | 0.206 |
| FB | p | ETc_Orchard level | 0.975 | 0.826 | 0.296 | 0.982 | 0.982 | 0.852 | 0.938 | 0.774 | 0.663 | 0.924 | 0.931 | 0.898 | 0.982 | 0.022 |
| Y | p | ETo | *0.062* | *0.064* | 0.983 | 0.045 | 0.156 | 0.020 | 0.008 | 0.024 | 0.033 | 0.218 | 0.007 | *0.088* | 0.401 | 0.009 |
| FB | p | ETo | 0.374 | 0.253 | 0.297 | 0.336 | 0.468 | 0.178 | 0.259 | 0.139 | *0.089* | 0.506 | 0.256 | 0.201 | 0.652 | *0.070* |
| Y | p | T_Orchard level : ETo | 0.459 | 0.468 | 0.316 | 0.378 | 0.707 | 0.265 | 0.192 | 0.305 | 0.284 | 0.804 | 0.190 | 0.516 | 0.925 | 0.114 |
| FB | p | T_Orchard level : ETo | 0.557 | 0.644 | 0.241 | 0.491 | 0.648 | 0.488 | 0.730 | 0.686 | 0.486 | 0.739 | 0.762 | 0.680 | 0.611 | 0.266 |
| Y | p | ETc_Orchard level : ETo | 0.756 | 0.775 | 0.013 | 0.869 | 0.485 | 0.961 | 0.857 | 0.991 | 0.921 | 0.623 | 0.854 | 0.602 | 0.283 | 0.588 |
| FB | p | ETc_Orchard level : ETo | 0.710 | 0.909 | 0.561 | 0.753 | 0.717 | 0.882 | 0.797 | 0.961 | 0.928 | 0.811 | 0.804 | 0.837 | 0.753 | 0.287 |

NIR – Near-infrared, NDVI - Normalized Difference Vegetation Index, NDRE - Normalized Difference Red Edge Index, GNDVI -Green Normalized Difference Vegetation Index, RVI - Ratio Vegetation Index, CVI - Chlorophyll vegetation index, CIRE - Chlorophyll index – Red edge, Dr_Height – drone image estimated tree height, Dr_Volume – drone image estimated tree volume, TIR – thermal infrared temperature. T – transpiration, ETc – evapotranspiration, ETo – reference evapotranspiration.

# APPENDIX D: SUMMARY OF COEFFICIENTS OF DETERMINATION OF LINEAR REGRESSIONS OF MEASURED TREE WATER USE PROPERTIES WITH IN-FIELD MEASURED TREE PROPERTIES

Table 42. Comparison of coefficients of determination ($R^2$) and Pearson p-values of simple linear regressions between measured or calculated individual tree canopy dimensions, fractional interception, leaf area index and transpiration and the ratio thereof to reference evapotranspiration for cultivar 'Wonderful' pomegranate orchards combined and separately over the 2023/2024 season. Bold black text indicates indices which related significantly to the measured parameters at a significa**nce level of 5% (p≤0.05)** and bold red italicized text at a **significance level of 10% (0.05<p≤0.1). Increased green colour intensity indicates increasing $R^2$** values.

| Level | Tree property | SI | Tree height | Across row width | In row width | Tree volume | Fractional interception | Ceptometer LAI | Tree canopy _LAI | Orchard LAI | Tree level transpiration | T:ETo |
|---|---|---|---|---|---|---|---|---|---|---|---|---|
| Orchards combined | Transpiration | $R^2$ | 0.421 | 0.463 | 0.151 | 0.242 | 0.431 | 0.438 | 0.102 | 0.083 | 1 | 0.654 |
| | Transpiration:ETo | $R^2$ | 0.588 | 0.524 | 0.143 | 0.220 | 0.560 | 0.503 | 0.068 | 0.136 | 0.654 | 1 |
| | Transpiration | p | <0.0001 | <0.0001 | 0.021 | 0.003 | <0.0001 | <0.0001 | *0.061* | *0.094* | 0 | <0.0001 |
| | Transpiration:ETo | p | <0.0001 | <0.0001 | 0.025 | 0.004 | <0.0001 | <0.0001 | 0.131 | 0.029 | <0.0001 | 0 |
| Y | Transpiration | $R^2$ | 0.230 | 0.397 | 0.354 | 0.538 | 0.238 | 0.390 | 0.378 | 0.389 | 1 | 0.380 |
| FB | Transpiration | $R^2$ | 0.005 | 0.090 | - | 0.003 | 0.013 | 0.055 | 0.055 | 0.055 | 1 | 0.885 |
| Y | Transpiration:ETo | $R^2$ | 0.673 | 0.455 | 0.361 | 0.422 | 0.559 | 0.520 | 0.528 | 0.522 | 0.380 | 1 |
| FB | Transpiration:ETo | $R^2$ | 0.005 | 0.178 | - | 0.042 | 0.001 | 0.023 | 0.023 | 0.023 | 0.885 | 1 |
| Y | Transpiration | p | 0.032 | 0.003 | 0.006 | 0.000 | 0.029 | 0.003 | 0.004 | 0.003 | 0 | 0.004 |
| FB | Transpiration | p | 0.794 | 0.278 | - | 0.838 | 0.688 | 0.401 | 0.401 | 0.401 | 0 | <0.0001 |
| Y | Transpiration:ETo | p | <0.0001 | 0.001 | 0.005 | 0.002 | 0.000 | 0.000 | 0.000 | 0.000 | 0.004 | 0 |
| FB | Transpiration:ETo | p | 0.800 | 0.117 | - | 0.466 | 0.895 | 0.592 | 0.592 | 0.592 | <0.0001 | 0 |

SI - Statistical indicator, LAI – Leaf area index, T – Transpiration, ETo – reference evapotranspiration.

Table 43. Comparison of coefficients of determination ($R^2$) of simple linear regressions between individual tree sap flow derived transpiration and the transpiration to reference evapotranspiration (ETo) ratio, respectively, with measured or calculated individual tree canopy dimensions, fractional interception and leaf area indices, respectively. Data were collected for the young (Y, green gradient colour) and full bearing (FB, red gradient colour) cultivar 'Wonderful' pomegranate orchards at Avontuur and Welgemoed, respectively, on days that drone surveys were conducted over the 2023/2024 season. Bold text indicates indices with significant potential to model the measured parameters at a significance level of 5% ($p \leq 0.05$). Increased colour intensity indicates increasing $R^2$ values.

| Site | Survey | Tree Property | Tree height | Across row Width | In row width | Tree volume | Fractional interception | Ceptometer LAI | Tree canopy _LAI | Orchard LAI |
|---|---|---|---|---|---|---|---|---|---|---|
| Y | 1 | Transpiration | 0.618 | 0.746 | 0.744 | 0.822 | 0.619 | 0.447 | 0.438 | 0.447 |
| Y | 2 | Transpiration | **0.993** | 0.824 | 0.551 | **0.910** | **0.957** | **0.974** | **0.943** | **0.971** |
| Y | 3 | Transpiration | 0.865 | 0.878 | 0.848 | **0.983** | **0.986** | **0.930** | **0.947** | **0.933** |
| Y | 4 | Transpiration | 0.868 | 0.533 | 0.729 | 0.783 | **0.913** | **0.961** | **0.968** | **0.962** |
| Y | 5 | Transpiration | 0.356 | 0.426 | 0.540 | 0.598 | 0.170 | 0.084 | 0.083 | 0.084 |
| FB | 1 | Transpiration | 0.302 | **0.931** | - | <0.0001 | **0.941** | 0.002 | 0.002 | 0.002 |
| FB | 2 | Transpiration | 0.047 | 0.710 | - | 0.387 | 0.072 | 0.121 | 0.121 | 0.121 |
| FB | 3 | Transpiration | 0.048 | **0.996** | - | 0.185 | 0.272 | 0.002 | 0.002 | 0.002 |
| FB | 4 | Transpiration | 0.794 | 0.069 | - | 0.272 | 0.211 | 0.065 | 0.065 | 0.065 |
| FB | 5 | Transpiration | - | - | - | - | - | - | - | - |
| Y | 1 | Transpiration:ETo | 0.618 | 0.746 | 0.744 | 0.822 | 0.619 | 0.447 | 0.438 | 0.447 |
| Y | 2 | Transpiration:ETo | **0.993** | 0.824 | 0.551 | **0.910** | **0.957** | **0.974** | **0.943** | **0.971** |
| Y | 3 | Transpiration:ETo | 0.865 | 0.878 | 0.848 | **0.983** | **0.986** | **0.930** | **0.947** | **0.933** |
| Y | 4 | Transpiration:ETo | 0.868 | 0.533 | 0.729 | 0.783 | **0.913** | **0.961** | **0.968** | **0.962** |
| Y | 5 | Transpiration:ETo | 0.356 | 0.426 | 0.540 | 0.598 | 0.170 | 0.084 | 0.083 | 0.084 |
| FB | 1 | Transpiration:ETo | 0.302 | **0.931** | - | <0.0001 | **0.941** | 0.002 | 0.002 | 0.002 |
| FB | 2 | Transpiration:ETo | 0.047 | 0.710 | - | 0.387 | 0.072 | 0.121 | 0.121 | 0.121 |
| FB | 3 | Transpiration:ETo | 0.048 | **0.996** | - | 0.185 | 0.272 | 0.002 | 0.002 | 0.002 |
| FB | 4 | Transpiration:ETo | 0.794 | 0.069 | - | 0.272 | 0.211 | 0.065 | 0.065 | 0.065 |
| FB | 5 | Transpiration:ETo | - | - | - | - | - | - | - | - |

Table 44. Comparison of Pearson p-values (p) of simple linear regressions between selected individual tree sap flow derived transpiration and the transpiration to reference evapotranspiration (ETo) ratio, respectively, with measured or calculated individual tree canopy dimensions, fractional interception and leaf area indices, respectively. Data were collected for the young (Y, green gradient colour) and full bearing (FB, red gradient colour) cultivar 'Wonderful' pomegranate orchards at Avontuur and Welgemoed, respectively, on days that drone surveys were conducted over the 2023/2024 season. **Bold black text indicates indices which related significantly to the measured parameters at a significance level of 5% (p≤0.05) and bold red italicized text at a significance level of 10% (0.05<p≤0.1).**

| Site | Survey | Tree Property | Tree height | Across row width | In row width | Tree volume | Fractional interception | Ceptometer LAI | Tree canopy _LAI | Orchard LAI |
|---|---|---|---|---|---|---|---|---|---|---|
| Y | 1 | Transpiration | 0.214 | 0.136 | 0.137 | *0.093* | 0.213 | 0.331 | 0.338 | 0.331 |
| Y | 2 | Transpiration | 0.004 | *0.092* | 0.257 | 0.046 | 0.022 | 0.013 | 0.029 | 0.015 |
| Y | 3 | Transpiration | *0.070* | *0.063* | *0.079* | 0.009 | 0.007 | 0.036 | 0.027 | 0.034 |
| Y | 4 | Transpiration | *0.069* | 0.270 | 0.146 | 0.115 | 0.044 | 0.020 | 0.016 | 0.019 |
| Y | 5 | Transpiration | 0.403 | 0.348 | 0.265 | 0.227 | 0.588 | 0.711 | 0.712 | 0.710 |
| FB | 1 | Transpiration | 0.450 | 0.035 | - | 1.000 | 0.030 | 0.952 | 0.952 | 0.952 |
| FB | 2 | Transpiration | 0.783 | 0.157 | - | 0.378 | 0.732 | 0.653 | 0.653 | 0.653 |
| FB | 3 | Transpiration | 0.860 | 0.039 | - | 0.717 | 0.651 | 0.973 | 0.973 | 0.973 |
| FB | 4 | Transpiration | 0.109 | 0.737 | - | 0.478 | 0.540 | 0.746 | 0.746 | 0.746 |
| FB | 5 | Transpiration | - | - | - | - | - | - | - | - |
| Y | 1 | Transpiration:ETo | 0.214 | 0.136 | 0.137 | *0.093* | 0.213 | 0.331 | 0.338 | 0.331 |
| Y | 2 | Transpiration:ETo | 0.004 | *0.092* | 0.257 | 0.046 | 0.022 | 0.013 | 0.029 | 0.015 |
| Y | 3 | Transpiration:ETo | *0.070* | *0.063* | *0.079* | 0.009 | 0.007 | 0.036 | 0.027 | 0.034 |
| Y | 4 | Transpiration:ETo | *0.069* | 0.270 | 0.146 | 0.115 | 0.044 | 0.020 | 0.016 | 0.019 |
| Y | 5 | Transpiration:ETo | 0.403 | 0.348 | 0.265 | 0.227 | 0.588 | 0.711 | 0.712 | 0.710 |
| FB | 1 | Transpiration:ETo | 0.450 | 0.035 | - | 1.000 | 0.030 | 0.952 | 0.952 | 0.952 |
| FB | 2 | Transpiration:ETo | 0.783 | 0.157 | - | 0.378 | 0.732 | 0.653 | 0.653 | 0.653 |
| FB | 3 | Transpiration:ETo | 0.860 | 0.039 | - | 0.717 | 0.651 | 0.973 | 0.973 | 0.973 |
| FB | 4 | Transpiration:ETo | 0.109 | 0.737 | - | 0.478 | 0.540 | 0.746 | 0.746 | 0.746 |
| FB | 5 | Transpiration:ETo | - | - | - | - | - | - | - | - |

Table 45. Comparison of coefficients of determination ($R^2$) of simple linear regressions between averaged measured or calculated tree canopy dimensions, fractional interception and leaf area index, orchard level transpiration and evapotranspiration and the ratios thereof to ETo for orchards combined over the 2023/2024 season. Pearson p-values (p) are indicated in the bottom part of the table. Bold black text indicates indices which related significantly to the measured parameters at a signi**ficance level of 5% (p≤0.0**5) and bold red italicized text at a **significance level of 10% (0.05<p≤0.1). Increased green colour intensity indicates increasing $R^2$** values.

| Tree property | SI | Tree height | Across row width | Tree volume | Fractional interception | Ceptometer LAI | Tree canopy LAI | Orchard LAI |
|---|---|---|---|---|---|---|---|---|
| Orchard level transpiration | $R^2$ | 0.450 | 0.452 | 0.351 | 0.291 | 0.356 | 0.737 | 0.058 |
| Orchard level ETc | $R^2$ | 0.369 | 0.447 | 0.529 | 0.385 | 0.509 | 0.108 | 0.497 |
| Orchard level T:ETo | $R^2$ | 0.623 | 0.494 | 0.324 | 0.576 | 0.551 | 0.466 | 0.338 |
| Orchard level ETc:ETo | $R^2$ | 0.672 | 0.724 | 0.780 | 0.697 | 0.742 | 0.348 | 0.394 |
| Orchard level transpiration | p | *0.069* | *0.068* | 0.122 | 0.167 | 0.118 | 0.006 | 0.565 |
| Orchard level ETc | p | 0.110 | *0.070* | 0.041 | 0.101 | 0.047 | 0.428 | *0.051* |
| Orchard level T:ETo | p | 0.020 | *0.052* | 0.141 | 0.029 | 0.035 | *0.062* | 0.130 |
| Orchard level ETc:ETo | p | 0.013 | 0.007 | 0.004 | 0.010 | 0.006 | 0.123 | *0.096* |

SI - Statistical indicator, LAI – Leaf area index, T – Transpiration, ETc – Evapotranspiration, ETo – reference evapotranspiration.

Table 46. Comparison of coefficients of determination ($R^2$) of simple linear regressions between averaged measured or calculated tree canopy dimensions, fractional interception and leaf area index, orchard level upscaled transpiration and evapotranspiration and the ratios thereof to reference evapotranspiration for the young (Y) and full bearing (FB) orchards over the 2023/2024 season. Bold text indicates indices which related significantly to the measured parameters at a significance level **of 5% (p≤0.05). Increased** colour intensity indicates increasing $R^2$ values. Transpiration was determined using sap flow and orchard evapotranspiration by surface renewal (young orchard) and eddy covariance (full bearing orchard).

| Site[1] | Variable | Tree height | Across row width | Tree volume | Fractional interception | Ceptometer LAI[2] | Tree canopy LAI | Orchard LAI |
|---|---|---|---|---|---|---|---|---|
| Y | Orchard level transpiration | **0.948** | 0.009 | 0.088 | **0.901** | **0.817** | **0.796** | **0.811** |
| FB | Orchard level transpiration | 0.103 | **0.791** | **0.758** | 0.355 | 0.397 | 0.397 | 0.397 |
| Y | Orchard level ETc | 0.036 | 0.365 | 0.397 | 0.003 | 0.001 | 0.000 | 0.001 |
| FB | Orchard level ETc | **0.658** | **0.746** | **0.757** | **0.963** | **0.848** | **0.848** | **0.848** |
| Y | ETo | **0.762** | 0.298 | 0.064 | **0.543** | 0.348 | 0.351 | 0.347 |
| FB | ETo | 0.045 | 0.252 | 0.260 | 0.041 | 0.381 | 0.381 | 0.381 |
| Y | T : ETo | 0.202 | **0.615** | **0.481** | 0.056 | 0.004 | 0.006 | 0.004 |
| FB | T : ETo | **0.566** | **0.998** | **1.000** | 0.013 | 0.025 | 0.025 | 0.025 |
| Y | ETc : ETo | 0.048 | 0.206 | 0.403 | 0.107 | 0.121 | 0.097 | 0.114 |
| FB | ETc : ETo | **0.957** | **0.988** | **0.990** | **0.671** | **0.468** | **0.468** | **0.468** |

LAI -Leaf area index, T – Transpiration, ETc – evapotranspiration, ETo - Reference evapotranspiration.

Table 47. Comparison of Pearson p-values (p) of simple linear regressions between averaged measured or calculated tree canopy dimensions, fractional interception and leaf area index, orchard level upscaled transpiration, orchard level evapotranspiration and the ratios of the latter two variables to reference evapotranspiration for the young (Y) and full bearing (FB) cultivar 'Wonderful' pomegranate orchards over the 2023/2024 season. Bold black text indicates indices which related significantly to the measured parameters at a significance level of **5% (p≤0.05) and bold red italicized text at a significance level of 10% (0.05<p≤0.1).** Transpiration was determined using sap flow and orchard evapotranspiration by surface renewal (young orchard) and eddy covariance (full bearing orchard).

| Site[1] | Variable | Tree height | Across row width | Tree volume | Fractional interception | Ceptometer LAI | Tree canopy LAI | Orchard LAI |
|---|---|---|---|---|---|---|---|---|
| Y | Orchard level transpiration | 0.005 | 0.882 | 0.628 | 0.014 | 0.035 | 0.042 | 0.037 |
| FB | Orchard level transpiration | 0.792 | 0.302 | 0.328 | 0.594 | 0.566 | 0.566 | 0.566 |
| Y | Orchard level ETc | 0.759 | 0.280 | 0.254 | 0.936 | 0.953 | 0.992 | 0.963 |
| FB | Orchard level ETc | 0.398 | 0.336 | 0.328 | 0.124 | 0.255 | 0.255 | 0.255 |
| Y | ETo | *0.053* | 0.341 | 0.680 | 0.156 | 0.295 | 0.293 | 0.296 |
| FB | ETo | 0.733 | 0.388 | 0.380 | 0.744 | 0.267 | 0.267 | 0.267 |
| Y | T:ETo | 0.448 | 0.116 | 0.194 | 0.702 | 0.922 | 0.903 | 0.919 |
| FB | T:ETo | 0.458 | 0.032 | 0.006 | 0.927 | 0.899 | 0.899 | 0.899 |
| Y | ETc:ETo | 0.723 | 0.443 | 0.250 | 0.590 | 0.567 | 0.611 | 0.579 |
| FB | ETc:ETo | 0.133 | *0.071* | *0.063* | 0.389 | 0.520 | 0.520 | 0.520 |

LAI -Leaf area index, T – Transpiration, ETc – evapotranspiration, ETo - Reference evapotranspiration

# APPENDIX E: ORCHARD HOMOGENEITY SUMMARY STATISTICS

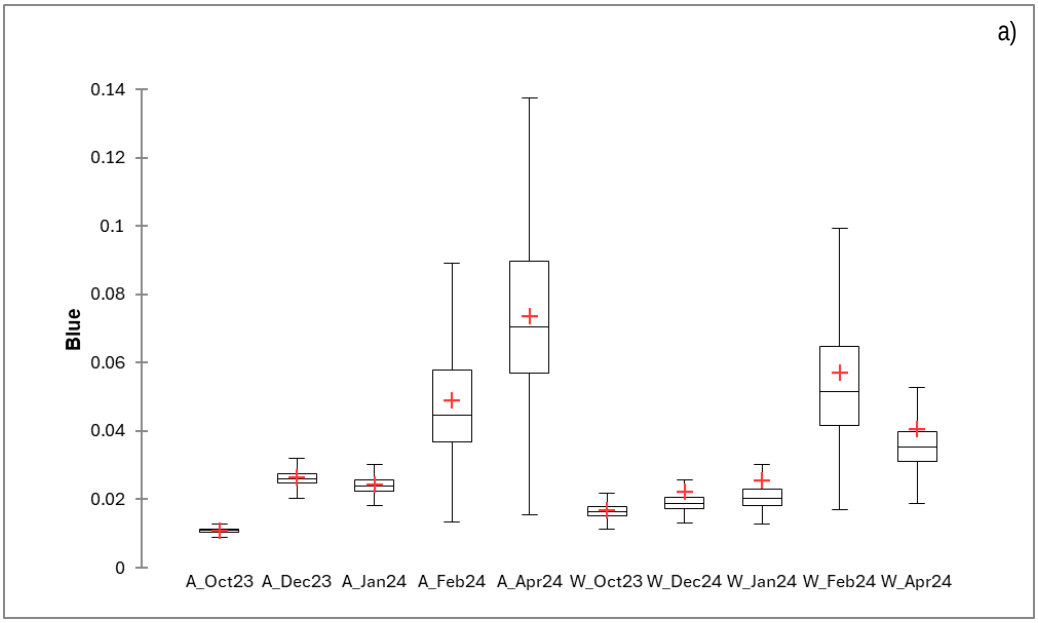


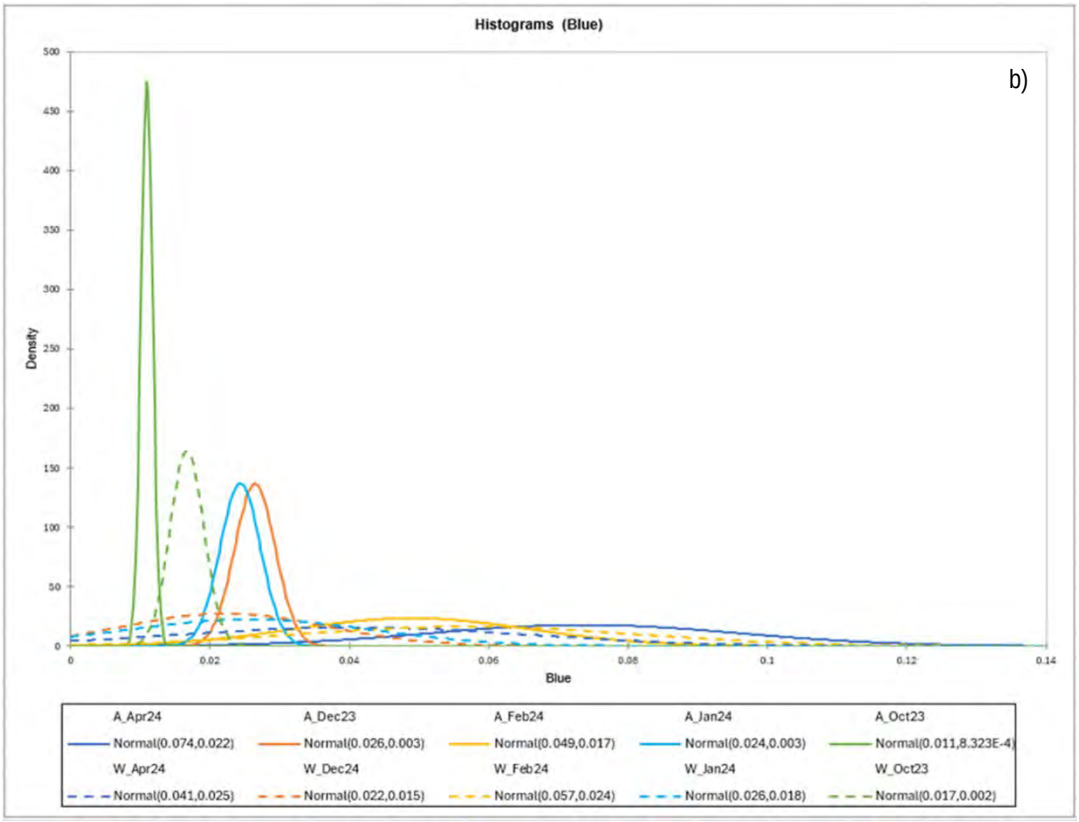


Figure 86. Comparison of variation in the blue spectral band reflectance derived from multispectral drone images from five drone surveys (October and December 2023, January, February and April 2024) conducted for the young (A, at Avontuur) and full bearing (W, at Welgemoed) pomegranate orchards over the 2023/2024 growing season. The data distribution according to boxplot (a) indicates the minimum, lower quartile (25th percentile), median, upper quartile (75$^{th}$ percentile), and maximum. The histograms (b) indicate the normal distribution, average and standard deviation of data per survey per orchard.

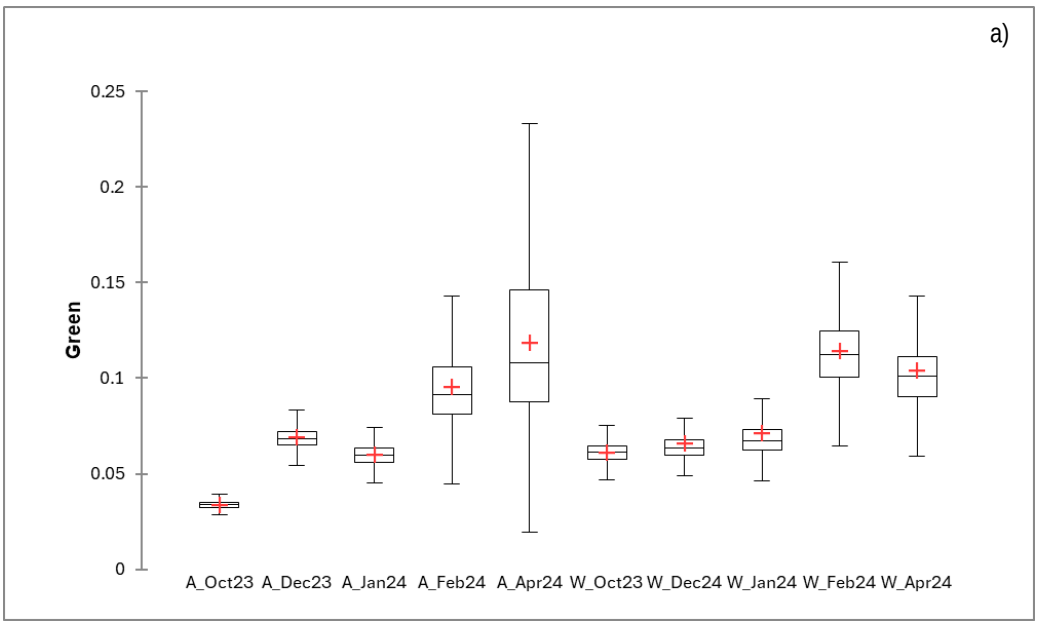


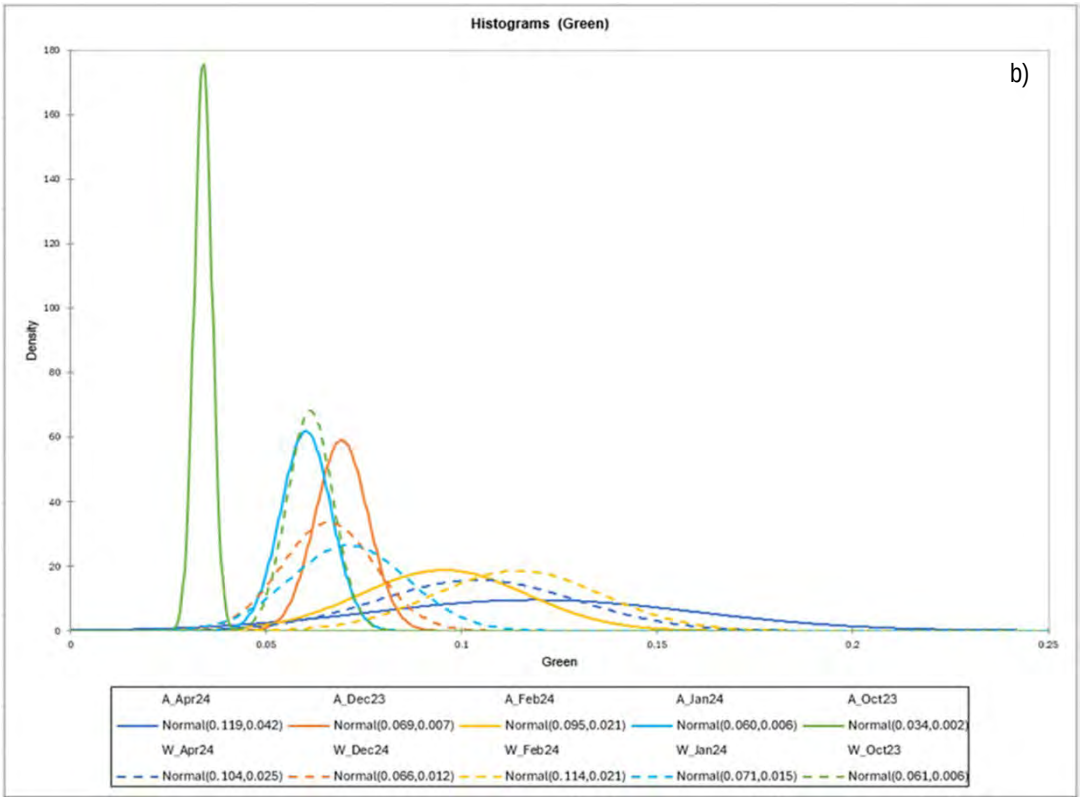


Figure 87. Comparison of variation in the green spectral band reflectance derived from multispectral drone images from five drone surveys (October and December 2023, January, February and April 2024) conducted for the young (A, at Avontuur) and full bearing (W, at Welgemoed) pomegranate orchards over the 2023/2024 growing season. The data distribution according to boxplot (a) indicates the minimum, lower quartile (25th percentile), median, upper quartile (75$^{th}$ percentile), and maximum. The histograms (b) indicate the normal distribution, average and standard deviation of data per survey per orchard.

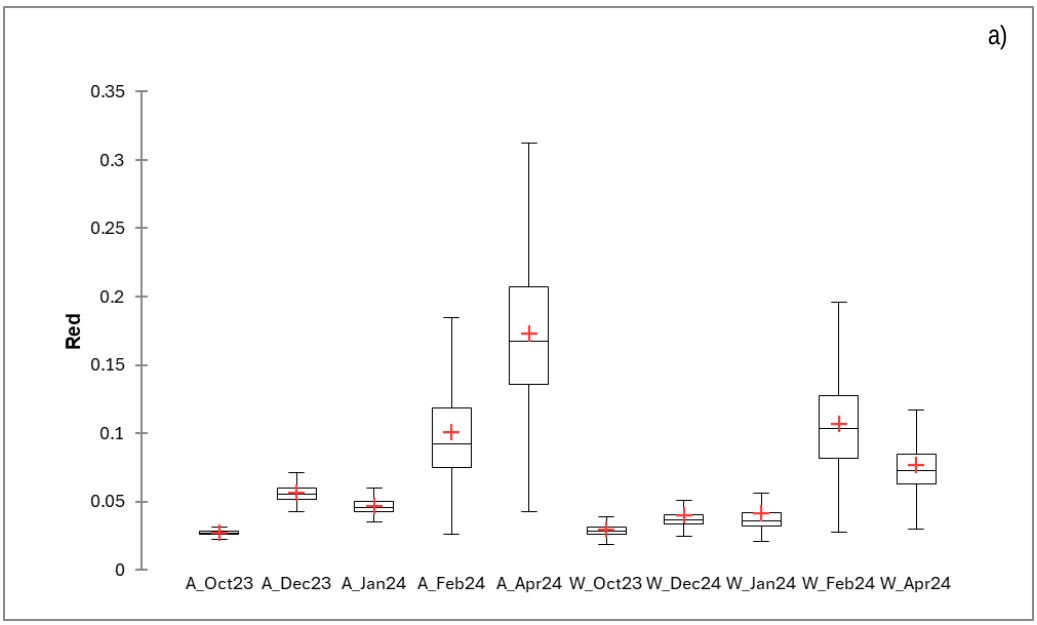


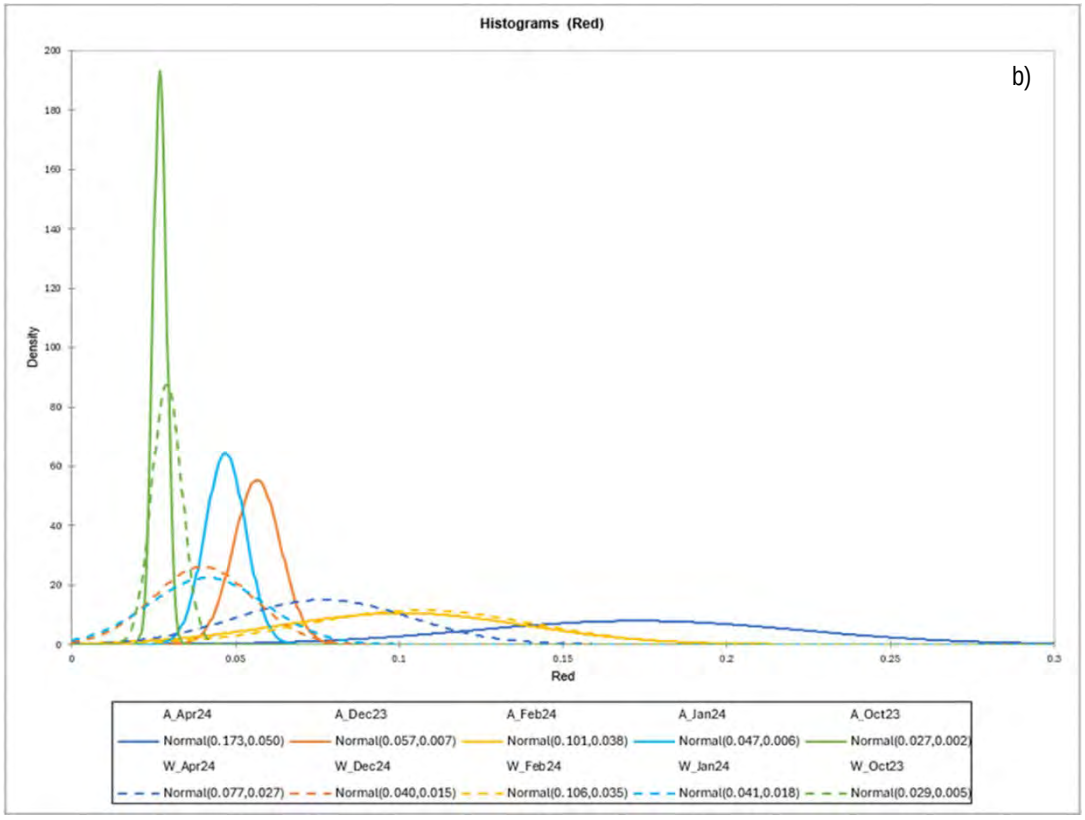


Figure 88. Comparison of variation in the red spectral band reflectance derived from multispectral drone images from five drone surveys (October and December 2023, January, February and April 2024) conducted for the young (A, at Avontuur) and full bearing (W, at Welgemoed) pomegranate orchards over the 2023/2024 growing season. The data distribution according to boxplot (a) indicates the minimum, lower quartile (25th percentile), median, upper quartile (75$^{th}$ percentile), and maximum. The histograms (b) indicate the normal distribution, average and standard deviation of data per survey per orchard.

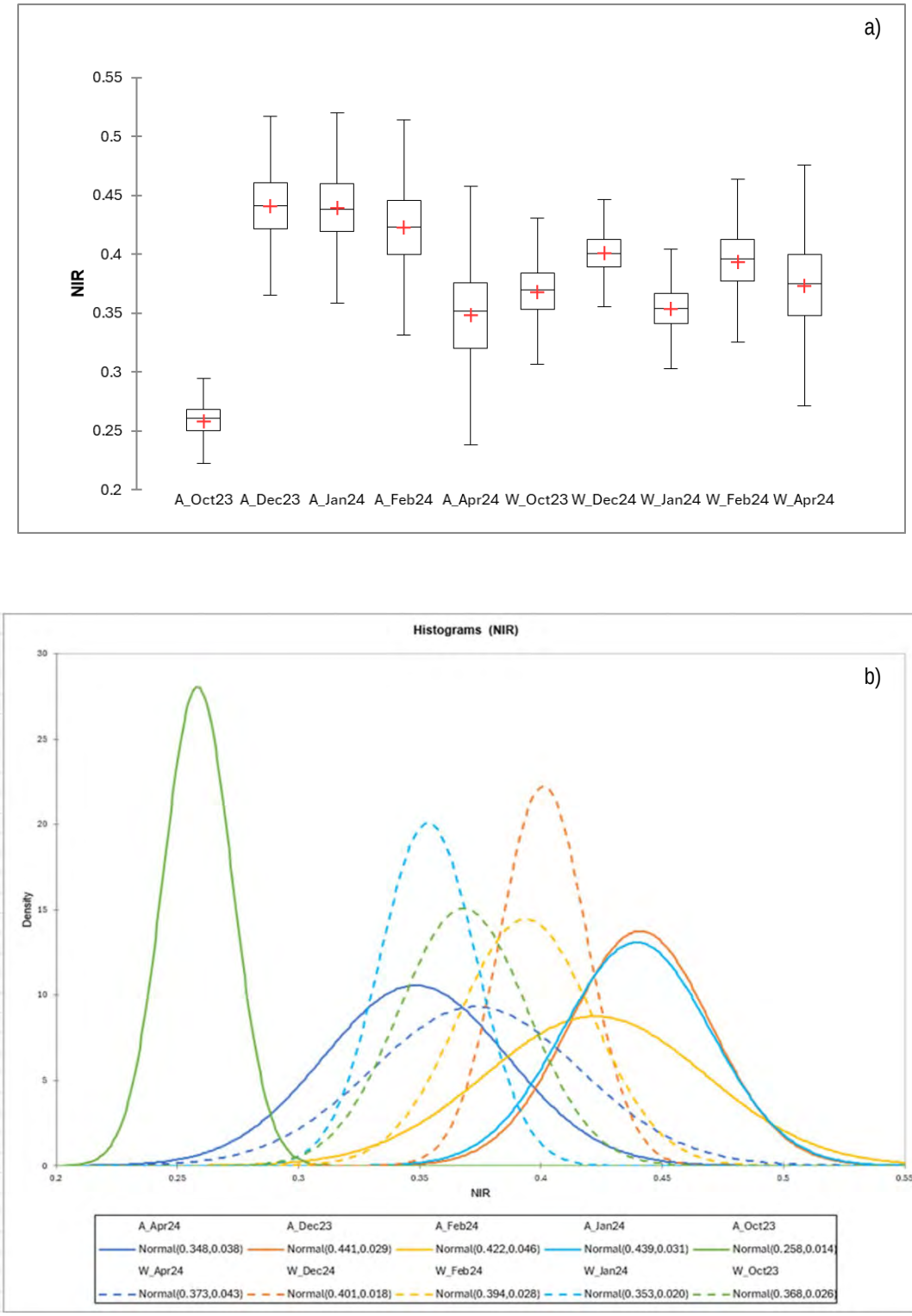


Figure 89. Comparison of variation in the near-infrared (NIR) spectral band reflectance derived from multispectral drone images from five drone surveys (October and December 2023, January, February and April 2024) conducted for the young (A, at Avontuur) and full bearing (W, at Welgemoed) pomegranate orchards over the 2023/2024 growing season. The data distribution according to boxplot (a) indicates the minimum, lower quartile (25th percentile), median, upper quartile (75$^{th}$ percentile), and maximum. The histograms (b) indicate the normal distribution, average and standard deviation of data per survey per orchard.

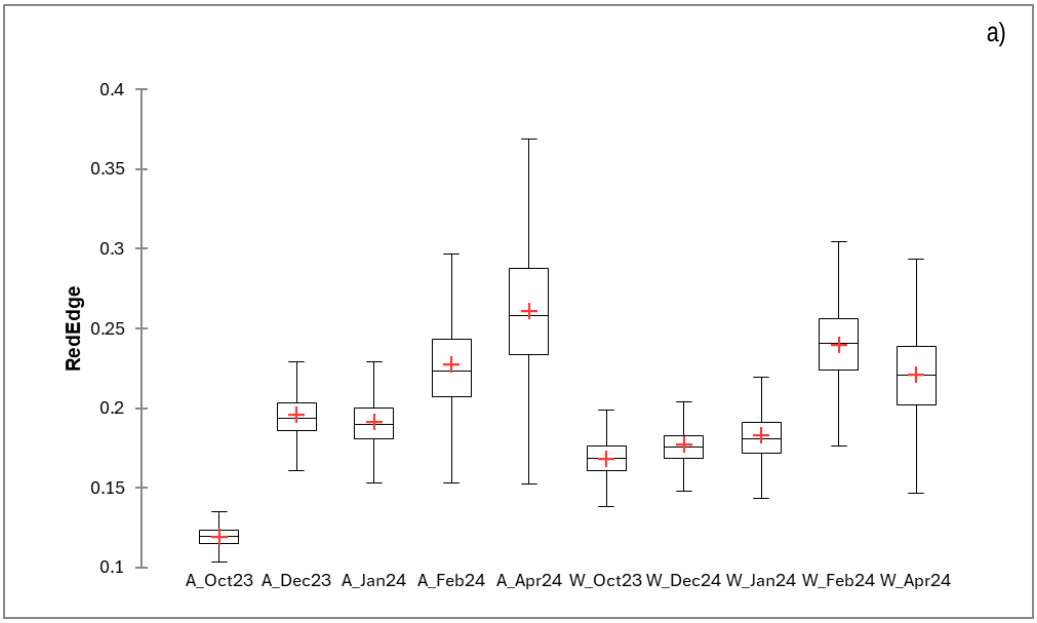


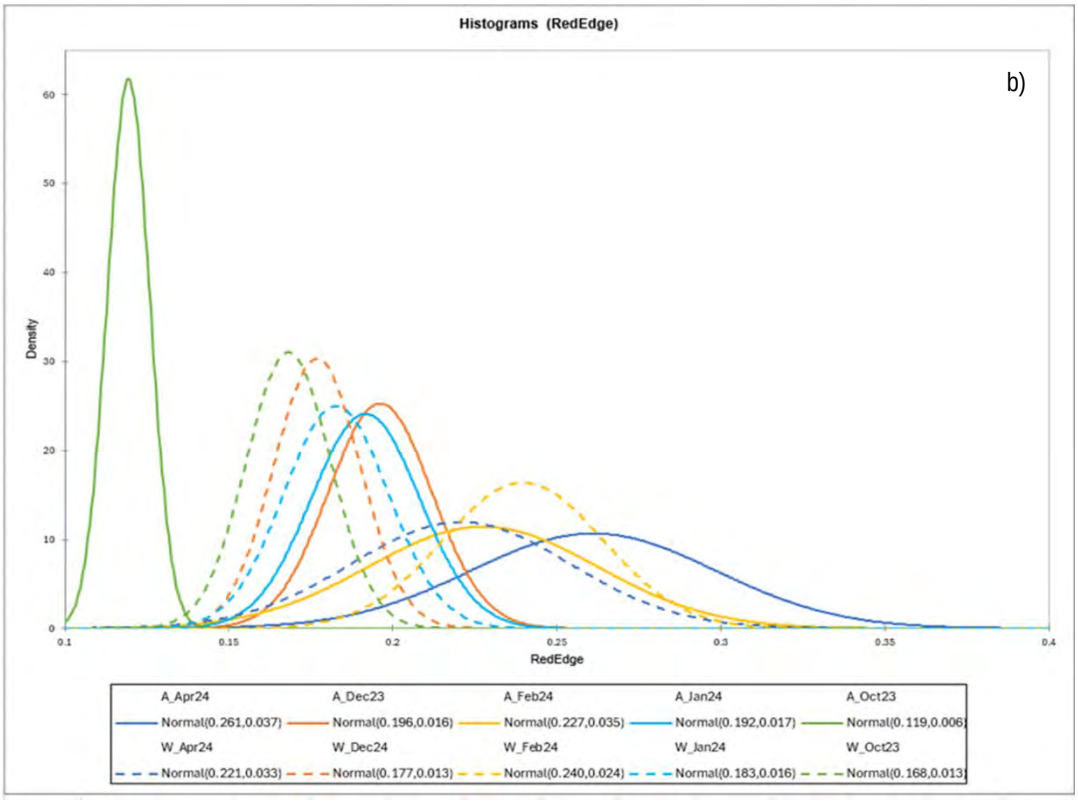


Figure 90. Comparison of variation in the RedEdge spectral band reflectance derived from multispectral drone images from five drone surveys (October and December 2023, January, February and April 2024) conducted for the young (A, at Avontuur) and full bearing (W, at Welgemoed) pomegranate orchards over the 2023/2024 growing season. The data distribution according to boxplot (a) indicates the minimum, lower quartile (25th percentile), median, upper quartile (75$^{th}$ percentile), and maximum. The histograms (b) indicate the normal distribution, average and standard deviation of data per survey per orchard.

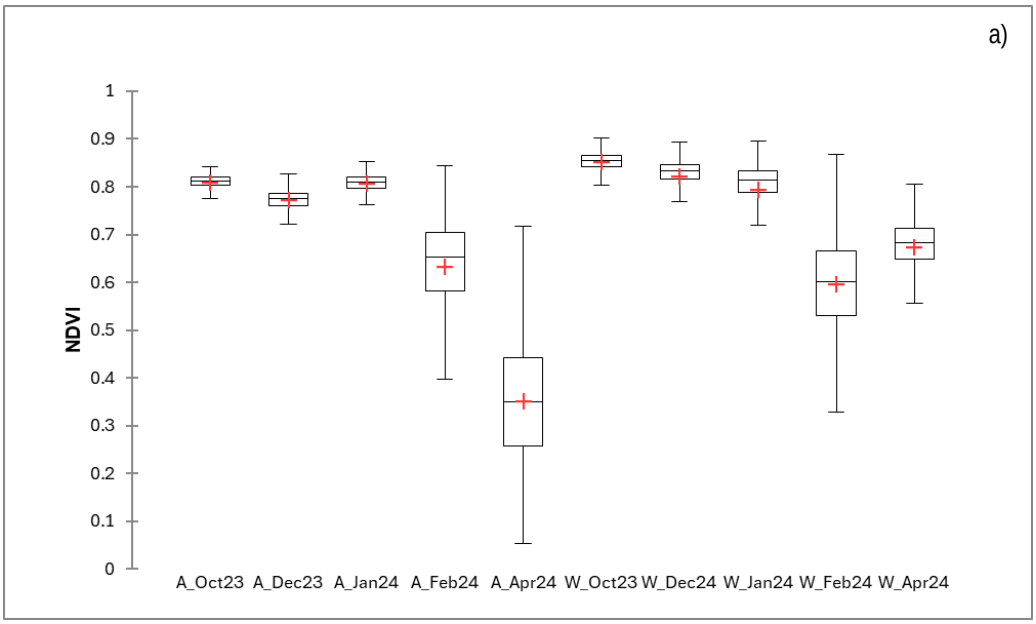


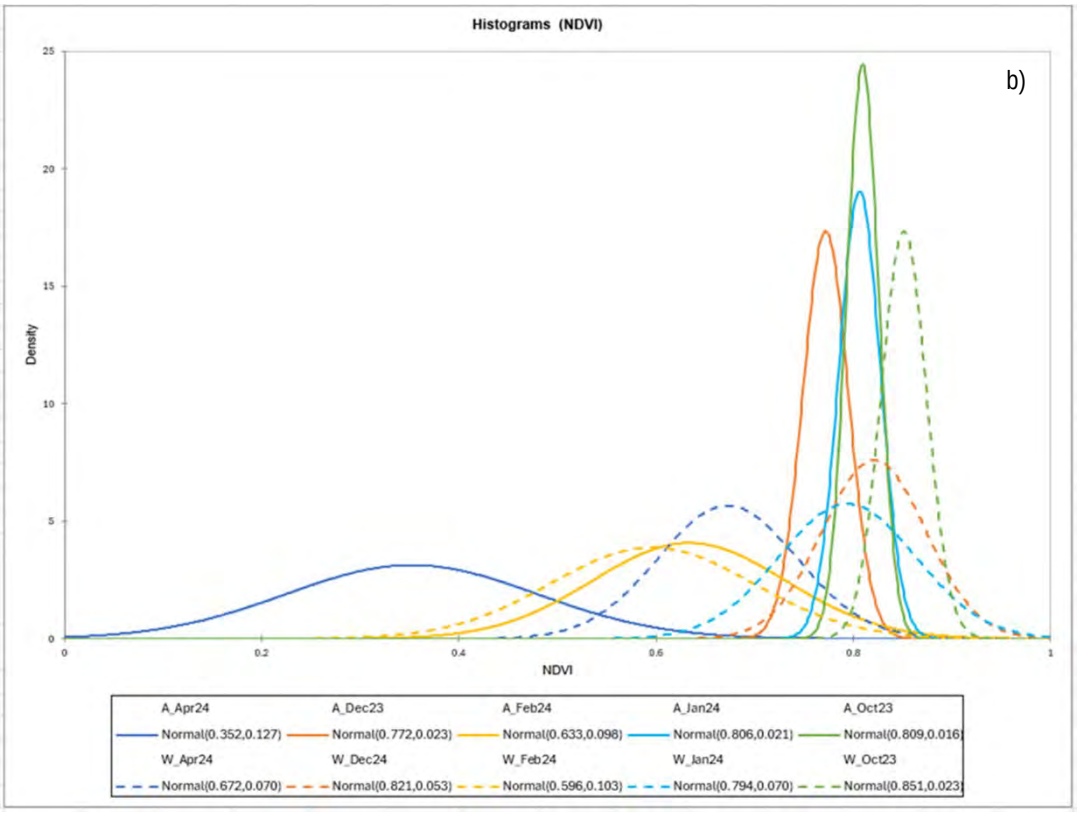


Figure 91. Comparison of variation in the Normalized Difference Vegetation Index (NDVI) derived from multispectral drone images from five drone surveys (October and December 2023, January, February and April 2024) conducted for the young (A, at Avontuur) and full bearing (W, at Welgemoed) pomegranate orchards over the 2023/2024 growing season. The data distribution according to boxplot (a) indicates the minimum, lower quartile (25th percentile), median, upper quartile (75$^{th}$ percentile), and maximum. The histograms (b) indicate the normal distribution, average and standard deviation of data per survey per orchard.

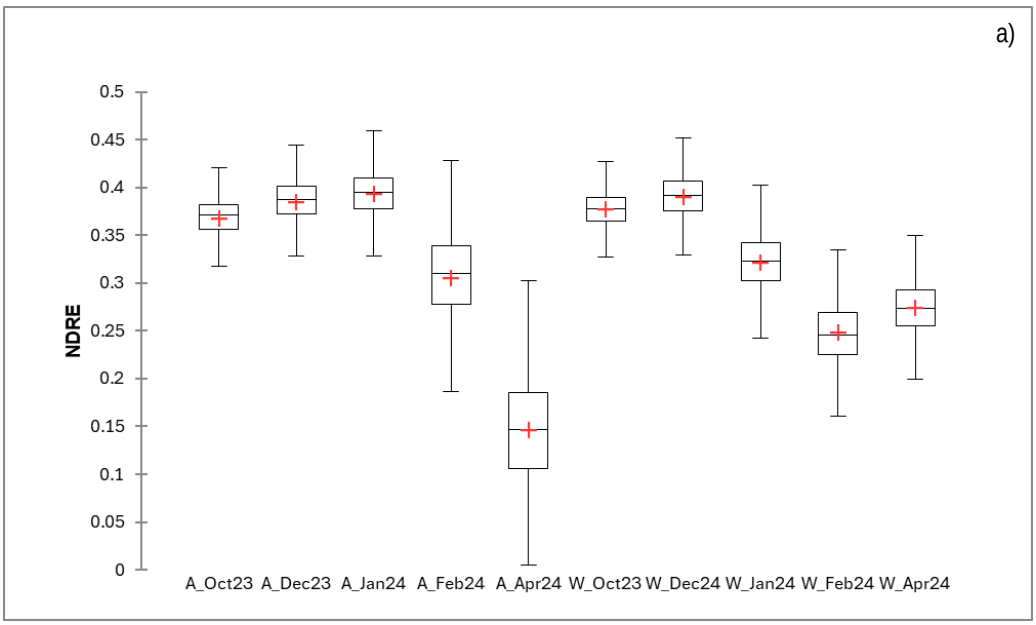


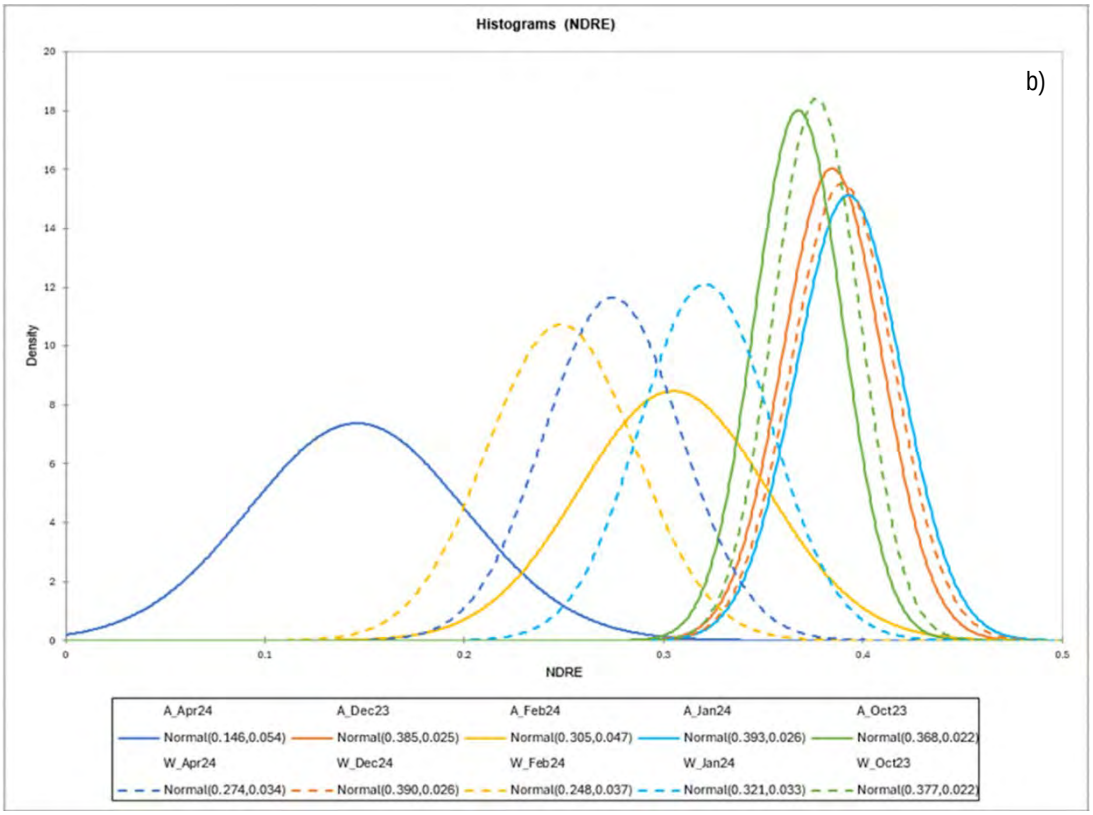


Figure 92. Comparison of variation in the Normalized Difference Red Edge index (NDRE) derived from multispectral drone images from five drone surveys (October and December 2023, January, February and April 2024) conducted for the young (A, at Avontuur) and full bearing (W, at Welgemoed) pomegranate orchards over the 2023/2024 growing season. The data distribution according to boxplot (a) indicates the minimum, lower quartile (25th percentile), median, upper quartile (75$^{th}$ percentile), and maximum. The histograms (b) indicate the normal distribution, average and standard deviation of data per survey per orchard.

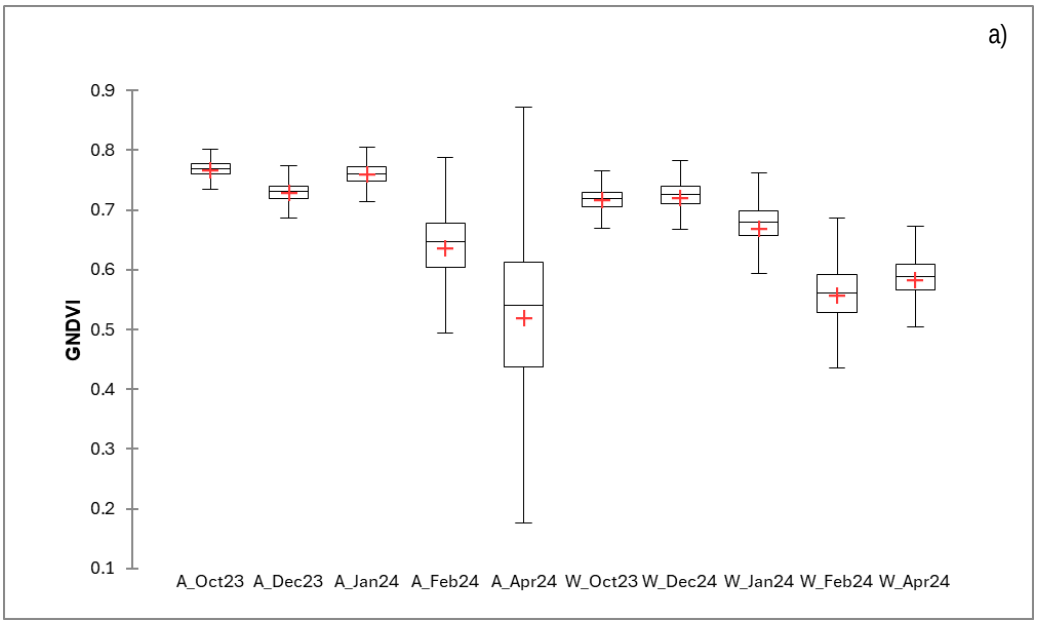


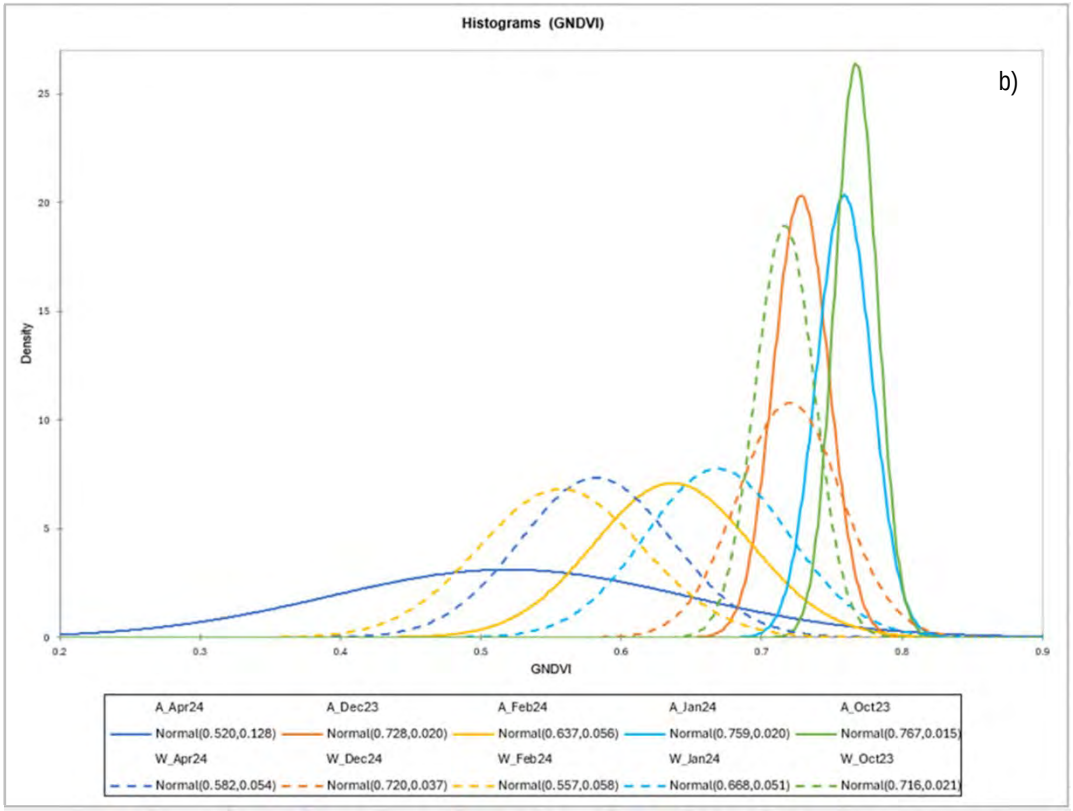


Figure 93. Comparison of variation in the Green Normalized Difference Vegetation Index (GNDVI) derived from multispectral drone images from five drone surveys (October and December 2023, January, February and April 2024) conducted for the young (A, at Avontuur) and full bearing (W, at Welgemoed) pomegranate orchards over the 2023/2024 growing season. The data distribution according to boxplot (a) indicates the minimum, lower quartile (25th percentile), median, upper quartile (75$^{th}$ percentile), and maximum. The histograms (b) indicate the normal distribution, average and standard deviation of data per survey per orchard.

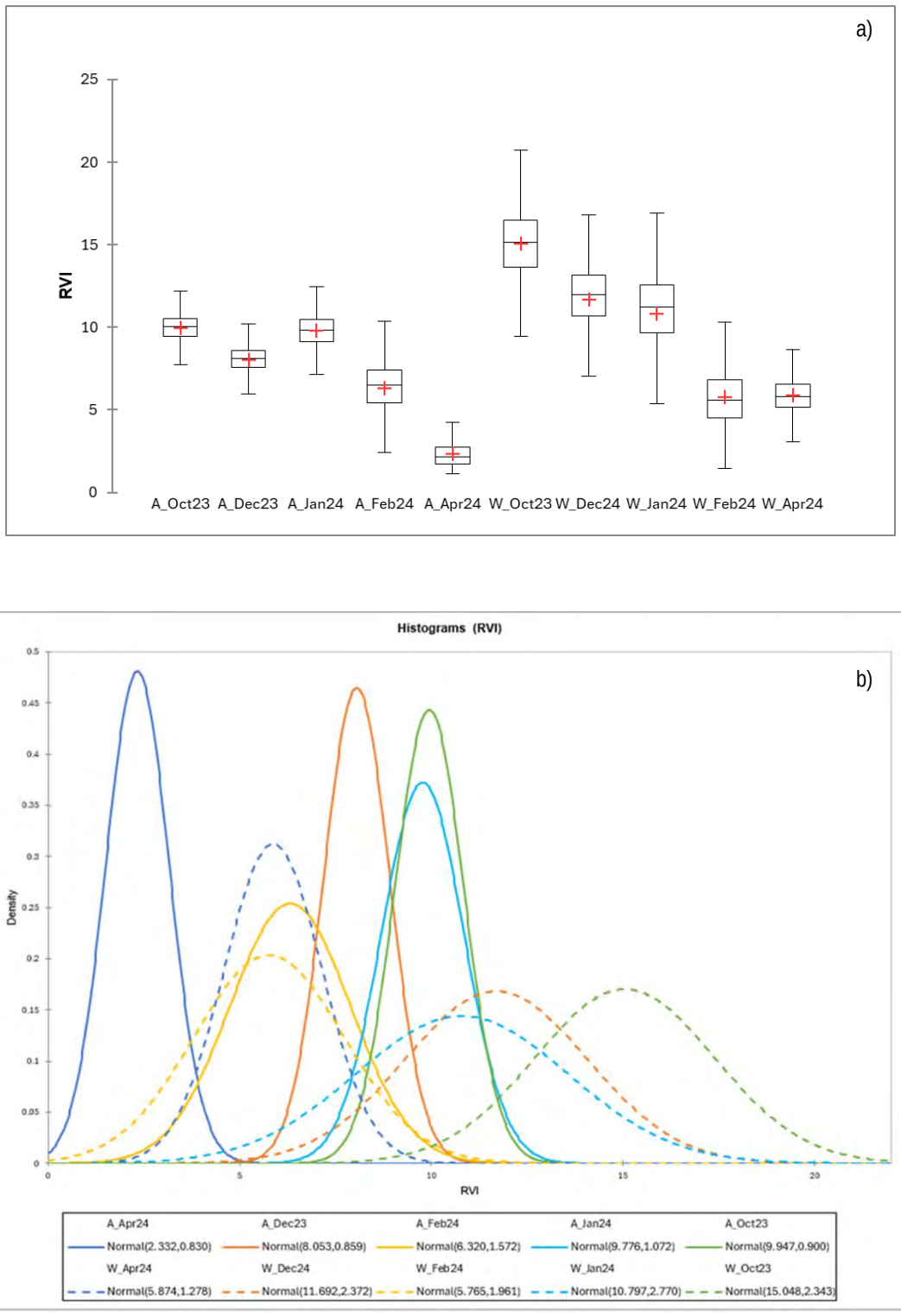


Figure 94. Comparison of variation in the Ratio Vegetation Index (RVI) derived from multispectral drone images from five drone surveys (October and December 2023, January, February and April 2024) conducted for the young (A, at Avontuur) and full bearing (W, at Welgemoed) pomegranate orchards over the 2023/2024 growing season. The data distribution according to boxplot (a) indicates the minimum, lower quartile (25th percentile), median, upper quartile (75$^{th}$ percentile), and maximum. The histograms (b) indicate the normal distribution, average and standard deviation of data per survey per orchard.

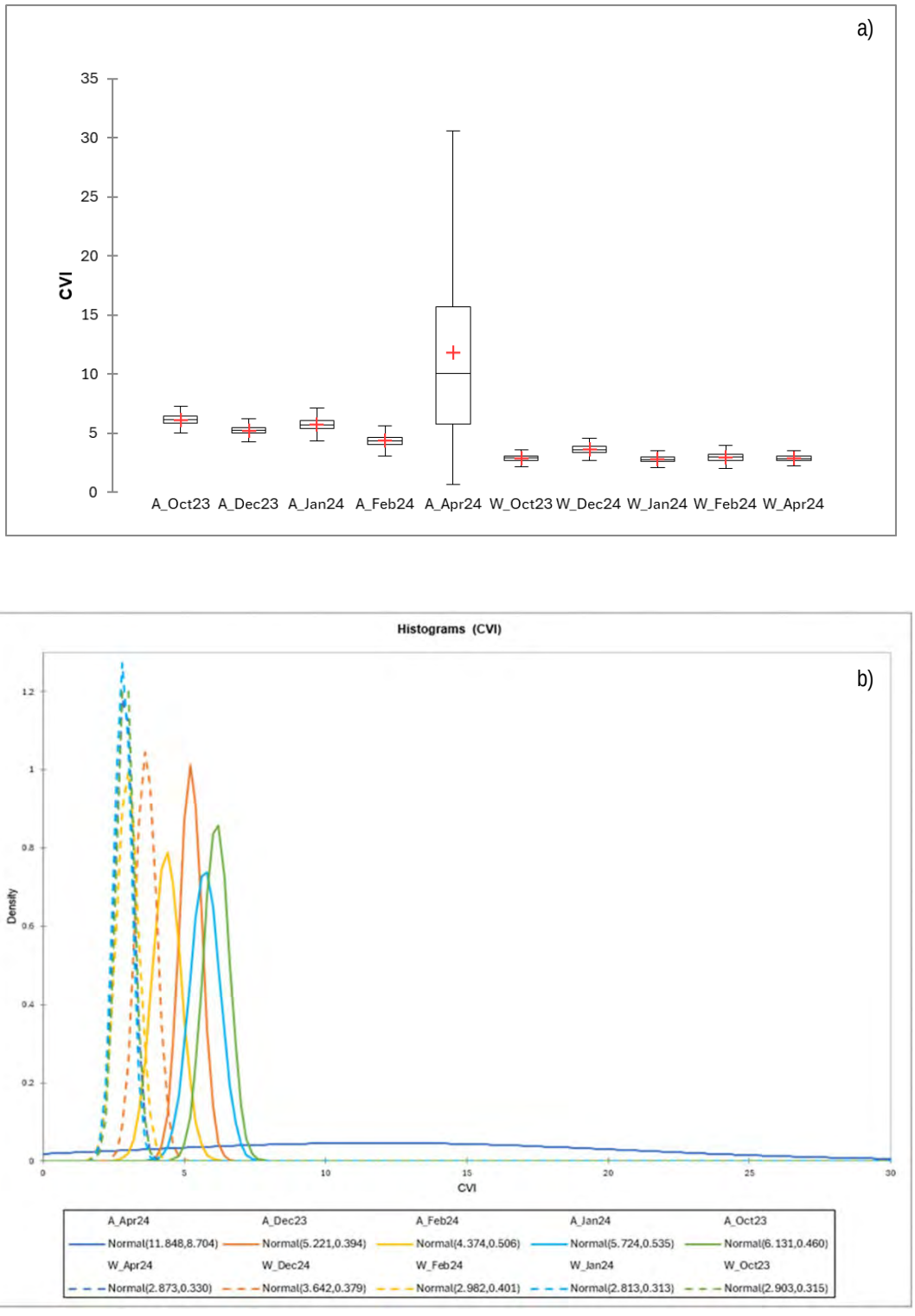


Figure 95. Comparison of variation in the Chlorophyll Vegetation Index (CVI) derived from multispectral drone images from five drone surveys (October and December 2023, January, February and April 2024) conducted for the young (A, at Avontuur) and full bearing (W, at Welgemoed) pomegranate orchards over the 2023/2024 growing season. The data distribution according to boxplot (a) indicates the minimum, lower quartile (25th percentile), median, upper quartile (75$^{th}$ percentile), and maximum. The histograms (b) indicate the normal distribution, average and standard deviation of data per survey per orchard.

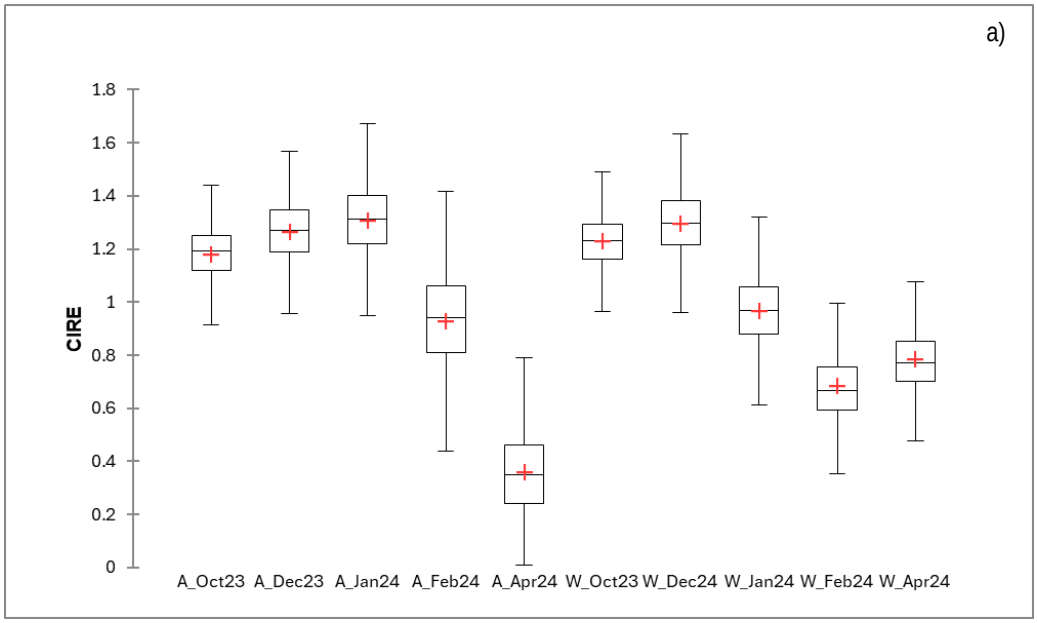


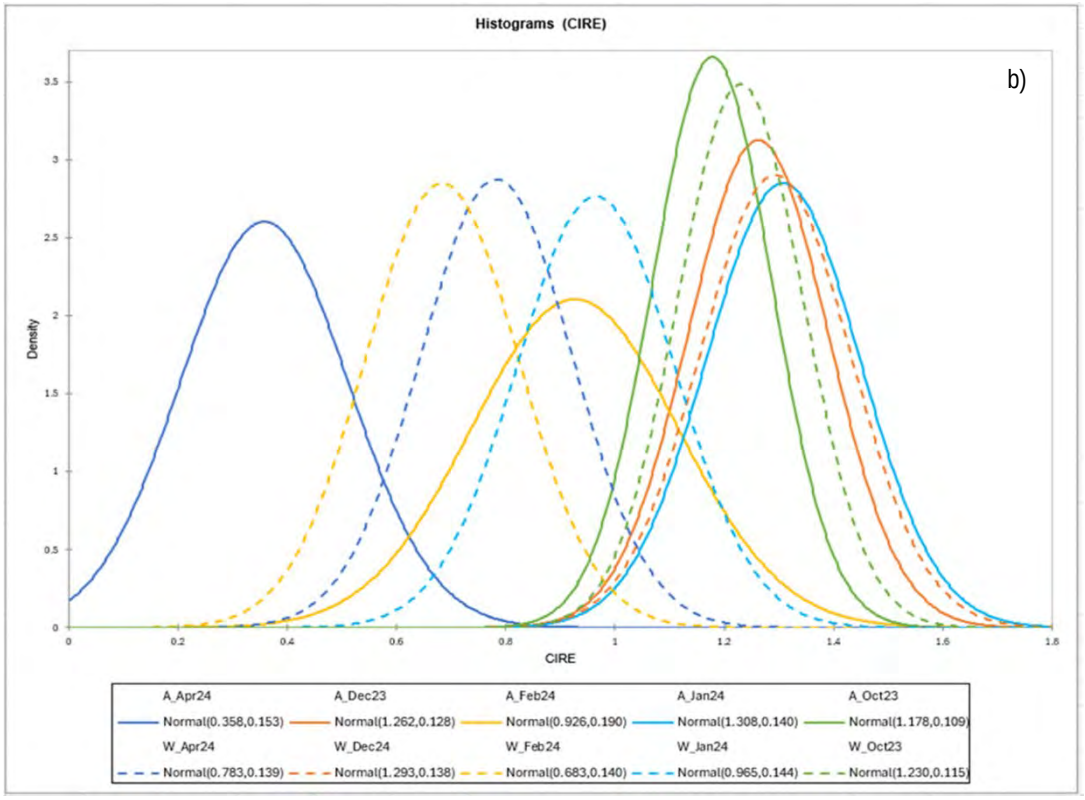


Figure 96. Comparison of variation in the Chlorophyll Index – Red Edge (CIRE) derived from multispectral drone images from five drone surveys (October and December 2023, January, February and April 2024) conducted for the young (A, at Avontuur) and full bearing (W, at Welgemoed) pomegranate orchards over the 2023/2024 growing season. The data distribution according to boxplot (a) indicates the minimum, lower quartile (25th percentile), median, upper quartile (75$^{th}$ percentile), and maximum. The histograms (b) indicate the normal distribution, average and standard deviation of data per survey per orchard.

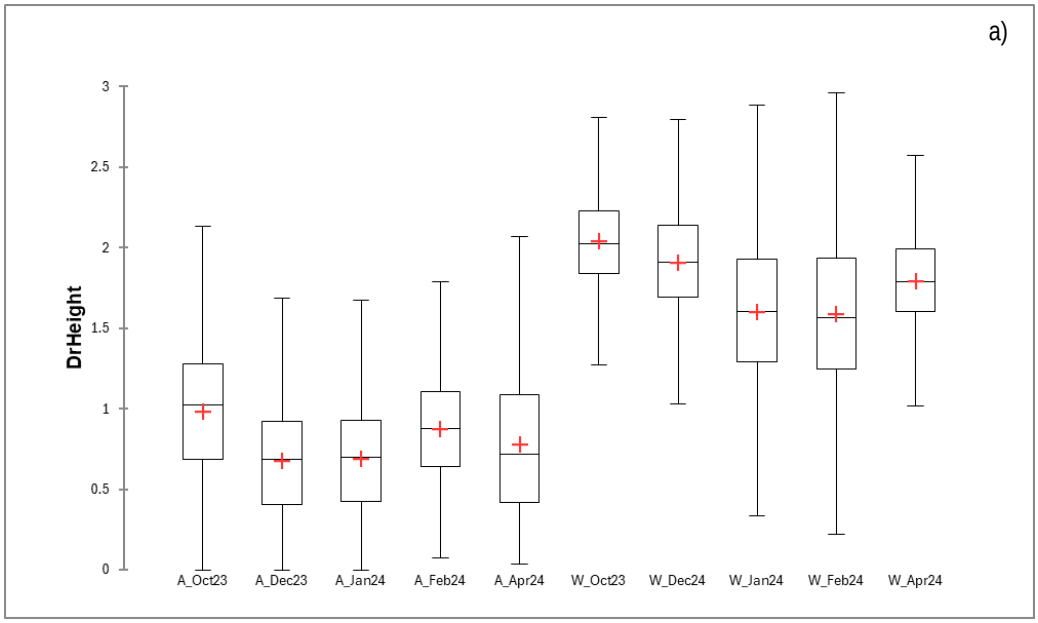


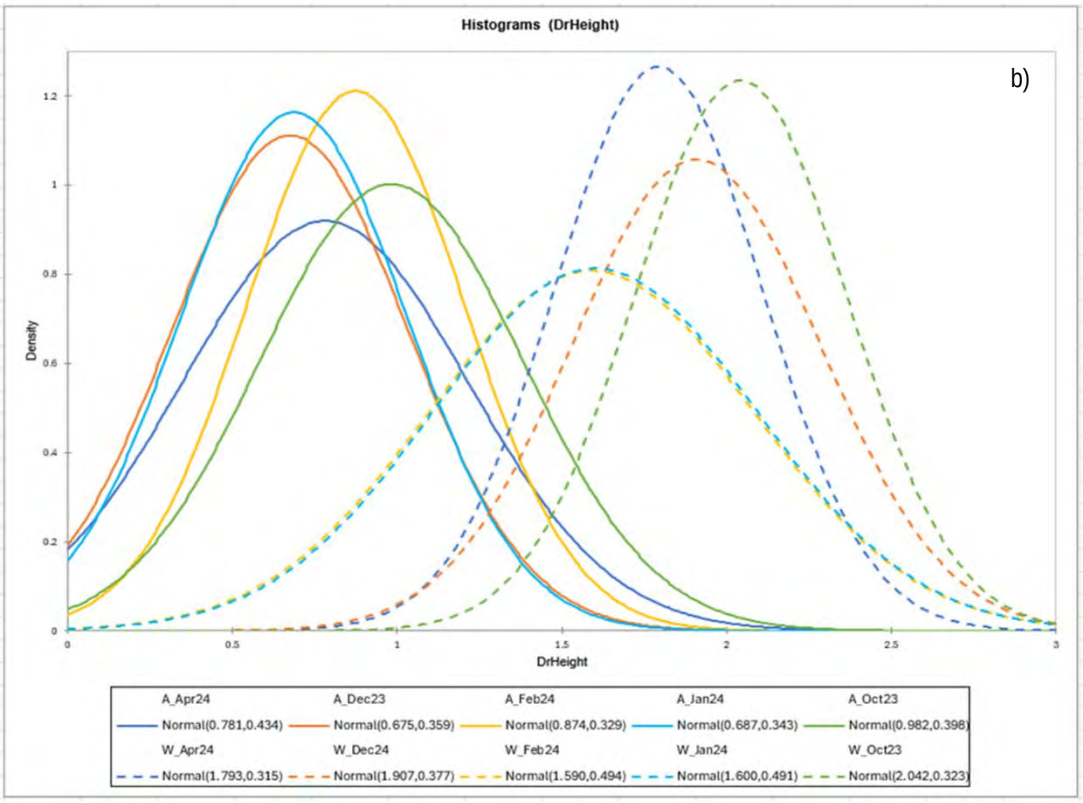


Figure 97. Comparison of variation in the drone estimated tree height (DrHeight) derived from multispectral drone images from five drone surveys (October and December 2023, January, February and April 2024) conducted for the young (A, at Avontuur) and full bearing (W, at Welgemoed) pomegranate orchards over the 2023/2024 growing season. The data distribution according to boxplot (a) indicates the minimum, lower quartile (25th percentile), median, upper quartile (75$^{th}$ percentile), and maximum. The histograms (b) indicate the normal distribution, average and standard deviation of data per survey per orchard.

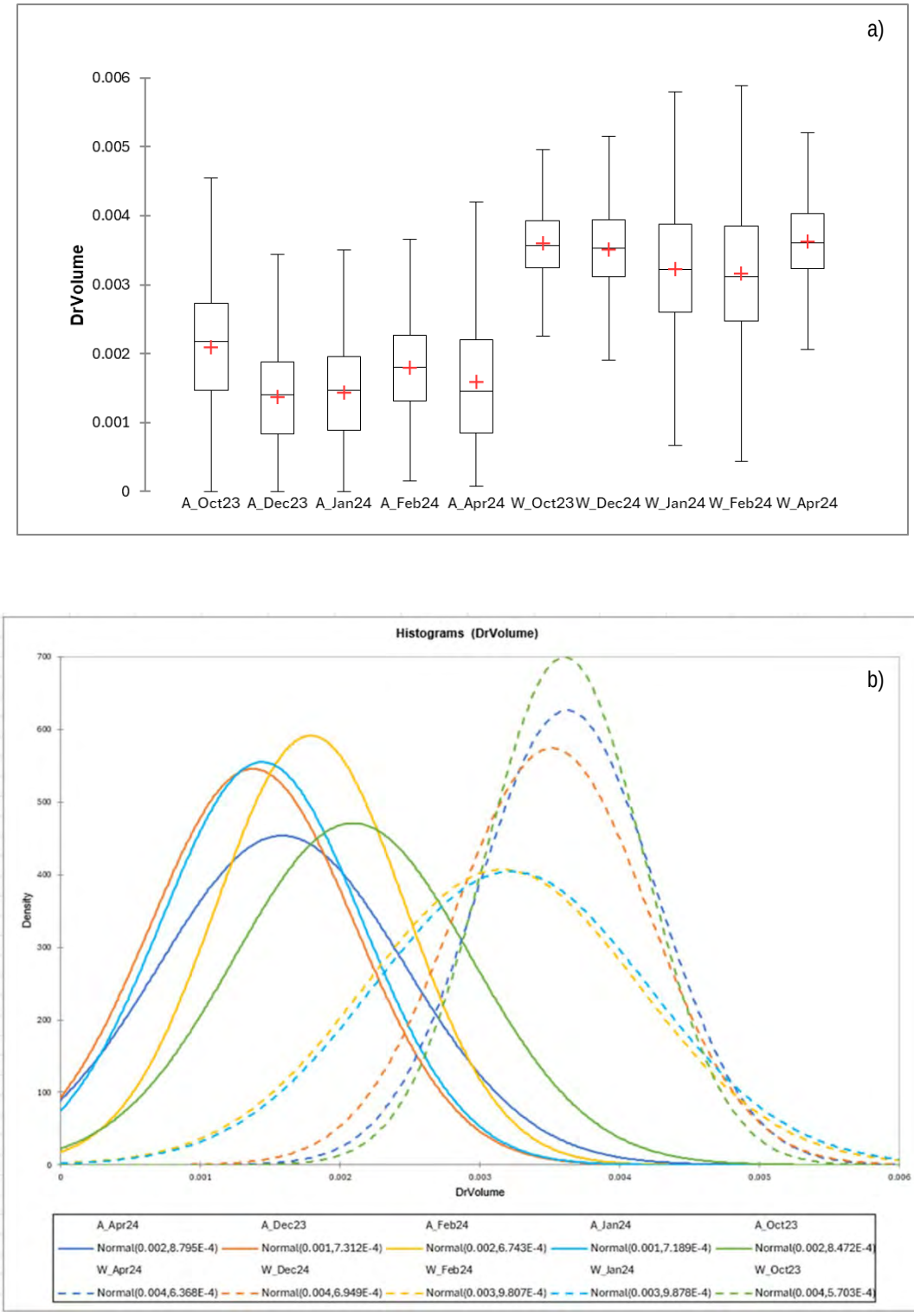


Figure 98. Comparison of variation in the drone estimated tree volume (DrVolume) derived from multispectral drone images from five drone surveys (October and December 2023, January, February and April 2024) conducted for the young (A, at Avontuur) and full bearing (W, at Welgemoed) pomegranate orchards over the 2023/2024 growing season. The data distribution according to boxplot (a) indicates the minimum, lower quartile (25th percentile), median, upper quartile (75$^{th}$ percentile), and maximum. The histograms (b) indicate the normal distribution, average and standard deviation of data per survey per orchard.

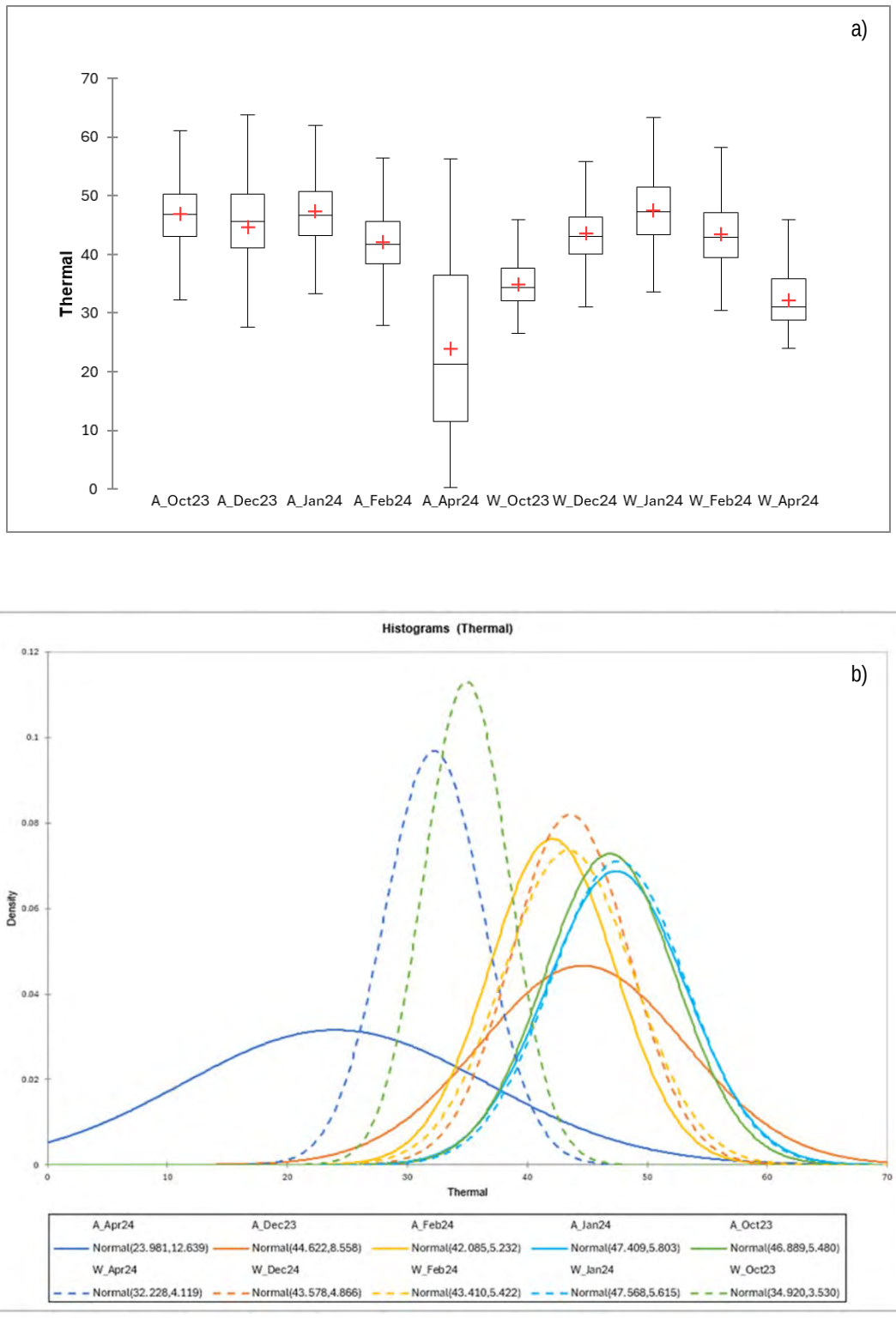


Figure 99. Comparison of variation in thermal infrared temperature (TIR) derived from thermal drone images from five drone surveys (October and December 2023, January, February and April 2024) conducted for the young (A, at Avontuur) and full bearing (W, at Welgemoed) pomegranate orchards over the 2023/2024 growing season. The data distribution according to boxplot (a) indicates the minimum, lower quartile (25th percentile), median, upper quartile (75$^{th}$ percentile), and maximum. The histograms (b) indicate the normal distribution, average and standard deviation of data per survey per orchard.

Table 48. Summary statistics for drone image derived spectral bands, indices, tree height, tree volume and thermal infrared temperature for five surveys conducted during the 2023/2024 growing season for a young (A, Avontuur) and full bearing (W, Welgemoed) cultivar 'Wonderful' pomegranate orchard.

| Drone variable | Site | Survey | No. of observations | Minimum | Maximum | 1st Quartile | Median | 3rd Quartile | Mean | Standard deviation (n-1) |
|---|---|---|---|---|---|---|---|---|---|---|
| Blue | A | Oct-23 | 5173 | 0.009 | 0.023 | 0.010 | 0.011 | 0.011 | 0.011 | 0.001 |
| Blue | A | Dec-23 | 5172 | 0.019 | 0.074 | 0.025 | 0.026 | 0.028 | 0.026 | 0.003 |
| Blue | A | Jan-24 | 5173 | 0.018 | 0.046 | 0.023 | 0.024 | 0.026 | 0.024 | 0.003 |
| Blue | A | Feb-24 | 5173 | 0.014 | 0.166 | 0.037 | 0.045 | 0.058 | 0.049 | 0.017 |
| Blue | A | Apr-24 | 5173 | 0.016 | 0.160 | 0.057 | 0.071 | 0.090 | 0.074 | 0.022 |
| Blue | W | Oct-23 | 5226 | 0.010 | 0.040 | 0.015 | 0.016 | 0.018 | 0.017 | 0.002 |
| Blue | W | Dec-23 | 5707 | 0.013 | 0.113 | 0.017 | 0.019 | 0.021 | 0.022 | 0.015 |
| Blue | W | Jan-24 | 5707 | 0.013 | 0.104 | 0.018 | 0.020 | 0.023 | 0.026 | 0.018 |
| Blue | W | Feb-24 | 5707 | 0.017 | 0.176 | 0.042 | 0.052 | 0.065 | 0.057 | 0.024 |
| Blue | W | Apr-24 | 5707 | 0.015 | 0.279 | 0.031 | 0.035 | 0.040 | 0.041 | 0.025 |
| Green | A | Oct-23 | 5173 | 0.025 | 0.057 | 0.032 | 0.034 | 0.035 | 0.034 | 0.002 |
| Green | A | Dec-23 | 5172 | 0.048 | 0.135 | 0.065 | 0.068 | 0.072 | 0.069 | 0.007 |
| Green | A | Jan-24 | 5173 | 0.044 | 0.108 | 0.056 | 0.059 | 0.063 | 0.060 | 0.006 |
| Green | A | Feb-24 | 5173 | 0.029 | 0.223 | 0.081 | 0.091 | 0.106 | 0.095 | 0.021 |
| Green | A | Apr-24 | 5173 | 0.019 | 0.288 | 0.087 | 0.108 | 0.146 | 0.119 | 0.042 |
| Green | W | Oct-23 | 5226 | 0.030 | 0.093 | 0.058 | 0.061 | 0.065 | 0.061 | 0.006 |
| Green | W | Dec-23 | 5707 | 0.047 | 0.133 | 0.060 | 0.063 | 0.068 | 0.066 | 0.012 |
| Green | W | Jan-24 | 5707 | 0.042 | 0.131 | 0.063 | 0.067 | 0.073 | 0.071 | 0.015 |
| Green | W | Feb-24 | 5707 | 0.039 | 0.208 | 0.100 | 0.112 | 0.125 | 0.114 | 0.021 |
| Green | W | Apr-24 | 5707 | 0.034 | 0.311 | 0.091 | 0.101 | 0.111 | 0.104 | 0.025 |
| NIR | A | Oct-23 | 5173 | 0.183 | 0.301 | 0.250 | 0.260 | 0.268 | 0.258 | 0.014 |
| NIR | A | Dec-23 | 5172 | 0.276 | 0.643 | 0.422 | 0.441 | 0.461 | 0.441 | 0.029 |
| NIR | A | Jan-24 | 5173 | 0.276 | 0.561 | 0.419 | 0.438 | 0.460 | 0.439 | 0.031 |
| NIR | A | Feb-24 | 5173 | 0.137 | 0.643 | 0.400 | 0.423 | 0.446 | 0.422 | 0.046 |
| NIR | A | Apr-24 | 5173 | 0.127 | 0.491 | 0.320 | 0.352 | 0.376 | 0.348 | 0.038 |
| NIR | W | Oct-23 | 5226 | 0.190 | 0.472 | 0.353 | 0.370 | 0.384 | 0.368 | 0.026 |
| NIR | W | Dec-23 | 5707 | 0.265 | 0.478 | 0.390 | 0.401 | 0.412 | 0.401 | 0.018 |
| NIR | W | Jan-24 | 5707 | 0.228 | 0.437 | 0.341 | 0.354 | 0.366 | 0.353 | 0.020 |
| NIR | W | Feb-24 | 5707 | 0.184 | 0.496 | 0.378 | 0.396 | 0.412 | 0.394 | 0.028 |
| NIR | W | Apr-24 | 5707 | 0.145 | 0.537 | 0.348 | 0.375 | 0.399 | 0.373 | 0.043 |
| Red | A | Oct-23 | 5173 | 0.022 | 0.054 | 0.026 | 0.027 | 0.028 | 0.027 | 0.002 |
| Red | A | Dec-23 | 5172 | 0.039 | 0.134 | 0.052 | 0.055 | 0.060 | 0.057 | 0.007 |
| Red | A | Jan-24 | 5173 | 0.035 | 0.099 | 0.043 | 0.046 | 0.050 | 0.047 | 0.006 |
| Red | A | Feb-24 | 5173 | 0.026 | 0.320 | 0.075 | 0.092 | 0.119 | 0.101 | 0.038 |
| Red | A | Apr-24 | 5173 | 0.043 | 0.363 | 0.135 | 0.167 | 0.207 | 0.173 | 0.050 |

| Drone variable | Site | Survey | No. of observations | Minimum | Maximum | 1st Quartile | Median | 3rd Quartile | Mean | Standard deviation (n-1) |
|---|---|---|---|---|---|---|---|---|---|---|
| Red | W | Oct-23 | 5226 | 0.016 | 0.066 | 0.026 | 0.028 | 0.031 | 0.029 | 0.005 |
| Red | W | Dec-23 | 5707 | 0.024 | 0.130 | 0.033 | 0.036 | 0.040 | 0.040 | 0.015 |
| Red | W | Jan-24 | 5707 | 0.021 | 0.122 | 0.032 | 0.036 | 0.042 | 0.041 | 0.018 |
| Red | W | Feb-24 | 5707 | 0.028 | 0.279 | 0.082 | 0.104 | 0.127 | 0.106 | 0.035 |
| Red | W | Apr-24 | 5707 | 0.022 | 0.343 | 0.062 | 0.073 | 0.084 | 0.077 | 0.027 |
| RedEdge | A | Oct-23 | 5173 | 0.087 | 0.166 | 0.115 | 0.119 | 0.123 | 0.119 | 0.006 |
| RedEdge | A | Dec-23 | 5172 | 0.125 | 0.328 | 0.186 | 0.193 | 0.203 | 0.196 | 0.016 |
| RedEdge | A | Jan-24 | 5173 | 0.138 | 0.283 | 0.181 | 0.190 | 0.200 | 0.192 | 0.017 |
| RedEdge | A | Feb-24 | 5173 | 0.070 | 0.442 | 0.207 | 0.223 | 0.243 | 0.227 | 0.035 |
| RedEdge | A | Apr-24 | 5173 | 0.118 | 0.404 | 0.233 | 0.258 | 0.288 | 0.261 | 0.037 |
| RedEdge | W | Oct-23 | 5226 | 0.084 | 0.218 | 0.161 | 0.169 | 0.176 | 0.168 | 0.013 |
| RedEdge | W | Dec-23 | 5707 | 0.126 | 0.237 | 0.168 | 0.175 | 0.183 | 0.177 | 0.013 |
| RedEdge | W | Jan-24 | 5707 | 0.130 | 0.264 | 0.172 | 0.181 | 0.191 | 0.183 | 0.016 |
| RedEdge | W | Feb-24 | 5707 | 0.092 | 0.349 | 0.224 | 0.241 | 0.256 | 0.240 | 0.024 |
| RedEdge | W | Apr-24 | 5707 | 0.071 | 0.406 | 0.202 | 0.221 | 0.239 | 0.221 | 0.033 |
| NDVI | A | Oct-23 | 5173 | 0.619 | 0.841 | 0.802 | 0.812 | 0.820 | 0.809 | 0.016 |
| NDVI | A | Dec-23 | 5172 | 0.544 | 0.828 | 0.761 | 0.775 | 0.787 | 0.772 | 0.023 |
| NDVI | A | Jan-24 | 5173 | 0.567 | 0.855 | 0.797 | 0.809 | 0.819 | 0.806 | 0.021 |
| NDVI | A | Feb-24 | 5173 | 0.138 | 0.844 | 0.581 | 0.652 | 0.704 | 0.633 | 0.098 |
| NDVI | A | Apr-24 | 5173 | 0.054 | 0.771 | 0.257 | 0.349 | 0.442 | 0.352 | 0.127 |
| NDVI | W | Oct-23 | 5226 | 0.662 | 0.914 | 0.841 | 0.854 | 0.866 | 0.851 | 0.023 |
| NDVI | W | Dec-23 | 5707 | 0.501 | 0.894 | 0.815 | 0.833 | 0.847 | 0.821 | 0.053 |
| NDVI | W | Jan-24 | 5707 | 0.379 | 0.895 | 0.788 | 0.814 | 0.833 | 0.794 | 0.070 |
| NDVI | W | Feb-24 | 5707 | 0.175 | 0.879 | 0.531 | 0.600 | 0.666 | 0.596 | 0.103 |
| NDVI | W | Apr-24 | 5707 | 0.156 | 0.831 | 0.649 | 0.682 | 0.712 | 0.672 | 0.070 |
| NDRE | A | Oct-23 | 5173 | 0.148 | 0.421 | 0.356 | 0.371 | 0.382 | 0.368 | 0.022 |
| NDRE | A | Dec-23 | 5172 | 0.155 | 0.457 | 0.372 | 0.387 | 0.401 | 0.385 | 0.025 |
| NDRE | A | Jan-24 | 5173 | 0.183 | 0.459 | 0.377 | 0.394 | 0.410 | 0.393 | 0.026 |
| NDRE | A | Feb-24 | 5173 | 0.070 | 0.470 | 0.278 | 0.310 | 0.339 | 0.305 | 0.047 |
| NDRE | A | Apr-24 | 5173 | 0.004 | 0.340 | 0.106 | 0.147 | 0.185 | 0.146 | 0.054 |
| NDRE | W | Oct-23 | 5226 | 0.256 | 0.474 | 0.365 | 0.377 | 0.390 | 0.377 | 0.022 |
| NDRE | W | Dec-23 | 5707 | 0.254 | 0.475 | 0.376 | 0.391 | 0.407 | 0.390 | 0.026 |
| NDRE | W | Jan-24 | 5707 | 0.174 | 0.442 | 0.302 | 0.323 | 0.342 | 0.321 | 0.033 |
| NDRE | W | Feb-24 | 5707 | 0.101 | 0.418 | 0.225 | 0.245 | 0.269 | 0.248 | 0.037 |
| NDRE | W | Apr-24 | 5707 | 0.084 | 0.491 | 0.255 | 0.274 | 0.293 | 0.274 | 0.034 |
| GNDVI | A | Oct-23 | 5173 | 0.597 | 0.806 | 0.760 | 0.769 | 0.777 | 0.767 | 0.015 |
| GNDVI | A | Dec-23 | 5172 | 0.523 | 0.780 | 0.719 | 0.730 | 0.741 | 0.728 | 0.020 |

| Drone variable | Site | Survey | No. of observations | Minimum | Maximum | 1st Quartile | Median | 3rd Quartile | Mean | Standard deviation (n-1) |
|---|---|---|---|---|---|---|---|---|---|---|
| GNDVI | A | Jan-24 | 5173 | 0.559 | 0.805 | 0.749 | 0.761 | 0.772 | 0.759 | 0.020 |
| GNDVI | A | Feb-24 | 5173 | 0.308 | 0.787 | 0.604 | 0.646 | 0.678 | 0.637 | 0.056 |
| GNDVI | A | Apr-24 | 5173 | 0.032 | 0.886 | 0.437 | 0.540 | 0.613 | 0.520 | 0.128 |
| GNDVI | W | Oct-23 | 5226 | 0.572 | 0.775 | 0.705 | 0.718 | 0.730 | 0.716 | 0.021 |
| GNDVI | W | Dec-23 | 5707 | 0.494 | 0.792 | 0.711 | 0.726 | 0.740 | 0.720 | 0.037 |
| GNDVI | W | Jan-24 | 5707 | 0.378 | 0.780 | 0.657 | 0.680 | 0.699 | 0.668 | 0.051 |
| GNDVI | W | Feb-24 | 5707 | 0.299 | 0.746 | 0.529 | 0.561 | 0.592 | 0.557 | 0.058 |
| GNDVI | W | Apr-24 | 5707 | 0.219 | 0.721 | 0.567 | 0.588 | 0.609 | 0.582 | 0.054 |
| RVI | A | Oct-23 | 5173 | 4.263 | 12.410 | 9.434 | 10.037 | 10.551 | 9.947 | 0.900 |
| RVI | A | Dec-23 | 5172 | 3.383 | 10.662 | 7.550 | 8.106 | 8.617 | 8.053 | 0.859 |
| RVI | A | Jan-24 | 5173 | 3.638 | 13.436 | 9.138 | 9.843 | 10.490 | 9.776 | 1.072 |
| RVI | A | Feb-24 | 5173 | 1.320 | 11.828 | 5.418 | 6.483 | 7.407 | 6.320 | 1.572 |
| RVI | A | Apr-24 | 5173 | 1.114 | 7.719 | 1.720 | 2.151 | 2.729 | 2.332 | 0.830 |
| RVI | W | Oct-23 | 5226 | 5.234 | 23.246 | 13.664 | 15.124 | 16.493 | 15.048 | 2.343 |
| RVI | W | Dec-23 | 5707 | 3.031 | 19.084 | 10.682 | 11.989 | 13.146 | 11.692 | 2.372 |
| RVI | W | Jan-24 | 5707 | 2.223 | 20.028 | 9.676 | 11.250 | 12.566 | 10.797 | 2.770 |
| RVI | W | Feb-24 | 5707 | 1.429 | 17.092 | 4.494 | 5.597 | 6.824 | 5.765 | 1.961 |
| RVI | W | Apr-24 | 5707 | 1.378 | 11.921 | 5.163 | 5.826 | 6.560 | 5.874 | 1.278 |
| CVI | A | Oct-23 | 5173 | 3.621 | 8.391 | 5.857 | 6.154 | 6.431 | 6.131 | 0.460 |
| CVI | A | Dec-23 | 5172 | 2.970 | 7.012 | 4.983 | 5.227 | 5.476 | 5.221 | 0.394 |
| CVI | A | Jan-24 | 5173 | 3.377 | 7.642 | 5.367 | 5.727 | 6.078 | 5.724 | 0.535 |
| CVI | A | Feb-24 | 5173 | 2.583 | 8.650 | 4.036 | 4.335 | 4.667 | 4.374 | 0.506 |
| CVI | A | Apr-24 | 5173 | 0.681 | 144.968 | 5.788 | 10.023 | 15.716 | 11.848 | 8.704 |
| CVI | W | Oct-23 | 5226 | 1.815 | 5.617 | 2.709 | 2.879 | 3.067 | 2.903 | 0.315 |
| CVI | W | Dec-23 | 5707 | 2.501 | 6.902 | 3.391 | 3.619 | 3.858 | 3.642 | 0.379 |
| CVI | W | Jan-24 | 5707 | 1.938 | 5.719 | 2.607 | 2.766 | 2.961 | 2.813 | 0.313 |
| CVI | W | Feb-24 | 5707 | 1.935 | 5.926 | 2.721 | 2.976 | 3.217 | 2.982 | 0.401 |
| CVI | W | Apr-24 | 5707 | 1.462 | 4.590 | 2.720 | 2.870 | 3.035 | 2.873 | 0.330 |
| CIRE | A | Oct-23 | 5173 | 0.347 | 1.476 | 1.117 | 1.192 | 1.252 | 1.178 | 0.109 |
| CIRE | A | Dec-23 | 5172 | 0.366 | 1.683 | 1.190 | 1.271 | 1.346 | 1.262 | 0.128 |
| CIRE | A | Jan-24 | 5173 | 0.448 | 1.717 | 1.219 | 1.311 | 1.401 | 1.308 | 0.140 |
| CIRE | A | Feb-24 | 5173 | 0.151 | 1.773 | 0.811 | 0.940 | 1.060 | 0.926 | 0.190 |
| CIRE | A | Apr-24 | 5173 | 0.009 | 1.044 | 0.241 | 0.350 | 0.462 | 0.358 | 0.153 |
| CIRE | W | Oct-23 | 5226 | 0.692 | 1.821 | 1.163 | 1.230 | 1.295 | 1.230 | 0.115 |
| CIRE | W | Dec-23 | 5707 | 0.690 | 1.827 | 1.214 | 1.297 | 1.383 | 1.293 | 0.138 |
| CIRE | W | Jan-24 | 5707 | 0.422 | 1.614 | 0.878 | 0.969 | 1.055 | 0.965 | 0.144 |
| CIRE | W | Feb-24 | 5707 | 0.229 | 1.463 | 0.594 | 0.665 | 0.754 | 0.683 | 0.140 |

| Drone variable | Site | Survey | No. of observations | Minimum | Maximum | 1st Quartile | Median | 3rd Quartile | Mean | Standard deviation (n-1) |
|---|---|---|---|---|---|---|---|---|---|---|
| CIRE | W | Apr-24 | 5707 | 0.184 | 1.978 | 0.703 | 0.772 | 0.853 | 0.783 | 0.139 |
| DrHeight | A | Oct-23 | 5173 | 0.000 | 2.134 | 0.689 | 1.024 | 1.279 | 0.982 | 0.398 |
| DrHeight | A | Dec-23 | 5172 | 0.000 | 1.956 | 0.408 | 0.686 | 0.923 | 0.675 | 0.359 |
| DrHeight | A | Jan-24 | 5173 | 0.000 | 1.924 | 0.423 | 0.699 | 0.930 | 0.687 | 0.343 |
| DrHeight | A | Feb-24 | 5173 | 0.072 | 2.141 | 0.643 | 0.879 | 1.104 | 0.874 | 0.329 |
| DrHeight | A | Apr-24 | 5173 | 0.035 | 2.244 | 0.420 | 0.717 | 1.086 | 0.781 | 0.434 |
| DrHeight | W | Oct-23 | 5226 | 0.704 | 6.146 | 1.839 | 2.023 | 2.227 | 2.042 | 0.323 |
| DrHeight | W | Dec-23 | 5707 | 0.015 | 5.661 | 1.693 | 1.912 | 2.137 | 1.907 | 0.377 |
| DrHeight | W | Jan-24 | 5707 | 0.000 | 3.685 | 1.289 | 1.602 | 1.928 | 1.600 | 0.491 |
| DrHeight | W | Feb-24 | 5707 | 0.184 | 3.948 | 1.245 | 1.567 | 1.937 | 1.590 | 0.494 |
| DrHeight | W | Apr-24 | 5707 | 0.081 | 3.030 | 1.603 | 1.786 | 1.994 | 1.793 | 0.315 |
| DrVolume | A | Oct-23 | 5173 | 0.000 | 4.543 | 1.466 | 2.179 | 2.723 | 2.091 | 0.847 |
| DrVolume | A | Dec-23 | 5172 | 0.000 | 3.985 | 0.830 | 1.398 | 1.881 | 1.374 | 0.731 |
| DrVolume | A | Jan-24 | 5173 | 0.000 | 4.034 | 0.887 | 1.465 | 1.950 | 1.440 | 0.719 |
| DrVolume | A | Feb-24 | 5173 | 0.148 | 4.383 | 1.316 | 1.799 | 2.261 | 1.789 | 0.674 |
| DrVolume | A | Apr-24 | 5173 | 0.072 | 4.550 | 0.851 | 1.455 | 2.203 | 1.584 | 0.880 |
| DrVolume | W | Oct-23 | 5226 | 1.243 | 10.851 | 3.246 | 3.572 | 3.931 | 3.605 | 0.570 |
| DrVolume | W | Dec-23 | 5707 | 0.027 | 10.428 | 3.119 | 3.523 | 3.937 | 3.513 | 0.695 |
| DrVolume | W | Jan-24 | 5707 | 0.000 | 7.419 | 2.596 | 3.225 | 3.881 | 3.221 | 0.988 |
| DrVolume | W | Feb-24 | 5707 | 0.366 | 7.842 | 2.474 | 3.114 | 3.847 | 3.157 | 0.981 |
| DrVolume | W | Apr-24 | 5707 | 0.165 | 6.121 | 3.238 | 3.609 | 4.029 | 3.622 | 0.637 |
| Thermal | A | Oct-23 | 5173 | 29.517 | 69.010 | 43.081 | 46.879 | 50.307 | 46.889 | 5.480 |
| Thermal | A | Dec-23 | 5172 | 0.000 | 68.931 | 41.164 | 45.580 | 50.246 | 44.622 | 8.558 |
| Thermal | A | Jan-24 | 5173 | 33.349 | 70.150 | 43.181 | 46.742 | 50.763 | 47.409 | 5.803 |
| Thermal | A | Feb-24 | 5173 | 26.362 | 63.924 | 38.432 | 41.675 | 45.652 | 42.085 | 5.232 |
| Thermal | A | Apr-24 | 5173 | 0.186 | 56.297 | 11.551 | 21.300 | 36.481 | 23.981 | 12.639 |
| Thermal | W | Oct-23 | 5226 | 26.501 | 48.446 | 32.082 | 34.369 | 37.606 | 34.920 | 3.530 |
| Thermal | W | Dec-23 | 5707 | 31.117 | 66.749 | 40.126 | 43.083 | 46.419 | 43.578 | 4.866 |
| Thermal | W | Jan-24 | 5707 | 33.552 | 69.341 | 43.443 | 47.244 | 51.464 | 47.568 | 5.615 |
| Thermal | W | Feb-24 | 5707 | 30.476 | 67.170 | 39.510 | 42.900 | 47.061 | 43.410 | 5.422 |
| Thermal | W | Apr-24 | 5707 | 24.017 | 45.895 | 28.857 | 31.057 | 35.925 | 32.228 | 4.119 |

NIR – Near-infrared, NDVI - Normalized Difference Vegetation Index, NDRE - Normalized Difference Red Edge Index, GNDVI -Green Normalized Difference Vegetation Index, RVI - Ratio Vegetation Index, CVI - Chlorophyll vegetation index, CIRE - Chlorophyll index – Red edge, Dr_Height – drone image estimated tree height, Dr_Volume – drone image estimated tree volume, TIR – thermal infrared temperature

# APPENDIX F: CAPACITY BUILDING

## 1. Students

Uncertainties with regard to suppliers to conduct the drone surveys and lack of funding for a bursary hampered recruitment of a student for this project. The stem water potential and physiological data collected in 2023/2024 was related to the drone image derived spectral bands and indices and will be included in the thesis of Daniel Havenga supervised by Dr Dzikiti on the water use and water productivity project (C2020/2021-00404). He assisted in the writing of Chapter 6 of the final report for project C2020/2021-00943. Mr Daniel Havenga (Student number 21898138) registered in February 2023 for an MSc in Horticulture at Stellenbosch University with Dr Dzikiti as supervisor. The title of his thesis is "Water use efficiency of pomegranate". He reregistered in 2025 and is expected to complete his studies by March 2026.

## 2. Institutional capacity building

Dr T. Volschenk attended an online short course: Introduction to field data collection and UAV data pre-processing held by ARC NRE, 17 October 2023.